Université Fédérale
Toulouse Midi-Pyrénées

THÈSE

En vue de l'obtention du

DOCTORAT DE L'UNIVERSITÉ DE TOULOUSE

Délivré par l'Université Toulouse 3 - Paul Sabatier

Présentée et soutenue par

Marine CAZENAVE

Le 15 octobre 2018

Caractérisation multi-site de la distribution osseuse corticale et de l'organisation du réseau trabéculaire du squelette postcrânien de *Paranthropus robustus*: implications taxonomiques, fonctionnelles et paléobiologiques

---

Ecole doctorale : **BSB - Biologie, Santé, Biotechnologies**

Spécialité : **ANTHROPOBIOLOGIE**

Unité de recherche :
AMIS - Laboratoire d'Anthropologie Moléculaire et Imagerie de Synthèse

Thèse dirigée par
José BRAGA et Anna OETTLE

Rapporteurs
M. Frederick E. Grine, Rapporteur
Mme Emmanuelle Pouydebat, Rapporteur

Jury
M. Frederick E. Grine, Rapporteur
M. Damiano Marchi, Examinateur
M. Norbert Telmon, Examinateur
M. José Braga, Directeur de thèse
Mme Anna C. Oettlé, Co-directeur de thèse
M. Roberto Macchiarelli, Co-directeur de thèse

ACKNOWLEDGMENTS (IN FRENCH)

Remerciements,

Je dédie ces quelques lignes à toutes les personnes et les institutions qui par leur accueil, leur collaboration et leur soutien ont contribué de près ou de loin à la réalisation de ce projet de recherche. Je remercie également ceux qui ont accepté d'évaluer ce travail.

Au cours de ces dernières années, M. J. Braga (AMIS, Toulouse & Wits Univ., Johannesburg) a été successivement enseignant puis tuteur de mémoire de M1 et de M2, et enfin directeur de thèse. Je souhaiterais le remercier pour son encadrement, pour m'avoir accueillie au sein de son équipe et m'avoir offert l'opportunité de travailler sur ce sujet de recherche passionnant dans le contexte paléoanthropologique exceptionnel d'Afrique du Sud. M. Braga m'a permis d'acquérir une expérience scientifique incontestablement riche, et notamment une expérience de terrain à Kromdraai particulièrement formatrice, m'apportant ainsi une formation complète et de qualité.

J'adresse également mes remerciements à Mme A. Oettlé (Université de Pretoria & SMU, Pretoria) pour la qualité de son suivi et de son encadrement, pour son investissement et ses précieux conseils. Ses connaissances, notamment sur l'anatomie humaine et sur les institutions sud-africaines, ont largement contribué à nourrir ce travail. Je la remercie également pour son aide au quotidien ainsi que pour tous les échanges culturels.

L'opportunité m'est ici offerte de remercier grandement et très sincèrement M. R. Macchiarelli (Université de Poitiers & MNHN, Paris) qui a été protagoniste de mon parcours universitaire depuis ma L2, tour à tour tuteur de mémoire en L3, M1 et M2, et finalement co-encadrant de thèse. Je souhaiterais souligner la qualité de son encadrement et de son accompagnement. Son important investissement/implication, son soutien et son aide au cours de ces sept dernières années, malgré la distance et les difficultés, ont été essentiels à ma formation et à mes débuts dans le domaine de la recherche. En outre, ses connaissances, son professionnalisme et sa rigueur ont largement contribué à la réalisation de ce projet de recherche. Je le remercie pour les conseils avisés prodigués, le partage de son expérience tout au long de ce parcours, sa patience, et les occasions professionnelles successives qu'il a pris soin de me proposer.

Je tiens à remercier très sincèrement M. F.E. Grine (Stony Brook University, New York) et Mme E. Pouydebat (MNHN, Paris) qui ont tous deux accepté de juger et de rapporter ce travail. Un grand merci également à M. D. Marchi (University of Pisa) et à M. N. Telmon (AMIS, Toulouse) de venir officier dans ce jury de soutenance.

J'adresse mes remerciements les plus sincères à M. F. Thackeray (Wits Univ., Johannesburg) pour son aide généreuse et précieuse tout au long de mes séjours en Afrique du Sud depuis mon M2. Les très nombreuses discussions scientifiques depuis ces quatre dernières années m'ont permis d'appréhender le contexte de la paléoanthropologie en Afrique du Sud. Son aide, concernant notamment les rencontres avec différents chercheurs et l'accès aux collections, a été incontestablement essentielle pour la mise en place et le bon déroulement de ce projet de recherche. Je le remercie sincèrement pour son soutien indéfectible dans les différents travaux de recherche. Enfin, un grand merci de m'avoir fait découvrir toutes les richesses de l'Afrique du Sud.

Je remercie M. É. Crubézy, directeur du laboratoire AMIS de l'Université de Toulouse III, Paul Sabatier et M. M.C. Bosman Directeur du Département d'Anatomie de l'Université de Pretoria pour avoir autorisé mon inscription en thèse au sein de leurs unités. Je remercie également l'Ecole Doctorale pour leur aide et compréhension quant aux difficultés liées à la distance.

Au cours de ma formation en paléoanthropologie, j'ai eu la chance de bénéficier directement de l'expérience de différents chercheurs, qui représentent pour moi un entourage proche et un soutien précieux.

Je remercie notamment Mme A. Beaudet (Wits Univ., Johannesburg), de m'avoir tout d'abord formée aux outils d'imagerie 3D et d'avoir partagé ses connaissances sur la caractérisation de l'endo-structure osseuse, puis de m'avoir accueillie à Toulouse lors de mes déplacements en L3; Un grand merci également pour les innombrables conseils avisés, échanges scientifiques, aides précieuses et surtout pour ta patience; Merci d'avoir partagés ces nombreux moments riches en expériences professionnelles et humaines depuis ma L2 (merci par exemple d'avoir partagé les logements pour les conférences, même si nos choix ont pu s'avérer imprudents).

Je remercie très sincèrement M. C. Zanolli (AMIS, Toulouse), pour m'avoir accueillie, accompagnée et formée aux outils d'acquisitions micro-tomographiques et aux techniques d'imagerie pendant mes stages en L2 et L3 à Trieste en Italie mais également pour son soutien et son aide prodigués depuis lors; merci d'être toujours disponible pour répondre à mes questions ou simplement discuter.

Je remercie Mme C. Theye (Université de Pretoria) pour son aide généreuse et infaillible qu'elle m'a apportée à maintes reprises depuis mon M1 et surtout durant mes séjours en Afrique du Sud. Je souhaiterais la remercier notamment pour sa présence indispensable lors des transports de fossiles, son aide pour la sélection, manipulation et transport du matériel ostéologique, pour ses relectures innombrables et pour toutes les autres bienveillances et autres services; Merci également pour ta patience et ta bonne humeur constante (merci par exemple d'avoir accepté cadavres et squelettes dans le bureau et tous les désagréments olfactifs associés).

Merci à M. A. Mazurier (Université de Poitiers), pour la mise à disposition d'éléments de sa base de données et pour sa gentillesse pendant mes différents passages à l'Université de Poitiers.

Ce travail de recherche a bénéficié de l'investissement de différents chercheurs, ingénieurs et techniciens qui ont, par leur disponibilité et compétence, facilité l'accès aux collections et aux plateformes d'imagerie et contribué à la constitution de l'échantillon de cette thèse.

Je remercie M. H. Fourie, M. L. Kgasi, Mme S. Potze, et Mme M. Tawane du Ditsong National Museum of Natural History (DNMNH) de Pretoria, pour l'accès et l'emprunt du matériel fossile ainsi que pour leur efficacité et professionnalisme.

Je tiens à remercier également M. J. Heaton (Birmingham-Southern College & Wits Univ., Johannesburg & DNMNH, Pretoria) et M. T. Pickering (University of Wisconsin, Madison & Wits Univ., Johannesburg & DNMNH, Pretoria) de m'avoir généreusement proposé une collaboration pour l'étude inédite de la structure interne du fémur proximal de P. robustus *SWT1/LB-2 de Swartkrans.*

Pour l'accès au registre tomographique du spécimen H. *aff.* erectus *Gombore IB, je remercie M. R. Macchiarelli (Université de Poitiers & MNHN, Paris), Mme M. Endalamaw (ARCCH, Addis Ababa), M. B. Endga Redae (ARCCH, Addis Ababa) et toute l'équipe de l'Italian Archaeological Mission de Melka Kunture et Balchit ainsi que M. Y. Assefa (ARCCH,*

Addis Ababa), Mme M. Mussi (Università di Roma Sapienza), M. Y.D. Tsegaye (ARCCH, Addis Ababa) et M. Y. Yilm (ARCCH, Addis Ababa) pour leur soutien pour les acquisitions tomographiques.

Pour leur confiance et leur aide pour l'accès au matériel comparatif ostéologique humain et de Papio *de la Pretoria Bone Collection du Département d'Anatomie de l'Université de Pretoria, je souhaiterais remercier Mme E. L'Abbé et Mme G. Kruger; Merci d'avoir été toujours disponible afin de trouver les meilleures solutions possibles. Je remercie également M. G. Lewis d'avoir autorisé l'emprunt d'un cadavre pour des acquisitions micro-tomographiques. Je remercie le Comité d'Ethique de l'Université de Pretoria pour avoir soutenu le projet de thèse et autorisé les analyses.*

Je tiens à remercier M. N. Bacci et M. B. Billings de la R.A. Dart Collection pour leur disponibilité à maintes reprises pour l'accès au matériel comparatif humain et gorille. Je souhaiterais également les remercier pour leur intérêt apporté à ce projet de recherche et les nombreux échanges scientifiques.

Je remercie M. D. Morris de m'avoir accueillie au McGregor Museum de Kimberley et d'avoir accepté l'emprunt de fémurs de la collection ostéologique de populations Khoesan.

Je remercie également M. M. Nakatsukasa (Kyoto University), M. Nakamura (Kyoto University) et Y. Shintaku (Japan Monkey Centre, Inuyama) pour l'accès et les acquisitions micro-tomographiques de trois patellae de femelles chimpanzés et je remercie M. M. Nakatsukasa (Kyoto University) pour ses conseils dans le cadre de la collaboration sur l'étude de la patelle P. robustus *SKX 1084. Je remercie M. R. Macchiarelli (Université de Poitiers & MNHN, Paris) et M. A. Mazurier (Université de Poitiers) pour l'accès au registre synchrotron de deux fémurs de chimpanzés et de la patella de Regourdou 1. Je souhaiterais remercier M. B. Zipfel pour l'accès au squelette d'un individu* Pan troglodytes *et un individu* Pan paniscus *et je remercie Mme L. Hutten du Département d'Archéologie de l'Université de Cape Town pour l'accès au matériel ostéologique comparatif de* Papio.

Je remercie M. E. Gilissen (MRAC, Tervuren) et M. Wim Wendelen (MRAC, Tervuren) pour leur accueil au Musée royal de l'Afrique centrale et également pour leur aide dans l'accès aux collections.

Un remerciement particulier à M. F. de Beer (Necsa, Pelindaba), M. J. Hoffman (Necsa, Pelindaba) et M. L. Bam (Necsa, Pelindaba) pour leurs collaborations aux différents travaux de recherches, et notamment pour les acquisitions micro-tomographiques à la South African Nuclear Energy corporation (Necsa) à Pelindaba et pour les nombreux échanges scientifiques sur les outils d'acquisitions; Merci d'avoir été toujours très arrangeants et disponibles et d'avoir accepté de manipuler et de scanner du matériel délicat. Je souhaitais également remercier M. K. Jakata (Wits Univ., Johannesburg) pour les acquisitions micro-tomographiques à l'Evolutionary Studies Institute de l'Université du Witwatersrand de Johannesburg. Je remercie M. F. Bernardini (ICTP, Trieste), M. L. Bondioli (National Museum "L. Pigorini", Rome) M. C. Tuniz (ICTP, Trieste) et M. C. Zanolli (AMIS, Toulouse) pour les acquisitions micro-tomographiques des patellae de Krapina et de Velia conservées au Muséum National "L. Pigorini" de Rome.

Je remercie M. R. Macchiarelli (Université de Poitiers & MNHN, Paris) pour les images X-ray du fémur H. erectus *KNM-WT 15000-G de Nariokotome réalisées par lui-même, M. L. Bondioli (National Museum "L. Pigorini", Rome) et M. M. Rossi (Universitá di Bologna) en collaboration avec M.G. Leakey (Nairobi), A. Walker (State College) and C.V. Ward (Columbia) et l'assistance technique de M. G. Abungu (Nairobi) et M. F.M. Kirera (Nairobi)*

Pendant mon parcours professionnel et notamment pendant ces trois années de thèse, j'ai eu la chance de nouer des contacts professionnels constructifs et enrichissants avec différents chercheurs.

Je souhaitais remercier tout particulièrement M. P. O'Higgins (HYMS, University of York) de m'avoir accueillie dans son laboratoire lors d'un stage de L3 et pour tout son soutien, son aide et ses conseils prodigués depuis lors

Pour les diverses discussions constructives, je voudrais remercier Mme M. Bamford (Wits Univ., Johannesburg), Mme P. Bayle (PACEA, Bordeaux), M. J. Benoit (Wits Univ., Johannesburg), M. L. Bruxelles (INRAP, Nïmes & IFAS, Johannesburg & Wits Univ., Johannesburg), M. K. Carlson (University of Southern California, Los Angeles), Mme M. Carmen Arriaza (Wits Univ., Johannesburg), M. R. Clarke (Wits Univ., Johannesburg), M. T. Cucchi (MNHN, Paris), Mme K. Kuman (Wits Univ., Johannesburg), M. J.-B. Fourvel (TRACE, Toulouse), M. D. Gommery (MNHN, Paris), M. J. Hawks (Wits Univ., Johannesburg), Mme T. Jashawalishi (Wits Univ., Johannesburg & University of Southern California, Los Angeles & Georgian National Museum, Tbilisi), M. M. Lague (Stokton University), Mme M. Pina (University of Tokyo), M. L. Puymerail (ADES, Marseille), Mme C. Steininger (Wits Univ., Johannesburg), M. D. Stratford (Wits Univ., Johannesburg), Mme A. Val (Wits Univ., Johannesburg), M. B. Zipfel (Wits. Univ., Johannesburg).

Je tiens à remercier M. P. Adalian (ADES, Marseille) et M. P. Swider (IMFT, Toulouse) pour avoir accepté de former mon comité de thèse et m'avoir adressé leurs commentaires particulièrement constructifs pour mon travail de thèse.

Je remercie tous les membres du Kromdraai Research Project avec lesquelles j'ai eu la grande opportunité de partager une expérience de terrain.

Je remercie également profondément M. A. El-Albani (Hydrasa, Poitiers) et M. A. Meunier (Hydrasa, Poitiers) pour leur accueil toujours chaleureux à l'Université de Poitiers et leur soutien.

Pour le financement de cette thèse, je remercie l'European Commission (EACEA), Erasmus Mundus programme, AESOP and AESOP+ consortia coordonné par M. J. Braga (AMIS, Toulouse). Je tiens à remercier particulièrement Mme E. Balonas. Je remercie également la NRF pour la bourse de mobilité du programme Knowledge Interchange and Collaboration (KIC) m'ayant permise de présenter les travaux sur l'étude de l'humérus distal à la East African Association for Paleoanthropology And Paleontology (EAAPP) Sixth Biennial Conference.

Je tenais à remercier très sincèrement tous les membres du Département d'Anatomie de l'Université de Pretoria pour leur chaleureux accueil, leur soutien pour leur gentillesse et leur attention à mon égard. Je tiens à remercier tout particulièrement Mme E. L'Abbé, Mme M.-C. Dussault et Mme G. Kruger pour leur aide dans toutes les démarches administratives et au quotidien. Je remercie mes camarades de thèse Mme R. Holgate, Mme A. Ridel, Mme C. Sutherland, et Mme C. Theye qui à travers des échanges et partages d'expériences ont contribué au bon déroulement de ce projet de recherche. Ainsi que tous les doctorants post-doctorants que j'ai rencontrés au cours de mon séjour au Département et qui ont contribué à enrichir ce travail de thèse, je pense notamment à Mme M. Galland et M. S. Renni. Je remercie également M. E. de Jager, Mme L. Liebenberg, M. E. Marakalla, Mme M. Pretorius, Mme Y. Scholtz, M. A. VanSchoor pour leur disponibilité et pour tous les bons moments partagés.

Je remercie chaleureusement tous les membres du laboratoire AMIS qui m'ont soutenue et aidée pendant ces trois années je tiens à remercier tout particulièrement Mme M.-H. Escalier, à la fois pour son aide précieuse dans les différentes démarches administratives mais également pour son soutien constant. Un immense merci à M. J. Dumoncel, qui a mis en place des outils méthodologiques informatiques innovants et qui armé d'une grande patience a toujours pris le temps de répondre à mes innombrables questions et a toujours été enthousiaste pour développer des projets innovants. Je remercie sincèrement M. C. Zanolli pour ces nombreux conseils avisés et son soutien. Je remercie aussi Mme A. Nengovhela et Mme N.

Ngoloyi, camarades de thèse, à qui je souhaite bonne chance pour la suite de leur parcours. Merci aussi à M. P. Gérard, M. D. Ginibrière, Mme D. Nikolaeva et M. D. Pierron.

Un remerciement pour tous mes camarades et amis rencontrés tout au long de ce parcours et qui encore aujourd'hui par leur soutien participent à mon épanouissement professionnel, je pense notamment à Cécilia et Valentin. Un grand merci à toutes ces belles rencontres en Afrique du Sud, Alice, Alienor, Celso, Clarissa, François, Graham, JP, Julien, Kobus, Kuda, Lunga, Mabuti, Mamasila, Marine, Rachel, Robert, Shanene, Sophie, Swapiwe, pour tous ces extraordinaires moments riches en échanges culturels et expériences. Un grand merci à Audrey (de ta cousine préférée) pour son rôle indispensable de médiatrice avec l'Ecole Doctorale, qui n'a jamais refusé de se déplacer à l'Ecole Doctorale ou au laboratoire AMIS, d'imprimer ou de récupérer des documents dès qu'il en était nécessaire. Enfin, ce projet de recherche n'aurait jamais pu se réaliser sans les encouragements de ma famille à qui je dédie ce travail. Un immense merci à mes parents et leur conjoint respectif qui malgré les craintes et les difficultés liées à la distance me laissent voguer vers des mers inconnues, et même plus, m'encouragent et me soutiennent. Merci à mes frères et sœurs, pour leur compréhension et leur patience mais aussi à toute ma famille. Mes dernières pensées vont bien évidemment à Etienne pour sa curiosité sans limites, son enthousiasme face à mes choix et décisions professionnelles et son soutien indéfectible.

CONTENTS

LIST OF FIGURES

LIST OF TABLES

Table 3.2.2.1.G. Two-sample t-test via Monte-Carlo permutation between the *P. robustus* specimens (SK 82, and SK 97), the human (n = 12) and *Pan* (n = 2) samples for the superior (S) and inferior (I) cortical thicknesses ratio (S/I) assessed from the base of neck (0) to the head-neck junction (100%). Significant differences are shown in bold.

Table 3.2.2.1.H. Bone volume fraction (BV/TV, in %) and degree of anisotropy (DA) of the volume of interest sampling the centre of the femoral head extracted following the protocol established by Ryan et al. (2018), measured using BoneJ and Quant3D and assessed in the two *P. robustus* specimens SWT1/LB-2 and SK 3121 from Swartkrans in comparison to the measurements performed by Ryan et al. (2018) shown in italic.

Table 3.2.2.2.A. Muscles of the gluteal and thigh region in extant Humans and information about their origin(s) and attachment(s) according to their principal function (Standring, 2008; Levangie and Norkin, 2005).

Table 3.2.2.3.A. Bone volume fraction (BV/TV, in %), trabecular thickness (Tb.Th., in mm), and degree of anisotropy (DA) of the volume of interest sampling the infero-lateral portion of the femoral head (hVOI) assessed in *P. robustus* from Swartkrans (SK 82, SK 97, SK 3121, SKW 19 and SWT1/LB-2), in extant Humans (n = 12; s.d., standard deviation), *Pan* (n = 2), *Gorilla* (n = 2) and *Papio* (n = 4).

Table 3.3.2.1.A. Composition of the recent human sample of patellae detailed using high resolution µXCT scanning.

Table 3.3.2.1.B. Individual data and descriptive statistics of the maximum thickness of the cortico-trabecular complex (in mm) standardised by the medio-lateral breadth of the patella (% values) measured from the articular surface in correspondence to the central (aCTT) and medial (bCTT) volumes of interest in a comparative sample of 12 recent Humans; s.d., standard deviation; min., minimum value; max., maximum value.

Table 3.3.2.1.C. Individual data and descriptive statistics of the bone volume fraction (BV/TV, in %), trabecular thickness (Tb.Th., in mm), and degree of anisotropy (DA) of the central (aVOI) and medial (bVOI) volumes of interest of the patella assessed in a comparative sample of 12 recent Humans, but excluding the outliers indicated in italics; s.d., standard deviation; min., minimum value; max., maximum value.

Table 3.3.2.1.D. Descriptive statistics of the cortico-trabecular complex standardised by the medio-lateral breadth of the patella (% values) and bone density (BV/TV in %) measured from the anterior surface in correspondence to the central (aCTT) volumes of interest in recent Humans (n = 12), a Neanderthal representative (Regourdou 1), *Pan* (n = 2) and *Papio* (n = 6); s.d., standard deviation. Note that this specific measurement is not available for SKX 1084.

Table 3.3.2.2.A. Bone volume fraction (BV/TV, in %), trabecular thickness (Tb.Th., in mm), and degree of anisotropy (DA) of the central (aVOI) and medial (bVOI) volumes of interest of the patella, assessed in a sample of recent Humans (n = 12), a Neanderthal sample consisting of Regourdou 1 and three specimens from Krapina (Pa 1, Pa 3, Pa 5), and in a *Pan* sample.

Table 3.4.1.A. Composition and degree of epiphyseal fusion of the extant human subadult sample from the R.A. Dart Collection (University of the Witwatersrand, Johannesburg) used in the comparisons with the TM 1517-labelled postcranial elements representing *P. robustus*.

Table 3.4.4.A. Dental and skeletal age estimates based on extant human and *Pan* reference models for the dental development condition shown by the right hemi-mandible TM 1517b (J. Braga, pers. comm.) and the maturation indicators of the distal humerus, proximal ulna and distal hallucial phalanx forming the TM 1517 fossil assemblage; M = male; F = female.

Table 3.4.4.B. Extant human and chimpanzee ages corresponding to the observed maturational condition of the permanent teeth of the right mandible TM 1517b (belonging to the *P. robustus* type specimen) and those of the distal humerus TM 1517g, the proximal ulna TM 1517e and the distal hallucial phalanx TM 1517k.

Table 4.A. Summary of the cortico-trabecular condition/features observed at various postcranial sites in *Australopithecus*, early *Homo* (including erectus-like), Neanderthals, extant Humans, *Pan*, *Gorilla*, and *Papio* with respect to the reference condition/features expressed in *Paranthropus robustus*. << : sensibly lower value; < : lower value; -- : sensibly less developed/expressed; - : slightly less developed/expressed; □: comparable/similar; > : higher value; >> : sensibly higher value; + : slightly more developed/expressed; ++ : sensibly more developed/expressed; ≠ : different condition; ? : uncertain condition; n.a. : not available information.

1. Introduction

1.1. *Paranthropus robustus*: A historical account

The hominin taxon *Paranthropus robustus* was established in 1938 by the paleontologist R. Broom, following the discovery of craniodental and postcranial remains at the Plio-Pleistocene cave site of Kromdraai B, situated on the southern side of the Blaauwbank stream in Gauteng, South Africa (Broom, 1938a). In comparison to the previously established taxon *Australopithecus africanus* (Dart, 1925), discovered in 1924 at Taung, North West Province, and the *A. transvaalensis* fossils discovered in 1936 at Sterkfontein (ca 2 km west of Kromdraai) and later renamed *Plesianthropus transvaalensis*, Broom noticed that the more robust cranium of TM 1517 had a shorter and flatter face, ectocranial crests, smaller canines and incisors and differently shaped premolar and molar tooth crowns (Broom, 1938a). In his study of the new fossils from Kromdraai, Broom suggested that these differences were worthy of recognition at the generic level and thus designated the specimen, TM 1517, as the holotype of *P. robustus*. At that time, the assemblage reported by Broom included the left half of a young adult calvarium (TM 1517a), an associated right mandibular corpus (TM 1517b), several isolated teeth (TM 1517c) (Broom, 1938a), as well as the distal end of a right humerus (TM 1517g), part of a proximal end of a right ulna (TM 1517e), and a manual distal phalanx from rays II to V (TM 1517o) (Broom, 1938b), all from the same matrix as the holotype skull (TM 1517a, b, c) and thus assigned to the same individual. Later on, several isolated hand and foot bones (TM 1517 h, i, j, l, m, n) and a right talus (TM 1517d) were also discovered in the same matrix and thus attributed to the same individual (Broom, 1942).

Since their initial description, the attribution of the isolated hand and foot remains and their association to the *P. robustus* holotype have been debated (Broom and Scheppers, 1946; Day, 1978; Day and Thornton, 1986; Skinner et al., 2013). At present, the postcranial elements reported as most likely associated with the individual TM 1517, include the proximal ulna (TM 1517e), the distal humerus (TM 1517g), the distal hallucial phalanx (TM 1517k) and the ulnar diaphysis (KB 5522). The latter was discovered in breccia similar to that of TM 1517 "block of matrix" (Thackeray et al., 2005). Subsequent discoveries at Kromdraai B were made during four distinct periods of field work: 1955-56, under the direction of B. Brain; 1977-80, by I. Vrba; 1993-2002, by J.F. Thackeray; and, since 2002, within the research activity of the Kromdraai Research Project co-directed by J.F. Thackeray and J. Braga (Braga et al., 2016a,

2017). Up to 2014, a total of 22 hominin specimens forms the Kromdraai fossil assemblage. This assemblage constitutes a minimum number of nine individuals representing *P. robustus*, including four juveniles, four young adults and one subadult (Thackeray et al., 2001; Braga et al., 2013, 2016a, 2017).

Following his initial discoveries at Kromdraai in 1949, Broom announced the recovery of the first fossil hominin remains (SK 2 and SK 6) at Swartkrans, another breccia-filled cave complex discovered in November 1948 in the Blaauwbank valley. Based on this new material, Broom created the new taxon *P. crassidens* (Broom, 1949). According to Broom, the reason for labelling a new species distinct from *P. robustus*, was based on in the fact that the teeth from Swartkrans were much larger than those from Kromdraai. This original distinction at specific level between *P. robustus* from Kromdraai and *P. crassidens* from Swartkrans was mostly supported at the time on the basis of features mainly affected by wear, such as the morphology and size of the mandibular deciduous first molar, the canine and the first permanent mandibular molar (Grine, 1982, 1985, 1988). The distinction between *P. crassidens* and *P. robustus* was later lowered to subspecies level by Robinson (1954) and is currently no longer in use (Wood, 2015).

In early 1949, J.T. Robinson found a mandible (SK 15), an isolated third lower premolar (P_3) (SK 18a), the buccal half of an isolated fourth premolar (P_4) (SK 43), and the proximal end of a radius (SK 18b), all presumed to be from the same individual (Broom and Robinson, 1949). Two months after these discoveries, an incomplete mandibular corpus with the right first and second molars (M_1 and M_2) (SK 45) and a palate with a lateral incisor (I_2) stump and fragmented third premolar (P_3) (SK 80) were unearthed at the same site. The SK 15 mandible and specimens SK 18a, SK 18b, SK 45 and SK 80, currently attributed to *Homo erectus*, were described as representing a human-like creature, *Telanthropus capensis* (Broom and Robinson, 1949, 1950). Since then, hominin fossils at Swartkrans assigned to *Homo* sp. have been recovered from Members 1 and 2, and some researchers have suggested that one, or more, hominin postcranial fossil(s) from Member 3 may also belong to *Homo* (Susman, 1988, 1989, 2004; Susman and Brain, 1988; Susman et al., 2001; Pickering et al., 2012). However, since species identification in the hominin fossil record commonly relies upon craniodental morphology, the taxonomic attribution of isolated postcranial remains at this site is made difficult by the presence of two hominin genera (Susman et al., 2001). The site of Swartkrans is extraordinarily rich. Over 200 hominin specimens (cranial and postcranial) representing more than 80 individuals were recovered in the first phases of excavation (Brain, 1981). In addition, over 120 additional hominin specimens belonging to more than 60 individuals have been retrieved during the

second phase (1979-1986) (Brain, 1993). On the basis of the craniodental records provided by Brain (1981, 1993), the relative abundance of *P. robustus* in the Swartkrans Members 1-3 hominin assemblage has been estimated at 96%, with the remaining 4% more likely representing the taxon *Homo* (Moggi-Cecchi et al., 2010).

Other South African sites have contributed to enlarge the *P. robustus* hypodigm. The Plio-Pleistocene site of Drimolen, located approximately 5.5 km north of Kromdraai, with its over 80 specimens recovered since its discovery by A. Keyser in 1992, is the second largest contributor after Swartkrans (Keyser et al., 2000; Moggi-Cecchi et al., 2010; Wood, 2015). Besides the number of fossils discovered, another characteristic of this site is the preservation quality of the hominin remains. In fact, Drimolen has yielded the most complete skull attributed to *P. robustus* (DNH 7) and a mandible with an almost complete dentition (DNH 8). The assemblage is mostly constituted of craniodental specimens (n = 63), among which there are 47 isolated teeth. According to the estimates provided by Keyser et al. (2000), *P. robustus* represents about 84% of the hominin fossil remains. The remaining 16% is represented by *Homo*. The large sample of dental remains of *P. robustus* indicates a considerable intraspecific variation encompassing the range of metrical and morphological variation observed in the samples from Swartkrans and Kromdraai (Keyser, 2000). This evidence would support the idea of a single species of *Paranthropus* inhabiting the region during the Plio-Pleistocene.

The sites of Cooper, situated between the caves at Sterkfontein to the west, and Kromdraai to the east, and that of Gondolin, situated 24 km northwest of Sterkfontein, have also yielded *P. robustus* remains. More specifically, in Cooper's cave, known since 1938, but systematically excavated only since 2001, seven hominin specimens have been recovered and, with the exception of that labelled COA-1, which has been assigned to *Homo* sp. (Berger et al., 1995; de Ruiter et al., 2009) and of a lumbar vertebra of an unknown early hominin (de Ruiter et al., 2009), all have been assigned to *P. robustus* (de Ruiter et al., 2009; Val et al., 2014). At Gondolin cave, discovered by MacKenzie in 1977 (MacKenzie, 1994) and then excavated by Vrba (Vrba, 1982; Watson, 1993), a possible *Homo* lower molar (GDA-1) and a large *P. robustus* M2 (GDA-2), have been recovered (Menter et al., 1999).

1.2. *Paranthropus*: Origin(s) and phylogeny

Remains of "robust" australopiths are typically attributed to one of three species which are in turn conventionally assigned to the genera *Australopithecus* or *Paranthropus*. These three species, systematically subsumed within the genus *Paranthropus* in the present study, are *P. aethiopicus*, *P. boisei* and the previously described *P. robustus*.

So far, the oldest species among the "robust" australopithecus is *P. aethiopicus* (Chamberlain and Wood, 1987), originally described as *Paraustralopithecus aethiopicus* (Arambourg and Coppens, 1968) from Ethiopia (Omo) and later on discovered at West Turkana, Kenya (Walker et al., 1986) and Laetoli, Tanzania (Harrison, 2011). This taxon covers the time span between 2.66 Ma and 2.3 Ma (rev. in Wood and Boyle, 2016). As presently interpreted, the hypodigm of this taxon includes a well-preserved adult cranium from West Turkana (KNM-WT 17000), together with mandibles (e.g., KNM-WT 16005) and isolated teeth from the Shungura Formation (Leakey and Walker, 1988). The only postcranial remain considered part of the *P. aethiopicus* hypodigm is a proximal tibia (EP 1000/98) from Laetoli, found in 1998 (Harrison, 2011). Globally, the craniodental morphology of *P. aethiopicus* resembles that of *P. boisei* (see below), but the face of the former is more prognathic, the cranial base is less flexed, the brain is perhaps smaller, the posterior attachments of the temporalis muscle are better developed, the incisors are inferred to be larger (judging from their preserved alveoli) and the postcanine teeth, especially the mandibular premolars, are less morphologically specialized (Arambourg and Coppens, 1968; Rak and Kimbel, 1991, 1993; Walker et al., 1993; Suwa et al., 1994; White and Falk, 1999; Wood and Constantino, 2007; Wood and Schroer, 2013, 2017).

First discovered at Olduvai Gorge, Tanzania, and originally labelled *Zinjanthropus boisei* (Leakey, 1959), the taxon *P. boisei* is currently known from (deposit dated around 2.3 Ma to 1.3 Ma) outcropping at Koobi Fora, Kenya (Leakey and Walker, 1988; Wood, 1991; Brown et al., 1993; Prat et al., 2003), Chesowanja, Kenya (Szalay, 1971; Howell, 1978; Gowlett et al., 1981; Wood, 1991), Omo, Ethiopia (Alemseged et al., 2002), Konso (formerly Konso Gardula), Ethiopia (Suwa et al., 1997) and likely Malema, in Malawi (Kullmer et al., 1999) (rev. in Wood and Boyle, 2016). The hypodigm, mostly consisting of craniodental remains, includes some skulls (the one from Konso being especially complete and well preserved), several well-preserved crania, and many mandibles and isolated teeth (rev. in Wood and Constantino, 2007). Conversely, except for elements from the recently discovered partial skeleton likely belonging to one individual from Level 4 BK at Olduvai Gorge (Domiguez-Rodrigo et al., 2013), there is

a lack of secure craniodental and postcranial associated remains convincingly sampling *P. boisei* (Wood and Constantino, 2007). This taxon combines a massive, wide and flat face to large-crowned premolars and molars and small-crowned anterior teeth. The attachment area of the masseter muscle on the lower aspect of the flared zygomatic arch is pronounced and the strong crests on the braincase are indicative of a hypertrophied temporalis muscle. The mandibles are also especially large and robust and the craniodental complex, as a whole, shows even more extreme adaptations to forceful mastication than does *P. robustus* (rev. in Wood and Constantino, 2007, Wood and Schroer, 2013, 2017).

As summarised in the previous section, the taxon *P. robustus* was established to accommodate the partial TM 1517 from Kromdraai. Since then, the presence of this taxon has also been shown at Swartkrans, Drimolen, Cooper, and Gondolin (see section 1.1.; rev. in Braga et al., 2016a). Most evolutionary scenarios consider that *P. robustus* did not occur prior to 2.0 Ma (Braga et al., 2016b, 2017; Wood and Boyle, 2016). In addition to the distinction between *P. robustus* and *P. boisei* convincingly made by Tobias (1967), Suwa (1988) observed that several dental and cranial features on *P. robustus* contrast to the more derived conditions displayed by the post-2.3 Ma eastern African *P. boisei* (Suwa, 1988). Even though the discoveries of megadont hominins at Konso and craniodental specimens such as KNM-ER 23000 from Koobi Fora (Brown et al., 1993), Omo 323-896, in Ethiopia (Alemseged et al., 2002) and Gondolin (Grine et al., 2012) prompted researchers to suggest that *Paranthropus* taxonomy, as a whole (e.g., Delson, 1997), should be reassessed, there is still strong evidence that *P. robustus* is distinct from *P. boisei* (Tobias, 1967; Rak, 1983; Kimbel, 2007; Wood and Constantino, 2007; Wood and Schroer, 2013, 2017; Wood and Boyle, 2016).

In this context, what are the evolutionary relationships between the representatives of this taxon from Southern and Eastern Africa? Did *P. boisei* and *P. robustus* evolve from a recent common ancestor, thus forming a monophyletic group, or did they evolve independently? (Kimbel, 2007; Wood and Constantino, 2007; Wood and Schroer, 2013, 2017). As mentioned by Wood and Constantino (2007), if the two species evolved from a recent common ancestor, as the less derived *P. robustus* is apparently more recent than the more derived *P. boisei*, this would either imply several reversals in cranial morphology or, more likely, that *P. robustus* existed prior to its current date of first appearance. Alternatively, if the two species arose independently, then it would be a case of homoplasy, with both lineages exhibiting a morphological trend towards masticatory hypertrophy and extreme postcanine megadontia that evolved separately in East and South Africa in response to similar selective pressures.

Some studies suggest that the shared craniodental morphology of the "robust" australopiths is homoplasious (e.g., Wood, 1988; Skelton and McHenry, 1992; Turner and Wood, 1993a, b; Emonet et al., 2012; Schroer and Wood, 2015) and thus, that the species should be placed within the genus *Australopithecus*. Indeed, all of the features of this "robust" australopith clade relate to adaptations for heavy mastication and appear to be functionally integrated and potentially ''non-independent''. Already at the time that previous assumptions about the morphoclines within the taxon *Paranthropus* deserved revision, the discoverers of the so-called "Black Skull" KNM-WT 17000, a specimen showing a number of highly specialised features, suggested that early hominin phylogeny was more complex than had been suggested as the fossil from Kenya proved evidence of (Walker et al., 1986). However, several studies have since provided support for *Paranthropus* monophyly and the balance of the cladistic evidence tends to support such view (e.g., Turner and Wood, 1993a; Corruccini, 1994; Strait et al., 1997, 2018; Kimbel et al., 2004; Strait and Grine, 2004; for the methodological issue, see Strait et al., 2015). Most significantly is the fact that in a cladistic analysis of hominin relationships, *Paranthropus* monophyly was supported in every instance, even when masticatory characters were excluded (Strait et al., 1997). Therefore, retention of *Paranthropus* as a distinct genus is warranted until convincing evidence demonstrates otherwise. However, even within the most parsimonious scenario of monophyly, the evolutionary relationships within the genus *Paranthropus* remain somewhat unresolved. The hypothesis of *P. aethiopicus* as a potential ancestor is most commonly accepted (Kimbel, 2007; Wood and Constantino, 2007; Wood and Schroer, 2013, 2017). Alternatively, Braga et al. (2013, 2016b, 2017) suggested that a phylogenetic model rests on the discovery of non-*aethiopicus*-like but more *P. robustus*/*P. boisei*-like hominins securely dated from between 3.0 and 2.3 Ma. In the event of the occurrence of a pre-2.3 Ma *P. robustus* Southern African form, this alternative hypothesis would entail the parallel evolution of certain 'robust' craniodental traits in the *aethiopicus* species.

1.3. *Paranthropus*: Locomotor behaviour

Plio-Pleistocene hominins display a variety of skeletal adaptations for habitual terrestrial bipedalism (e.g., Stern, 2000; Ward, 2002, 2013; Ruff et al., 2016) but some aspects of their gait kinematics remain unresolved (DeSilva et al., 2013, 2018; Ruff and Higgins, 2013; Harcourt-Smith, 2016; Hatala et al., 2016; Su and Carlson, 2017). While there is accumulating evidence that arboreal behaviour represented an important component of the early hominin locomotor repertoire, its variable nature and occurrence in the different taxa remain uncertain (Ruff, 2008a, 2009; DeSilva, 2009; Lovejoy et al., 2009; Zipfel et al., 2011; Green and Alemseged, 2012; Churchill et al., 2013; Ward, 2013; Marchi, 2015; Kappelman et al., 2016; Ruff et al., 2016; Rein et al., 2017; Kivell et al., 2018a) as well as when the manipulative transition to habitual tool manufacture occurred (Pouydebat et al., 2008; Skinner et al., 2015; Marchi et al., 2017).

The postcranial remains confidently attributed to *P. boisei* are quantitatively scarce (rev. in Domiguez-Rodrigo et al., 2013; see supra section 1.2), while the hypodigm of *P. robustus* is more representative. However, given the nature of the South African cave deposits and the most frequent dynamics of accumulation of the remains (Brain, 1981, Vrba, 1981; Braga and Thackeray, 2016), it should be noted that a number of postcranial specimens have been attributed to *P. robustus* not only on comparative anatomical ground, but also because of the contextual absence of remains unambiguously representing early *Homo*, or by default (see supra section 1.1). Within the postcranial assemblage attributed to *P. robustus*, some specimens are especially suitable for providing biomechanical information on its locomotor behaviour.

Reconstruction of the gait of *Paranthropus* pattern has typically relied on external morphology. As a whole, the indicators provide unequivocal evidence that the locomotor behaviour of *Paranthropus* combined a form of terrestrial bipedality, which may have differed from that of modern Humans, with a certain degree of arboreal component, but likely to a lower extent than typical in *Australopithecus* (Day, 1969; Jolly, 1970; Leakey, 1971, 1972; Robinson, 1972; Grine, 1988; Susman and Brain, 1988; Susman, 1989; Harcourt-Smith and Aiello, 2004; Susman and de Ruiter, 2004; Gebo and Schwartz, 2006; Domiguez-Rodrigo et al., 2013).

Arborealism in *Paranthropus* has been suggested from analyses of limb proportions (McHenry, 1978), functional morphology of various forelimb elements (Lague and Jungers, 1996; Aiello et al., 1999; Patel, 2005; Gebo and Schwartz, 2006; McHenry et al., 2007) and inner ear morphology (Spoor et al., 1994). For instance, the *P. robustus* distal humerus TM 1517g, from Kromdraai, presents similarities to the *A. afarensis*' epiphyseal morphology, with

a blend of human-like, chimp-like, and unique features distinct from early *Homo* and consistent with an arboreal component (McHenry and Corruccini, 1975; Lague and Jungers, 1996; Lague, 2014). Similarly, the cross-sectional morphology of the distal humeral shaft from Tanzania OH 80-10, representing *P. boisei*, and TM 1517g humerus are distinct from the typical human morphology (Lague, 2015). However, the extent to which distal humeral diaphyseal shape responds to habitual limb use (or is phylogenetically constrained) is unclear. On this matter, Lague (2015) claimed that humeral diaphyseal shape, at least partly, relates to different patterns of force transmission through the elbow. In 1991, Grine and Susman reported that proximal and distal radial morphology in *Paranthropus* is similar to that of *A. africanus* and *A. afarensis*, and distinct from *Homo*. They noted that the overall morphology of the radius in *Paranthropus* indicates enhanced stability for the elbow joint, enhanced forearm flexion, and wrist extension capabilities compatible with a climbing function (Grine and Susman, 1991). Although *Paranthropus* was certainly not participating in specialised richochetal brachiation ("ballistic flight"), Patel (2005) showed that the *Paranthropus* proximal radius alludes to an arboreal behaviour because of a number of similitudes between *Paranthropus* and extant hylobatids whose elbow joint is adapted for both stability and suspensory behaviour. Moreover, a morphology indicating a locomotor repertoire, including arboreal locomotion, has also been described for the specimen OH 36, a *P. boisei* ulna from Olduvai Gorge (Aiello et al., 1999). Finally, another independent signal suggesting compatibility in locomotor behaviour between *P. robustus* and *A. africanus*, thus including an arboreal repertoire, comes from the CT-based pioneering study of the semi circular canal morphology performed by Spoor et al. (1994).

Evidence for terrestrial bipedalism in *Paranthropus* stems from functional morphological analyses of manual and pedal remains (Susman, 1988, 1989; Susman and Brain, 1988; Gebo, 1992), limb proportions (McHenry, 1978; Grausz et al., 1988) and morphological analyses of various hindlimb elements (e.g., Day, 1969; McHenry, 1975a, b, c, 1976). Lovejoy and co-workers (1973) argued that *Paranthropus* (and australopith) coxo-femoral morphology conformed to biomechanical patterns: “fully commensurate with erect striding as is that of modern man” (Lovejoy et al., 1973: 78). More recently, DeSilva (2009) found that the angle between the plane of the ankle joint and the long axis of the tibia of the specimen KNM-ER 1500 falls within the modern human range of variation, thus suggesting that *P. boisei* did not have an inverted ankle nor an ankle joint capable of extreme dorsiflexion. Lack of these features in the ankle of *P. boisei* would have compromised its ability to traverse arboreal substrates and climb in an ape-like manner. However, according to Susman (1989), evidence from foot remains suggests mobility and flexibility in *P. robustus*, but associated with an incompletely

adducted great toe, thus representing a compromise between the extant ape and the human condition. Accordingly, it would appear that *Paranthropus* was essentially bipedal, but had a foot that did not toe-off precisely like in modern Humans (Susman and de Ruiter, 2004). Moreover, according to Susman and Brain (1988), while the global morphology of the metatarsal SKX 5017 is compatible with a human-like foot posture and range of extension (dorsiflexion) at the hallucial metatarso-phalangeal joint, its distal articular surface indicates that a human-like toe-off mechanism was absent.

There are also divergent perspectives on the functional significance of postcranial morphological traits observed in early hominins, notably whether they constitute primitive retentions by stabilising selection, pleiotropy, or other ontogenetic mechanisms of little adaptive importance, or if they really indicate major differences in actual locomotion-related biomechanical environment (Ward, 2002, 2013; Haile-Selassie et al., 2010; Ruff et al., 2016). As noted by a number of authors, developmentally plastic traits, such as trabecular organisation and cortical bone structure should reflect, at least in part, the mechanical loading environment of the animal while it was alive, allowing for more nuanced reconstructions of its behaviour (Kivell, 2016; Ruff et al., 2016).

Some studies have addressed the issue of locomotor behaviour in *Paranthropus* specifically using phenotypically plastic traits (see infra section 1.4.1; rev. in Kivell, 2016). By using a series of calibrated radiographs, Macchiarelli et al. (1999, 2001) have comparatively described the trabecular architecture of some South African gracile and robust australopith ilia (including the *P. robustus* specimens SK 50, SK 3155 and TM 1605) and concluded that a loading regime commensurate with a bipedal gait exists in both taxa, but is somewhat different from that typical of modern Humans. The trabecular bone fabric structure at the femoral head of *P. robustus* and *A. africanus*, more similar to that of modern Humans and Pleistocene *Homo* than to the typical extant ape condition, is also consistent with a human-like form of bipedal locomotion, including a more limited range of habitual hip joint postures during gait (e.g., a more extended hip) (Ryan et al., 2018). In addition, in their recent microtomographic-based study of a large sample of proximal femora, Ryan et al. (2018) did not mention structural differences in the trabecular arrangement at the femoral head between *P. robustus* and *A. africanus*. Studies of cortical distribution at the femoral neck confirmed a bipedal gait in australopiths, but somewhat different from that typical of modern Humans. Ruff and Higgins (2013) and Ruff et al. (2016) showed that, especially at mid-neck, australopiths (including the two *Paranthropus* specimens SK 82 and SK 97) have relatively less asymmetric superior and inferior neck cortices than modern Humans, while they are closer to modern Humans than non-

human hominoids at the base of the neck (Ruff and Higgins, 2013). The authors thus concluded that, while clearly adapted for terrestrial bipedality, australopiths likely experienced a greater lateral displacement of the body centre of gravity over the stance limb during the support phase of gait, which in turn resulted in a slightly altered gait kinematics compared to *Homo* (Ruff and Higgins, 2013; Ruff et al., 2016). A comparative analysis of the CT-based cross-sectional geometry of the proximal diaphysis of the femur provided the first evidence of similar biomechanical properties between South African *P. robustus* and Eastern African *P. boisei*, both different from the conditions displayed by *H. erectus* and modern Humans, respectively (Ruff et al., 1999). Accordingly, Ruff et al. (1999) concluded that such distinction between *Paranthropus* and *Homo* indicates an increased level of mechanical loading on the lower limb of the former, consistent with a slightly altered pattern of bipedal gait relative to that of fossil and extant Humans. In addition, Bleuze (2010) comparatively assessed cross-sectional geometry of the femoral midshaft and showed that all *Paranthropus* fossil femora follow the modern human-like pattern of a greater cortical area than *Pan*, but that the relationships between medio-lateral relative to antero-posterior bending strength are not significantly different among *Paranthropus*, modern Humans and *Pan*.

The trabecular organisation of the *Paranthropus*' talus has also been investigated in a biomechanical perspective, but the results are somewhat contradictory (DeSilva and Devlin, 2012; Su et al., 2013; Su and Carlson, 2017). While DeSilva and Devlin (2012) found no taxon-specific features of the cancellous network virtually divided in four regions, Su et al. (2013) suggested that the antero-medial region of the KNM-ER 1464 talus may have transmitted body weight to the midfoot in a similar manner than in extant Humans, while the lateral aspect may have been subjected to more variable loading conditions. More recently, in their comparative study of the australopith talus, Su and Carlson (2017) showed that, in strut orientation, KNM-ER 1464 and TM 1517 globally fit the human pattern in the anterior-medial subregion, while primary strut orientation in this region in *A. africanus* (e.g., StW 486) is ape-like. The authors concluded that, while *Paranthropus* may have had a human-like medial weight shift during the last half of stance phase, *Australopithecus* did not (Su and Carlson, 2017).

The trabecular structural arrangement of the first metatarsal (Mt) in *P. robustus* suggests habitual bipedalism characterised by hyper dorsiflexion at the metatarsophalangeal joint (Komza et al., 2018), although the authors recently stated that it is unclear to which locomotor behaviour this was linked (Komza et al., 2018). Whilst SKX 5017 (*P. robustus*) and SK 1813 (taxonomic affiliation uncertain) show a low degree of anisotropy (DA), suggesting increased

mobility at this site, differences in their trabecular distributions imply variable locomotion modes in Plio-Pleistocene hominins (Komza et al., 2018).

As seen in *A. africanus* and *H. habilis*, the diaphysis of the fifth metatarsal in *P. robustus* also shows a human-like dorsoplantar reinforcement for resisting dorsoplantar loading, but enhanced through cortical thickening rather than by increasing dorsoplantar external dimensions, as seen in Humans (Dowdeswell et al., 2016). In this respect, *P. robustus*, *H. habilis* and *H. naledi* do not exhibit the human-like distal tapering in cortical thickness of the Mt5s observed also in *A. africanus* and *H. erectus*. The authors thus concluded that selective pressures on metatarsal structure experienced by these hominins likely differed from those experienced by extant Humans (Dowdeswell et al., 2016).

Because of the potential amount of valuable biomechanical information recorded at endostructural bony level and the significant technological advances now allowing the subtle virtual extraction of such information at high resolution and with no risk for the integrity of the fossil specimens (e.g., Macchiarelli and Weniger, 2011; Weber, 2015), an increasing number of studies are expanding the functionally-related evidence extracted from fossil hominin remains and extant hominid taxa. However, given the variety of adaptations for habitual terrestrial bipedalism and degree of arboreality displayed by early hominins (e.g., Stern, 2000; Ward, 2002, 2013; Ruff et al., 2016), biomechanical studies combining the topographic analysis of cortical bone distribution with the structural signal from the cancellous network assessed at different sites of the axial and appendicular skeleton are still rare, especially in *Paranthropus*.

1.4. Aims of the research project

Differential taxonomic diagnosis in the hominin fossil record is primarily based on the critical comparative assessment of craniodental anatomy and morphological variation performed by taking into account the evidence from a number of extant and extinct taxa (e.g., Grine et al., 1996; Wood and Lieberman, 2001; Scott and Lockwood, 2004; Strait and Grine, 2004; Braga et al., 2013; Wood and Boyle, 2016). Therefore, the rarity of unambiguously associated craniodental and postcranial remains complicates the already implicitly difficult task of identifying and confidently allocating isolated fragmentary elements sampling the axial and the appendicular skeleton (e.g., Susman et al., 2001; Wood and Constantino, 2007; Dominguez-Rodrigo et al., 2013; Hlusko et al., 2015; Lague, 2015; Wood and Boyle, 2016). With special reference to the taxon *Paranthropus*, as yet, there is only one well-authenticated *P. boisei* partial skeleton from Olduvai Gorge, Tanzania, which preserves a humerus, a radius, a femur and a tibia, collectively labelled as OH 80 (Dominguez-Rodrigo et al., 2013). Not surprisingly, given the specific geo-environmental and taphonomic context of the fossil-bearing South African caves, only one *P. robustus* partial skeleton, constituting the assemblage TM 1517 and attributed to the TM 1517a, b, c craniodental holotype from Kromdraai (Broom, 1938a), has been identified so far (Broom, 1938b). As a whole, it is supposed to include a distal humerus, a humeral diaphysis, a proximal ulna, a distal hallucial phalanx and possibly a talus (Broom, 1938b, 1942, 1943; Thackeray et al., 2001, 2005).

Our ability to assign isolated postcranial elements to the taxon *Paranthropus* is especially impaired by its chronological overlap with early human taxa in the Eastern and Southern African deposits and also because of a number of similarities in their axial and appendicular skeletal features (McHenry, 1975b; Susman and Brain, 1988; Grine and Susman, 1991; Keyser et al., 2000; Susman et al., 2001; Susman and de Ruiter, 2004; McHenry et al., 2007; Moggi-Cecchi et al., 2010; Lague, 2015; Braga et al., 2016b). In addition, with special reference to the South African cave context, following the recent discovery at Malapa of well-preserved remains of a new, approximately 2 Ma old australopith species, *A. sediba* (Berger et al., 2010), and because of the still open question of the distinctive features characterising "early *Homo*" and *Paranthropus* (Broom, 1949, 1952; Broom and Robinson, 1949; Robinson, 1954; Clarke and Howell, 1972; Grine, 1982, 1985, 1988, 2005; Schwartz and Tattersall, 2003; Curnoe, 2010; Braga et al., 2016b), Late Pliocene-Early Pleistocene hominin taxonomic diversity is revealing more complex than previously assumed (rev. in Wood and Boyle, 2016). In the light of the

currently expanding evidence, reconsideration of some attributions and the list of specimens within the hypodigm is thus required.

Because of uncertainties concerning the identity of some specimens collected from the South African fossil hominin-bearing cave deposits, different palaeobiologically (including functionally) related aspects of the *P. robustus* postcranial skeleton remain poorly known or are of uncertain meanings (for instance, the degree of sexual dimorphism). The matter of the locomotor behaviour in this taxon is also still controversial (e.g., Robinson, 1972; Lovejoy et al., 1973; Susman and Brain, 1988; Grine and Susman, 1991; Lague and Jungers, 1996; Susman and de Ruiter, 2004; Patel, 2005; Ruff and Higgins, 2013; Wood and Schroer, 2013; Lague, 2014; Ruff et al., 2016).

Recent advances in primate bone biology show that, besides the influence of a number of biological factors on skeletal morphology, and the imprint of a strong genetic component in the resulting evolutionary adaptive skeletal bauplan, the local arrangement of cortical and trabecular tissues is intimately related to the biomechanical environment. This evidence is based on the now well-documented ability of bone to adjust, as mechanosensitive tissue, to its loading environment nearly all along life (rev. in Kivell, 2016; see section 1.4.1). While some questions concerning the nature of the functional relationships between the "container" (the cortical shell) and the "contents" (the inner structural organisation) remain a matter of research, the assessment of bone morphometric properties in selected regions of the postcranial skeleton allows the comparative reconstruction of habitual functionally-related loads, even in extinct taxa. Nonetheless, the extraction of this endostructural signature from the fossil record is limited by the need of assuring the integrity of the specimens, as well as by the usual "noise depth" resulting from the impact of taphonomic dynamics. However, a significant progress in the non-invasive analytical and imaging techniques and elaboration methods, grant by now, the safe virtual exploration and fine characterisation of the inner features of mineralised tissue, including in fossil specimens. These non-invasive techniques allow for the identification, modelling and "easy" sharing (simply impossible even a few years ago) of relevant information useful for comparatively assessing the morphostructural skeletal changes in an adaptive, evolutionary perspective (e.g., Mazurier et al., 2006; Sutton, 2008; Clément and Geffard-Kuriyama, 2010; Bayle et al., 2011; Sanchez et al., 2012; Cunningham et al., 2014; Le Cabec et al., 2015; Weber, 2015; Braga, 2016; Ryan and Sukhdeo, 2016; Davies et al., 2017; Schillinger et al., 2018).

In this research project we explored, extracted and assessed the endostructural conformation patterns at different joint sites of the postcranial skeleton on a number of

specimens commonly, or tentatively, attributed to *P. robustus*, by means of high resolution X-ray micro-tomography and advanced techniques of virtual imaging, coupled with two- and three-dimensional quantitative analyses. We specifically finely characterised, in detail, the patterns of distribution and topographic thickness variation of the cortical shell and the site-specific textural properties of the cancellous network at the distal humerus, the proximal ulna, the ilium, the proximal femur, the patella, and the distal hallucial phalanx. On a comparative ground, we aimed at (i) identifying some endostructural bony features characteristic of *P. robustus*, if any, thus tentatively providing a reference framework for the attribution of isolated fossil specimens from commingled assemblages; (ii) deconstructing the biomechanical (loading) environment that shaped the cortical and cancellous bone arrangement at the elbow, the hip, and the knee joints; (iii) assessing variation and, whenever possible, sex- and age-related differences in this taxon.

A preliminary account of the goals and research strategies of this project has been presented and discussed in occasion of the 1843èmes journées de la *Société d'Anthropologie de Paris* (Poitiers, 24-26/1/2018): Cazenave M. - Caractéristiques endostructurales du squelette postcrânien de *Paranthropus robustus*. Implications taxinomiques, fonctionnelles et paléobiologiques. *Bulletins et Mémoires de la Société d'Anthropologie de Paris* 30: S13 (https://bmsap.revuesonline.com/articles/lvbmsap/abs/2018/01/lvbmsap201830S1pS9/lvbmsap201830S1pS9.html).

1.4.1. Bone: An endostructural perspective

There is a general consensus that, besides the role played by the genetic component during individual development and growth in determining the essential of the evolutionary adaptive bauplan of the skeletal system, which follows a taxon-specific pattern (e.g., Lovejoy et al., 1999), and the influence exerted on bone by a variable number of biological factors (e.g., metabolism, heath status, age, etc.), within the limits determined by a variety of functional and rheological constraints, cortical and trabecular tissues constantly interact with the local biomechanical environment. Bone remodels nearly all along life to adjust structurally to the external and internal loads, by partial alteration of their shape, mass and microstructure (Huiskes, 2000; Layon and Skerry, 2001; Lieberman et al., 2003, 2004; Pearson and Lieberman, 2004; Mittra et al., 2005; Ruff et al., 2006; Skerry, 2008; Barak et al., 2011; Gosman et al., 2011; Raichlen et al., 2015; Barak and Black, 2017; Agostini et al., 2018; for a review, see Kivell, 2016). Indeed, as cortical thickness distribution and cancellous network organisation

(textural properties) tend to reflect, locally, the nature, direction, frequency, and magnitude of such loads, measures of topographic variation of the cortical shell and of trabecular thickness, volume, fabric and textural anisotropy, represent proxies for tentatively deciphering the taxon-specific dynamic relationships between individuals and their biomechanical environments.

Loadings engender stresses, which in turn cause strains (Martin and Burr, 1989; Rubin et al., 1990; Turner, 1998). These basic mechanical stimuli determine bone adaptive responses of bone through mechanotransduction (i.e., the mechanisms guiding the responses of bone cells to loading) which operates at a cellular level via modelling and remodelling phenomena (e.g., Martin et al., 1998; Currey, 2002; Lieberman et al., 2003; Ruimerman et al., 2005; Ruff et al., 2006; Bonewald and Johnson, 2008; Gosman et al., 2011).

Three types of bone cells are involved in the formation and maintenance of bone tissues: osteoblasts, osteocytes and osteoclasts. Osteoblasts synthesise bone material. They are concentrated near the periosteum and produce an organic matrix rich in collagen. Osteoblasts are gradually surrounded by newly formed matrix and become osteocytes. Osteocytes are found in cavities within the matrix situated between the lamellae. Some molecular exchanges between osteocytes and blood vessels take place through the small amount of extracellular substance located between the osteocytes and the matrix. Finally, osteoclasts, as multinucleated giant cells, are involved in bone resorption and remodelling (Martin et al., 1998; rev. in Jilka, 2003).

Once a strain is produced, bone cells react in one of the following four ways: (i) If the magnitude of the strain is not sufficient, or if there are physiological disruptions, there might be no cellular response (Frost, 1987, 1988; Turner, 1998; Bikle et al., 1995; Skerry, 2000; Schoenau, 2005); (ii) Osteoblasts synthetise bone tissue (i.e., modelling) in response to a relatively important strain (Rubin et al., 1990; Turner and Pavalko, 1998; Currey, 2003); (iii) Osteoclasts resorb bone tissue under low load conditions (Turner and Pavalko, 1998; Bikle and Halloran, 1999; Frost, 1999); (iv) Bone tissue is remodelled, a process accomplished by the assemblage of osteoclasts and osteoblasts into discrete temporary anatomic structures called basic multicellular units (BMUs), where osteoclasts move to resorb the surface of the bone which is thus again deposited by the osteoblasts (Martin and Burr, 1989; Rubin et al., 1990; Frost, 1999; Currey, 2002, 2003; Jilka, 2003).

Mechanotransduction is a multistep process which implies the conversion of mechanical forces into local mechanical signals that, in turn, initiate a direct response from bone cells. This response is followed by the transduction of the mechanical signal into a biochemical response and a cell-to-cell signalling, which involves communication from sensor cells (probably osteocytes) to effector cells (osteoblasts or osteoclasts) (Turner and Pavalko, 1998). This

communication probably acts within a larger complex system called the "mechanostat", a term coined by H.M. Frost, which describes the mechanism that monitors bone metabolism (i.e., longitudinal growth, bone modelling and remodelling activities) in relation to mechanical usage (Frost, 1987, 1998, 2003; Turner, 1998; Schoenau, 2005). The physiological procedure of cell activation to loading is still unclear, although many studies have shown that the key mechanism relies on osteocyte-osteoblast communication (Rubin et al., 1990; Cowin et al., 1991; Marotti et al., 1992; Mikuni-Takagaki, 1999; Cullinane and Einhorn, 2002; Bonewald and Johnson, 2008).

Variation in both cortical and trabecular bone formation is valuable when assessing the individual-environmental dynamic interactions (Kivell, 2016). Trabecular or cancellous bone is a light and porous bone enclosing large spaces that give a honeycombed or spongy-like appearance. The bone matrix is composed of rods (i.e., trabeculae) and plates (Martin et al., 1998; Macho et al., 2005; Buie et al., 2007; Volpato, 2007). Trabecular bone formation and maintenance throughout ontogeny are influenced by a number of factors, such as the underlying genetic patterning (Cunningham and Black, 2009a, b), vascular patterning and the positioning of growth plates (Cunningham and Black, 2010), changes in hormone levels (Simkin et al., 1987; Karlsson et al., 2001; Yeni et al., 2011) and variation in cellular processes and constraints on bone design (Lieberman, 1997). In this early phase, bone is both actively modelled and remodelled and is considered to be more responsive to mechanical stimuli than adult bone (Pearson and Lieberman, 2004). However, mechanics may also have a lasting effect on trabecular structure later in life, even in nearly inactive adults (Pettersson et al., 2010; but see Karlsson et al., 2000).

The concept that the basic genetic blueprint of the trabecular structure - for which the general functional role is to provide strength and transfer external loads away from the joint and towards cortical bone (Currey, 2002; Barak et al., 2008) - can be subsequently changed by variation in load and/or habitual individual activities (rev. in Kivell, 2016), has received support from a variety of studies developed at different scales and by different analytical techniques. These include: (i) in vivo experimental studies testing directly functional adaptation of trabecular bone (e.g., Biewener et al., 1996; Guldberg et al., 1997; Mittra et al., 2005; Pontzer et al., 2006; Chang et al., 2008; Polk et al., 2008; Barak et al., 2011; Harrison et al., 2011); (ii) computational studies testing the maintenance of a particular trabecular structure adapted for the biomechanical load experienced (e.g., Levenston et al., 1994; Huiskes et al., 2000; Fox and Keaveny, 2001; Keaveny et al., 2001; Gupta et al., 2007); (iii) finite element (FE) modelling quantifying and validating the mechanical properties and functional significance of trabecular

bone (e.g., Hollister et al., 1994; van Rietbergen et al., 1995, 1999; Kabel et al., 1999; Ulrich et al., 1999; Homminga et al., 2004; Ryan and van Rietbergen, 2005; Nguyen et al., 2013, 2014); (iv) comparative populational and intertaxic functional analyses, essentially using primates, on cancellous bone organisation at different skeletal sites and joints (e.g., Fajardo and Müller, 2001; Ryan and Ketcham, 2002a, 2005; Volpato, 2007; Ryan and Shaw, 2012, 2015; Scherf et al., 2013; Tsegai et al., 2013; Matarazzo, 2015; Barak et al., 2017; Tsegai et al., 2017).

The trabecular bone volume fraction (BV/TV, in %; sometimes also referred to as "density") and its degree of alignment (i.e., anisotropy) are considered as the most biomechanically informative features of the trabecular architecture (Goldstein et al., 1993; Odgaard et al., 1997; van Rietbergen et al., 1998; Stauber et al., 2006; Maquer et al., 2015). Qualitative and/or quantitative variation (textural properties) is used in an increasing number of studies relying on cancellous network to reconstruct the postural, locomotor and behavioural modes of extinct hominoids (e.g., Macchiarelli et al., 1999, 2001; Rook et al., 1999; Volpato, 2007; Barak et al., 2013a; Su et al., 2013; Chirchir et al., 2015; Skinner et al., 2015; Zeininger et al., 2016; Su and Carlson, 2017).

Consisting of closely packed osteons (i.e., the "Haversian systems"), cortical bone is dense and compact and forms the outer layer of bones. The physiological processes responsible for modelling and remodelling are similar in trabecular and cortical bone (Eriksen, 2010) (see above). However, compared to trabecular bone, cortical bone is less metabolically active (Huiskes et al., 2000; Jacobs, 2000; Currey, 2002) and remodels slower (2-3% in adult humans compared to 25% for the trabecular tissue; Eriksen, 1986, 2010). Despite the still incomplete understanding of cortical bone modelling/remodelling dynamics, experimental studies demonstrate that topographic variation in its morphology and thickness largely reflects biophysical (mechanical) loads (e.g., Jones et al., 1977; van der Meulen et al., 1993, 1996; Ruff et al., 1994, 2006; van der Meulen and Carter, 1995; Robling et al., 2002; Carlson and Judex, 2007; Carlson and Marchi, 2014; Christen et al., 2014). Accordingly, analyses of: (i) cross-sectional geometric properties assessed at several diaphyseal points (e.g., Ruff, 2002, 2008a, b, 2009; Carlson, 2005; Marchi, 2005; Sarringhaus et al., 2005; Carlson et al., 2006, 2008; Trinkaus and Ruff, 2012; Volpato et al., 2012; Ruff and Higgins, 2013; Shaw and Stock, 2013; Davies and Stock, 2014; Ruff et al., 2015; rev. in Carlson and Marchi, 2014); (ii) site-specific cortical thickness topographic variation (e.g., Bondioli et al., 2010; Morimoto et al., 2011; Puymerail, 2011, 2013; Puymerail et al., 2012; Jashashvili et al., 2015); (iii) profiles across the articular surfaces (sometimes including both cortical bone and the underlying trabecular structure) (e.g., Mazurier, 2006; Patel and Carlson, 2007; Mazurier et al., 2010; Carlson et al.,

2013) have been extensively performed to extract function-related information in both extant and fossil primate taxa.

Even though cortical and trabecular bone respond differently to strains (Carlson and Judex, 2007) - the trabecular bone changes being more localised than measured in cortical bone (Rubin et al., 2001, 2002; Judex et al., 2004; Barak et al., 2011) - the "container" (cortex) and the "contents" (cancellous network) interact in resisting and adapting bone shape to loads (Carlson and Judex, 2007; Volpato, 2007). Thus, combined information on cortical thickness topographic variation and cancellous textural arrangement provides valuable support for assessing the individual-environmental dynamic interactions (Kivell, 2016). Indeed, the primate studies that have jointly analysed both components revealed interesting compensatory effects between the two tissues (e.g., Skedros et al., 2004, 2012; Carlson and Judex, 2007; Carlson et al., 2008; Lazenby et al., 2008; Shaw and Ryan, 2012; Tsegai et al., 2017).

As previously mentioned, special care should be taken in translating any pattern of inner bony arrangement (structural signature) into a "mechanical behaviour", as there are various aspects of bone biology and functional adaptation that are not fully understood. Our knowledge is still incomplete concerning the following limiting aspects: (i) the genetic and systemic factors that shape trabecular and cortical tissues and bone as a whole (Lieberman, 1996; Carlson et al., 2008; Havill et al., 2010; Wallace et al., 2010; Paternoster et al., 2013; Tsegai et al., 2016); (ii) the relative influence of the duration, frequency, polarity and magnitude of the loads, which is extremely difficult to disentangle (e.g., Rubin and Lanyon, 1985; Frost, 1987; Skerry and Lanyon, 1995; Biewener et al., 1996; Barak et al., 2011); (iii) and how these factors might vary among the taxa (e.g., Turner, 2001) and depending on the age (e.g., Pearson and Lieberman, 2004), the body mass (e.g., Biewener, 1990; Doube et al., 2011; Barak et al., 2013b; Ryan and Shaw, 2013), and of course the anatomical region (e.g., Morgan and Keaveny, 2001; Rubin et al., 2001, 2002; Judex et al., 2004; Barak et al., 2011; Saers et al., 2016).

Finally, it is worth noting here that, ideally, functional inferences, primarily relying on the inner bony structural organisation, should also at least tentatively consider the broader context of the immediately related muscles, connective tissues and of the other stress-carrying elements (notably ligaments and tendons), i.e., the global loading environment in which bone grows and adapts, which affects bony recording sensitivity (Hall, 1985; Sinclair et al., 2013; Kivell, 2016). Of course, such information is extremely limited on extinct taxa and is commonly inferred on comparative ground (e.g., Lovejoy et al., 2002).

2. Materials

2.1. *P. robustus*

For the purposes of the present research work, the following isolated postcranial remains, commonly allocated to the taxon *P. robustus*, were examined: four distal humeri TM 1517g, SK 24600, SKX 10924 and SKX 34805, five proximal femoral ends SK 82, SK 97, SK 3121, SKW 19 and SWT1/LB-2, as well as the patella SKX 1084. We also investigated the proximal end of the right ulna TM 1517e and the distal hallucial phalanx TM 1517k, in order to verify the suggestion that TM 1517 represents a partial skeleton of a single late adolescent-young adult individual (Broom, 1938b, 1942, 1943; Thackeray et al., 2001, 2005; Braga et al., 2013, 2016a, b; Skinner et al., 2013). Finally, in the perspective of extracting and characterising the cortical and cancellous organisation of the australopith coxo-femoral complex as a functional unit in three-dimensions, we also scanned and preliminary examined the ilia TM 1605 and SK 50, both attributed to *P. robustus*.

2.1.1. The Kromdraai site

The Plio-Pleistocene site of Kromdraai is situated 50 km northwest of Johannesburg and approximately 2 km east of the Sterkfontein Cave, on the southern side of the Blaauwbank stream (Braga et al., 2016a). It has long been considered as two distinct localities: Kromdraai A (KA) and Kromdraai B (KB). The KA locality, younger than KB according to biochronological interpretations, is situated about 30 m to the west of KB and provided faunal remains and some stone tools, but no fossil hominins (Brain, 1975; Vrba, 1981; Kuman et al., 1997). The KB locality yielded the type specimen of *P. robustus* (TM 1517) (Broom, 1938a, b, 1942, 1943) and a rich assemblage of other fossil hominin remains discovered from 1938 to 2014 (Thackeray et al., 2001; Braga and Thackeray, 2003; Braga et al., 2013). This assemblage includes at least one specimen attributed to early *Homo* (Braga and Thackeray, 2003; Braga et al., 2016a; but see Grine et al., 2009), while all remaining fossil hominins represent the taxon *P. robustus* (Broom, 1938a, b; Vrba, 1981; Thackeray et al., 2001; Braga et al., 2016a), with a few (i.e., specimens found in situ Member 3) possibly corresponding to a primitive form of this lineage (Braga et al., 2013, 2016b).

The first detailed stratigraphic analysis of the site was produced in 1977, during the excavation work performed by Vrba (1981). Since then, the stratigraphy has been refined by Partridge in 1982, who identified five successive members with a geometry corresponding to a talus formed at the base of a single entrance located about 10 m above the current landscape (Partridge, 1982; Vrba and Panagos, 1982). Towards the western side, a split in the stratigraphic sequence has been recorded, with only Members 1 to 3 being found in this area. Member 1 consists of a dark stony breccia corresponding to that originally identified by Brain (1958) and which represents most of the cavity infill. This member yielded only microfauna and two baboon teeth (Vrba and Panagos, 1982). The upper surface of this member corresponds to an erosional truncation. Member 2 lies on Member 1 (Partridge, 1982). No fossils have been discovered in this stratigraphic unit. Resting on Member 2, Member 3 is a fine-grained breccia. The infill of Member 3 yielded the main assemblage of fossil vertebrates discovered during Vrba's (1981) excavations. According to Vrba (1981), most of the hominin remains found at this site, including those discovered by R. Broom, come from this breccia. Member 4 is a stony breccia, including blocks of chert and dolomite. Micro- and macrofauna were discovered in this unit. Finally, Member 5, made up of silts covering abundant broken stones and blocks, represents the last phase of sedimentary deposit.

Based on the evidence accumulated during the past years of excavations, a revised stratigraphic interpretation of KB has recently been proposed (Bruxelles et al., 2016). Accordingly, the breccia accumulation has been divided into four main phases: Member 1; Members 2, 3 and 4; Members 5 and 6; and Member 7. In the updated stratigraphy, Members 1 and 2, defined by Partridge (1982), have been maintained. Conversely, the previous Member 3 has been divided into Member 3 and Submember 4.1, while the Members 4 and 5 correspond to Submembers 4.2 and 4.3 respectively. Finally, the previous Members 1, 2 and 3 of the KB West formation have been relabelled as Member 5, 6 and 7, respectively. The type specimen TM 1517 is from the so-called “holotype block”, which was identified as a conglomerate of breccias from Members 5 and 6.

So far, attempts to obtain absolute dates for the site provided varying results. Paleomagnetistic analyses provided an age between 2.0 and 1.77 Ma for KB (Thackeray et al., 2002). However, this magnetostratigraphic record was later reinterpreted by Herries et al. (2009) and the deposits estimated to be slightly younger, between 1.8 and 1.6 Ma. Nonetheless, on the basis of biochronological arguments (McKee et al., 1995; Heaton, 2006; Pickford, 2013), the oldest KB fossil assemblage could be about 2.6 Ma old. In support of this view, it has been suggested that some of the KB hominin specimens from the chronostratigraphic period between

Sterkfontein Member 4 and Swartkrans Member 1, might represent a more primitive, thus slightly older form of *P. robustus*, compared to the remains representing this taxon from other South African sites (Grine, 1988; Tobias, 1988; Kaszycka, 2002; Kuman and Clarke, 2000; Braga et al., 2013).

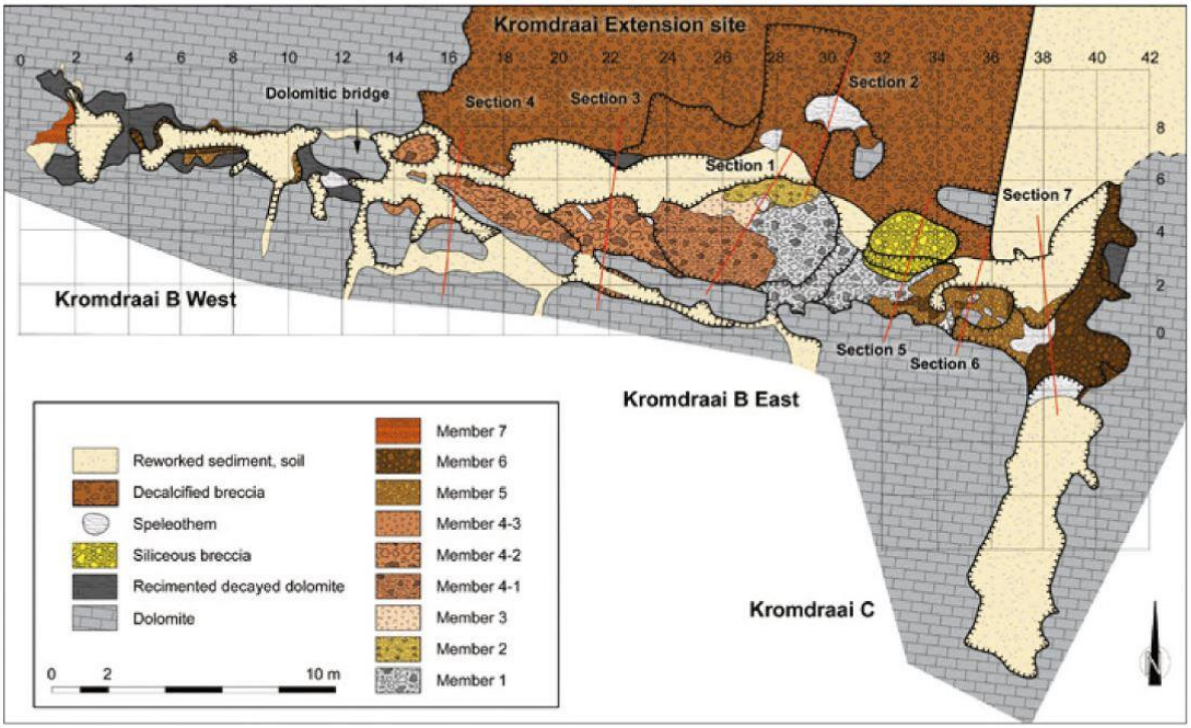

Fig. 2.1.1.A. Map of Kromdraai B formation (from Bruxelles et al., 2016).

2.1.2. The Swartkrans site

Swartkrans, situated on the northern side of the Blaauwbank Valley, has delivered rich fossil finds. With some 29 fossil remains assigned to early *Homo*, it represents the site that delivered the largest sample of *P. robustus* (about 400 specimens) (Brain, 1981, 1993; Grine et al., 1996; de Ruiter, 2001; Moggi-Cecchi et al., 2010; Pickering et al., 2012), and the first South African site providing unambiguous evidence for the co-occurrence of multiple hominin taxa (Broom and Robinson, 1950).

Most of its original roof has been removed by erosion, thus exposing the fossil bearing sediments on the surface. Excavations at Swartkrans began in the late 1940s under the supervision of R. Broom and J.T. Robinson (Brain, 1981). The stratigraphy is complex, with evidence of several cycles of deposition and erosion (Brain, 1993). Brain (1993) recognised

five remaining members incorporating six discrete fossiliferous deposits. Member 4, commonly referred as the Middle-Late Pleistocene because of distribution of Middle Stone Age artefacts (Brain, 1993) and Member 5, dated to around 12.000-9.000 years (Brain, 1993; Watson, 1993; Sutton et al., 2009) do not appear to contain hominin fossil remains. The fossil hominin specimens investigated in this research project are from Members 1, 2 and 3.

Member 1 (formerly *pink breccia*; Brain, 1958) contains two depositional subunits, the Lower Bank (LB) and the Hanging Remnant (HR), which are, respectively, the oldest and second oldest preserved deposits of the formation. Taking into consideration various dating methods, the most accurate dating of Member 1 is between 2.31 and 1.64 Ma. This estimation was based (i) on the cosmogenic nuclide burial dating method applied by Gibbon and co-authors (2014), (ii) on the dating results of the flowstone layers under- and overlying the Member 1 deposits sampled at two locations by Pickering and co-workers (2011) and (iii), also taking into account the previous results provided by Curnoe et al. (2001) and Balter et al. (2008) and discussed by Herries et al. (2009).

Dating of the Member 2 breccia block was more problematic. However, based on U-Pb dates provided by Balter et al. (2008; see also Herries et al., 2009; Gibbon et al., 2014), this unit should range between 1.36 and 1.1 Ma, a chronology which is compatible with the biochronological estimates assessed by Vrba (1975) and by Delson (1988) on the basis of the primate and bovid fossil assemblages, both relatively abundant in the hominin-bearing units of this cave site.

Member 3 yielded some stone artefacts (Leakey, 1970), as well as evidence of bone technology and controlled use of fire (Brain, 1993). Based on geomorphological criteria and on biochronology, the age of Member 3 has initially been estimated around 1.0 Ma (Brain, 1993), but since refined by U-Pb (0.83 ± 0.21 Ma; Balter et al., 2008) and ESR dating methods (1.04-0.61 Ma; Curnoe et al., 2001). The most recent chronological assessment using the cosmogenic nuclide burial dating indicate an age of 0.96 ± 0.09 Ma (Gibbon et al., 2014).

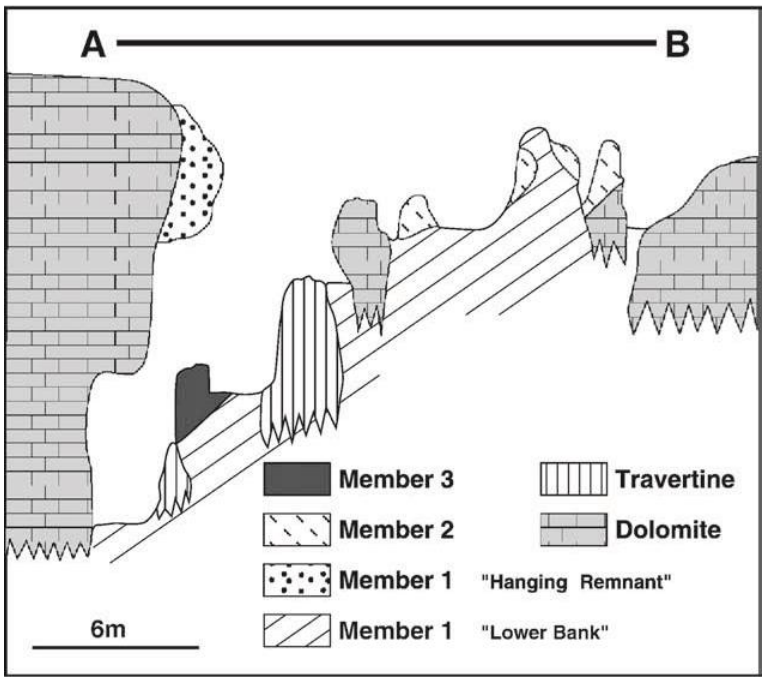

Fig. 2.1.2.A. Cross section of the Swartkrans deposits (from Balter et al., 2008).

2.1.3. Summarised description of the P. robustus *specimens*

TM 1517g (Fig. 2.1.3.A), originally reported by Broom (1938b) and later detailed by Straus (1948), is an incomplete but well-preserved right distal humerus from Kromdraai B, found in association with the proximal ulna (TM 1517e) in the so-called "holotype block" (Braga et al., 2016b; Bruxelles et al., 2016). Within the *P. robustus* assemblage, the partial humerus, TM 1517g, has been commonly used as a reference specimen for taxonomic purposes (Straus, 1948; Senut, 1981a; Susman, 1989; Lague and Jungers, 1996; Susman et al., 2001; McHenry and Brown, 2008; Churchill et al., 2013; Lague, 2014, 2015; Di Vincenzo et al., 2015; Ryan and Sukhdeo, 2016). TM 1517g is housed at the Ditsong National Museum of Natural History, Pretoria. While incomplete, these two specimens fit so well that there is little doubt they belonged to the same right upper limb, likely from the same individual represented by the type skull TM 1517 (Robinson, 1972; Thackeray et al., 2001; Skinner et al., 2013; Braga et al., 2017). The distal humeral specimen has a maximum length of 56.7 mm and presents the entire distal articular epiphysis with a 20.0 mm long and 23.0 mm deep trochlea and a biepicondylar width of 54.0 mm. At the most distal part of the shaft, it has a medio-lateral diameter of 31.0 mm and an antero-posterior thickness of 13.0 mm (Straus, 1948). While its outer surface is rather well preserved, the anterior aspect of the capitulum lacks a bony flake. A crack runs

supero-inferiorly through the capitulum and the lateral epicondyle, while another more oblique crack cuts the most medial aspect of the trochlea to the superior end of the medial epicondyle. In general, the specimen does not show evidence for subaerial weathering alteration (stage 0; Behrensmeyer, 1978) apart from slightly on the lateral facet (stage 1; Behrensmeyer, 1978). A generalised manganese dioxide coating is present with only a few bare dots on the lateral aspect (stage 1; Val and Stratford, 2015), while other spots obscure previous bone surface modifications on the trochlea and capitulum (stage 4; Val and Stratford, 2015). As in TM 1517e, bore holes, likely representing insect damage, are visible on the posterior surface of the lateral epicondyle. Within the *P. robustus* assemblage, this partial humerus has been commonly used as a reference specimen for taxonomic purposes (Straus, 1948; Senut, 1981a; Susman, 1989; Lague and Jungers, 1996; Susman et al., 2001; McHenry and Brown, 2008; Churchill et al., 2013; Lague, 2014, 2015; Di Vincenzo et al., 2015; Ryan and Sukhdeo, 2016).

Fig. 2.1.3.A. Anterior (A) and posterior (B) views of the right humerus TM 1517g from Kromdraai.

SKX 10924 (Fig. 2.1.3.B) is a 58.5 mm long distal left humeral end from Swartkrans Member 3, first described by Susman et al. (2001). It is housed at the Evolutionary Studies Institute of the University of the Witwatersrand, Johannesburg. Based on comparisons with SKX 34805 (Susman, 1989), and notably because of its "rounded" cross section, this specimen

was originally allocated to *Homo*, but an attribution to *Paranthropus* has been more recently proposed (McHenry and Brown, 2008) and then supported by GM analyses (Lague, 2014, 2015). The shaft retains only 37 mm of bone proximal to the biepicondylar axis (43.8 mm). The trochlea (15.0 mm on its anterior surface) and the capitulum (13.8 mm wide) are preserved. On its outer shaft surface, longitudinal cracks run on the anterior and posterior surfaces ending in a ‘‘Y’’ shape, with one limb heading to the medial pillar and the other toward the lateral pillar. The specimen has suffered some post-mortem damage visible on its posterior surface. Small chunks of bone are also absent at the level of the medial epicondyle and on the lateral edge of the trochlea. However, there is no evidence of subaerial weathering alteration (stages 0 to 1; Behrensmeyer, 1978). The specimen is heavily stained with manganese dioxide (stage 4; Val and Stratford, 2015). While it lacks tooth marks such as scores, pits and punctures, insect damage is found on its posterior surface. Among its morphological characteristics useful for taxonomic assessment, the following should be recalled: the lateral epicondyle does not rise prominently above or proximal to the supero-medial edge of the capitulum; the articular features are not sharply defined; the capitulum is positioned on the anterior surface; the zona conoidea, between the trochlea and the capitulum, is indistinct; the central sulcus of the trochlea is not deeply grooved; the supracondylar ridge is evident, but not pronounced; the olecranon fossa is large, ellipsoidal and lacks a sharp crest, or edge, on its lateral wall (Susman et al., 2001; McHenry and Brown, 2008; Churchill et al., 2013; Dusseldorp et al., 2013 [in Suppl. Mat.]; Lague, 2014, 2015; Ryan and Sukhdeo, 2016).

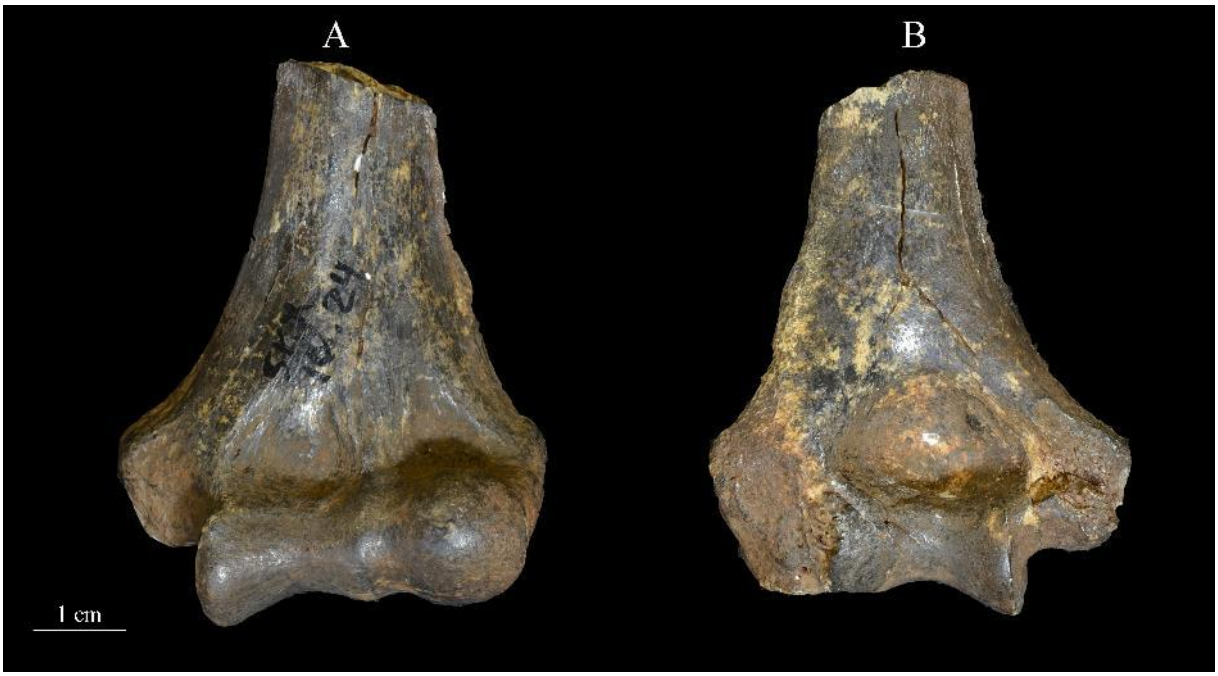

Fig. 2.1.3.B. Anterior (A) and posterior (B) views of the left humerus SKX 10924 from Swartkrans.

SK 82 (Fig. 2.1.3.C) is a proximal right femoral end recovered in 1949 from the Hanging Remnant in Member 1 of Swartkrans. It is housed at the Ditsong National Museum of Natural History, Pretoria. The specimen was attributed to *P. robustus* by Napier (1964), who firstly identified and described its non *Homo*-like morphology. Later on, in attributing the large majority (about 95%) of the taxonomically diagnostic craniodental material from Swartkrans Member 1 to *Paranthropus*, Grine (1989) provided support to Napier's original attribution. Compared to other specimens commonly considered as conspecific, SK 82 likely represents a male individual because of its femoral head size (maximum diameter: 34.4 mm) (Susman et al., 2001). Beside the head, it presents the neck (mid-neck supero-inferior diameter: 30.6 mm; mid-neck antero-posterior diameter: 20.5 mm), the trochanteric region and 137 mm of the upper shaft (Robinson, 1972). It is rather well preserved, but a fracture exists just at its head-neck junction. Close to the virtually complete fovea capitis, it lacks some cortical bone. Distally, a fracture is filled by matrix; in frontal view, a number of vertically-oriented shallow and thin cracks join the distal fracture. The greater trochanter bears some minor damage, while the lesser trochanter is nearly complete, including at the crest. The shaft portion has suffered some cracking on the posterior, lateral, and medial aspects (Robinson, 1972). Large spots of manganese dioxide are spread all over its anterior and posterior surfaces (stage 4; Val and Stratford, 2015), obscuring the traces of possible previous bone surface modifications. Compared to *H. sapiens*, SK 82 has a significantly smaller femoral head, a relatively longer neck (61 mm; Lovejoy, 1975) and antero-posteriorly compressed (or, more appropriately, supero-inferiorly expanded, relative to the femoral head breadth; Ruff and Higgins, 2013) (Robinson, 1972; Lovejoy et al., 1973; Ruff et al., 2016). The neck-shaft angle (119°; Lovejoy et al., 1973) is slightly more accute than commonly seen in *H. sapiens* (Lovejoy et al., 1973; Ruff and Higgins, 2013; Ruff et al., 2016). The lateral face of the greater trochanter bears a somewhat less protuberant appearance than is the case in *H. sapiens* (Robinson, 1972). In addition, it is projected laterally and positioned below the femoral head (Harmon, 2009). At the broken limit of the proximal shaft, SK 82 shows a thick cortex indicating an increased medio-lateral relative to antero-posterior bending strength compared to modern Humans, but not as extreme as typical in *H. erectus* (Ruff et al., 1999). Estimated body mass of this individual is 37.1-45.3 kg (Pickering et al., 2012; Ruff et al., 2018a).

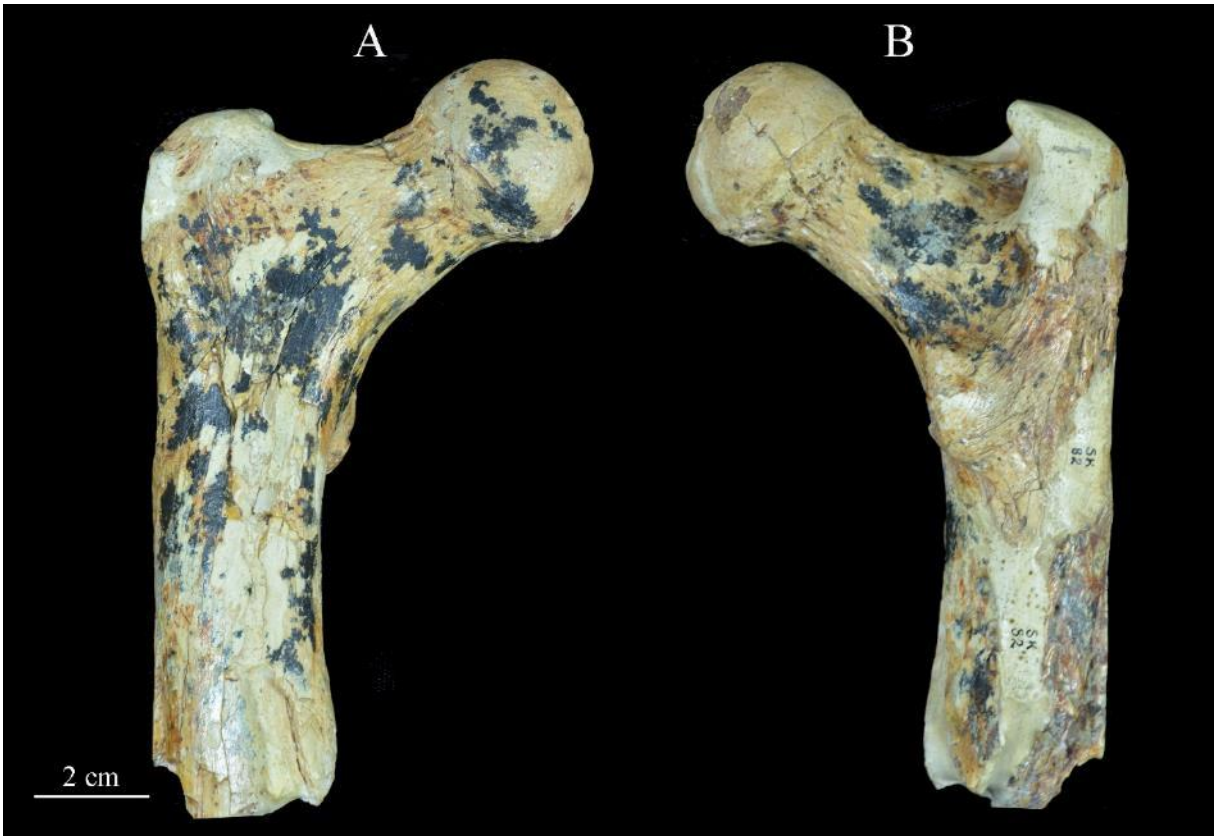

Fig. 2.1.3.C. Anterior (A) and posterior (B) views of the right proximal femoral end SK 82 from Swartkrans.

SK 97 (Fig. 2.1.3.D) is also a right proximal femoral end recovered in 1949 from the Hanging Remnant in Member 1 of Swartkrans, attributed to *P. robustus* by Napier (1964; see also Grine, 1989) and very likely representing a male individual (Susman et al., 2001). It presents the head (maximum diameter: 38.4 mm), the neck (mid-neck supero-inferior diameter: 30.9 mm; mid-neck antero-posterior diameter: 19.8 mm), the trochanteric region and 118 mm of the proximal shaft (Robinson, 1972). It is housed at the Ditsong National Museum of Natural History, Pretoria. Similar to SK 82, its head and neck are rather well preserved, even with two fractures running from the fovea capitis to the neck. A number of fine cracks are also present. There is some external damage on the greater trochanter, especially along the crest from the proximal portion down onto the quadrate tubercle. The lesser trochanter has also suffered little surface damage, as has the distal portion of the preserved shaft (Robinson, 1972). Besides the damages, the surface does not reveal weathering (stage 1; Behrensmeyer, 1978). Compared to the condition of SK 82, no spots of manganese are found on its surface. With a shaft angle of

115° and a neck length of 66 mm, SK 97 closely resembles SK 82 in morphology, proportions and cross-sectional geometry of the shaft (Robinson, 1972; Ruff et al., 1999; Ruff and Higgins, 2013). It has been noted that the morphology of the greater and lesser trochanters approach that of the modern Humans, even with some differences concerning the medial extension of the area of attachment of the gluteus minimus muscle onto the neck (Lovejoy, 1975). Estimated body mass of this individual is 43.2-53.8 kg (Pickering et al., 2012; Ruff et al., 2018a).

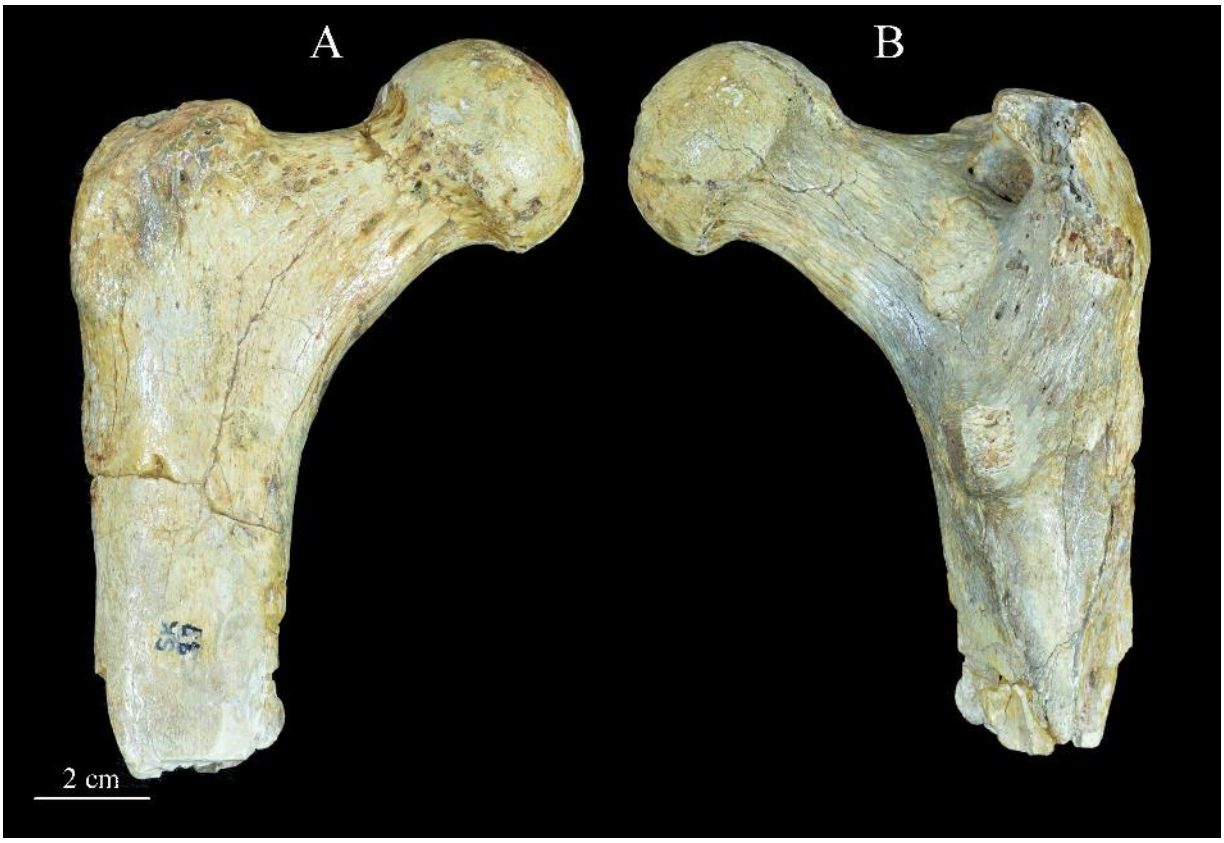

Fig. 2.1.3.D. Anterior (A) and posterior (B) views of the right proximal femoral end SK 97 from Swartkrans.

SK 3121 (Fig. 2.1.3.E) is a right proximal femoral end recovered some time before 1970 from Member 2 of Swartkrans. It is housed at the Ditsong National Museum of Natural History, Pretoria. It was originally described by Susman et al. (2001) who attributed it to *P. robustus* essentially because of the antero-posterior compression of its preserved neck portion (mid-neck supero-inferior diameter: 20.0 mm; mid-neck antero-posterior diameter: 15.7 mm), a feature also shown by SK 82 and SK 97 (Pickering et al., 2012). Within the assemblage of proximal femora attributed so far to *P. robustus*, SK 3121 displays the smallest articular end (maximum

diameter: 29.9 mm), which suggests its more likely attribution to the female sex. This specimen consists of a well preserved femoral head and a neck of about 23 mm. While incomplete, it is relatively well preserved, although the fovea capitis is filled by consolidated matrix. A horizontal crack is visible on the upper part of the most lateral region of the neck, while a vertical crack is found inferiorly. No insect damage or manganese dioxide black spots are present on the outer surface of this specimen. As opposed to SKW 19 (see below), its head-neck junction is rather smooth. Compared to SK 82 and SK 97, SK 3121 shows a more *A. africanus*-like, rounder cross-sectional shape at mid-neck level (Harmon, 2009). Estimated body mass of this individual is 24.1-30.0 kg (Pickering et al., 2012; Ruff et al., 2018a).

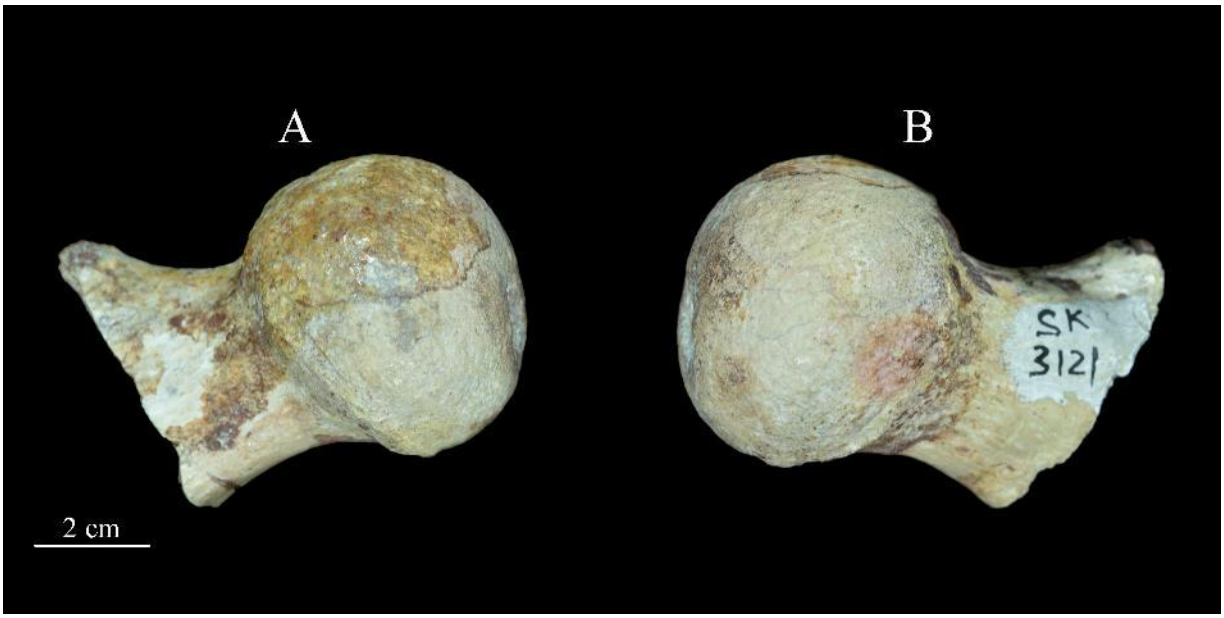

Fig. 2.1.3.E. Anterior (A) and posterior (B) views of the right proximal femoral end SK 3121 from Swartkrans.

SKW 19 (Fig. 2.1.3.F), recovered by C.K. Brain after 1970 from the Hanging Remnant in Member 1 of Swartkrans, represents a right proximal femoral end. It was first detailed by Susman et al. (2001) and attributed to *P. robustus* given its antero-posteriorly compressed neck. It is housed at the Evolutionary Studies Institute of the University of the Witwatersrand, Johannesburg. Within the *Paranthropus* sample of proximal femora available so far, SKW 19 is considered to represent a female individual because of its relatively small size (Pickering et al., 2012) (maximum head diameter: 31.9 mm). It consists of a relatively well-preserved femoral head and of a minor portion (8-10 mm long) of the neck (Susman et al., 2001). No

insect damage or manganese dioxide black spots are present on its surface. The fovea capitis is large, but relatively shallow, with a prominent rim. The head-neck junction is particularly marked, likely because of the recent fusion of the articular end, indicating that this specimen represents a young adult individual. Estimated body mass of this individual is 27.7-35.3 kg (Pickering et al., 2012; Ruff et al., 2018a).

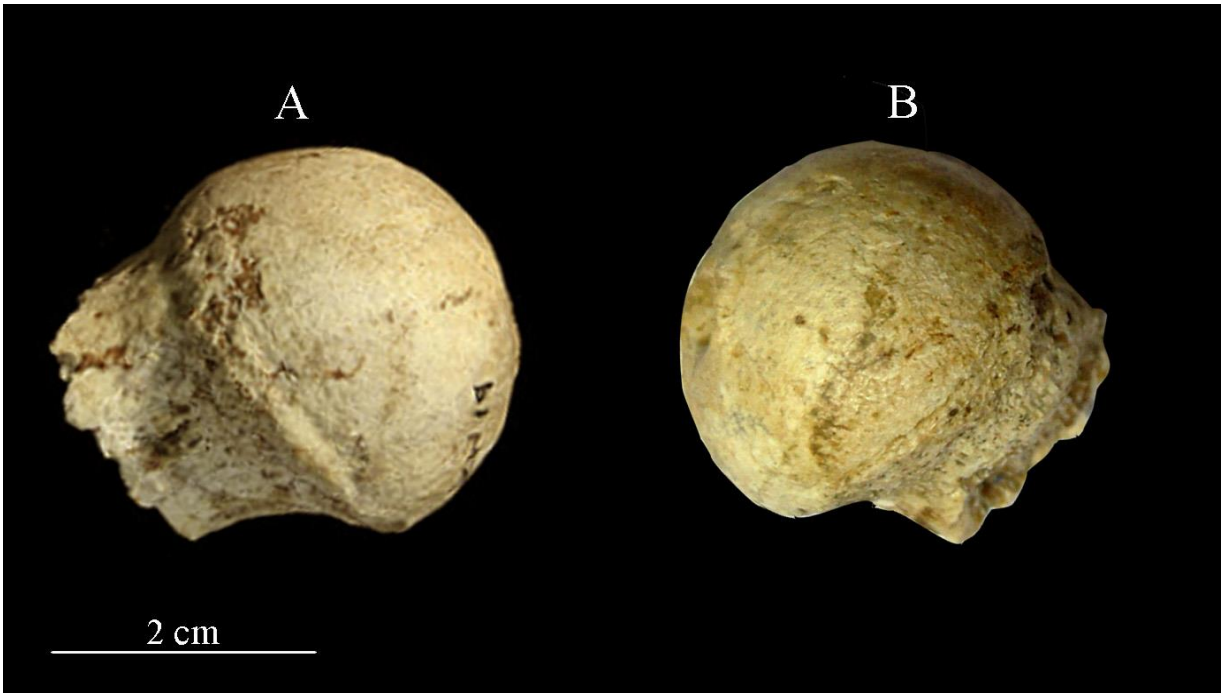

Fig. 2.1.3.F. Anterior (A) and posterior (B) views of the right proximal femoral end SKW 19 from Swartkrans.

Recovered in 2010 from the Lower Bank in Member 1 of Swartkrans, SWT1/LB-2 (Fig. 2.1.3.G) represents a right proximal femoral end originally in two pieces, but with good contact between the two sections. It is housed at the Ditsong National Museum of Natural History, Pretoria. It presents the head (maximum diameter: 35.2 mm), an antero-posteriorly flattened and long neck (mid-neck supero-inferior diameter: 27.4 mm; estimated mid-neck antero-posterior diameter: 18.4 mm) and a minor portion of the proximal diaphysis, but lacks most of the greater trochanter. The specimen's external surface is relatively well-preserved (weathering stage 0; Behrensmeyer, 1978), without conspicuous or inconspicuous tooth marks such as scores, pits and punctures, but a crenulation pattern on the anterior aspect of the greater trochanter is suggestive of carnivore chewing damage (Pickering et al., 2012). Although it bears only minor biochemical erosion in the form of a few localized, shallow linear features appearing

on the cortex, manganese dioxide spots are spread over the head and the trochanteric region. Estimated body mass of this individual (37.1-45.8 kg; Pickering et al., 2012; Ruff et al., 2018) is heavier than assessed in the likely female specimens SK 3121 (24.1-30.0 kg) and SKW 19 (27.7-35.3 kg) and nears the estimates for the larger SK 82 and SK 97 specimens (37.1-45.3 kg and 43.2-53.8 kg, respectively) (Pickering et al., 2012).

Fig. 2.1.3.G. Anterior view of the right proximal femoral end SWT1/LB-2 from Swartkrans.

SKX 1084 (Fig. 2.1.3.H) represents the superior two-thirds of an undistorted, relatively well preserved, although incomplete left patella recovered from Swartkrans Member 2. It is housed at the Evolutionary Studies Institute at the University of the Witwatersrand, Johannesburg. First described by Susman (1989), this fossil has a medio-lateral breadth of 30.2 mm (Susman, 1989) and an antero-posterior thickness near its centre of 13.0 mm (original measure), while its maximum height could not be assessed. This patella sample is that of an adult individual as indicated by its ossification, general morphology and degree of development of some longitudinal markings present on its anterior surface (likely related to the quadriceps tendon), even if some surface rugosity may have been locally accentuated by mineral matrix dissolution. As a whole, this specimen shows an only modest degree of mineralisation. It presents the entire base, which slopes antero-inferiorly from behind. However, its cortical shell is chipped all along the supero-posterior margin, approximately at the insertion of the vastus intermedius tendon, thus revealing an underlying trabecular network partially filled by

sediment. The lateral border is almost intact, but the specimen lacks the apex and almost its entire medial border, apart from its uppermost portion. Posteriorly, the portion which articulates with the lateral lip of the femoral trochlea is virtually intact. The attribution of SKX 1084 to the taxon *P. robustus* mostly relies on its modest size compared to the mean human figures, as well as to the context of its discovery (Susman, 1989).

Fig. 2.1.3.H. Anterior (A) and posterior (B) views of the left patella SKX 1084 from Swartkrans.

TM 1517e (Fig. 2.1.3.I) is a right proximal ulnar fragment from the site of Kromdraai B, recovered in the so-called "holotype block" (Braga et al., 2016b; Bruxelles et al., 2016). Originally reported by Broom (1938b) and then more extensively described by Broom and Schepers (1946), TM 1517e is considered part of the type specimen of *P. robustus* (Broom, 1938b; Broom and Schepers, 1946), representing a dentally late adolescent individual (Braga et al., 2016a). It is housed at the Ditsong National Museum of Natural History, Pretoria. The proximal end, which includes the trochlear notch and the olecranon process, is about 38.5 mm long with a medio-lateral breadth of 23.0 mm and an antero-posterior thickness of 20.5 mm. The specimen, as a whole, is moderately well preserved but the proximal and distal portions of the trochlear notch, the radial notch and the entire coronoid process are missing. In addition, some chunks of bone are missing on the supero-medial and postero-lateral aspects of the olecranon and some flakiness is perceived on the postero-lateral surface. No signs of surface weathering (stage 0; Behrensmeyer, 1978) could be detected, while sparse manganese dioxide

coating ranges from a few dots on the lateral aspect (stage 1; Val and Stratford, 2015) to spots completely covering the postero-medial surface and the anterior articular facet (stage 4; Val and Stratford, 2015). Among other modifications, bore holes, likely representing insect damage are found in the supero-lateral aspect and < 1 mm pits affect the lateral and superior surfaces. The coronoid fossa is well marked and relatively deep. The olecranon is not strongly developed, being much as it is in recent Humans, while there is a prominent ridge on the medial surface, corresponding to the attachment of the ulnar collateral ligament (Robinson, 1972; Le Gros Clark, 1947).

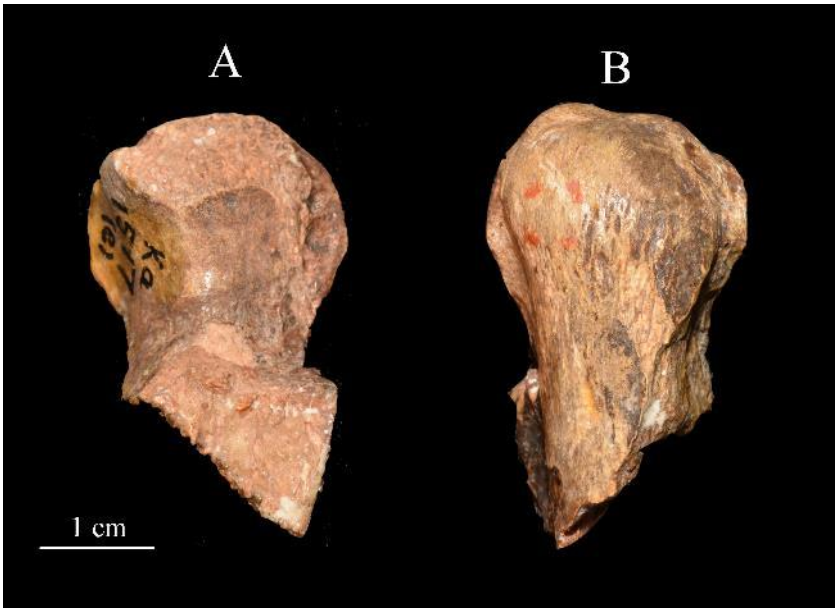

Fig. 2.1.3.I. Anterior (A) and posterior (B) views of the right proximal ulna TM 1517e from Kromdraai.

TM 1517k (Fig. 2.1.3.J) is a distal left phalanx of the hallux discovered in 1942, which apparently also comes from the "holotype block". It is housed at the Ditsong National Museum of Natural History, Pretoria. According to the first descriptions by Broom (1942) and Robinson (1972), it represents a second or third toe. However, Day (1978) and Day and Thornton (1986) later defined it as a distal phalanx of the hallux, mainly because of the attachment for the flexor hallucis longus tendon. The specimen, which is 12.5 mm long and 8.3 mm wide, is entirely preserved, but, especially on the dorsal surface, its outer contour suffered some taphonomic alterations (including insect damage). Conversely, only few dots of manganese dioxide staining are present.

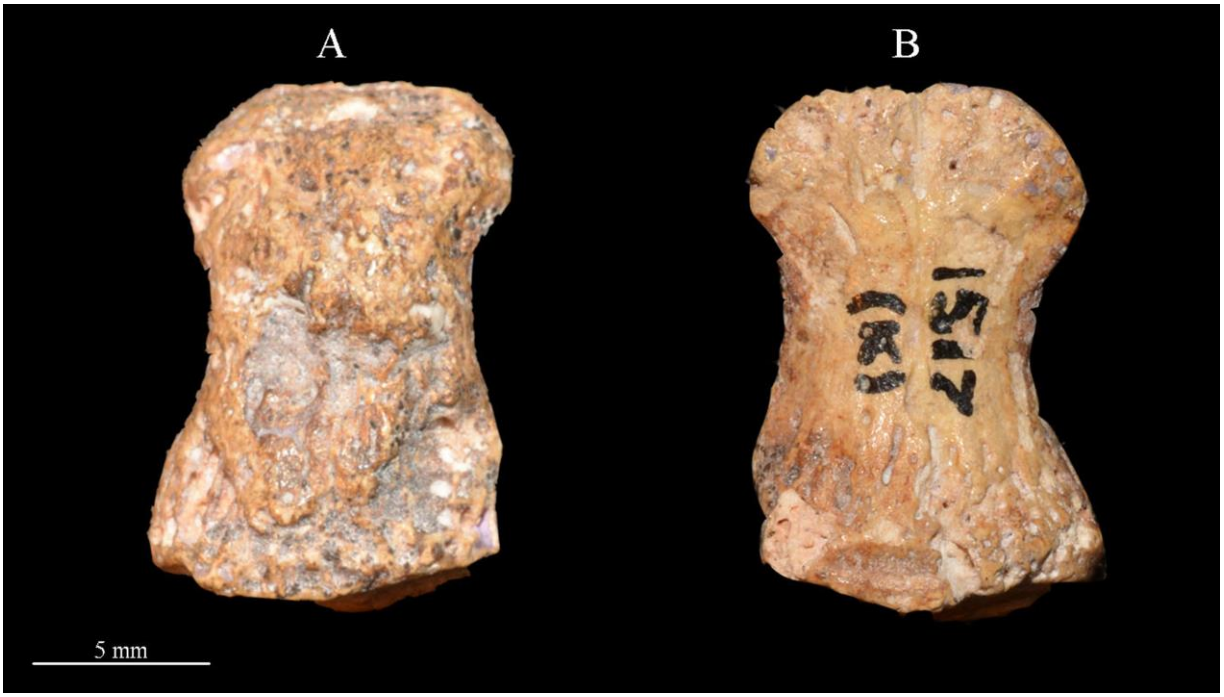

Fig. 2.1.3.J. Dorsal (A) and plantar (B) views of the hallucial phalanx TM 1517k from Kromdraai.

SK 50 (Fig. 2.1.3.K) is a right partial hip bone from an adult individual discovered at Swartkrans in the Hanging Remnant of Member 1. It is housed at the Ditsong National Museum of Natural History, Pretoria. First described by Broom and Robinson (1950) and then by Robinson (1972), it was attributed to *P. robustus* (initially *P. crassidens*) as it is "less like that of modern man than is that of *H. africanus*" (Robinson, 1972: 88). SK 50 includes about the lower half of a 168 mm wide iliac blade (McHenry, 1975c), the acetabular part of the pubis (acetabulum depth: 22.5 mm; McHenry, 1975c) and most of the body of the ischium and of the anterior superior iliac spine. A portion of the ischial ramus is also present, but it is broken and displaced. Conversely, most of the surface of the ischial tuberosity is missing, as is the region of the ischial spine and the lesser sciatic notch. However, the posterior surface of the remaining iliac portion is rather well preserved, while in the anterior region of the blade, three cracks run transversely, the thickest one crossing the upper portion of the acetabulum. The outer surface of this specimen is well preserved (weathering stage 0; Behrensmeyer, 1978), but manganese dioxide spots are found on all remaining regions of the fossil.

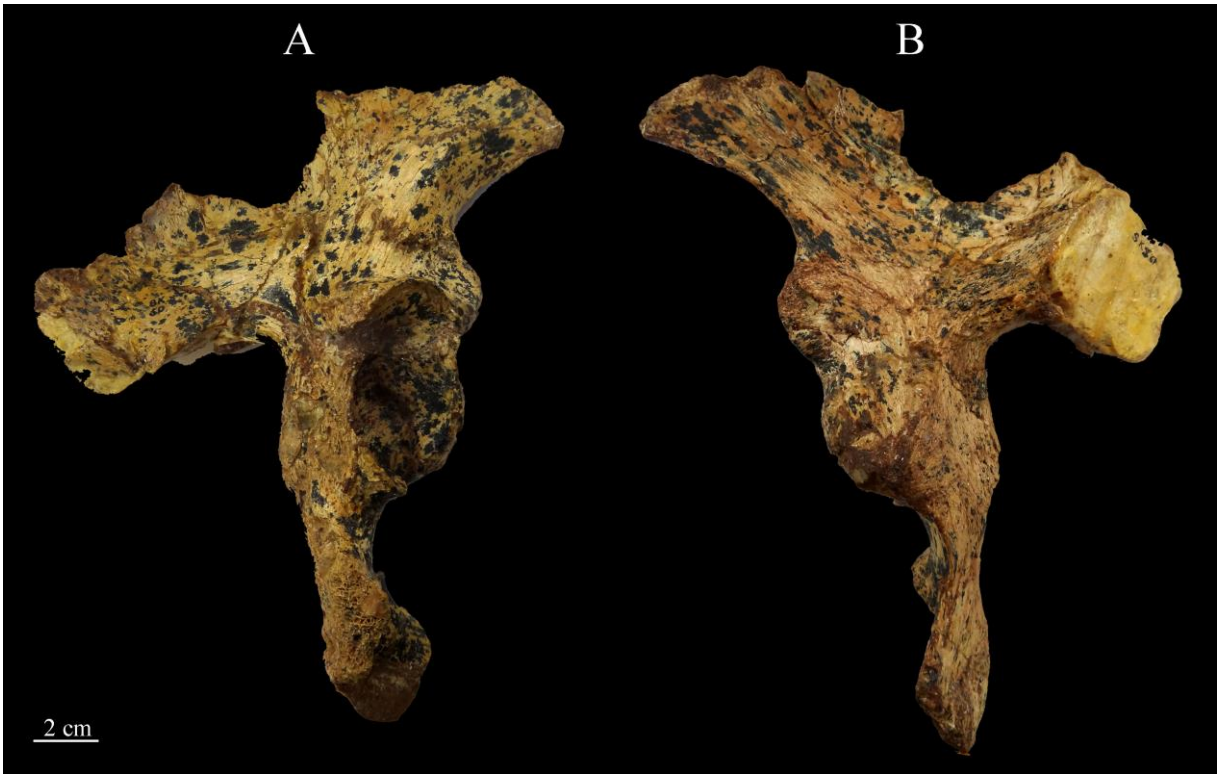

Fig. 2.1.3.K. Lateral (A) and medial (B) views of the right hip bone SK 50 from Swartkrans.

TM 1605 (Fig. 2.1.3.L) is an incomplete left hip bone recovered in 1954 at Kromdraai B in the decalcified breccia. It is housed at the Ditsong National Museum of Natural History, Pretoria. First described by Robinson (1972), it was attributed to *P. robustus* based on comparisons with specimen SK 50. TM 1605 is less robust than SK 50 and therefore could have been female (Robinson, 1972). It is commonly considered as an adult individual (Robinson, 1972; Brain, 1981, Skinner et al., 2013; Braga et al., 2016b), but Thompkins (1977) reported it as possibly immature. While incomplete, TM 1605 is extremely well preserved. It consists of most of the ilium (thickness: 10.4 mm) and the upper part of the acetabulum. However, the entire iliac crest, the ischium and the pubis are absent and only a small part of the auricular region is present. On both anterior and posterior surfaces, some cracks run supero-inferiorly from the greater sciatic notch. Some horizontal cracks are also found on the upper portion of the medial iliac fossa. The width of the incomplete auricular surface has been estimated as 24.3 mm and the angle between the blade and the sacral articular surface as 64.2° (McHenry, 1975c). At the easily palpable acetabulo-cristal buttress, the compact bone reached a thickness of 1.5 mm (Robinson, 1972).

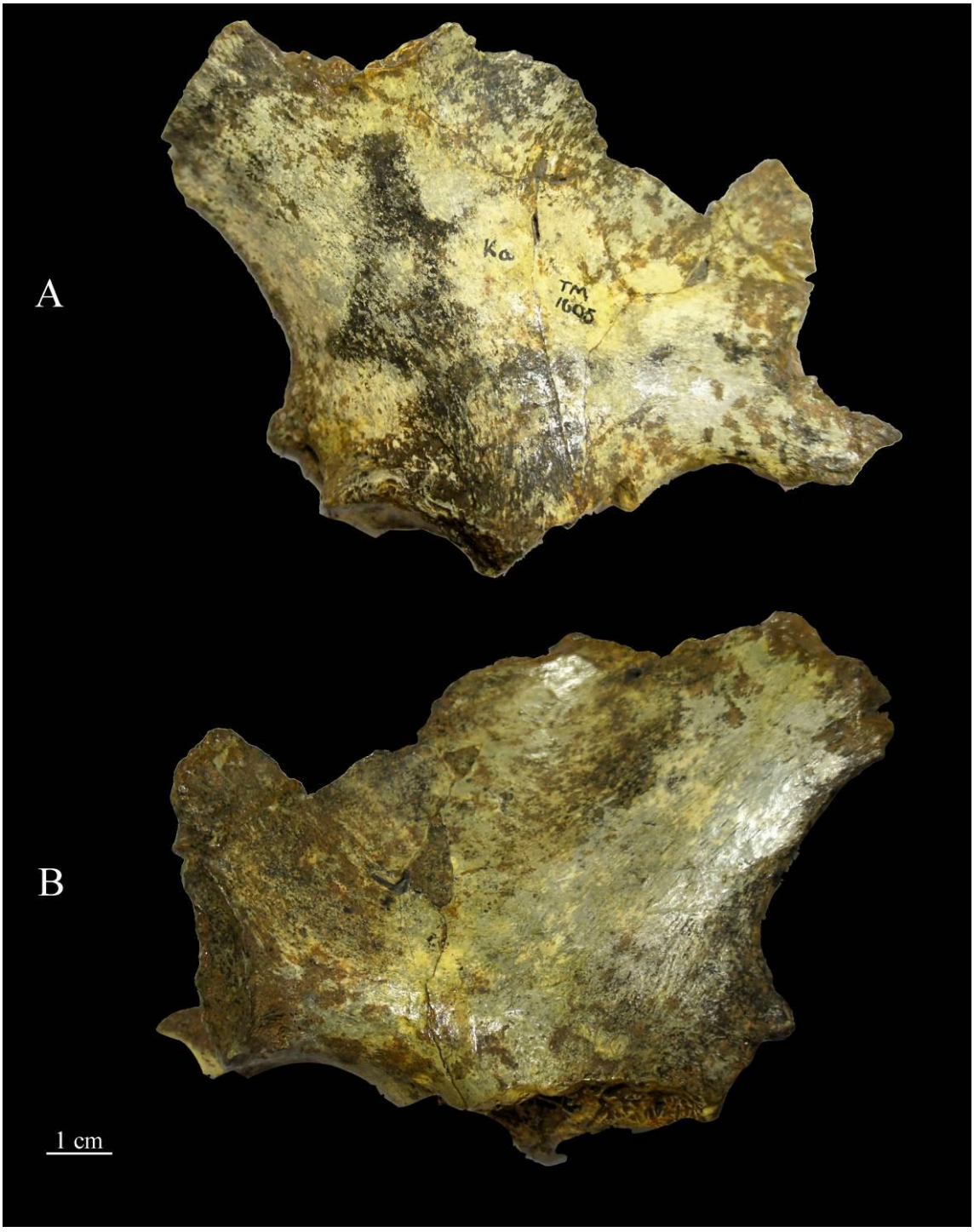

Fig. 2.1.3.L. Lateral (A) and medial (B) views of the partial hip bone TM 1605 from Kromdraai.

2.2. Comparative materials

For each investigated element of the postcranial skeleton representing the taxon *P. robustus*, we composed a comparative sample tentatively consisting of fossil *Homo* representatives and extant catharrine taxa. More specifically, our fossil human sample includes the two distal humeri SK 24600 and SK 34805 from Swartkrans, South Africa, attributed to early *Homo*, the *Homo* aff. *erectus* distal humerus Gombore IB (GOM IB) from Melka Kunture, Ethiopia, and a sample of four Neanderthal patellae, including three specimens from Krapina, Croatia (Pa1, 3, 5) and Regourdou 1, France. The comparative sample of extant catharrines includes representatives from five taxa: extant Humans, *Pan, Gorilla* and *Papio*. The following sections are devoted to the description of this comparative sample.

2.2.1. Comparative fossil specimens

SK 24600 (Fig. 2.2.1.A), described by Susman et al. (2001), is a distal part of a left humerus of 59.3 mm from the Lower Bank of Swartkrans Member 1 currently stored at the Ditsong National Museum of Natural History, Pretoria. In their original description, Susman and co-workers (2001: 617) stated that "comparisons with TM 1517 and KNM-ER 271 as well as with modern Humans, chimpanzees and bonobos, suggest that SK 24600 samples *Paranthropus*". However, based on the results of a recent geometric morphometric (GM) comparative analysis, this specimen has been allocated to early *Homo* (Lague, 2015). SK 24600 presents the trochlea, the capitulum and the epicondyles (biepicondylar diameter: 44.7 mm). Its external surface is only locally altered by minor erosions, limited damages and cracks, notably at the lateral epicondyle, the antero-lateral edge of the capitulum, the antero-medial edge of the trochlea, the posterior surface of the lateral epicondyle and the posterior surface of the shaft, just above the olecranon fossa. Large spots of manganese dioxide are spread all over the specimen.

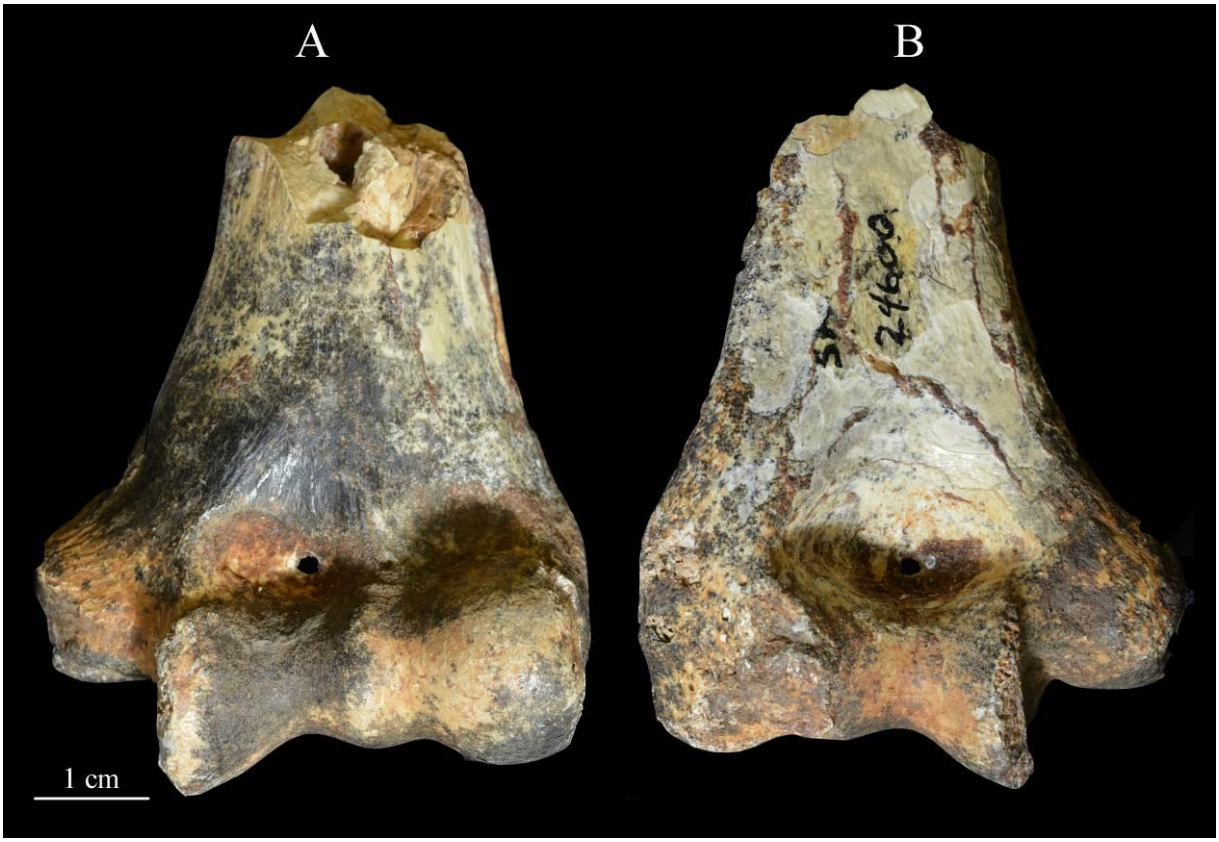

Fig. 2.2.1.A. Anterior (A) and posterior (B) views of the left distal humerus SK 24600 from Swartkrans.

SKX 34805 (Fig. 2.2.1.B), originally reported by Susman (1989), is a distal part of a right humerus of 80.7 mm from the Hanging Remnant in the Member 1 of Swartkrans. The specimen is stored at the Evolutionary Studies Institute of the University of the Witwatersrand, Johannesburg. In his original description, Susman stated that "(t)his specimen is a reasonably good match for TM 1517 in both size and shape, and on this basis it most likely belongs to *Paranthropus*" (Susman, 1989: 462). However, based on its cross-sectional shape and comparisons with the expanded record later available at Swartkrans, this specimen has since been allocated to *Homo* (Susman et al., 2001; Dusseldorp et al., 2013; Lague, 2015), more specifically, to *H*. aff. *erectus* (Lague, 2015). It lacks a portion of each condyle, as well as the trochlea and the capitulum, but presents the upper part of the epicondyles (biepicondylar diameter: 47.2 mm). The external surface of the remaining regions is well preserved, with no conspicuous damages or cracks, but scores are observed on the posterior and anterior surfaces of the shaft. The specimen is also heavily stained with manganese dioxide.

Fig. 2.2.1.B. Anterior (A) and posterior (B) views of the right distal humerus SK 34805 from Swartkrans.

Gombore IB (GOM IB; Fig. 2.2.1.C), originally reported by Chavaillon and co-workers (1977) and by Senut (1979; see also Senut, 1981a, b), is a distal third of a left humerus from a *Homo* aff. *erectus* robust individual, stored at the National Museum of Ethiopia, Addis Ababa. It was discovered in 1976 in the Oldowan tool-bearing level of Gombore I, one of the Early to Middle Pleistocene localities forming the Melka Kunture archaeological and paleontological site complex along the Upper Awash Valley, on the Ethiopian highlands (Chavaillon and Piperno, 2004; Gallotti and Mussi, 2015). GOM IB has been more recently investigated by Puymerail et al. (2014) and by Di Vincenzo et al. (2015). While incomplete, this specimen is finely preserved. However, longitudinal cracks run on the anterior and posterior external surfaces of the shaft. A horizontal crack at the mid-preserved shaft is found all around the specimen. Minor local erosion is found on the posterior shaft surface and on the posterior aspect of the most distal articular surface.

Fig. 2.2.1.C. Anterior (A) and posterior (B) views of the left distal humerus GOM IB from Melka Kunture.

For the study of the patella, we considered a comparative sample consisting of four adult European Neanderthals represented by two right (Pa1 and Pa3) and one left (Pa5) patellae from the OIS 5 Croatian site of Krapina, stored at the Croatian Natural History Museum, Zagreb (Radovčić et al., 1988), and the left patella from the OIS 4 partial skeleton Regourdou 1, from the homologous rock shelter in Dordogne, France, stored at the Musée d'Art et d'Archéologie du Périgord, Périgueux (Bayle et al., 2011; Maureille et al., 2015) (Fig. 2.2.1.D). While local erosion is commonly found at the bases and around the apices, the five specimens were selected because of their particularly fine degree of preservation and modest level of mineralisation.

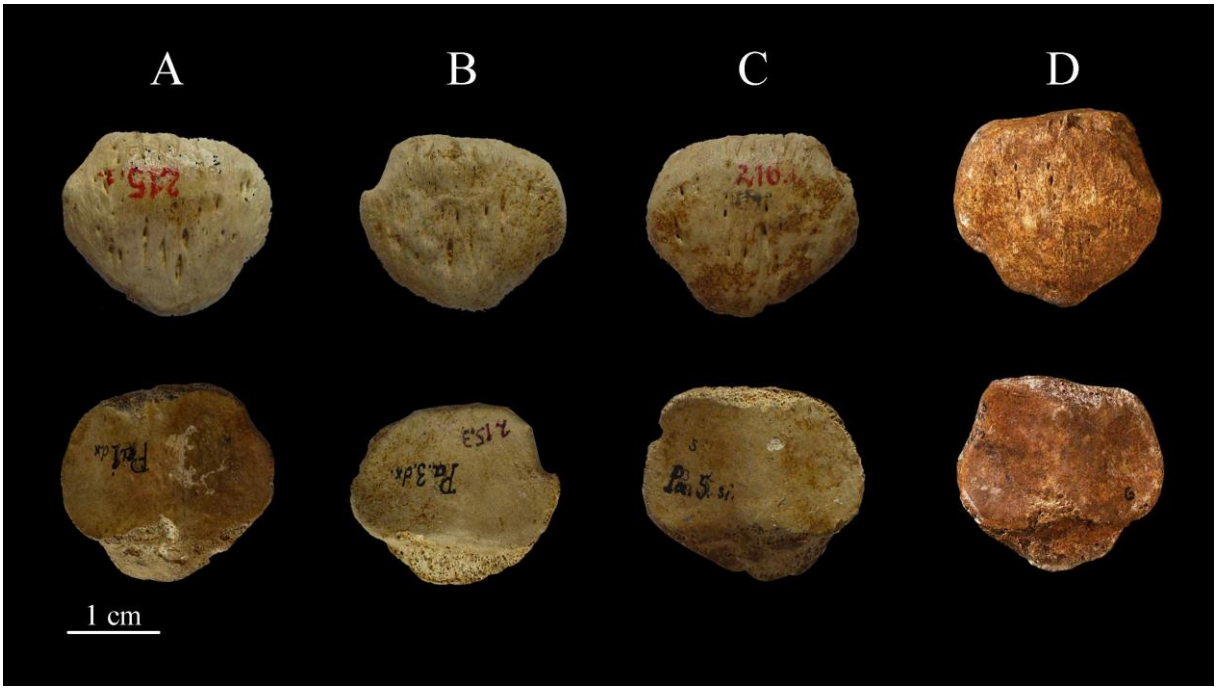

Fig. 2.2.1.D. Anterior (upper row) and posterior (lower row) views of the Neanderthal patellae Pa1 (A), Pa3 (B), Pa5 (C) from Krapina, Croatia, and of Regourdou 1, France (D).

2.2.2. Comparative extant samples

For the study of the internal structural organisation of the distal humerus, we examined a comparative extant human sample composed of 12 adult individuals selected from the Pretoria Bone Collection stored in the Department of Anatomy at the University of Pretoria (L'Abbé et al., 2005). The sample includes two male and four female individuals of African origin, aged 23-29 years, and four male and two European-derived female individuals, aged 41-58 years.

The extant human sample used for the comparative endostructural analysis of the proximal femur consists of 12 femora from adult individuals of African origin (seven males and five females, aged 26-54 years) selected from the McGregor Museum of Kimberley (Morris, 1984), the Pretoria Bone Collection, and the R.A. Dart skeletal collection at the University of the Witwatersrand, Johannesburg (Dayal et al., 2009). We also used the digital radiographic records of 214 proximal femora, sampling adult individuals of both sexes, from the Imperial Roman osteological collection of Isola Sacra (Macchiarelli and Bondioli, 2000). In this specific study, *Pan* is represented by one femur from a *P. troglodytes* and a *P. paniscus* adult skeleton, stored at the Evolutionary Studies Institute of the University of the Witwatersrand, two *P. troglodytes* femora from the primate osteological collections of the Muséum national d'Histoire

naturelle, Paris and the CT-based records of seven adult *P. troglodytes* femora from the Primate Research Institute, Kyoto University (Digital Morphology Museum, KUPRI; http://dmm.pri.kyoto-u.ac.jp/dmm/WebGallery/index.html). We also examined the proximal femora of two male *Gorilla* from the R.A. Dart skeletal collection. In addition, four *Papio* femora, curated at the Pretoria Bone Collection, were investigated.

The comparative extant material used in the study of the patellar bone consists of 12 human specimens from six individuals of African ancestry (four males and two females aged between 24-29 years) selected from the Pretoria Bone Collection, and from six individuals (two likely males and four likely females whose estimated age at death ranges between 30 and 50 years) from the Imperial Roman graveyard of Velia, Italy, stored at the National Prehistoric Museum of Rome (Beauchesne and Agarwal, 2017). In addition, we studied two female chimpanzee patellae from the Mahale skeletal collection stored at the Japan Monkey Centre of Inuyama, and six *Papio* patellae curated at the Pretoria Bone Collection.

For the comparative study of the TM 1517-labelled postcranial elements, suggested to represent a single late adolescent or young adult *P. robustus* (Broom, 1938b, 1942, 1943; Thackeray et al., 2001, 2005; Braga et al., 2013, 2016a, b; Skinner et al., 2013), we used an extant human sample of subadult individuals consisting of five humeri, six ulnae and six distal hallucial phalanges from the R.A. Dart Collection. For each bone, we selected three male and three female individuals. More specifically, for each corresponding element of the TM 1517 and for each sex, our sample included one specimen of which the epiphysis of the corresponding elements is unfused, one individual with faint traces of recent epiphyseal fusion and one individual where the corresponding epiphysis is fused. However, in the sample comprising of distal humerus only two females are presented, as a female specimen showing traces of recent fusion was lacking. Information on this assemblage is summarised in Table 2.2.1.A below:

Table 2.2.1.A. Composition and degree of epiphyseal fusion of the extant human subadult sample used in the comparisons with the TM 1517-labelled postcranial elements representing *P. robustus*.

bone	sex	degree of epiphyseal fusion	age (years)
distal humerus	M	not fused	15
=	M	traces of recent fusion	16
=	M	fused	17
=	F	not fused	12
=	F	fused	14

proximal ulna	M	not fused	16
=	M	traces of recent fusion	16
=	M	fused	17
=	F	not fused	13
=	F	traces of recent fusion	13
=	F	fused	14
distal hallucial phalanx	M	not fused	15
=	M	traces of recent fusion	16
=	M	fused	17
=	F	not fused	12
=	F	traces of recent fusion	13
=	F	fused	14

Finally, in the perspective of extracting and characterising the cortical and cancellous organisation of the australopith coxo-femoral complex as a functional unit in three-dimensions we have scanned and preliminary examined the iliac bone of an extant human female individual of South African origin, aged 32 years, from the Pretoria Bone Collection.

All extant human and non-human specimens used here for comparisons were selected because of their lack of any macroscopic evidence of outer or inner alteration and of obvious pathological changes. Depending on their nature and location, the specimens were scanned by means of medical computed tomography (CT), X-ray microtomography (µCT), or synchrotron radiation microtomography (SR-µCT). Details about these comparative materials are provided in Table 2.2.1.B.

Table 2.2.1.B. The postcranial extant material used for comparisons with *P. robustus*. For each skeletal element, the equipment used for scanning is indicated as follows: CT = medical computed tomography; µCT X-ray = microtomography; SR-µCT = synchrotron radiation microtomography.

taxon	**sample size / equipment**	**collection**
humerus		
human	12/µCT	PBC[1]
ilium		
human	1/µCT	PBC[1]
femur		
human	12/µCT (+214 X-ray films)	McGM[2], PBC[1], Dart[3], NPMR[4]
Pan	2/µCT; 2/SR-µCT; 7/CT	ESI[5], MNHM[6], PRI[7]

Gorilla	2/µCT	Dart[3]
Papio	4/µCT	PBC[1]
patella		
human	12/µCT	PBC[1], NPMR[4]
Pan	2/µCT	MSC[8]
Papio	6/µCT	PBC[1]
humerus + ulna + distal hallux phalanx		
human	17/µCT	Dart[3]

[1] Pretoria Bone Collection, Department of Anatomy, University of Pretoria, South Africa
[2] McGregor Museum of Kimberley, South Africa
[3] R.A. Dart skeletal Collection, University of the Witwatersrand, Johannesburg, South Africa
[4] National Prehistoric Museum of Rome, Italy
[5] Evolutionary Studies Institute of the University of the Witwatersrand, Johannesburg, South Africa
[6] Muséum national d'Histoire naturelle, Paris, France
[7] Primate Research Institute, Kyoto University, Japan
[8] Mahale skeletal collection, Japan Monkey Centre of Inuyama, Japan

3. Results

3.1. Distal humerus

The humerus, particularly its distal end, is among the most represented remains in the Plio-Pleistocene hominin fossil record and is often used in comparative analyses to assess early hominin postcranial variation and evolution (e.g., Patterson and Howells, 1967; McHenry, 1971; McHenry and Corruccini, 1975; Senut, 1981a, b; Feldesman, 1982; Senut and Tardieu, 1985; Susman, 1989; Lague and Jungers, 1996; Bacon, 2000; Susman et al., 2001; McHenry and Brown, 2008; Lague, 2014, 2015; Di Vincenzo et al., 2015). However, the degree and significance of morphological variation among the hominin distal humeri have been a recurrent matter of discussion among palaeoanthropologists. Some researchers argued that differences imply functional diversity and deserve taxonomic separation (e.g., Patterson and Howells, 1967; McHenry and Corruccini, 1975; Senut, 1981b; Senut and Tardieu, 1985; McHenry and Brown, 2008; Lague, 2015; Di Vincenzo et al., 2015), while others note that the degree of morphological variation is not of sufficient magnitude to deserve taxonomic or functional distinctions (e.g., Hill and Ward, 1988; Lague and Jungers, 1996; Bacon, 2000).

Disagreement among researchers also concerns the evolutionary trends in distal humeral morphology, which have been widely debated because of the primitive vs. derived status of some anatomical features (Straus, 1948; Patterson and Howells, 1967; Kay and McHenry, 1973; McHenry, 1973; McHenry and Corruccini, 1975; McHenry et al., 1976; Senut, 1979, 1981a, b, 1986; Feldesman, 1982; Senut and Tardieu, 1985; Rockwell, 1994; Lague and Jungers, 1996; Bacon, 2000; Yokley and Churchill, 2006). A number of studies suggest that some features do not follow a linear path of increasing "modernisation" through the time, rather noting that the earliest known hominin distal humeri already show modern-like features, while a number of specimens later in time, appear more primitive (McHenry and Brown, 2008). However, other works conclude that earlier hominin distal humeri appear ape-like, whereas later specimens are more similar to the derived human condition (Feldesman, 1982; Lague and Junger, 1996; Richmond and Junger, 2008). In his comprehensive morphometric study, Lague (2014: 105) concluded that “the pattern of distal humeral morphology that characterised the earliest species of *Australopithecus* remained remarkably stable throughout the evolution of the genus. This basic morphological pattern, possibly primitive for all hominins, continued to be exhibited by members of *P. robustus*, perhaps as late as 1 Ma at Swartkrans”. He also stated that “after 2

Ma, a subtly more human-like elbow morphology is apparent among specimens attributed to early *Homo*, as well as among isolated specimens that may represent either *Homo* or *Paranthropus boisei*".

The challenge of allocating isolated and fragmentary postcranial elements to one of the penecontemporaneous Plio-Pleistocene hominin species (see supra section 1.4) is a major issue in palaeoanthropology, which limits the accurate assessment of the degree of inter- and intraspecific diversity based on the anatomy and morphological variation at the elbow joint. Considering the long-term debate about the assignment of some isolated remains to *Paranthropus* or *Homo*, the distal humerus is a leading example of such difficulties (e.g., Patterson and Howells, 1967; Senut, 1981a; Susman, 1989; Lague and Jungers, 1996; Bacon, 2000; Susman et al., 2001; Churchill et al., 2013; Lague, 2014, 2015; Di Vincenzo et al., 2015). Fortunately, the discovery in 1938 of the distal humeral end TM 1517g assigned to the *P. robustus* holotype at Kromdraai (see supra sections 1.1 and 2.1.3) and the recent discovery at Olduvai Gorge, Tanzania, of craniodental remains confidently attributed to *P. boisei* in association with postcranial elements representing the partial skeleton OH 80 (Domínguez-Rodrigo et al., 2013), now provide a stronger foundation for testing taxonomic hypotheses regarding isolated hominin humeri.

Following the observation of a possible dichotomy in diaphyseal morphology between *Paranthropus* and *Homo*, the former showing a broad medio-lateral breadth and a flat antero-posterior thickness (Susman et al., 2001; but see also Leakey, 1971), the potential taxonomic significance of the distal humeral diaphyseal shape has been assessed in a study on the cross-sectional outline variation in Early Pleistocene specimens attributable to *Paranthropus* and *Homo*, to test the hypothesis that the fossils can be divided into distinct morphotypes (Lague, 2015). The results show that the comparative analysis of the most distal cross-sectional shape grants distinction among three morphs present in Eastern and Southern Africa between ca 2.0 and 1.0 Ma ago: *Paranthropus*, *Homo erectus*, and non-*erectus* early *Homo*. Following such study (Lague, 2015), specimens attributed to non-*erectus* early *Homo* are unique among hominins, displaying a flat antero-posterior thickness relative to medio-lateral width, while *H. erectus*' morphology is more similar to that of modern Humans, with a high degree of antero-posterior flattening. Finally, in both Eastern and Southern Africa macro-regions, *Paranthropus* is characterised by a somehow intermediate morphology between the two forms of fossil *Homo*.

By this study, Lague (2015) provided clear evidence about the value of using the cross-sectional humeral diaphyseal shape, which shows a high degree of diversity in early hominins, for taxonomic identification of isolated remains.

A direct relationship between loading environment and cross-sectional geometry (CSG) has been experimentally tested (e.g., Stock and Pfeiffer, 2001; Stock, 2006) and is supported by studies of bilateral asymmetry (Jones et al., 1977; Ruff and Jones, 1981; Trinkaus et al., 1994; Sakaue, 1997; Shaw and Stock, 2009; Warden et al., 2009; Volpato et al., 2011; Ireland et al., 2014; Trinkaus et al., 2014). Accordingly, CSG properties of the humeral diaphysis have been extensively used in previous studies to measure diaphyseal strength and to provide mechanical loading information on the forearm in fossil hominins (Ruff et al., 1993; Trinkaus et al., 1994; Trinkaus and Churchill, 1999; Trinkaus et al., 1999; Ruff, 2008a, 2009; Ruff et al., 2016) and past populations (Ruff et al., 1993; Trinkaus and Churchill, 1999; Ledger et al., 2000; Marchi et al., 2006; Macintosh et al., 2017; Trinkaus, 2018). Therefore, beyond their taxonomic implications, the complementary results of our research project might provide direct functional evidence for clarifying the specific forearm loading environment in *P. robustus*.

Given the well-documented ability of long bones to adjust structurally to their loading environment, i.e., of recording relevant biomechanical information during life, but also of preserving the signature of their genetic-related evolutionary adaptive bauplan (Lovejoy et al., 1999; Currey, 2002; Volkman et al., 2003; Lieberman et al., 2004; Pearson and Lieberman, 2004; Ruff et al., 2006; Carlson et al., 2008; Middleton et al., 2008; Wallace et al., 2010, 2012; Gosman et al., 2011; Ryan and Shaw, 2013; Carlson and Marchi, 2014; Nadell and Shaw, 2015; Kivell, 2016; Agostini et al., 2018), the still poorly investigated inner structural features of the distal humerus in early hominins should provide further evidence of taxonomic significance. A thicker cortical bone and the diffuse presence of trabeculae nearly obstructing the most distal portion of the medullary cavity have been reported among the common features in *Paranthropus* (Susman et al., 2001; Dominguez-Rodrigo et al., 2013). However, to the best of our knowledge, the endostructural organisation of Plio-Early Pleistocene distal humeri attributed to *Paranthropus* or *Homo* (rev. in Lague, 2015) and the possible existence of some taxon-specific features, remain unexplored.

The primary aim of our project is, therefore, to characterise the still unreported endostructural morphology of five Early Pleistocene distal humeri from South Africa (TM 1517g, SK 24600, SKX 10924, SKX 34805) and Ethiopia (Gombore IB), which have been previously investigated only for their cross-sectional outer morphology (Lague, 2015), in order to compare for their coherence the eso- and endostructural signals.

Preliminary results of the study of the *P. robustus* distal humerus have been presented to the *6th Biennial Conference of the East African Association for Paleoanthropology and Paleontology* (Addis Ababa, 30/7-2/8/2017): Cazenave M., Braga J., Oettlé A., Thackeray J.F.,

de Beer F., Hoffman J.W., Endalamaw M., Enga Redae B. & Macchiarelli R. - The endostructural bony organization at the distal humerus: do *Paranthropus* and early *Homo* differ? (https://eaappinfo.wordpress.com/2017-2/2017-conference-abstracts/). The methods of data acquisition and the results *in extenso* of this study are detailed in the paper "Inner structural organization of the distal humerus in *Paranthropus* and *Homo*" published in 2017 in the *Comptes Rendus Palevol* (vol. 16, 521-532) and are provided in section 3.1.1.

3.1.1. Paper published in 2017 in the Comptes Rendus Palevol *(vol. 16, 521-532)*

C. R. Palevol 16 (2017) 521–532

Contents lists available at ScienceDirect

Comptes Rendus Palevol

www.sciencedirect.com

Human Palaeontology and Prehistory (Palaeoanthropology)

Inner structural organization of the distal humerus in *Paranthropus* and *Homo*

Organisation de la structure interne de l'humérus distal chez Paranthropus *et* Homo

Marine Cazenave[a,b,*], José Braga[b,c], Anna Oettlé[d,a], John Francis Thackeray[c], Frikkie de Beer[e], Jakobus Hoffman[e], Metasebia Endalamaw[f], Blade Engda Redae[f], Laurent Puymerail[g], Roberto Macchiarelli[h,i]

[a] *Department of Anatomy, University of Pretoria, Pretoria, South Africa*
[b] *Computer-assisted Palaeoanthropology Team, UMR 5288 CNRS–Université Paul-Sabatier, 37, allées Jules-Guesde, 31000 Toulouse, France*
[c] *Evolutionary Studies Institute and School of Geosciences, University of the Witwatersrand, Johannesburg, South Africa*
[d] *Department of Anatomy and Histology, Sefako Makgatho Health Sciences University, Ga-Rankuwa, Pretoria, South Africa*
[e] *South African Nuclear Energy Corporation, Pelindaba, South Africa*
[f] *Authority for Research and Conservation of Cultural Heritage (ARCCH), National Museum of Ethiopia, Addis Ababa, Ethiopia*
[g] *UMR 7268 CNRS–Université d'Aix–Marseille–EFS, 13344 Marseille, France*
[h] *UMR 7194 CNRS–Muséum national d'histoire naturelle, 75013 Paris, France*
[i] *Unité de formation géosciences, Université de Poitiers, 86073 Poitiers, France*

ARTICLE INFO

Article history:
Received 27 February 2017
Accepted after revision 13 June 2017
Available online 1 August 2017

Presented by Roberto Macchiarelli and Clément Zanolli

Keywords:
Distal humerus
Inner structure
Cortical bone topography
Paranthropus
Homo

ABSTRACT

The taxonomic attribution of isolated hominin distal humeri has been a matter of uncertainty and disagreement notwithstanding their relative abundance in the fossil record. Four taxonomically-based morphotypes, respectively representing *P. boisei*, *P. robustus*, non-*erectus* early *Homo* and *H. erectus*, have been identified based on the cross-sectional outer shape variation of an assemblage of Plio-Pleistocene eastern and southern African specimens (Lague, 2015). However, the existence of possible differences between *Paranthropus* and *Homo* in the inner structural organisation at this skeletal site remains unexplored. We used noninvasive imaging techniques to tentatively characterize the endostructural organization of five early Pleistocene distal humeri from South Africa (TM 1517g, SK 24600, SKX 10924, SKX 34805) and Ethiopia (Gombore IB), which have been variably attributed to *Paranthropus* or *Homo*. While the investigated specimens reveal diverse degrees of inner preservation related to their taphonomic and diagenetic history, in all but SK 24600 from Swartkrans we could comparatively assess some geometric properties at the most distal cross-sectional level (%CA, I_x/I_y, I_{max}/I_{min}) and quantify cortical bone thickness topographic variation across the preserved shaft portions by means of a 2-3D Relative Cortical Thickness index. Whenever possible, we also provided details about the site-specific organization of the cancellous network and measured the same parameters in a comparative sample of twelve adult extant humans. For most features, our results indicate two main patterns: the first includes the specimens TM 1517g, SKX 10924 and SKX 34805, while the second endostructural morphotype sets apart the robust *Homo* aff. *erectus* Gombore IB specimen from Melka Kunture, which more closely resembles the condition displayed by our

* Corresponding author. Computer-assisted Palaeoanthropology Team, UMR 5288 CNRS–Université Paul-Sabatier, Toulouse, France.
E-mail address: marine.cazenave4@gmail.com (M. Cazenave).

http://dx.doi.org/10.1016/j.crpv.2017.06.002
1631-0683/© 2017 Académie des sciences. Published by Elsevier Masson SAS. All rights reserved.

comparative human sample. Notably, marked differences in the amount and pattern of proximodistal cortical bone distribution have been detected between Gombore IB and SKX 34805 from Swartkrans. Given its discordant outer and inner signatures, we conclude that the taxonomic status of SKX 34805 deserves further investigations.

© 2017 Académie des sciences. Published by Elsevier Masson SAS. All rights reserved.

Mots clés :
Humérus distal
Structure interne
Topographie de l'os cortical
Paranthropus
Homo

RÉSUMÉ

Malgré leur abondance relative dans le registre fossile, l'attribution taxinomique d'huméri distaux isolés d'hominines a souvent été sujet d'incertitudes et de désaccords. Sur la base de variations de la morphologie externe de sections transversales d'un ensemble de spécimens du Plio-Pléistocène d'Afrique orientale et méridionale, quatre morphotypes, représentant respectivement *P. boisei*, *P. robustus*, premier *Homo* non-*erectus* et *H. erectus*, ont été récemment identifiés (Lague, 2015). Cependant, l'existence de possibles différences entre *Paranthropus* et *Homo* dans l'organisation de la structure interne de ce site squelettique reste inconnue. Nous avons utilisé des techniques d'imagerie non invasives pour caractériser l'organisation endostructurale de cinq huméri distaux d'Afrique du Sud (TM 1517g, SK 24600, SKX 10924 et SKX 34805) et d'Éthiopie (Gombore IB), qui ont été variablement attribués, soit à *Paranthropus*, soit à *Homo*. Même si les spécimens étudiés révèlent des variations dans leur préservation dues à leur histoire taphonomique et diagénétique, à l'exception de SK 24600 provenant de Swartkrans, nous avons pu analyser comparativement des paramètres de géométrie de section au niveau de la coupe transversale la plus distale de la diaphyse (%CA, I_x/I_y, I_{max}/I_{min}) et quantifier les variations topographiques d'épaisseur du tissu cortical le long de la portion diaphysaire préservée à l'aide d'indices 2–3D. Nous avons aussi apporté des précisions sur l'organisation site-spécifique du réseau trabéculaire et mesuré les mêmes variables dans un échantillon comparatif composé de douze humains actuels adultes. Pour la plupart des caractères, nos résultats indiquent deux patrons principaux : le premier réunit les spécimens TM 1517g, SKX 10924 et SKX 34805, tandis que le second morphotype endostructural distingue le spécimen robuste *Homo* aff. *erectus* de Melka Kunture, Gombore IB, qui se rapproche de la condition de l'échantillon comparatif humain. En particulier, des différences marquées dans la quantité et le patron de distribution proximo-distale de l'os cortical ont été détectées entre Gombore IB et SKX 34805 de Swartkrans. Compte tenu d'un certain dégrée d'hétérogénéité entre la morphologie externe et la signature morphostructurale interne, nous concluons que le statut taxonomique de SKX 34805 mérite d'autres analyses.

© 2017 Académie des sciences. Publié par Elsevier Masson SAS. Tous droits réservés.

1. Introduction

The rarity in the hominin fossil record of unambiguously associated craniodental and postcranial remains usually complicates the task of identifying isolated fragmentary elements from the axial and the appendicular skeleton (e.g., Domínguez-Rodrigo et al., 2013; Hlusko et al., 2015; Lague, 2015). This is especially true for the hominin-bearing southern African cave sites, where variably preserved remains of *Australopithecus*, *Paranthropus* and *Homo* have been sometimes discovered commingled and where taxonomic diversity is revealing wider than previously assumed (Berger et al., 2010, 2015).

An interesting case is represented by the long-term debate about the allocation to *Paranthropus* (or australopith *s.l.*, following some authors) or *Homo* of isolated remains of the distal humerus remains (e.g., Bacon, 2000; Churchill et al., 2013; Di Vincenzo et al., 2015; Lague, 2014, 2015; Lague and Jungers, 1996; Patterson and Howells, 1967; Senut, 1981a; Susman, 1989; Susman et al., 2001). While potentially well suited for assessing postcranial variation because of their abundance in the record and the biomechanical specificities of the hominin elbow joint, Plio-Pleistocene specimens from both eastern and southern Africa have nonetheless been the matter of frequent controversial attributions (rev. in Domínguez-Rodrigo et al., 2013; Lague, 2015).

Compared to humans, the surface morphology of the distal humerus of *Paranthropus* is reported to show a mediolaterally broader and anteroposteriorly flatter distal shaft cross section (but see Domínguez-Rodrigo et al., 2013 for OH 80–10) with a more medially elongated articular surface, a more prominent coronoid fossa and a position of the lateral epicondyle above the upper edge of the capitulum (rev. in Di Vincenzo et al., 2015). Conversely, a poorly distinct coronoid area, a more distal positioning of the lateral epicondyle relative to the capitulum, a thick and medially oriented medial epicondyle (epitrochlea), a more vertically developed (thus, sub-rounded) and anteriorly projecting capitulum, and a proportionally anteroposteriorly expanded contour of the distal shaft are more typical human features (e.g., Di Vincenzo et al., 2015; Domínguez-Rodrigo et al., 2013; Lague, 2014; Susman, 1989; Susman et al., 2001). Also, the presence of a distally flaring sharp

supracondylar crest, also present in apes (Lague, 2015), seems more common in later *Homo* than in *Paranthropus*, even if rather variable in its occurrence and degree of development within the same fossil sample (Lague, 2015). For the inner structural organization, a thicker cortical bone and the diffuse presence of trabeculae nearly obstructing the most distal portion of the medullary cavity have also been reported as common features in *Paranthropus* (Domínguez-Rodrigo et al., 2013; Susman et al., 2001).

Besides the interspecific differences, a certain degree of intraspecific variation in fossil hominin distal humeral shaft morphology has been reported (Domínguez-Rodrigo et al., 2013; Feuerriegel et al., 2016; Lague, 2014, 2015). Notable inter-population variation in humeral shape (more elliptical vs. more circular diaphyses) has been measured also in *Pan troglodytes*, and could partly be attributed to differences in activity levels (Carlson et al., 2008). With this respect, the role of the still poorly determined extent of intraspecific sexual dimorphism is commonly evoked (e.g., Domínguez-Rodrigo et al., 2013; Feuerriegel et al., 2016; Lague, 2014).

Given the well-documented ability of long bones to adjust structurally to their loading environment, i.e. of recording relevant biomechanical information during life, but also of preserving the signature of their genetic-related evolutionary adaptive *bauplan* (Carlson and Marchi, 2014; Carlson et al., 2008; Currey, 2002; Gosman et al., 2011; Kivell, 2016; Lieberman et al., 2004; Lovejoy et al., 1999; Middleton et al., 2008; Nadell and Shaw, 2015; Pearson and Lieberman, 2004; Ruff et al., 2006; Ryan and Shaw, 2013; Smith-Adaline et al., 2004; Volkman et al., 2003; Wallace et al., 2010, 2012), an increasing number of studies use high resolution imaging techniques to reveal the inner structure of the fossil hominin humerus (e.g., Kappelman et al., 2016; Ruff et al., 2016; Ryan and Sukhdeo, 2016).

In this study, we noninvasively explored and quantitatively characterized the still unreported endostructural organization of five early Pleistocene distal humeri from South Africa (TM 1517g, SK 24600, SKX 10924, SKX 34805) and Ethiopia (Gombore IB), which have been variably attributed to *Paranthropus* or *Homo* (rev. in Lague, 2015). By assuming that the inner features at this skeletal site – notably, cross-sectional geometric properties and cortical bone topography – are taxon-specific to an extent comparable to the outer morphological signature, which has been commonly considered in their taxonomic assessment, we compare for their coherence the two signals.

Specifically, we expect that the inner structural arrangement of the South African fossils attributed to *Homo* (notably, SKX 34805 and, likely, SK 24600; Lague, 2015) will more closely resembles that of the *Homo* aff. *erectus* distal humerus Gombore IB than the endostructural signature of those specimens commonly attributed to *Paranthropus* (i.e. TM 1517g and SKX 10924).

2. Materials and methods

2.1. Materials

Information on the five fossil hominin distal humeri considered in the present study (TM 1517g, SK 24600, SKX 10924, SKX 34805, and MK 76 GOM IB 7594), all undistorted and sampling nearly or full adult individuals, is summarized in Table 1. They are permanently stored at the Ditsong National Museum of Natural History, Pretoria (TM 1517g and SK 24600), the Evolutionary Studies Institute at the University of the Witwatersrand, Johannesburg (SKX 10924 and SKX 34805), and at the National Museum of Ethiopia, Addis Ababa (MK 76 GOM IB 7594).

Originally reported by Broom (1938a) and detailed by Straus (1948), TM 1517g is an incomplete but well-preserved right distal humerus from the South African site of Kromdraai B (KB), part of the type specimen of *Paranthropus robustus* (Broom, 1938b; Broom and Schepers, 1946), which represents a dentally late adolescent individual (Braga et al., 2016a). More recent field work and material revision (rev. in Braga and Thackeray, 2016) suggest that, while commonly referred to KB Member 3 (e.g., Herries et al., 2009; Skinner et al., 2013; Thackeray et al., 2001; Vrba, 1981), TM 1517g and the purportedly associated remains are possibly from Member 5 (Braga et al., 2016a, b; but see Bruxelles et al., 2016: 42).

SK 24600 is a 2.3-1.6 Ma old distal part of an intact left humerus from Swartkrans Member 1, South Africa, preserving approximately the same anatomical region as the specimen SKX 10924. In its original description, Susman and co-workers (Susman et al., 2001: 617) stated that "(t)hese differences, and comparisons with TM 1517 and KNM-ER 271 as well as with modern humans, chimpanzees and bonobos, suggest that SK 24600 samples *Paranthropus*." However, based on the results of a recent geometric morphometric (GM) comparative analysis, this specimen has been allocated to early *Homo* (Lague, 2015).

SKX 10924, chronologically the most recent among the fossil specimens examined here ($\leq$ 1.0 Ma), is an intact distal left humeral end from Swartkrans Member 3, which has been described by Susman et al. (2001). Based on comparisons with SKX 34805 (Susman, 1989), and notably because of its "rounded" cross section, this specimen was originally allocated to *Homo* and was suggested to represent a small body-sized, probably female individual (Susman et al., 2001: 616). However, while it has been noted that SKX 10924 is considerably smaller than the TM 1517 g *P. robustus* specimen from Kromdraai (Susman et al., 2001), McHenry and Brown (2008) still included it among the remains more likely sampling *P. robustus* (see also Grine, 2005a). Even if still listed among the human remains by Dusseldorp et al. (2013: Suppl. Mat.; see Herries et al., 2009), an attribution of SKX 10924 to *Paranthropus* has been recently supported also by GM analyses (Lague, 2014, 2015).

SKX 34805 is a 2.3–1.6 Ma old distal part of a right humerus from Swartkrans Member 1 lacking a portion of each condyle, as well as the trochlea and the capitulum (Susman, 1989). In its original description, Susman stated that "(t)his specimen is a reasonably good match for TM 1517 in both size and shape, and on this basis it most likely belongs to *Paranthropus*" (Susman, 1989: 462). However, based on its cross-sectional shape and comparisons with the expanded record at Swartkrans, this specimen has since been allocated to *Homo* (Lague, 2015; Susman et al., 2001;

Table 1
The fossil specimens used in the present study.
Tableau 1
Les spécimens fossiles inclus dans cette étude.

Specimen	Site	Age (Ma)	Taxonomic attribution[a]	References
TM 1517g	Kromdraai (possibly Member 5[b]), South Africa	~2.0?[c]	*Paranthropus robustus*	Braga et al., 2016a, b; Broom, 1938b; Broom and Schepers, 1946; Bruxelles et al., 2016; Churchill et al., 2013; Di Vincenzo et al., 2015; Lague, 2014, 2015; Lague and Jungers, 1996; McHenry and Brown, 2008; Ryan and Sukhdeo, 2016; Senut, 1981a; Skinner et al., 2013; Straus, 1948; Susman, 1989; Susman et al., 2001; Thackeray et al., 2001
SK 24600	Swartkrans, Member 1, South Africa	2.3–1.6[c]	*Paranthropus robustus*	Churchill et al., 2013; Lague and Jungers, 1996; McHenry and Brown, 2008; Ryan and Sukhdeo, 2016; Susman et al., 2001
			early *Homo*	Lague, 2014, 2015
SKX 10924	Swartkrans, Member 3, South Africa	≤ 1.0[d]	*Paranthropus robustus*	Churchill et al., 2013; Lague, 2014, 2015; McHenry and Brown, 2008; Ryan and Sukhdeo, 2016
			Homo sp.	Susman et al., 2001; Dusseldorp et al., 2013 (in Suppl. Mat.)
SKX 34805	Swartkrans, Member 1, South Africa	2.3–1.6[c]	*Paranthropus robustus*	Susman, 1989
			early *Homo*/ *Homo* aff. *erectus*	Dusseldorp et al., 2013 (in Suppl. Mat.); Lague, 2015; Susman et al., 2001
MK 76 GOM IB 7594 (GOM IB)	Gombore I, Melka Kunture, Ethiopia	1.6–1.5[e]	*Homo* aff. *erectus*	Carretero et al., 2009; Chavaillon et al., 1977; Churchill et al., 2013; Di Vincenzo et al., 2015; Puymerail et al., 2014; Ryan and Sukhdeo, 2016; Senut, 1979, 1981a, b

[a] In some papers cited in this study, the taxon *Paranthropus* is subsumed within *Australopithecus*.
[b] Braga et al., 2016a, b; Bruxelles et al., 2016.
[c] Balter et al., 2008; Curnoe et al., 2001; Gibbon et al., 2014; Pickering et al., 2011; Vrba, 1981, 1985.
[d] Balter et al., 2008; Brain, 1993; Gibbon et al., 2014; Herries et al., 2009.
[e] Morgan, 2014 (pers. comm. to R.M.); Morgan et al., 2012; Tamrat et al., 2014.

see also Dusseldorp et al., 2013), more specifically, to *H.* aff. *erectus* (Lague, 2015).

Finally, Gombore IB (MK 76 GOM IB 7594, hereafter GOM IB) is a finely preserved distal third of a left humerus from a *Homo* aff. *erectus* robust individual. It was discovered in 1976 in the Oldowan tool-bearing level of Gombore I, one of the early to middle Pleistocene localities forming the Melka Kunture archaeological and paleontological site complex along the Upper Awash Valley, on the Ethiopian highlands (Chavaillon and Piperno, 2004; Gallotti and Mussi, 2015). Originally reported by Chavaillon and co-workers (1977) and by Senut (1979; see also Senut, 1981a, b), GOM IB has been more recently investigated by Puymerail et al. (2014) and by Di Vincenzo et al. (2015). A refinement of the chronologies at Melka Kunture (Morgan et al., 2012; Tamrat et al., 2014) indicates that GOM IB is 1.6-1.5 Ma old (Morgan, 2014: pers. comm. to R.M.), thus just slightly younger than the juvenile human partial mandible from the nearby site of Garba IV (Zanolli et al., 2016).

For this study, we used an extant human (EH) sample consisting of twelve adult humeri selected from the Pretoria Bone Collection stored in the Department of Anatomy at the University of Pretoria, South Africa (L'Abbé et al., 2005). The sample includes two male and four female individuals of African origin aged 23–29 years, and four male and two female European-derived individuals aged 41–58 years. All specimens used in this study lack any macroscopic evidence of outer or inner alteration or pathological change.

2.2. Methods

The South African fossil specimens TM 1517g, SK 24600, SKX 10924 and SKX 34805 and the twelve humeri forming the extant human comparative sample (EH) have been scanned between 2015 and 2016 at the micro-focus X-ray tomography facility (MIXRAD) of the South African Nuclear Energy Corporation (Necsa), Pelindaba, at resolutions ranging from 33 μm (fossil specimens) to 90 μm isotropic voxel size (EH sample) using a Nikon XTH 225 ST equipment (Hoffman and de Beer, 2012). Acquisition parameters for each of the four fossil specimens were as follow: 125 kV and 110 mA current, with a frame rate of 4 frames per second and an angular increment of 1000/360° resulting in an exposure time of 0.25 s/projection; 0.10 mm of aluminium was used to "pre-filter" low-energy X-rays. The specimen GOM IB from Melka Kunture was scanned in 2013 at the Wudassie Diagnostic Centre of Addis Ababa, Ethiopia, using a Philips Brilliance16 medical CT equipment according to the following parameters: 140 kV voltage, 100 mA current, 1.76 s exposition time per projection, slice thickness of 0.6 mm, reconstruction increment of 0.3 mm (see Zanolli et al., 2016). The final volume was reconstructed with a voxel size of 147 × 147 × 300 μm. In all cases, special care was taken in orienting each specimen

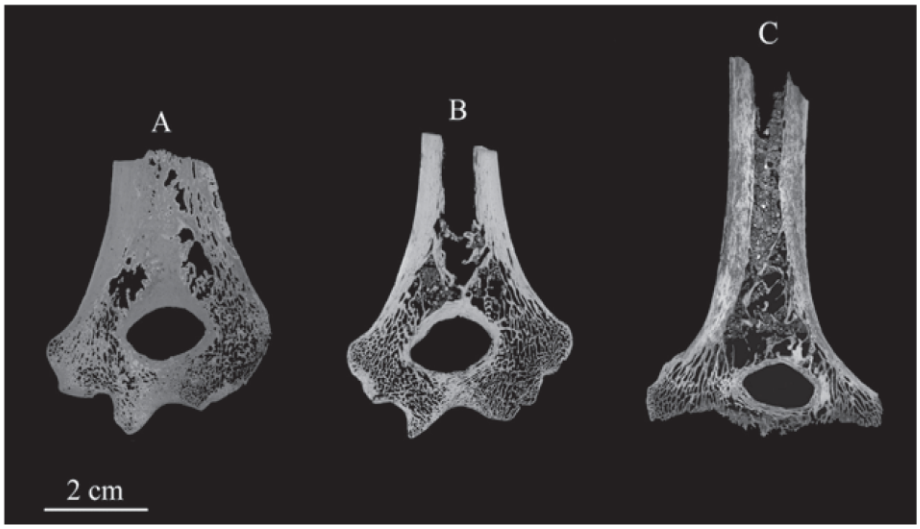

Fig. 1. µCT-based coronal slice of SK 24600 (A), SKX 10924 (B) and SKX 34805 (C), all from the site of Swartkrans, South Africa. Note their variable degree of inner preservation and the sedimentary infill and degree of mineralisation in SK 24600.
Fig. 1. Coupe coronale extraite des données µCT de SKX 24600 (A), SKX 10924 (B) et SKX 34805 (C) provenant du site de Swartkrans, Afrique du Sud. Noter le degré variable de conservation de la structure interne et du remplissage sédimentaire, ainsi que le degré de minéralisation pour SK 24600.

in a standardized way during acquisition (see comments in Wilson and Humphrey, 2015). Each diaphyseal axis was assessed as perpendicular to the coronal axis through the most medial and the most lateral points of the two epicondyles (the biepicondylar line). Coherence in orientation was then checked on the virtually reconstructed 3D models and, if needed, manually corrected by using Avizo© v.8.1 (Visualization Sciences Group Inc.).

In order to virtually isolate the cortical shell from the matrix variably filling the fossil specimens, to image their preserved inner morphology, and to quantify the cortical volume, a semi-automatic threshold-based segmentation with manual corrections was carried out (Spoor et al., 1993; see also Meyer and Beucher, 1990; Roerdink and Meijster, 2000) by using Avizo© v.8.1 (Visualization Sciences Group Inc.). In principle, while time-consuming because of frequent manual interventions, the segmentation process of SKX 10924, SKX 34805, and GOM IB did not present technical problems. As their endosteal contours were generally distinct at most shaft levels, the results of repeated performances independently run by two (in some cases, three) trained observers were consistent. However, because of its pervasive matrix infill, in SK 24600 the endosteal border was nearly invariably indistinguishable (Fig. 1), which presented challenges in using this specimen for the specific purposes of the present study (see infra section 3.1.). Also, some technical problems were encountered during the segmentation of TM 1517g, notably in precisely defining the endosteal contour along its lateral aspect.

Following the protocol established by Susman et al. (2001), and also adopted by Lague (2015), on each specimen we extracted a cross-sectional slice *a* at the humeral distal end, perpendicular to the major diaphyseal axis, approximately at the root of the medial crest slope, proximally to the biepicondylar line (Fig. 2). For the comparative assessment of proximodistal trends of thickness variation in cortex distribution across the shaft and for their 3D imaging, in all specimens except for the least preserved TM 1517g, we established an additional cross-sectional slice *b*, parallel to *a*, defined as the most proximal diaphyseal section (i.e. the most distant from *a*) preserving a complete periosteal and endosteal contour (Fig. 2). In our fossil sample, the maximal *a*–*b* distance is found in GOM IB, which also preserves the absolute longest shaft portion (biomechanical length in GOM IB has been estimated at ca. 339 mm, and its preserved shaft portion comprised between ca. 12% distally to ca. 30% proximally; Puymerail et al., 2014). However, to allow comparisons, we considered as reference the *a*–*b* distance found in SKX 34805 (36.4 mm), i.e. that of the second best preserved shaft following GOM IB. In SKX 10924, this distance measures 15.6 mm. However, it should be taken into account here that, because of the different preservation conditions among the investigated specimens and in the absence of percentages of their overall diaphyseal length, the shaft portions *a*–*b* do not necessarily fully coincide. Nonetheless, we estimate such differences as minimal and of negligible biomechanical relevance.

By using ImageJ and a custom macro (MomentMacro, available at: www.hopkinsmedicine.org/fae/mmacro.htm), at virtual slice level *a* we assessed the following cross-sectional geometric parameters (CSG) reflecting bone shaft morphological and rigidity characteristics: percent of cortical area (%CA), an estimate of resistance to compressive and tensile axial loading; the ratios second (I_x/I_y) and principal (I_{max}/I_{min}) moments of area, with the former ratio being a better estimate of rigidity about AP and ML anatomical planes and the latter shape ratio being the best reflection of true cross-sectional shape (Carlson, 2014; Ruff, 2002, 2008; Trinkaus and Ruff, 2012).

Cortical thickness varies topographically within each section and at various cross-sectional levels (for a schematic representation, see fig. 14.6 in White et al.,

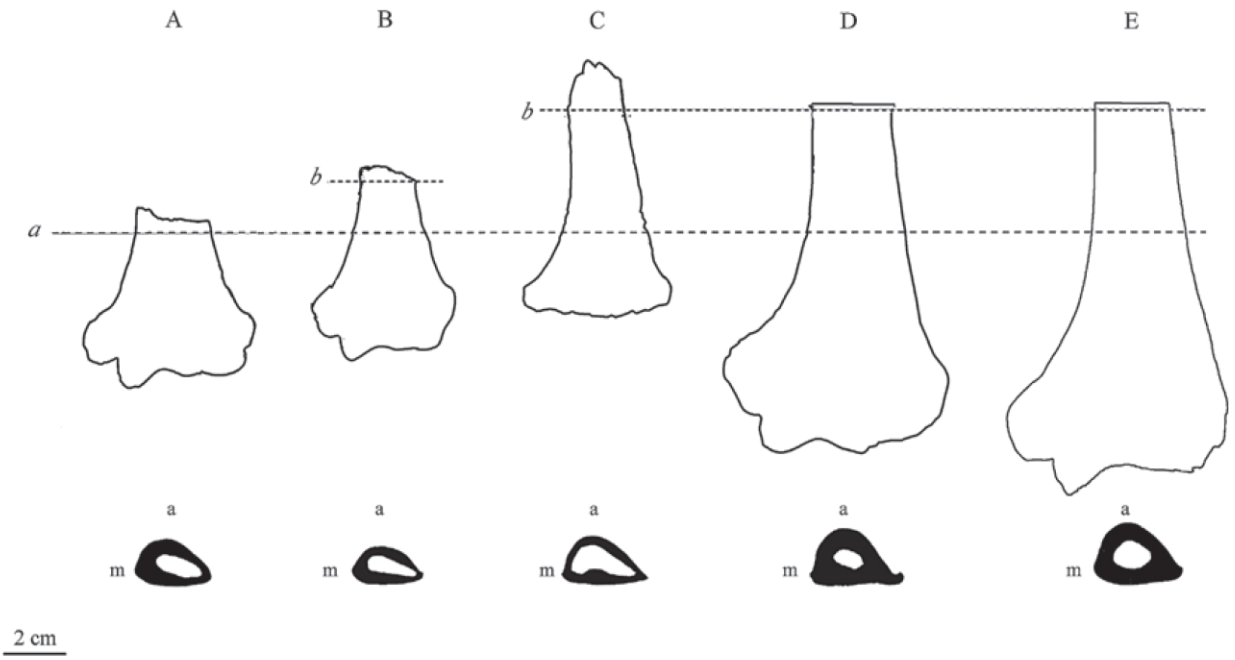

Fig. 2. Anterior view outline (upper row) and sketch of the cross section at level *a* (lower row) of the South African distal humeri TM 1517g (A), SKX 10924 (B) and SKX 34805 (C), of the Ethiopian specimen GOM IB (D), and of an extant human (EH) humerus. TM 1517g (A) and SKX 34805 (C) have been mirrored to be left. See the text (*2.2. Methods*) for details about the cross-sectional level *b*. The *a*–*b* distance measures 15.6 mm in SKX 10924 (B) and 36.4 mm in the remaining specimens. a: anterior; m: medial.

Fig. 2. Contours en vue antérieure (en haut) et schémas de la section extraite au niveau *a* (en bas) des huméri distaux sud-africains TM 1517g (A), SKX 10924 (B) et SKX 34805 (C), du spécimen éthiopien GOM IB (D) et d'un humérus humain actuel (EH). Un effet miroir a été appliqué pour TM 1517g (A) et SKX 34805 (C) afin d'obtenir des huméri gauches. Voir le texte (*2.2. Methods*) pour les détails à propos du niveau *b* de la coupe. La distance *a*–*b* est de 15,6 mm chez SKX 10924 (B) et de 36,4 mm pour les autres spécimens. A : antérieur ; m : médial.

2012). Accordingly, for the *a*–*b* shaft portion, we calculated a scale-free bi- (2D) and three-dimensional (3D) Relative Cortical Thickness (RCT) similarly to the analytical protocols used to allow a reliable comparative assessment of tooth enamel thickness variation in analyses using differently sized and shaped teeth (e.g., Grine, 2005b; Kono, 2004; Macchiarelli et al., 2006; Martin, 1985; Olejniczak et al., 2008). The 2D RCT is the average cortical thickness (2D ACT) multiplied by 100 and divided by the square root of the medullary cavity area (ma, in mm^2) (2D RCT = 2D ACT $\times$ 100/$ma^{1/2}$), where 2D ACT is the ratio between cortical area (CA, in mm^2) and the endosteal contour length (ecl, in mm) (2D ACT = CA/ect, in mm); the 3D RCT is the average cortical thickness (3D ACT) multiplied by 100 and divided by the cube root of the medullary cavity volume (mv, in mm^3) (3D RCT = 3D ACT $\times$ 100/$mv^{1/3}$), where 3D ACT is the ratio between cortical volume (cv, in mm^3) and the area of the endosteal surface (aes, in mm^2) (3D ACT = cv/aes, in mm) (for the Relative Enamel Thickness, see technical details in Olejniczak et al., 2008). As the Relative Enamel Thickness (RET) provides a scale-free measure of the enamel tissue with respect to the dentine, which is especially appropriate for interspecies comparisons (Martin, 1985), the RCT finely assesses cortical bone thickness across a shaft portion with respect to the space occupied by the medullary cavity (and by the struts as well). This synthetic descriptor of bone thickness variation adds useful complementary information, notably at volumetric scale, to the traditional geometric parameters punctually assessed at cross-sectional level and allows a finer interpretation of the long bone morphometric maps (Bondioli et al., 2010).

Intra- and inter-observer tests for measurement accuracy showed differences less than 4%.

For each anatomical projection (i.e. anterior, posterior, medial and lateral views), cortical thickness topographic distribution between *a* and *b* has been virtually rendered in all fossil specimens except TM 1517g using a chromatic scale increasing from dark blue (thin) to red (thick) (Bayle et al., 2011; Bondioli et al., 2010; Mazurier et al., 2010; Puymerail, 2011, 2013; Puymerail et al., 2012; Volpato et al., 2011).

Given the variable degree of endostructural preservation of the South African specimens (see infra 3.1) and the modest resolution of the CT record available for the distal humerus from Melka Kunture, in this study we did not assess the textural properties of the cancellous network, but uniquely provided, whenever possible, information on the presence/absence and type of trabecular structures.

3. Results

3.1. Inner preservation

The fossil specimens considered in this study show a variable degree of inner preservation and quality of the structural signal, ranging from rather good to very poor. As previously noted for the cancellous network of some South African australopith iliac blades (Macchiarelli et al., 1999), the inner structural conservation is unrelated to the outer preservation conditions, and here it extensively varies between specimens from the same site (or even from the same Member, as is the case of SK 24600 and SKX 34805

from Swartkrans) and between areas within the same specimen (Fig. 1).

In TM 1517g, the cancellous struts at the very distal shaft portion and epiphyseal end are arranged in a distinctly appreciable network, even if the trabeculae boundaries are locally masked by a matrix infill. Conversely, in SK 24600 the entire cavity is filled by highly cemented permeating matrix, which nearly invariably inhibits the identification of the cortex-cavity boundary because of their close material contrast (Fig. 1A). Additionally, in this specimen, the preserved cancellous network has a low contrast between the bone and the matrix due to similar densities of the two entities which cannot be satisfactorily overcome by digital image processing of the currently available record. Accordingly, SK 24600 has been a posteriori excluded from all quantitative analyses performed in this study.

Among the investigated fossil specimens, SKX 10924 revealed the most finely preserved inner structure (Fig. 1B). However, while its cancellous network is virtually intact, the identification of the bone-cavity boundary was locally disturbed by the presence of a relatively thin matrix layer, which obliged us to carry out a number of manual corrections to the semi-automatic threshold-based segmentation. The last specimen from Swartkrans included in this study, SKX 34805 also showed a sufficiently well-preserved cancellous network but, compared to SKX 10924, it is variably filled with a consolidated matrix whose density was, anyhow, distinct enough from that of the cortex (Fig. 1C).

Finally, despite its medullary cavity being filled with matrix, the preservation conditions of the Ethiopian specimen GOM IB, where only the cancellous network at its distal end showed a low bone-matrix contrast, permitted an unambiguous segmentation of its cortex.

3.2. Structural arrangement and cortical thickness variation

At cross-sectional level *a*, a mediolaterally broad and proportionally anteroposteriorly flattened elliptically-shaped medullary cavity is noticeable in TM 1517g (M-L/A-P diameter ratio: 1.7), SKX 10924 (ratio: 1.9) and SKX 34805 (ratio: 1.8) (Fig. 2A-C), while GOM IB (Fig. 2D) shows a sub-ovoid outline (i.e. slightly more expanded anteroposteriorly compared to an elliptically-shaped outline; M-L/A-P diameter ratio: 1.6), more closely approaching the extant human condition represented in our comparative sample (Fig. 2E), where it varies from sub-ovoid to sub-rounded (mean ratio: 1.5 ± 0.15).

At this distal shaft level, notably towards the lateral aspect, a variable number of relatively thick trabecular struts, occasionally crossing the cavity at various points, are present in all fossil specimens, which is commonly not the case in extant humans (besides our reference sample, see also Diederichs et al., 2009). Struts are especially numerous and thick in SKX 10924 and, to a slightly minor extent,

Table 2
Cross-sectional geometric properties (CSG) of the distal humeral diaphysis assessed at section *a* (see Fig. 2) in four fossil specimens and in the extant human reference sample (EH). s.d.: standard deviation.
Tableau 2
Paramètres de géométrie de section (CSG) mesurés à la section *a* (voir Fig. 2) pour quatre spécimens fossiles et pour notre échantillon humain actuel de référence (EH). s.d. : déviation standard.

Specimen/ sample	%CA	I_x/I_y	I_{max}/I_{min}
TM 1517 g	75.7	0.43	2.43
SKX 10924	72.4	0.35	2.94
SKX 34805	62.9	0.40	2.51
GOM IB	89.7	0.51	2.33
extant humans (EH)	63.2	0.92	1.94
(s.d.)	(11.6)	(0.61)	(0.31)

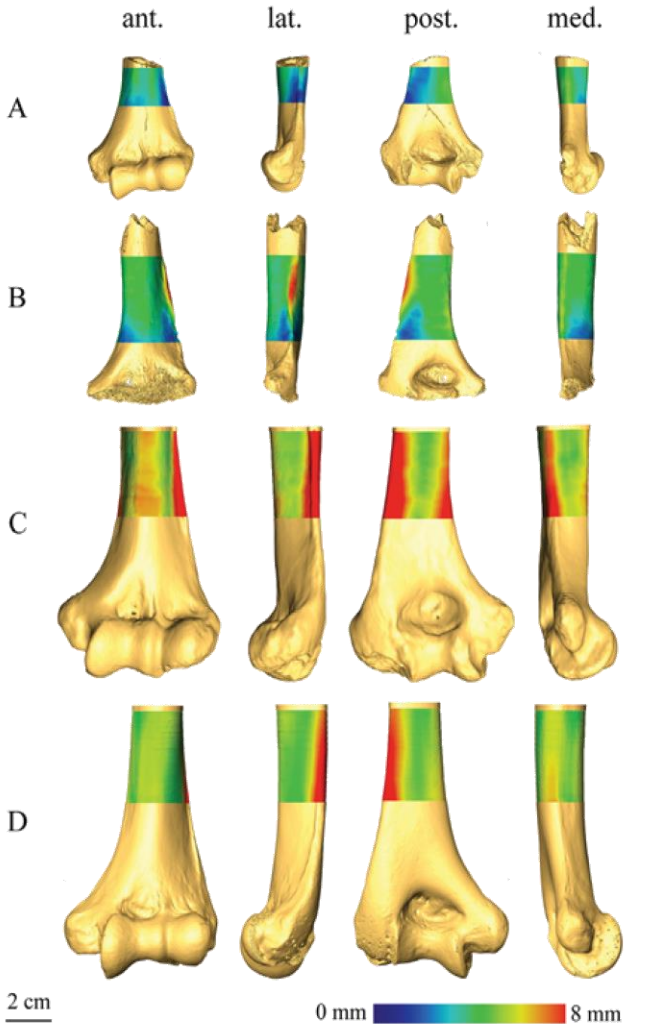

Fig. 3. (μ)CT-based maps of cortical bone thickness topographic distribution in anterior (ant.), posterior (post.), medial (med.), and lateral (lat.) views assessed along the shaft portion *a*–*b* (see Fig. 2) in the South African distal humeri SKX 10924 (A) and SKX 34805 (B), in the Ethiopian specimen GOM IB (C), and in an extant human (EH) humerus (D). SKX 34805 has been mirrored to be left. Thickness rendered by a chromatic scale increasing from dark blue (0 mm) to red (8 mm) for the *a*–*b* shaft portion (see Fig. 2).
Fig. 3. Reconstruction sur base microtomographique de la distribution topographique des variations d'épaisseur de l'os cortical dans la portion diaphysaire *a*–*b* (voir Fig. 2) des huméri distaux sud-africains SKX 10924 (A) et SKX 34805 (B), du spécimen éthiopien GOM IB (C) et d'un humérus humain actuel (EH, D) en vues antérieure (ant.), postérieure (post.), médiale (med.) et latérale (lat.). Un effet miroir a été appliqué pour SKX 34805 (B) afin d'obtenir un humérus gauche. Les épaisseurs sont représentées selon une échelle chromatique variant du bleu foncé (0 mm) au rouge (8 mm) pour la portion de diaphyse *a*–*b* (voir Fig. 2).

in SKX 34805, where they can locally form some plate-like structures (Gibson, 1985; Stauber and Müller, 2006), including towards the medial portion. Because of the permeating infill, the cancellous pattern is however difficult to discern in TM 1517g, but here the struts are uniquely confined to the lateral quadrant, which is not the case in the two fossils from Swartkrans. Given its mediolaterally narrower cavity, in GOM IB the struts are less numerous, even if not necessarily thinner than seen in SKX 10924 and SKX 34805.

The values of the CSG properties measured at section *a* are shown in Table 2. For the percent of cortical area (%CA), the highest value is shown by the distal humerus from Melka Kunture (89.7), which is over 2 standard deviations (s.d.) beyond the average expressed by our comparative extant human sample (63.2 ± 11.6). Among the South African specimens, TM 1517g shows the highest value (75.7), while the two distal humeri from Swartkrans fall within 1 s.d. (SKX 10924: 72.4), or just near the mean of the reference sample (SKX 34805: 62.9). As a whole, the pattern for %CA is: GOM IB » TM 1517g > SKX 10924 > extant humans ≈ SKX 34805.

Variation for the ratio of anteroposterior vs. mediolateral second moments of area (I_x/I_y) is modest among the South African fossils (range: 0.35 in SKX 10924 to 0.43 in TM 1517g), whose values are exceeded by both GOM IB (0.51) and, to a greater extent, by the modern reference sample (0.92 ± 0.61). Because of the mediolateral expansion at such a distal diaphyseal level observed in all specimens (i.e. the maximum rigidity is in the mediolateral direction), this pattern is almost systematically reversed for the maximum vs. minimum second moments of area (I_{max}/I_{min}), where the results of all fossils (range: 2.33 in GOM IB to 2.94 in SKX 10924) are from 2 s.d. (GOM IB, TM 1517g, SKX 34805) to 4 s.d. (SKX 10924) beyond the average value of the comparative human sample (1.94 ± 0.31).

According to four anatomical views, the morphometric maps of cortical bone thickness topographic variation across the shaft portion *a*–*b* in SKX 10924, SKX 34805, GOM IB, and in an extant human (EH) representative selected within our comparative sample because of its average cortical distribution (3D RCT values), are shown in Fig. 3. As previously specified, such virtual rendering was not technically possible for TM 1517g because of its too limited preserved portion.

While the limited preserved shaft portion of SKX 10924 precludes a detailed 1:1 comparison, the 3D maps confirm a closer affinity in cortical bone distribution pattern between the two specimens from Swartkrans, on one hand, and GOM IB and the average extant human condition, on the other hand, the latter invariably displaying absolutely and relatively thicker bone at all sites. Specifically, the South African fossils share relatively thicker bone across most of the posteromedial and the proximal part of the anterior aspects (in SKX 34805 the thickest bone corresponds to its relatively developed lateral supracondylar crest), and a thinner area along the distolateral portion of the posterior surface, a region where GOM IB and all modern human humeri conversely show thicker bone. In GOM IB, and in the comparative human sample as well, thinner bone is found anteriorly, anterolaterally (when the lateral supracondylar crest is not considered) and along the mid-third of the posterior aspect. Similarly to SKX 34805 and to the extant human figures, cortical thickening in GOM IB indeed corresponds here to a well-developed and vertically extended lateral supracondylar crest forming the sharp pinched and slightly undulating border of the distal shaft (Puymerail et al., 2014). Thickened bone in the Ethiopian specimen is also found along its medial crest, which is more marked in this *Homo* aff. *erectus* humerus compared to the two South African fossils.

Although the absolute values cannot be systematically compared, to determine the extent of the differences among the morphometric maps, we calculated the trends of proximodistal variation of the 2D RCT (Table 3). The results confirm a trend of cortical bone thinning in SKX 34805 (−66%) and, by contrast, of thickening in GOM IB (+61%). The incomplete signal from SKX 10924 (shorter *a*–*b* portion) basically supports the evidence from the other more complete shaft from Swartkrans (−42%). Variation for this parameter expressed by our human reference sample (from −60% thinning to +17% thickening) is marked and requires additional investigation, but at present we have no data enough to even tentatively relate such variation to any

Table 3
Bi- (2D RCT) and three-dimensional cortical thickness (3D RCT) of the distal humeral diaphysis assessed within the portion comprised between section *b* and section *a* (see Fig. 2) in three fossil specimens and in the extant human reference sample (EH).
Tableau 3
Épaisseur corticale de la diaphyse humérale mesurée en 2–3D sur une portion de diaphyse comprise entre la section *b* et la section *a* (voir Fig. 2) dans trois spécimens fossiles et dans notre échantillon humain actuel de référence (EH).

Specimen/ sample	2D RCT total shaft portion *b* to *a* % change	2D RCT anterior shaft portion *b* to *a* % change	2D RCT posterior shaft portion *b* to *a* % change	3D RCT total shaft portion proximal[a] to distal[b] % change
SKX 10924[c]	−42%	−30%	−18%	–
SKX 34805	−66%	−39%	−23%	−41%
GOM IB	+61%	+90%	+81%	+51%
extant humans (EH) (range)	−60% to +17%	−33% to +12%	−38% to +26%	−37% to +9%

[a] Proximal is the shaft portion comprised between *b* and the *a*–*b* mid-distance level (see Fig. 2); it is equal in location to SKX 34805 and GOM IB, but not to SKX 10924.
[b] Distal is the shaft portion comprised between the *a*–*b* mid-distance level and *a* (see Fig. 2); it is equal in location to SKX 34805 and GOM IB, but not to SKX 10924.
[c] In SKX 10924, proximal level *b* approximately corresponds to the *a*–*b* mid-distance level of SKX 34805 and GOM IB (see Fig. 2).

individual information available in our files (e.g., sex, age at death). The comparisons for 3D RCTs assessed in SKX 34805 and GOM IB for their relative proximal and distal portions of the *a*–*b* shaft segment provide the same indication of proportional global volumetric thinning in the South African (−41%) and of thickening in the Ethiopian (+51%) specimen. When the more variably shaped medial and lateral aspects are excluded and the 2D RCT is separately calculated for the anterior and the posterior portions at the same cross sections *a* and *b*, we note that the trend (thinning or thickening) is always more marked on the anterior aspect across the distal diaphysis, including in SKX 10924 (Table 3). Finally, even though variation in recent humans requires some in-depth analyses performed on larger samples, the amount of changes in cortical bone thickness expressed in our reference sample by the 3D RCT is lower than the measured variation in the three fossil specimens (Table 3), and is compatible with the evidence from other CT-based studies of clinical interest (e.g., Diederichs et al., 2009).

4. Discussion and conclusions

In his extensive GM-based study of the outer cross-sectional shape variation of a representative sample of eastern and southern African fossil hominin distal humeri, Lague (2015) identified the following four morphotypes (group configuration): *P. boisei* (OH 80, KNM-ER 739, 1504, 6020, 1591), *P. robustus* (TM 1517, SKX 10924; recently, the specimen DNH 32 from Drimolen, South Africa, has been added to this list; Lague and Menter, 2017), non-*erectus* early *Homo* (OH 62, ER 3735, SK 24600, SKX 19495, SK 2598), and *H. erectus* (WT 15000, ER 1808, SKX 34805). Following his results, distal humeri representing non-*erectus* early *Homo* are distinguishable because of their degree of relative anteroposterior flattening, while the morphology of *H. erectus* is more similar to that typical of more recent humans. In this context, *Paranthropus s.l.* specimens from both eastern and southern Africa are characterized by a morphology intermediate with respect to the features that differentiate non-*erectus* early *Homo* and *H. erectus*. Accordingly, the lower diaphyses of *P. boisei* (not considered in our study) and of non-*erectus* early *Homo* are "unusually AP flattened (ML broad) among both fossil hominins and extant hominids, though non-*erectus Homo* humeri are most extreme in this regard and markedly different from the more modern human-like specimens attributed to *H. erectus*" (Lague, 2015: 27). Fresh evidence from the *A. sediba*'s ulna shows that, in aspects of its size and shape, the outer morphology of its elbow, which shows adaptations to suspensory and climbing behaviours (Rein et al., 2017), falls within the range of variation of eastern and southern australopiths, including some specimens commonly attributed to *P. robustus*, such as TM 1517 and SK 10294 (Churchill et al., 2013).

For most structural parameters of the distal humerus considered in the present study, we schematically observed two main patterns: the first globally grouping the South African fossils, and the second pattern setting apart the specimen from Melka Kunture (GOM IB), more closely resembling the extant human condition. In principle, even if the southern African fossil sample provides evidence of variation, a "dichotomy" is found here for: (i) the elliptical (proportionally flatter) vs. the ovoid (proportionally more expanded anteroposteriorly) outline of the medullary cavity at the distal diaphyseal cross section *a*, even if, in this case, the position of SKX 34805 can be seen as intermediate; (ii) thinner vs. thicker cortices (%CA) as measured at the same cross-sectional level; (iii) a cortical bone distribution pattern of proximodistal thinning vs. thickening across the portion*a*–*b* (as revealed by the 2–3D Relative Cortical Thickness parameters). With special reference to the latter aspect, the results unequivocally distinguish GOM IB from the organizational pattern shared by the two specimens from Swartkrans available to us for such kind of analysis (SKX 10924 and SKX 34805) (see also Fig. 3).

Conversely, even if a tendency for "dichotomy" between GOM IB and the South African fossils is traceable for the I_x/I_y and I_{max}/I_{min} ratios, the differences at the most distal diaphyseal level are modest and a dominant maximum rigidity in the mediolateral plane is shown by all specimens. However, it should be also noted that, compared to the global pattern shown by the extant reference sample, the three South African fossils share a looser connection between the two ratios, indicating a more oblique orientation component of their maximum rigidity, i.e. a less stereotyped mediolateral maximum rigidity at the humeroulnar joint. With this respect, among the fossils considered in the present study, GOM IB is again the specimen more closely approaching the modern pattern, and also that displaying the most developed, thickest and vertically extended lateral supracondylar crest, i.e. the origin of *M. brachioradialis*. Differences in the development of such muscle, which is responsible for both flexion of the forearm and pronation of a supine forearm, and supination of a prone forearm, are associated in extant humans with differences in flexion to extension movement patterns at the elbow (Rhodes and Knüsel, 2005). Specifically, in humans the *M. brachioradialis* primarily acts as elbow stabilizer during flexion tasks (Boland et al., 2008). Nonetheless, it is also true that a certain variation in the degree of expression of the supracondylar crest, as well as in the differences between maximum second moment of area, I_{max}, and second moment of area in the mediolateral plane, I_y (range: from 0 up to 48%) are present even within our limited reference sample.

Because of a number of reasons explained in the methodological section, in this study we did not systematically assess the textural properties of the cancellous network. It seems nonetheless interesting to note that, besides the ambiguous evidence from TM 1517g because of its low bone-matrix contrast, the two specimens from Swartkrans share the presence of more numerous and thick struts, locally resulting into a more closed network of plate-like structures from the accumulation of more material in the cell wall (Dalstra and Huiskes, 1995; Gibson, 1985; Stauber and Müller, 2006). At any comparable site, struts are invariably thicker in the fossil specimens than in the extant human humeri available to us, which is consistent with the process of skeletal gracilisation and trabecular bone density reduction occurred in recent humans (Chirchir et al., 2015, 2017; Ryan and Shaw, 2015). It is also noticeable that the medullary cavity of the OH

80-10 distal humerus fragment from the *P. boisei* partial skeleton of Olduvai Gorge, Tanzania, is filled by trabecular bone (Domínguez-Rodrigo et al., 2013). On the other hand, probably because of its narrower lumen resulting from a thicker cortex, GOM IB displays less numerous and less projecting struts, mostly confined to the very distal end.

When our results are considered in a taxonomic perspective, we note that the first pattern more coherently associates two likely *Paranthropus* representatives – TM 1517g from Kromdraai and SKX 10924 from Swartkrans – to a specimen more likely representing early *Homo* or *H.* aff. *erectus*– SKX 34805, again from Swartkrans. The second pattern unambiguously distinguishes the distal humerus of *Homo* aff. *erectus* from Melka Kunture from all other specimens, and frequently even clusters it near the extant human condition. Additionally, in this limited fossil assemblage, the closest endostructural signatures are clearly shown by SKX 10924 (even if incomplete) and SKX 34805. Relevant here also the evidence that the thickest cortex at any site across the distal shaft end is found in GOM IB (*Homo*) and not in any *Paranthropus*. Whenever SKX 34805 and GOM IB are grouped as conspecific (Lague, 2015), or at least congeneric (Susman et al., 2001), among the fossil specimens used in the present study they respectively show the absolutely lower (%CA: 62.9) and higher (%CA: 89.7) amount of cortical bone at section *a*.

Indeed, a relevant result here concerns the structural differences measured between SKX 34805 and GOM IB in their relative and absolute amount of cortical bone and distribution pattern shown across a comparable portion of 36.4 mm at the distal humeral shaft. This shows that even specimens with similar diaphyseal shape (Lague, 2015) may differ substantially in relative cortical thickness. Variations in the amount of cortical bone tissue (commonly measured by %CA) reflect site-specific differences in the bone's ability to buffer pure axial compression and tension, i.e. differential structural reinforcements of the diaphysis (Ruff, 2008; Trinkaus and Ruff, 2012). Accordingly, even if we cannot discard here the possible influence on the endostructural bony arrangement of sex-related (or even of age-related) differences, nor that of a different handedness (for a recent discussion on hand specialization in early *Homo*, see Frayer et al., 2016; for its impact on humeral cross-sectional shape variation and cortical bone thickness distribution, see Lague, 2015 and Volpato et al., 2012, respectively), we anyhow assume that the two distinct conditions ("patterns") revealed by the South African and the Ethiopian specimens, whatever their taxonomic status, are primarily functionally-related and have biomechanical significance in terms of distal humeral strength.

In this perspective, we conclude that the taxonomic status of SKX 34805, which apparently combines a relatively *Homo*-like outer shape (Lague, 2014, 2015) with a more *Paranthropus*-like inner structural organization of the distal humerus (present study), deserves further investigation.

Acknowledgments

The present study contributes to the thematic issue of the *Comptes rendus Palevol* "Hominin biomechanics, virtual anatomy and inner structural morphology: From head to toe. A tribute to Laurent Puymerail", promoted by C. Zanolli and R. Macchiarelli. Some of the authors were fortunate enough to interact with Laurent and to benefit from his unique research work, unfortunately unfinished, on the structural organization of the distal humerus from Melka Kunture.

This version greatly benefited from the competent critical comments provided by three reviewers. We also acknowledge the valuable suggestions provided by K.J. Carlson (Johannesburg and Los Angeles), M.R. Lague (Galloway) and D. Marchi (Pisa) during various phases of this study. For access to the fossil and comparative materials stored in South Africa, we are especially grateful to the curators of the Ditsong National Museum of Natural History, Pretoria, and the Pretoria Bone Collection at the Department of Anatomy of the University of Pretoria. Within the activities of the Italian Archaeological Mission at Melka Kunture and Balchit, authorization for performing the CT-scan record of MK 76 GOM IB 7594 was provided by the Authority for Research and Conservation of Cultural Heritage (ARCCH) of the Federal Democratic Republic of Ethiopia, and R.M. acknowledges for their kind support Y. Assefa, M. Mussi, Y.D. Tsegaye and Y. Yilma. For technical collaboration, scientific contribution and/or discussion, we are very grateful to L. Bam (Pelindaba), A. Beaudet (Johannesburg), J. Benoit (Johannesburg), B. Billings (Johannesburg), L. Bruxelles (Toulouse and Johannesburg), R.J. Clarke (Johannesburg), M. Domínguez-Rodrigo (Madrid), J. Dumoncel (Toulouse), D. Hailu (Addis Ababa), K. Jakata (Johannesburg), T. Jashashvili (Johannesburg), L. Kgasi (Pretoria), D. Marchi (Pisa), A. Mazurier (Poitiers), S. Potze (Pretoria), C. Ridel (Pretoria), D. Stratford (Johannesburg), C. Theye (Pretoria), V. Volpato (Fribourg), C. Zanolli (Toulouse), B. Zipfel (Johannesburg). We acknowledge the DST-NRF for the financial support (Grant # UID23456) to establish the MIXRAD micro-focus X-ray tomography facility at Necsa. M.C. is funded by the European Commission (EACEA), Erasmus Mundus programme, AESOP and AESOP+ consortia coordinated by J.B.

References

Bacon, A.-M., 2000. Principal components analysis of distal humeral shape in Pliocene to recent African hominids: the contribution of geometric morphometrics. Am. J. Phys. Anthropol. 111, 479–487.

Balter, V., Blichert-Toft, J., Braga, J., Telouk, P., Thackeray, F., Albarède, F., 2008. U-Pb dating of fossil enamel from the Swartkrans Pleistocene hominid site. South Africa. Earth Planet. Sci. Lett. 267, 236–246.

Bayle, P., Bondioli, L., Macchiarelli, R., Mazurier, A., Puymerail, L., Volpato, V., Zanolli, C., 2011. Three-dimensional imaging and quantitative characterization of human fossil remains. Examples from the NESPOS database. In: Macchiarelli, R., Weniger, G.-C. (Eds.), Pleistocene databases. acquisition, storing, sharing. Wissenschaftliche Schriften des Neanderthal Museums 4, Mettmann, pp. 29–46.

Berger, L.R., de Ruiter, D.J., Churchill, S.E., Schmid, P., Carlson, K.J., Dirks, P.H.G.M., Kibii, J.M., 2010. *Australopithecus sediba*: a new species of *Homo*-like australopith from South Africa. Science 328, 195–204.

Berger, L.R., Hawks, J., de Ruiter, D.J., Churchill, S.E., Schmid, P., Delezene, L.K., Kivell, T.L., Garvin, H.M., Williams, S.A., DeSilva, J.M., Skinner, M.M., Musiba, C.M., Cameron, N., Holliday, T.W., Harcourt-Smith, W., Ackermann, R.R., Bastir, M., Bogin, B., Bolter, D., Brophy, J., Cofran, Z.D., Congdon, K.A., Deane, A.S., Dembo, M., Drapeau, M., Elliott, M.C., Feuerriegel, E.M., Garcia-Martinez, D., Green, D.J., Gurtov, A., Irish, J.D., Kruger, A., Laird, M.F., Marchi, D., Meyer, M.R., Nalla, S., Negash, E.W., Orr, C.M., Radov_ci_c, D., Schroeder, L., Scott, J.E., Throckmorton, Z., Tocheri, M.W., VanSickle, C., Walker, C.S., Wei, P., Zipfel, B., 2015. *Homo*

naledi, a new species of the genus *Homo* from the Dinaledi Chamber, South Africa. eLife 4, 1–35.
Boland, M.R., Spigelman, T., Uhl, T.L., 2008. The function of brachioradialis. J. Hand Surg. 33, 1853–1859.
Bondioli, L., Bayle, P., Dean, C., Mazurier, A., Puymerail, L., Ruff, C., Stock, J.T., Volpato, V., Zanolli, C., Macchiarelli, R., 2010. Technical note. Morphometric maps of long bone shafts and dental roots for imaging topographic thickness variation. Am. J. Phys. Anthropol. 142, 328–334.
Braga, J., Thackeray, J.F., 2016. Kromdraai, a birthplace of *Paranthropus* in the cradle of humankind. Sun Press, Johannesburg.
Braga, J., Thackeray, J.F., Bruxelles, L., Dumoncel, J., Fourvel, J.-B., 2016b. Stretching the time span of hominin evolution at Kromdraai (Gauteng, South Africa): recent discoveries. C.R. Palevol 16, 58–70.
Braga, J., Dumoncel, J., Duployer, B., Tenailleau, C., de Beer, F., Thackeray, J.F., 2016a. The Kromdraai hominins revised with an updated portrayal of differences between *Australopithecus africanus* and *Paranthropus robustus*. In: Braga, J., Thackeray, J.F. (Eds.), Kromdraai, a birthplace of *Paranthropus* in the cradle of humankind. Sun Press, Johannesburg, pp. 49–68.
Brain, C.K., 1993. Swartkrans: a cave's chronicle of early man. Transvaal Museum, Pretoria.
Broom, R., 1938a. Further evidence on the structure of the South African Pleistocene anthropoids. Nature 142, 897–899.
Broom, R., 1938b. The Pleistocene anthropoid apes of South Africa. Nature 142, 377–379.
Broom, R., Schepers, G.W.H., 1946. The South African Fossil Ape-M: the Australopithecinae, n. 2. Transvaal Museum Memoir, Pretoria.
Bruxelles, L., Maire, R., Couzens, R., Thackeray, J.F., Braga, J., 2016. A revised stratigraphy of Kromdraai. In: Braga, J., Thackeray, J.F. (Eds.), Kromdraai, a birthplace of *Paranthropus* in the cradle of humankind. Sun Press, Johannesburg, pp. 31–46.
Carlson, K.J., 2014. Linearity in the real world: an experimental assessment of nonlinearity in terrestrial locomotion. In: Carlson, K.J., Marchi, D. (Eds.), Reconstructing mobility. Environmental, behavioral and morphological determinants. Springer, New York, pp. 253–271.
Carlson, K.J., Marchi, D., 2014. In: Carlson, K.J., Marchi, D. (Eds.), Reconstructing mobility. Environmental, behavioral and morphological determinants. Springer, New York.
Carlson, K.J., Sumner, D., Morbeck, M., Nishida, T., Yamanaka, A., Boesch, C., 2008. Role of nonbehavioral factors in adjusting long bone diaphyseal structure in free-ranging *Pan troglodytes*. Int. J. Primatol. 29, 1401–1420.
Carretero, J.M., Haile-Selassie, Y., Rodriguez, L., Arsuaga, J.L., 2009. A partial distal humerus from the Middle Pleistocene deposits at Bodo, Middle Awash, Ethiopia. Anthropol. Sci. 117, 19–31.
Chavaillon, J., Chavaillon, N., Coppens, Y., Senut, B., 1977. Présence d'hominidé dans le site oldowayen de Gomboré I à Melka Kunturé, Ethiopie. C.R. Acad. Sci. Paris, Ser. D 285, 961–963.
Chavaillon, J., Piperno, M. (Eds.), 2004. Studies on the Early Paleolithic site of Melka Kunture, Ethiopia. Instituto Italiano di Preistoria e Protostoria, Florence.
Chirchir, H., Kivell, T.L., Ruff, C.B., Hublin, J.-J., Carlson, K.J., Zipfel, B., Richmond, B.G., 2015. Recent origin of low trabecular bone density in modern humans. PNAS USA 112, 366–371.
Chirchir, H., Ruff, C.B., Junno, J.-A., Potts, R., 2017. Low trabecular bone density in recent sedentary modern humans. Am. J. Phys. Anthropol. (online version).
Churchill, S.E., Holliday, T.W., Carlson, K.J., Jashashvili, T., Macias, M.E., Mathews, S., Sparling, T.L., Schmid, P., de Ruiter, D.J., Berger, L.R., 2013. The upper limb of *Australopithecus sediba*. Science 340, 1233477–1233481.
Curnoe, D., Grün, R., Taylor, L., Thackeray, F., 2001. Direct ESR dating of a Pliocene hominin from Swartkrans. J. Hum. Evol. 40, 379–391.
Currey, J.D., 2002. Bones: structure and mechanics. Princeton University Press, Princeton.
Dalstra, M., Huiskes, R., 1995. Load transfer across the pelvic bone. J. Biomech. 28, 715–724.
Diederichs, G., Issever, A.-S., Greiner, S., Linke, B., Korner, J., 2009. Three-dimensional distribution of trabecular bone density and cortical thickness in the distal humerus. J. Should. Elb. Surg. 18, 399–407.
Di Vincenzo, F., Rodriguez, L., Carretero, J.M., Collina, C., Geraads, D., Piperno, M., Manzi, G., 2015. The massive fossil humerus from the Oldowan horizon of Gombore I, Melka Kunture (Ethiopia, > 1.39 Ma). Quat. Sci. Rev. 122, 207–221.
Domínguez-Rodrigo, M., Pickering, T.R., Baquedano, E., Mabulla, A., Mark, D.F., Musiba, C., Pérez-González, A., 2013. First partial skeleton of a 1.34-million-year-old *Paranthropus boisei* from Bed II, Olduvai Gorge, Tanzania. PLoS ONE 8, e80347.
Dusseldorp, G., Lombard, M., Wurz, S., 2013. Pleistocene *Homo* and the updated Stone Age sequence of South Africa. S. Afr. J. Sci. 109, 1–7.
Feuerriegel, E.M., Green, D.J., Walker, C.S., Schmid, P., Hawks, J., Berger, L.R., Churchill, S.E., 2017. The upper limb of *Homo naledi*. J. Hum. Evol. 104, 155–173.
Frayer, D.W., Clarke, R.J., Fiore, I., Blumenschine, R.J., Pérez-Pérez, A., Martinez, L.M., Estebaranz, F., Holloway, R., Bondioli, L., 2016. OH-65: the earliest evidence for right-handedness in the fossil record. J. Hum. Evol. 100, 65–72.
Gallotti, R., Mussi, M., 2015. The unknown Oldowan: ~1.7-million-year-old standardized obsidian small tools from Garba IV, Melka Kunture, Ethiopia. PLoS ONE 10, e0145101.
Gibbon, R.J., Rayne, T., Sutton, M.B., Heaton, J.L., Kuman, K., Clarke, R.J., Brain, C.K., Granger, D.E., 2014. Quaternary geochronology cosmogenic nuclide burial dating of hominin-bearing Pleistocene cave deposits at Swartkrans, South Africa. Quat. Geochron. 24, 10–15.
Gibson, L.J., 1985. The mechanical behaviour of cancellous bone. J. Biomech. 18, 317–328.
Gosman, J.H., Stout, S.D., Larsen, C.S., 2011. Skeletal biology over the life span: a view from the surfaces. Am. J. Phys. Anthropol. 146, 86–98.
Grine, F.E., 2005a. Early *Homo* at Swartkrans, South Africa: a review of the evidence and an evaluation of recently proposed morphs. S. Afr. J. Sci. 101, 43–52.
Grine, F.E., 2005b. Enamel thickness of deciduous and permanent molars in modern *Homo sapiens*. Am. J. Phys. Anthropol. 126, 14–31.
Herries, A.I.R., Curnoe, D., Adams, J.W., 2009. A multi-disciplinary seriation of early *Homo* and *Paranthropus* bearing palaeocaves in southern Africa. Quat. Internat. 202, 14–28.
Hlusko, L.J., Reiner, W.B., Njau, J.K., 2015. A one-million-year-old hominid distal ulna from Olduvai Gorge, Tanzania. Am. J. Phys. Anthropol. 158, 36–42.
Hoffman, J.W., de Beer, F.C., 2012. Characteristics of the Micro-Focus X-ray tomography facility (MIXRAD) at Necsa in South Africa. In: 18th World Conference on non-destructive testing, Durban, South Africa.
Kappelman, J., Ketcham, R.A., Pearce, S., Todd, L., Akins, W., Colbert, M.W., Feseha, M., Maisano, J.A., Witzel, A., 2016. Perimortem fractures in Lucy suggest mortality from fall out of tall tree. Nature 537, 503–507.
Kivell, T.L., 2016. A review of trabecular bone functional adaptation: what have we learned from trabecular analyses in extant hominoids and what can we apply to fossils? J. Anat. 228, 569–594.
Kono, R.T., 2004. Molar enamel thickness and distribution patterns in extant great apes and humans: new insights based on a 3-dimensional whole crown perspective. Anthropol. Sc. 112, 121–146.
L'Abbé, E.N., Loots, M., Meiring, J.H., 2005. The Pretoria bone collection: a modern South African skeletal sample. Homo 56, 197–205.
Lague, M.R., 2014. The pattern of hominin postcranial evolution reconsidered in light of size-related shape variation of the distal humerus. J. Hum. Evol. 75, 90–109.
Lague, M.R., 2015. Taxonomic identification of Lower Pleistocene fossil hominins based on distal humeral diaphyseal cross-sectional shape. PeerJ 3, e1084.
Lague, M.R., Jungers, W.L., 1996. Morphometric variation in Plio-Pleistocene hominid distal humeri. Am. J. Phys. Anthropol. 101, 401–427.
Lague, M.R., Menter, C.G., 2017. DNH 32: a distal humerus of *Paranthropus robustus* from Drimolen, South Africa. Am. J. Phys. Anthropol. 162, S64 (255, abstract).
Lieberman, D.E., Polk, J.D., Demes, B., 2004. Predicting long bone loading from cross-sectional geometry. Am. J. Phys. Anthropol. 123, 156–171.
Lovejoy, C.O., Cohn, M.J., White, T.D., 1999. Morphological analysis of the mammalian postcranium: a developmental perspective. Proc. Nat. Acad. Sc. USA 96, 13247–13252.
Macchiarelli, R., Bondioli, L., Debénath, A., Mazurier, A., Tournepiche, J.F., Birch, W., Dean, M.C., 2006. How Neanderthal molar teeth grew. Nature 444, 748–751.
Macchiarelli, R., Bondioli, L., Galichon, V., Tobias, P.V., 1999. Hip bone trabecular architecture shows uniquely distinctive locomotor behaviour in South African australopithecines. J. Hum. Evol. 36, 211–232.
Martin, L.B., 1985. Significance of enamel thickness in hominoid evolution. Nature 314, 260–263.
Mazurier, A., Nakatsukasa, M., Macchiarelli, R., 2010. The inner structural variation of the primate tibial plateau characterized by high-resolution microtomography. Implications for the reconstruction of fossil locomotor behaviours. C.R. Palevol 9, 349–359.
McHenry, H.M., Brown, C.C., 2008. Side steps: the erratic pattern of hominin postcranial change through time. J. Hum. Evol. 55, 639–651.
Meyer, F., Beucher, S., 1990. Morphological segmentation. J. Vis. Comm. Image Represent. 1, 21–46.

Middleton, K.M., Shubin, C.E., Moore, D.C., Carter, P.A., Garland, T., Swartz, S.M., 2008. The relative importance of genetics and phenotypic plasticity in dictating bone morphology and mechanics in aged mice: evidence from an artificial selection experiment. Zoology 111, 135–147.
Morgan, L.E., Renne, P.R., Kieffer, G., Piperno, M., Gallotti, R., Raynal, J.-P., 2012. A chronological framework for a long and persistent archaeological record: Melka Kunture, Ethiopia. J. Hum. Evol. 62, 104–115.
Nadell, J.A., Shaw, C.N., 2015. Phenotypic plasticity and constraint along the upper and lower limb diaphyses of *Homo sapiens*. Am. J. Phys. Anthropol. 159, 410–422.
Olejniczak, A.J., Smith, T.M., Feeney, R.N., Macchiarelli, R., Mazurier, A., Bondioli, L., Radovčić, J., 2008. Dental tissue proportions and enamel thickness in Neandertal and modern human molars. J. Hum. Evol. 55, 12–23.
Patterson, B., Howells, W., 1967. Hominid humeral fragment from early Pleistocene of northwestern Kenya. Science 156, 64–66.
Pearson, O.M., Lieberman, D.E., 2004. The aging of Wolff's law: ontogeny and responses to mechanical loading in cortical bone. Yearb. Phys. Anthropol. 47, 63–99.
Pickering, T.R., Kramers, J.D., Hancox, P.J., de Ruiter, D.J., Woodhead, J.D., 2011. Contemporary flowstone development links early hominin bearing cave deposits in South Africa. Earth Planet. Sci. Lett. 306, 23–32.
Puymerail, L., 2011. Caractérisation de l'endostructure et des propriétés biomécaniques de la diaphyse fémorale : la signature de la bipédie et la reconstruction des paléo-répertoires posturaux et locomoteurs des Hominines. (PhD dissertation). Museum national d'histoire naturelle, Paris.
Puymerail, L., 2013. The functionally-related signatures characterizing the endostructural organisation of the femoral shaft in modern humans and chimpanzee. C.R. Palevol 12, 223–231.
Puymerail, L., Bondioli, L., Engda, B., Mazurier, A., Macchiarelli, R., 2014. The Early Pleistocene human distal humerus from Gombore I, Melka Kunture (Upper Awash basin, Ethiopia). Cortical bone topography and structural organization. Int. Symp. The Afr. Hum. Foss. Rec., 15–16 (Toulouse, http://www.tahfr.cnrs.fr, abstract).
Puymerail, L., Ruff, C.B., Bondioli, L., Widianto, H., Trinkaus, E., Macchiarelli, R., 2012. Structural analysis of the Kresna 11 *Homo erectus* femoral shaft (Sangiran, Java). J. Hum. Evol. 63, 741–749.
Rein, T.R., Harrison, T., Carlson, K.J., Harvati, K., 2017. Adaptation to suspensory locomotion in *Australopithecus sediba*. J. Hum. Evol. 104, 1–12.
Rhodes, J.A., Knüsel, C.J., 2005. Activity-related skeletal change in medieval humeri: cross-sectional and architectural alterations. Am. J. Phys. Anthropol. 128, 536–546.
Roerdink, J., Meijster, A., 2000. The watershed transform: definitions, algorithm and parallelization strategies. Fundam. Informat. 41, 178–228.
Ruff, C.B., 2002. Long bone articular and diaphyseal structure in Old World monkeys and apes. I. Locomotor effects. Am. J. Phys. Anthropol. 119, 305–342.
Ruff, C.B., 2008. Biomechanical analyses of archaeological human skeletons. In: Katzenberg, M.A., Saunders, S.R. (Eds.), Biological anthropology of the human skeleton. Alan R. Liss, New York, pp. 183–206.
Ruff, C.B., Burgess, M.L., Ketcham, R.A., Kappelman, J., 2016. Limb bone structural proportions and locomotor behavior in A.L. 288-1 ("Lucy"). PLoS ONE 11 (11), e0166095.
Ruff, C.B., Holt, B., Trinkaus, E., 2006. Who's afraid of the big bad Wolff? Wolff's law and bone functional adaptation. Am. J. Phys. Anthropol. 129, 484–498.
Ryan, T.M., Shaw, C.N., 2013. Trabecular bone microstructure scales allometrically in the primate humerus and femur. Proc. Roy. Soc. B 280, 20130172.
Ryan, T.M., Shaw, C.N., 2015. Gracility of the modern *Homo sapiens* skeleton is the result of decreased biomechanical loading. Proc. Nat. Acad. Sc. USA 112, 372–377.
Ryan, T.M., Sukhdeo, S., 2016. KSD-VP-1/1: Analysis of the postcranial skeleton using high-resolution computed tomography. In: Haile-Selassie, Y., Su, D.F. (Eds.), The Postcranial Anatomy of *Australopithecus afarensis*: new insights from KSD-VP-1/1. Vertebrate paleobiology and paleoanthropology Series. Springer, Dordrecht, pp. 39–62.
Senut, B., 1979. Comparison des hominidés de Gomboré IB et de Kanapoi : deux pièces du genre *Homo* ? Bull. Mem. Soc. Anthropol. Paris 6, 111–117.
Senut, B., 1981a. Outlines of the distal humerus in hominoid primates: application to some Plio-Pleistocene hominids. In: Chiarelli, B., Corruccini, R.S. (Eds.), Primate evolutionary biology. Springer-Verlag, Berlin, pp. 81–92.
Senut, B., 1981b. Humeral outlines in some hominoid primates and in Plio-Pleistocene hominids. Am. J. Phys. Anthropol. 56, 275–283.
Skinner, M.M., Kivell, T.L., Potze, S., Hublin, J.-J., 2013. Microtomographic archive of fossil hominin specimens from Kromdraai B, South Africa. J. Hum. Evol. 64, 434–447.
Smith-Adaline, E.A., Volkman, S.K., Ignelzi Jr., M.A., Slade, J., Platte, S., Goldstein, S.A., 2004. Mechanical environment alters tissue formation patterns during fracture repair. J. Orthop. Res. 22 (5), 1079–1085.
Spoor, F., Zonneveld, F., Macho, G., 1993. Linear measurements of cortical bone and dental enamel by computed tomography: applications and problems. Am. J. Phys. Anthropol. 91, 469–484.
Stauber, M., Müller, R., 2006. Volumetric spatial decomposition of trabecular bone into rods and plates: a new method for local bone morphometry. Bone 38, 475–484.
Straus, W.L., 1948. The humerus of *Paranthropus robustus*. Am. J. Phys. Anthropol. 6, 285–313.
Susman, R.L., 1989. New hominid fossils from the Swartkrans Formation (1979–1986 excavations), postcranial specimens. Am. J. Phys. Anthropol. 79, 451–474.
Susman, R.L., de Ruiter, D., Brain, C.K., 2001. Recently identified postcranial remains of *Paranthropus* and early *Homo* from Swartkrans Cave, South Africa. J. Hum. Evol. 41, 607–629.
Tamrat, E., Thouveny, N., Taieb, M., Brugal, J.-P., 2014. Magnetostratigraphic study of the Melka Kunture archaeological site (Ethiopia) and its chronological implications. Quat. Internat. 343, 5–16.
Thackeray, J.F., De Ruiter, D.J., Berger, L.R., Van Der Merwe, N.J., 2001. Hominid fossils from Kromdraai: a revised list of specimens discovered since 1938. Ann. Transv. Mus. 38, 43–56.
Trinkaus, E., Ruff, C.B., 2012. Femoral and tibial diaphyseal cross-sectional geometry in Pleistocene Homo. Paleo. Anthropol. 2012, 13–62.
Volkman, S.K., Galecki, A.T., Burke, D.T., Paczas, M.R., Moalli, M.R., Miller, R.A., Goldstein, S.A., 2003. Quantitative trait loci for femoral size and shape in a genetically heterogeneous mouse population. J. Bone Miner. Res. 18, 1497–1505.
Volpato, V., Couture, C., Macchiarelli, R., Vandermeersch, B., 2011. Endostructural characterization of the Regourdou 1 Neanderthal proximal arm: bilateral asymmetry and handedness. In: Condemi, S., Weniger, G.-C. (Eds.), Continuity and discontinuity in the peopling of Europe. Vertebrate paleobiology and paleoanthropology series. Springer, New York, pp. 175–178.
Volpato, V., Macchiarelli, R., Guatelli-Steinberg, D., Fiore, I., Bondioli, L., Frayer, D.W., 2012. Hand to mouth in a Neandertal: right handedness in Regourdou 1. PLoS ONE 7, e43949.
Vrba, E., 1981. The Kromdraai australopithecine site revisited in 1980: recent investigations and results. Ann. Transv. Mus. 33, 17–60.
Vrba, E.S., 1985. Early hominids in southern Africa: updated observations on chronological and ecological background. In: Tobias, P.V. (Ed.), Hominid evolution: past, present and future. Alan R. Liss, New York, pp. 195–200.
Wallace, I.J., Middleton, K.M., Lublinsky, S., Kelly, S.A., Judex, S., Garland, T., Demes, B., 2010. Functional significance of genetic variation underlying limb bone diaphyseal structure. Am. J. Phys. Anthropol. 143, 21–30.
Wallace, I.J., Tommasini, S.M., Judex, S., Garland Jr., T., Demes, B., 2012. Genetic variations and physical activity as determinants of limb bone morphology: an experimental approach using a mouse model. Am. J. Phys. Anthropol. 148, 24–35.
White, T.D., Black, M.T., Folkens, P.A., 2012. Human osteology, third ed. Academic Press, San Diego.
Wilson, L.A.B., Humphrey, L.T., 2015. A virtual geometric morphometric approach to the quantification of long bone bilateral asymmetry and cross-sectional shape. Am. J. Phys. Anthropol. 158, 541–556.
Zanolli, C., Dean, M.C., Assefa, Y., Bayle, P., Braga, J., Condemi, S., Endalamaw, M., Engda Redae, B., Macchiarelli, R., 2016. Structural organization and tooth development in a *Homo* aff. *erectus* juvenile mandible from the Early Pleistocene site of Garba IV at Melka Kunture, Ethiopian highlands. Am. J. Phys. Anthropol., http://dx.doi.org/10.1002/ajpa.23135.

3.1.2. Extended information

3.1.2.1. The extant human sample

Table 3.1.2.1.A. Composition of the extant human sample of distal humeri detailed using high resolution µXCT scanning.

specimen	sex	age (years)
EH 1	M	41
EH 2	M	51
EH 3	M	47
EH 4	F	29
EH 5	M	26
EH 6	F	23
EH 7	M	45
EH 8	M	27
EH 9	F	25
EH 10	F	26
EH 11	F	58
EH 12	F	48

Table 3.1.2.1.B. Individual values and descriptive statistics of cross-sectional geometric properties (CSG) of the distal humeral diaphysis assessed at section *a* in 12 extant Humans but excluding the outliers indicated in italics; s.d., standard deviation; min., minimum value; max., maximum value.

specimen	%CA	Ix/Iy	Imax/Imin
EH 1	*30.6*	*0.51*	2.06
EH 2	80.3	0.63	2.00
EH 3	68.2	0.50	2.00
EH 4	65.2	0.39	2.60
EH 5	80.8	0.52	2.04
EH 6	65.5	1.83	1.83
EH 7	64.3	0.51	2.02
EH 8	65.3	0.53	1.88
EH 9	59.4	0.53	1.90
EH 10	43.0	0.85	1.20
EH 11	48.6	1.92	1.93
EH 12	54.4	1.86	1.86

mean	63.2	0.92	1.94
s.d.	11.6	0.61	0.31
min.	43.0	0.39	1.20
max.	80.8	1.92	2.60

Table 3.1.2.1.C. Individual values of bi- (2D RCT) and three-dimensional cortical thickness (3D RCT) of the distal humeral diaphysis assessed at the section *b* and section *a* in three fossil specimens and in 12 extant Humans (EH).

specimen	location	2D RCT total shaft portion	2D RCT anterior shaft portion	2D RCT posterior shaft portion	3D RCT total shaft portion proximal (b)[1] to distal (a)[2]
SKX 10924	b	90	52	47	-
	a	52	36	38	-
SKX 34805	b	104	40	43	75
	a	36	24	34	44
GOM IB	b	133	48	43	100
	a	214	91	78	151
4926	b	74	39	40	58
	a	64	40	42	62
5155	b	93	48	45	77
	a	109	51	57	84
5293	b	62	39	35	27
	a	45	35	28	23
5957	b	94	45	52	57
	a	38	31	32	49
6030	b	104	47	49	85
	a	114	50	56	85
6177	b	77	35	45	28
	a	53	38	34	30
6188	b	53	32	32	45
	a	47	27	37	46
6199	b	71	33	42	46
	a	43	35	31	37
6234	b	42	24	23	35
	a	36	27	25	33
6257	b	28	21	18	26
	a	20	16	16	20
6390	b	37	31	25	61
	a	23	21	20	52
6432	b	34	23	30	69

a	33	21	25	43

[1] Proximal is the shaft portion between *b* and the *a*-*b* mid-distance level; it is equal in location to SKX 34805 and GOM IB, but not to SKX 10924.
[2] Distal is the shaft portion between the *a*-*b* mid-distance level and *a*; it is equal in location to SKX 34805 and GOM IB, but not to SKX 10924.

3.1.2.2. Cancellous network of the distal humerus

µXCT-based virtual coronal sections of the fossil distal humeri of the present study, detailed in the paper "Inner structural organization of the distal humerus in *Paranthropus* and *Homo*" published in 2017 in the *Comptes Rendus Palevol* (vol. 16, 521-532), are given in Fig. 3.1.2.2.A., providing complementary evidence of their degree of inner preservation and structural organisation. In TM 1517g, a matrix extensively fills the cells, but the matrix-trabeculae contrast is globally evident, even though densities may overlap at some spots, thus partially obscuring the signal despite hand-assisted segmentation. Variably sized lacunae and discontinuities are also present and some struts are locally highly mineralised. There is a crack of ca 15 mm running nearly vertically from the upper most part of the medial condyle to the epicondyle-trochlea junction, and another vertical crack of ca 18 mm is present laterally, running from the upper most part of the epicondyle to the capitulum. In the distal shaft, the struts are uniquely confined to the lateral quadrant. The struts at the very distal shaft portion and epiphyseal end are arranged in a distinctly appreciable network. A medial vertical bundle consisting of relatively thick rod-like trabeculae arises from the upper level towards the lower level of the olecranon fossa. Its outline parallels the inner cortical limit. Laterally, a vertical bundle of thin, long and well-oriented trabeculae arises from the upper portion of the lateral epicondyle and continues vertically to the lower level of the olecranon fossa. In the most distal region, corresponding to the trochleo-capitular portion, trabeculae radiate perpendicularly to the inferior outer surface in a fan-shaped outline. The region between the lower limit of the olecranon fossa and the outer surface of the trochlea shows the less structured and less dense trabecular network.

As stated in the paper published in 2017 in the *Comptes Rendus Palevol*, "In SK 24600 the entire cavity is filled by highly cemented permeating sediment which nearly invariably inhibits the identification of the cortex-cavity boundary because of their close material contrast". Additionally, following percolation of the mineral matrix through the cancellous network, in this specimen, the preserved trabeculae and the structural organisation cannot be

identified by using the µCT record available to us. With this respect it is likely that this issue may be circumvented in the future by using neutron-based µCT (see Beaudet et al., 2016).

The distal humerus SKX 10924, which, in the fossil assemblage considered in our research, revealed the most finely preserved inner structure, shows a denser cancellous network than the other South African specimens. In its distal shaft the trabeculae are especially numerous, thick and expanded. As seen in TM 1517g, SKX 10924 also reveals a medial trabecular bundle running from the upper region of the epicondyle to its lower region, a less dense lateral bundle of vertically well-oriented trabeculae running from the upper portion of the epicondyle to the lower level of the olecranon fossa (it is worth noting that few of the trabeculae of this bundle parallel the cortical inner limit), and a distal fan-shaped bundle of trabeculae radiating from the outer surface of the trochleo-capitular region. Conversely, differently from TM 1517g, in SKX 10924 the medial bundle shows a medially convex-like outline following the epicondyle and converging to the medial portion of the fan-shaped distal bundle.

While the most distal portion of SKX 34805 is absent, what is preserved confirms the presence of a medio-lateral diversity in cancellous architecture, as observed in TM 1517g and SKX 10924, with a dense medial bundle and a vertical lateral bundle composed of thin, well-oriented, plate-like trabeculae. However, we cannot verify the presence of an arched-shaped structure of the medial bundle as seen in SKX 10924. In the distal shaft of SKX 34805, the trabeculae are thick and expanded, where they can locally form plate-like structures (Gibson, 1985), including in the medial portion.

Finally, the medullary cavity of GOM IB is filled by sediments, but some structural details are anyhow appreciable even by using the medical CT-record available to us. Nonetheless, in this specimen we could not virtually extract and quantitatively assess the cancellous network properties. We note, regardless, that in GOM IB the struts are less numerous than in SKX 10924 and SKX 34805.

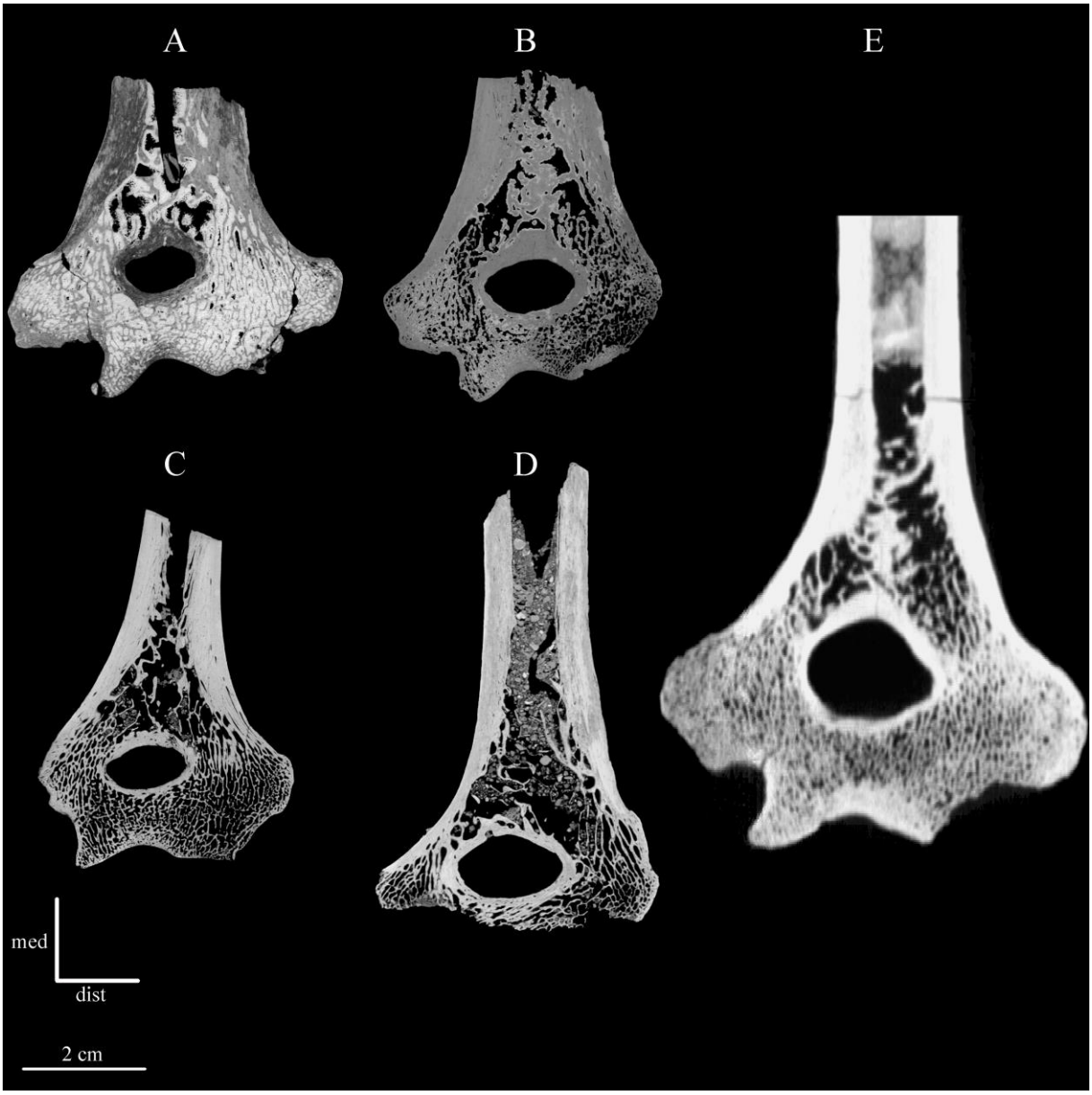

Fig. 3.1.2.2.A. µXCT-based virtual coronal sections of: the right distal humerus TM 1517g (A) from Kromdraai; the left distal humeri SKX 24600 (B), SKX 10924 (C), and the right distal humerus SKX 34805 (D) from Swartkrans; and the left partial humerus GOMB IB (E) from Melka Kunture, providing complementary evidence of their degree of inner preservation and structural organisation. TM 1517g (A) and SKX 34805 (D) are mirrored to be left.

µXCT-based virtual coronal sections extracted approximately across the centre of the 12 extant human distal humeri used as comparative material in the study published in 2017 in the *Comptes Rendus Palevol* (vol. 16, 521-532) are provided in Fig. 3.1.2.2.B., revealing their structural organisation and the amount of variation among the 12 specimens. These specimens

have been selected from the Pretoria Bone Collection at the Department of Anatomy of the University of Pretoria (L'Abbé et al., 2005). A certain degree of variation in endostructural arrangement of the distal humerus can be noticed in the reference human sample used in this study, especially in terms of cancellous network density. For instance, while specimens EH 1 (male, 41 years old) and EH 2 (male, 51 years old) show a rather dense bone, a looser cancellous network is found in EH 9, 10, 11 (all females ranging in age from 25 to 58 years). At present, the nature and meaning of such variation - which in the extant human reference sample used in this study does not seem to be age-related - cannot be fully assessed because of the limited sample size. However, such evidence suggests the possibility that endostructural variation at this skeletal site may also have characterised non-human hominins. However, except for EH 1, the medio-lateral differences noticed in the South African fossil assemblage are less evident in our comparative human sample where the trabeculae are more homogeneous, less oriented and show a more vacuolar network (or a loose cancellous pattern) than in the fossil specimens. In the human sample, the upper portion of the lateral bundle is the most structured region of the network, with vertically oriented and/or parallel struts to the endosteal margin. Finally, only few trabeculae are found in the medullary cavity of the human humeri.

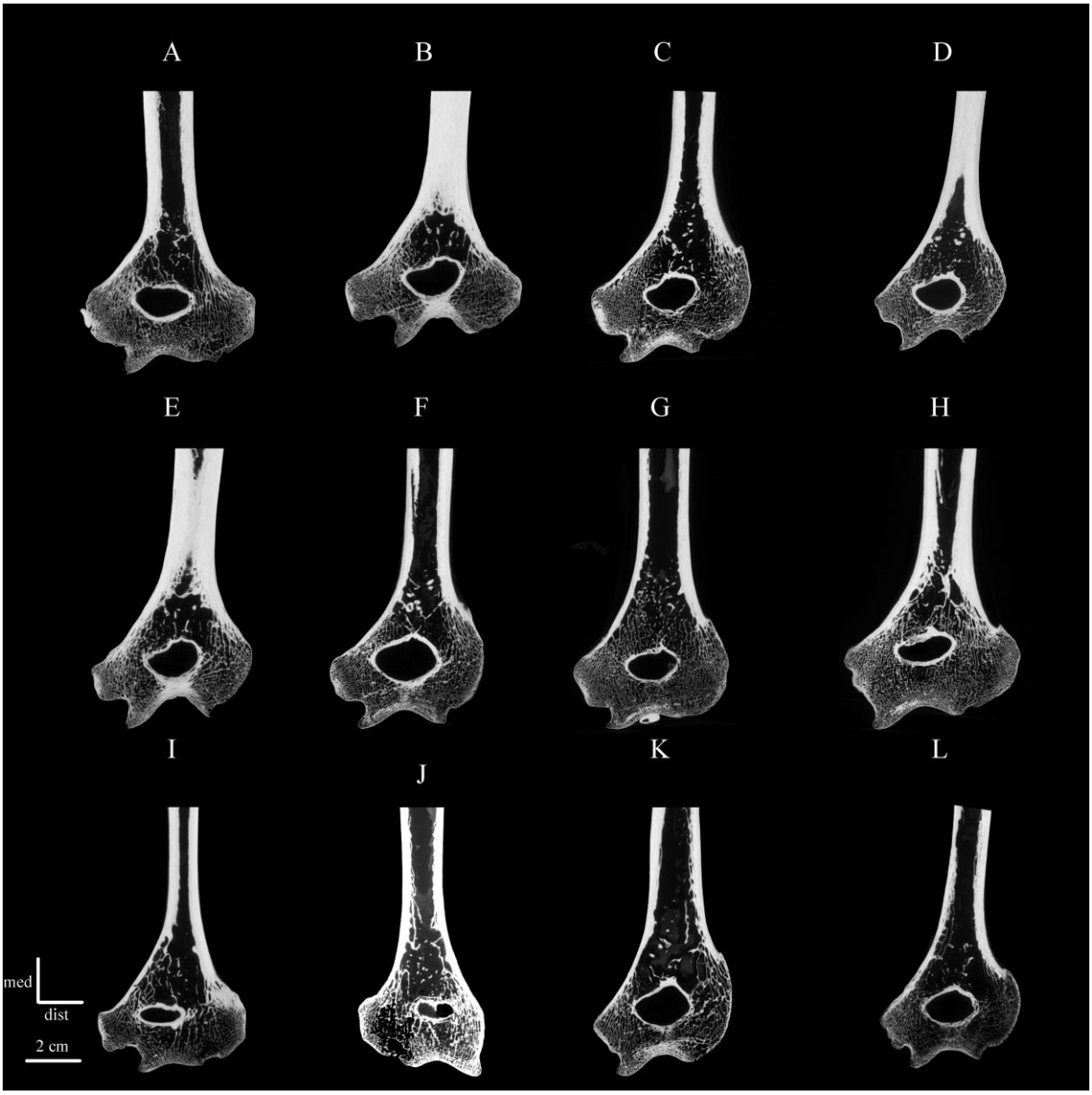

Fig. 3.1.2.2.B. µXCT-based virtual coronal sections extracted approximately across the centre of the 12 extant human distal humeri used in the study published in 2017 in the *Comptes Rendus Palevol* (vol. 16, 521-532). Upper row, from A to D: EH 1, 2, 3, 4; middle row, from E to H: EH 5, 6, 7, 8; lower row, from I to L: EH 9, 10, 11, 12. Sex and age information for each individual is provided in Table 3.1.2.1.D. Independent from their original side, all human specimens are presented here as left for direct comparison with Fig 3.1.2.2.A.

Table 3.1.2.2.A. Mean trabecular thickness measured at cross section level *a* and at two cross sections extracted 1 mm above and below level *a* in SKX 34805, SKX 10924 and in extant

Humans (n = 4). The value of TM 1517g uniquely refers to the section at level *a*. Trabeculae in the extant human humeri available to us are systematically thinner than in the fossil specimens, which confirms the process of skeletal gracilisation and trabecular bone density reduction that occurred in recent Humans (Chirchir et al., 2015; Ryan and Shaw, 2015); s.d., standard deviation.

specimen/sample	Tb.Th. (mm)
TM 1517g	0.41
SKX 34805	0.43
SKX 10924	0.61
extant Humans (EH)	0.35
(s.d.)	(0.03)

3.1.2.3. Loading environment of the distal humerus

The extent to which the distal humeral diaphysis responds to habitual limb use (or is phylogenetically constrained), is still unclear (Ibáñez-Gimeno et al., 2013; Lague, 2015). In extant Humans, three muscles find their origin at this region. The first is the medial head of the triceps brachii, which is part of the posterior group of elbow extensors. It has a particularly wide origin: from the entire posterior surface of the humeral shaft below the radial groove to ca 2.5 cm of the trochlea and to the medial border of the humerus. The anterior muscle is the brachialis, one of the major elbow flexors, which arises from the lower half of anterior humeral shaft. It starts on either side of the insertion of the deltoid and extends distally to ca 2.5 cm from the cubital articular surface. Finally, the brachioradialis muscle, an elbow flexor which is also responsible for both pronation of a supine forearm and supination of a prone forearm (Rhodes and Knüsel, 2005), arises from the proximal two-thirds of the lateral supracondylar humeral ridge and the anterior surface of the lateral intermuscular septum. Its fibres end above the mid-forearm level in a flat tendon which inserts on the lateral side of the distal end of the radius, usually just proximal to its styloid process (Levangie and Norkin, 2005; Standring, 2008; Kapandji, 2011).

At the distal epiphysis, the pronator teres - which has primary functions at the radio-ulnar joints - the flexor carpi radialis, the flexor carpi ulnaris, the flexor digitorum superficialis and the palmaris longus - having primary functions at the wrist, hand and fingers - all arising from a common tendon from the medial epicondyle of the humerus, are weak flexors of the elbow.

In addition, a number of muscles which also have actions at the wrist and fingers, insert onto the lateral humeral epicondyle through a common extensor tendon. These muscles include the extensor carpi radialis longus, the extensor carpi radialis brevis, the extensor digitorum communis, the extensor carpi ulnaris, and the extensor digiti minimi. In our human reference sample, obvious medio-lateral differences in trabecular organisation at the distal humeral epiphysis might relate to differences in the insertion and loading demands of these tendons.

In their study of the relationships between muscular development, humeral rigidity and diaphyseal shape, Ibáñez-Gimeno et al. (2013) showed that bone bending rigidities are mainly related to muscles crossing the shoulder joint (i.e., the supraspinatus, biceps brachii, subscapularis, deltoid, infraspinatus, pectoralis major, and teres major). Conversely, the muscles crossing the elbow but not the mid-distal humerus (i.e., the extensor digitorum communis, brachialis and flexor digitorum communis), as well as the triceps brachii, do not covary with rigidity. When assessed at 15% and 25%, the mechanical loading derived from the tendons of the flexor and extensor digitorum communis, which create ridges on the medial and lateral sides of the diaphysis, respectively, is apparently not as relevant as that derived from the shoulder muscles (Ibanez-Gimeno et al., 2013).

3.2. Proximal femur

In the mid 1800s, K. Culmann and G.H. von Meyer independently compared the trabecular architecture of a coronally (frontally) sectioned human proximal femur to the mathematically constructed stress trajectories of a curved crane-like beam that resembled a human femur loaded in single-legged stance (Culmann, 1866). Based on these works, J. Wolff stated that the similarities between trajectories in Culmann's crane and the arched trabecular patterns in the human proximal femur could not be coincidental, and hypothesised that ''the direction and pattern of loading influences, and/or controls, the pattern of the trabecular framework'' (Wolff, 1870). Since then, the inner structural organisation of the proximal femur has been the subject of a significant number of studies. The tentative aim of these studies involved the identification of the functional relationships between inner architecture and locomotor behaviour and the determination of the hip joint loading environment and biomechanics in Humans, non-human extant primates and fossil hominids (rev. in Skedros and Baucom, 2007).

In Humans, the upper femoral end displays a rather structured and topographically heterogeneous cancellous architecture, commonly described as consisting of two major and three minor systems, which face the complex set of postural and locomotion-related forces acting at the hip joint (Aiello and Dean, 1990; Levangie and Norkin, 2005; Kapandji, 2011). In addition, in modern Humans the femoral neck is characterised by a distinctly asymmetric cortical bone distribution resulting from a markably thinner superior and a thicker inferior cortex (Lovejoy, 1988, 2005; Ohman et al., 1997; Rafferty, 1998; Lovejoy et al., 2002; Ruff and Higgins, 2013; Ruff et al., 2016). This feature relates to reduced strains in the superior region of the neck due to the action of the gluteal abductors, producing a compressive force that counteracts tensile strains engendered by the neck bending because of weight bearing (Lovejoy, 1988, 2005; Lovejoy et al., 2002; Ruff and Higgins, 2013; Ruff et al., 2016).

In order to provide insight into bone and joint function and ultimately, locomotor behaviour, a number of studies on the bony inner structure in extant primates, including the trabecular organisation and cortical distribution, have primarily focused on the proximal femur (Rafferty and Ruff, 1994; Rafferty, 1998; Ohman et al., 1997; Demes et al., 2000; Lovejoy et al., 2002; MacLatchy and Müller, 2002; Ryan and Ketcham, 2002a, b, 2005; Viola, 2002; Ryan and van Rietbergen, 2005; Ryan and Krovitz, 2006; Fajardo et al., 2007; Scherf, 2007, 2008; Pina et al., 2011, 2012; Saparin et al., 2011; Ryan and Shaw, 2013; Scherf et al., 2013). While the intimate relationship between cancellous patterns and posturo-locomotor behaviour is often

unclear, these studies provide evidence of some structural differences in trabecular architecture across locomotor groups, where repetitive/stereotypical loading patterns are commonly associated with more anisotropic networks, while heterogeneous/variable patterns are associated with a less anisotropic (isotropic) cancellous organisation (e.g., Fajardo and Müller, 2001; MacLatchy and Müller, 2002; Ryan and Ketcham, 2002a, b, 2005; Ryan and Krovitz, 2006; Ryan and Walker, 2010; Saparin et al., 2011; Ryan and Shaw, 2012, 2015; Shaw and Ryan, 2012; Raichlen et al., 2015; Ryan et al., 2018; Tsegai et al., 2018). Comparative studies on cortical bone distribution across the femoral neck reveal a shared condition in hominoids of a thicker cortex consistent with their varied locomotor repertoire engendering variation in loading conditions. On the other hand, the asymmetrical cortex, as noted in Humans and some non-hominoid primates, is functionally related to the predominance of adducted positions of the femur in taxa where the hind limbs move predominantly along the parasagittal plane (Ohman et al., 1997; Rafferty, 1998; Demes et al., 2000; Lovejoy et al., 2002; Pina et al., 2011, 2012).

Developed in a comparative biomechanical perspective, a recent investigation of the cancellous network architecture of the australopith proximal femur reveals a highly anisotropic structure in both *A. africanus* and *P. robustus*, with principal strut orientations similar to that of recent Humans, which indicates that australopiths were human-like in many aspects of their bipedalism (Ryan et al., 2018). In addition, the human-like supero-inferior asymmetry in cortical bone distribution across the neck observed in australopiths suggests a full commitment to terrestrial bipedalism (Ohman et al., 1997; Lovejoy et al., 2002). However, a slightly less asymmetric supero-inferior ratio in australopiths than typical in Humans indicates that, while adapted for terrestrial bipedality, australopiths likely experienced a greater lateral displacement of the body centre of gravity over the stance limb during the support phase of gait, which in turn resulted into slightly altered gait kinematics compared to *Homo* (Ruff and Higgins, 2013; Ruff et al., 2016). Additionally, it should be noted that such studies do not really distinguish between the inner structural features of *Australopithecus* and *Paranthropus*, but rather tend to consider the structural signal from both taxa as a general australopith pattern (Ruff and Higgins, 2013; Ruff et al., 2016; Ryan et al., 2018).

Five proximal fossil femora attributed to *P. robustus* have been recovered at Swartkrans. Given the absence at this site of identified *Australopithecus* remains, on comparative ground, they have been attributed to *P. robustus*, not to early *Homo*, because they combine a small head with an antero-posteriorly compressed neck (or, more appropriately, a supero-inferiorly

expanded neck relative to the femoral head breadth; Ruff and Higgins, 2013) (see supra section 2.1.2 and 2.1.3).

In the frame of our research project, by using high resolution microtomography (µXCT) and 3D imaging techniques, the pattern of topographic thickness variation of the cortical shell and the site-specific textural properties of the cancellous network could be characterised in detail in the entire sample of proximal femoral ends from Swartkrans. The primary aim of the investigation was to tentatively identify, at this skeletal site, some taxon-specific features with respect to both *Australopithecus* and *Homo*, suitable for the taxonomic identification of isolated remains. In the light of previous tomographic- (CT) and µXCT-based studies of the inner bony arrangement in Human, non-human extant primate and fossil hominid proximal femoral ends, a further aim was to provide new quantitative information for deconstructing the adaptive functional demands that shaped the inner conformation of the hip joint in *P. robustus*, notably under the assumption that different forms of terrestrial bipedality were likely practiced by early hominins (Ruff et al., 2016: 19; for a review, see Ward, 2013). Finally, intra-specific variation and possible sex-related differences in *P. robustus* were also explored.

Following the research developed in the context of my Master thesis titled "*The inner structural morphology of the femoral head of* Paranthropus robustus" (Cazenave, 2015), preliminary results of the study of the *P. robustus* femur have been presented to the *5th Annual Meeting of the European Society for the Study of Human Evolution* (London, 10-12/9/2015): Cazenave M., Braga J., de Beer F., Hoffman J.W., Macchiarelli R. & Thackeray J.F. - The inner structural morphology of the femoral head of *Paranthropus robustus*. *Proceedings of the European Society for the Study of Human Evolution* 5: 68 (http://www.eshe.eu/static/eshe/files/PESHE/PESHE_4_2015_London.pdf); the *86th Annual Meeting of the American Association of Physical Anthropologists* (New Orleans, 19-22/4/2017): Cazenave M., Braga J., de Beer F., Hoffman J.W., Macchiarelli R., Oettlé A. & Thackeray J.F. - Site-specific cortical bone topographic variation across the whole neck assessed in two hominin proximal femora from Swartkrans Member 1, South Africa: SK 82 and SK 97. *American Journal of Physical Anthropology* 162, suppl. S64: 140 (https://onlinelibrary.wiley.com/doi/abs/10.1002/ajpa.23210). The results *in extenso* of this study are detailed in the manuscript entitled “The inner structural organisation of the proximal femoral end in *Paranthropus robustus*: Implications for the assessment of the australopith hip joint loading conditions” under review in the *Journal of Human Evolution* (ms. HUMEV_2018_160) and provided in the section 3.2.1.".

3.2.1. Manuscript HUMEV_2018_160 under review in the Journal of Human Evolution

The inner structural organisation of the proximal femoral end in *Paranthropus robustus*: Implications for the assessment of the australopith hip joint loading conditions

Marine Cazenave [a, b, *], José Braga [b, c], Anna Oettlé [d, a], Travis R. Pickering [e, f, g], Jason L. Heaton [h, c, g], Francis Thackeray [c], Frikkie de Beer [i], Jakobus Hoffman [i], Roberto Macchiarelli [j, k]

[a] *Department of Anatomy, University of Pretoria, Pretoria, South Africa*

[b] *Computer-assisted Palaeoanthropology Team, UMR 5288 CNRS-Université Paul-Sabatier, Toulouse, France*

[c] *Evolutionary Studies Institute and School of Geosciences, University of the Witwatersrand, Johannesburg, South Africa*

[d] *Department of Anatomy and Histology, Sefako Makgatho Health Sciences University, Ga-Rankuwa, Pretoria, South Africa*

[e] *Department of Anthropology, University of Wisconsin, Madison, USA*

[f] *Institute for Human Evolution, University of the Witwatersrand, Johannesburg, South Africa*

[g] *Plio-Pleistocene Palaeontology Section, Department of Vertebrates, Ditsong National Museum of Natural History (Transvaal Museum), Pretoria, South Africa*

[h] *Department of Biology, Birmingham-Southern College, Birmingham, USA*

[i] *South African Nuclear Energy Corporation SOC Ltd., Pelindaba, South Africa*

[j] *UMR 7194 CNRS-Muséum national d'Histoire naturelle, Musée de l'Homme, Paris, France*

[k] *Unité de Formation Géosciences, Université de Poitiers, Poitiers, France*

Keywords: Trabecular bone; Cortical bone; Functional morphology; Hominin biomechanics; X-ray micro-tomography

* Corresponding author.

E-mail address: marine.cazenave4@gmail.com (M. Cazenave).

ABSTRACT

Studies of the australopith (*Australopithecus* and *Paranthropus*) proximal femur have increasingly integrated information from the arrangement of the cortical and cancellous bone to allow functional-biomechanical inferences on the locomotor behavioural patterns. In both *A. africanus* and *P. robustus*, the cancellous bone organisation at the centre of the femoral head shows principal strut orientation similar to that of fossil and recent humans, which indicates that australopiths were human-like in many aspects of their bipedalism. However, by combining several outer features with cortical bone thickness distribution at the femoral neck, it has been suggested that, while adapted for terrestrial bipedality, australopiths displayed a slightly altered gait kinematics compared to *Homo*. To precise the adaptive functional requirements that shaped the inner bony conformation of the hip joint in *P. robustus*, we used techniques of virtual imaging applied to an X-ray micro-tomographic record to assess the internal structural organisation of five upper femora from Swartkrans, South Africa (SK 82, 97, 3121, SKW 19 and SWT1/LB-2). Specifically, we considered: whole cancellous bone architecture; site-specific textural properties at two spots of the head and the neck; and cortical bone distribution along the entire femoral neck compartment. Trabecular architecture in *P. robustus*, which is hardly distinguishable from that shown by *A. africanus*, more closely resembles the extant human condition than the less topographically contrasted and denser configuration of *Pan*. Nonetheless, nearly at all sites, cancellous network in *P. robustus* is denser, the struts thicker and the plate-like structures more common than in extant humans, especially in the likely males. Our record confirms that *P. robustus* had a thicker inferior cortex at the femoral neck, especially laterally. However, it provides evidence for a lower degree of asymmetry than previously reported, which implies possible differences in the loading environment of the hip joint between *Paranthropus* and *Australopithecus*.

1. Introduction

The evolutionary anatomy of the proximal femur has been extensively investigated in the australopiths (the term subsuming here *Australopithecus* and *Paranthropus*) because of its immediate relation with the locomotor repertoire (e.g., Lovejoy et al., 1973, 2002; Lovejoy, 1975, 1988; Ruff, 1995; Ohman et al., 1997; Ward, 2002, 2013; Ruff and Higgins, 2013; Ruff et al., 2016). Compared to the modern human condition, among other distinctive features, the australopith proximal femur shows a small head relative to the shaft breadth; a proportionally long and antero-posteriorly compressed neck (or, more appropriately, a supero-inferiorly expanded neck relative to the femoral head breadth; Ruff and Higgins, 2013); a reduced neck-shaft angle; a less laterally-projected greater trochanter positioned below the femoral head (e.g., Lovejoy et al., 1973; Lovejoy, 1975; McHenry, 1975; Tague and Lovejoy, 1986; Ruff, 1995, 2010; Ruff et al., 1999, 2016; Harmon, 2009; Berge and Goularas, 2010; Kibii et al., 2011; Ruff and Higgins, 2013). Likely to increase medio-lateral bending loads (Ruff and Higgins, 2013; Ruff et al., 2016), such anatomy is associated with a relatively wide biacetabular breadth which appears to have characterised all early hominin pelves (Gruss and Schmitt, 2015; Ruff, 2017; Vansickle, 2017). While it is still debated whether some morphological traits of the australopith hip joint evolved in response to functional demands or are retentions from an ancestral condition (see discussion in Ruff et al., 2016), it has been shown that a complex and changing pattern of natural selection drove hominin hip and femoral evolution; in this context, many traits commonly suggested to have played functional roles in a bipedal gait evolved as a result of natural selection (Grabowski and Roseman, 2015).

While initially based entirely on the external morphology, studies of the australopith proximal femur have increasingly incorporated information from the internal bony structure, an analytical shift which has added critical elements for functional-biomechanical inferences on the locomotor and behavioural patterns (Lovejoy, 1988; Ohman et al., 1997; Lovejoy et al., 2002; Ruff and Higgins, 2013; Chirchir et al., 2015; Ruff et al., 2016; Ryan et al., 2018; see also Ryan and Sukhdeo, 2016). Indeed, besides the influence of a number of biological (metabolic) factors on the inner bone organisation and the imprint of a genetic component in the resulting evolutionary adaptive bauplan (e.g., Lovejoy et al., 1999; Judex et al., 2004; Demissie et al., 2007; Havill et al., 2007, 2010; Bonewald and Johnson, 2008; O'Neill and Dobson, 2008; Gosman et al., 2011; Wallace et al., 2012; Johansson et al., 2015), the mechanosensitive bone tissues remodel during life to adjust the loading environment (e.g., Huiskes, 2000; Layon and Skerry, 2001; Lieberman et al., 2003, 2004; Pearson and Lieberman,

2004; Mittra et al., 2005; Ruff et al., 2006; Skerry, 2008; Barak et al., 2011, 2017; Gosman et al., 2011; Raichlen et al., 2015; rev. in Kivell, 2016). Accordingly, structural variation in cortical and trabecular bone can be used as proxy for assessing joint loading and thus inferring functional behaviours in extant and extinct organisms (Kivell, 2016; Ruff et al., 2016; Ryan et al., 2018).

Among the inner features of the hominin hip joint, the supero-inferior asymmetry in cortical bone thickness at the femoral neck has been especially considered (Ohman et al., 1997; Lovejoy et al., 2002; Ruff and Higgins, 2013; Ruff et al., 2016). Modern humans are characterised by a distinctly asymmetric distribution resulting from an absolutely thinner superior cortex and a thicker inferior cortex (Lovejoy, 1988, 2005; Ohman et al., 1997; Rafferty, 1998; Lovejoy et al., 2002; Ruff and Higgins, 2013; Ruff et al., 2016). The thinner superior cortex has been attributed to reduced strains in that region due to the action of the gluteal abductors producing a compressive force that counteracts tensile strains engendered by bending of the neck during weight bearing (Lovejoy, 1988, 2005; Lovejoy et al., 2002; Ruff and Higgins, 2013; Ruff et al., 2016). Conversely, great apes possess a more symmetrical distribution of cortical bone across the neck (Ohman et al., 1997; Rafferty, 1998), possibly because of alterations in positioning and functioning of the gluteal muscles (Stern and Susman, 1981).

The human-like supero-inferior asymmetry in cortical bone distribution across the femoral neck, as evidenced in *Australopithecus*, suggests a full commitment to terrestrial bipedalism (Ohman et al., 1997; Lovejoy et al., 2002). However, Ruff and Higgins (2013) show that, especially at mid-neck, australopiths have relatively less asymmetric superior and inferior neck cortices than modern humans, while they are closer to modern human than nonhuman hominoids at the base of the neck (Ruff and Higgins, 2013). Femoral neck cortical bone measures recently performed on the *A. afarensis* A.L. 288-1 partial skeleton ("Lucy") support a pattern of breadth ratios that fall close to the modern human figures, but that are slightly higher (Ruff et al., 2016). Based on a combination of several outer and inner features, it has been suggested that, while clearly adapted for terrestrial bipedality, australopiths likely experienced a greater lateral displacement of the body centre of gravity over the stance limb during the support phase of gait, which in turn resulted into a slightly altered gait kinematics compared to *Homo* (Ruff and Higgins, 2013; Ruff et al., 2016).

Until recently, investigation of the cancellous network architecture in the australopith proximal femur has produced limited results, none immediately related to gait patterns (see discussion in Lovejoy et al., 2002). Measures of trabecular bone fraction performed on three *A. africanus* femoral heads from Sterkfontein (StW 311, 403 and 527) and on the specimen KNM-

ER 738, a *P. boisei* or *Homo* sp. from the Omo-Turkana basin (Wood and Leakey, 2011), indicate values lying more than seven standard deviations above the recent modern human mean (Chirchir et al., 2015). However, a higher cancellous bone density at the femoral head and at other postcranial sites appears as a plesiomorphic feature of all extinct hominins, including pre-Holocene *H. sapiens* (Chirchir et al., 2015; see also Ryan and Shaw, 2015; Ryan et al., 2018). Nevertheless, relevant evidence on the australopith hip joint loading conditions was provided by Ryan and co-workers (2018) with assessments of fabric anisotropy, material orientation, and bone fraction in a trabecular bone volume of interest virtually extracted around the centre of the femoral head in six *A. africanus* (StW 99, 311, 392, 403, 479 and 501) and four *P. robustus* specimens (SK 82, 97, 3121 and SKW 19). By using a diverse comparative sample of extant catarrhines (*Pan*, *Gorilla*, *Pongo*, *Papio*) and Pleistocene and extant humans, they show a highly anisotropic trabecular bone structure in both *A. africanus* and *P. robustus*, with principal strut orientation similar to that of fossil and recent humans, which indicates that australopiths were human-like in many aspects of their bipedalism (Ryan et al., 2018).

Here we apply two- and three-dimensional (2D-3D) techniques of virtual imaging to assess the internal structural organisation of five variably preserved upper femoral ends from Swartkrans, South Africa, attributed to *P. robustus* (SK 82, 97, 3121, SKW 19 and SWT1/LB-2). In this assemblage, representing the totality of proximal femora within the hypodigm of *P. robustus*, SWT1/LB-2 is still unreported for its inner structure (Pickering et al., 2012). Specifically, we aim to provide further information to the micro-X-ray CT-based (µXCT) evidence of trabecular bone head structure reported by Ryan et al. (2018) on four out of five specimens from our sample, as well as to refine and expand previous XCT-based measures of neck cortical bone thickness performed on SK 82 and SK 97 by Ruff and Higgins (2013). Depending on the outer integrity and inner preservation quality of the specimens as revealed by our µXCT-based record, in this study we considered: (i) the general cancellous bone organisation (architecture); (ii) the site-specific textural properties of the network measured at two spots of the head and the neck; and (iii) the cortical bone distribution and thickness proportions all along the femoral neck. Under the assumption that different forms of terrestrial bipedality were likely practiced by early hominins (Ruff et al., 2016: 19; for a review, see Ward, 2013), we provide new information for tentatively deconstructing the adaptive functional requirements having shaped the inner bony conformation of the hip joint in *P. robustus* and, whenever possible, to identify intra-specific variation and possible sex-related differences in its structural organisation (Cazenave, 2015; Cazenave et al., 2015, 2017a).

2. Materials and Methods

2.1. Materials

2.1.1. Fossil specimens

The investigated specimens, SK 82, 97, 3121, SKW 19 and SWT1/LB-2, all adults from the Pleistocene cave deposits of Swartkrans, are shown in Figure 1. Apart for SKW 19, which is stored at the Evolutionary Studies Institute of the University of the Witwatersrand, Johannesburg, the remaining specimens forming the present *P. robustus* assemblage are curated at the Ditsong National Museum of Natural History, Pretoria.

SK 82, SK 97 and SKW 19 all derive from the Hanging Remnant while SWT1/LB-2 comes from the Lower Bank of the Member 1. According to cosmogenic nuclide burial dating (Gibbon et al., 2014), U/Pb dating of flowstone layers under- and overlying Member 1 (Pickering et al., 2011), and previous chronological estimates provided by Curnoe et al. (2001) and Balter et al. (2008), as discussed by Herries et al. (2009), the most accurate chronology of Member 1 ranges between 2.31 and 1.64 Ma. Conversely, SK 3121 comes from the Member 2 breccia block, whose dating has proved more problematic. However, based on U-Pb dates (Balter et al., 2008; see also Herries et al., 2009; Gibbon et al., 2014), chronology of this unit should range between 1.36 and 1.1 Ma, which is compatible with the biochronological framework assessed by Vrba (1975) and Delson (1988).

SK 82, discovered in 1949, represents a right proximal femoral end preserving the head (maximum diameter: 34.4 mm), the neck (mid-neck supero-inferior diameter: 30.6 mm), the trochanteric region and 137 mm of shaft (Robinson, 1972). It is rather well preserved, but a fracture exists just at its head-neck junction. Close to the virtually complete fovea capitis it lacks some cortical bone. Distally, a fracture is filled by matrix. The greater trochanter bears some minor damage, while the lesser trochanter is nearly complete, including at the crest. The shaft portion has suffered some cracking, mostly on the posterior, lateral, and medial aspects (Robinson, 1972). This specimen has been attributed to *P. robustus* by Napier (1964), who firstly identified and described its non *Homo*-like morphology. Later on, in attributing to *Paranthropus* the large majority (c. 95%) of the taxonomically diagnostic craniodental material from Swartkrans Member 1, Grine (1989) provided support to Napier's original attribution. Based on its femoral head diameter compared to other specimens considered as conspecific, SK

82 likely represents a male individual (Susman et al., 2001). Estimated body mass in this individual is 37.1-45.3 kg (Pickering et al., 2012; Ruff et al., 2018).

SK 97, also discovered in 1949, is a right proximal femur preserving the head (maximum diameter: 38.4 mm), the neck (mid-neck supero-inferior diameter: 30.9 mm), the trochanteric region, and 118 mm of shaft (Robinson, 1972). Similarly to SK 82, its head and neck are rather well preserved. However, two fractures run from the fovea capitis until the neck, and the specimen also shows a number of fine cracks. There are few outer damages on the greater trochanter, especially along the crest from the proximal portion down onto the quadrate tubercle. The lesser trochanter also has suffered a small amount of surface damage, as has the distal portion of the preserved shaft (Robinson, 1972). Attributed to *P. robustus* by Napier (1964; see also Grine, 1989) and very likely representing a male individual (Susman et al., 2001), SK 97 closely resembles to SK 82 in morphology, proportions, and cross-sectional geometry of the proximal shaft (Ruff et al., 1999; Ruff and Higgins, 2013). It has been noted that its greater and lesser trochanter approach the modern human morphology, even if some differences concern the medial extension of the area of attachment of the gluteus minimus onto the neck (Lovejoy, 1975). Estimated body mass in this individual is 43.2-53.8 kg (Pickering et al., 2012; Ruff et al., 2018).

SK 3121, discovered some time before 1970, is a right proximal femoral end bearing c. 23 mm of neck (mid-neck supero-inferior diameter: 20.0 mm), notably along its upper margin. Within the assemblage of proximal femora attributed so far to *P. robustus*, SK 3121 displays the smallest articular end (maximum diameter: 29.9 mm), which supports its attribution to the female sex. While incomplete, this specimen is relatively well preserved, but the fovea capitis is filled by consolidated matrix. Differently from SKW 19, its head-neck junction is rather smooth. According to Susman et al. (2001), the taxonomically most significant diagnostic feature of this fossil is represented by its antero-posteriorly compressed neck, a feature shared by all specimens investigated in the present study (Pickering et al., 2012). Estimated body mass in this individual is 24.1-30.0 kg (Pickering et al., 2012; Ruff et al., 2018).

SKW 19, discovered by C.K. Brain after 1970, represents a relatively well preserved right proximal femoral head (maximum diameter: 31.9 mm) only preserving a minor portion (8-10 mm long) of the neck (Susman et al., 2001). The fovea capitis is large but relatively shallow, with a prominent rim. The head-neck junction in this specimen is particularly marked, likely because of the recent fusion of the articular end, indicating this fossil represents a young adult individual. SKW 19 has been assigned to *P. robustus* based on its proportions and because of the antero-posterior compression expressed by its preserved neck portion (Susman et al., 2001).

Within the *Paranthropus* sample of proximal femora available so far, SKW 19 is considered to represent a female individual because of its relatively small size (Pickering et al., 2012). Estimated body mass in this individual is 27.7-35.3 kg (Pickering et al., 2012; Ruff et al., 2018).

SWT1/LB-2, discovered in 2010, represents a right proximal femur originally in two pieces, but with a good contact between the two sections. It preserves the head (maximum diameter: 35.2 mm), the neck (mid-neck supero-inferior diameter: 27.4 mm) and a minor portion of the proximal diaphysis; however, it lacks most of the greater trochanter. The specimen's outer surface is well-preserved. Minor biochemical erosion is apparent in the form of a few localised, shallow linear features appearing on the cortex (Pickering et al., 2012). This fossil shows a relatively small head and an antero-posterior flatness of the long neck, which also probably had a low angle. Estimated body mass in this individual (37.1-45.8 kg; Pickering et al., 2012; Ruff et al., 2018) is heavier than assessed in the likely females SK 3121 (24.1-30.0 kg) and SKW 19 (27.7-35.3 kg) and better fits the estimates of the larger and likely male SK 82 and SK 97 specimens (37.1-45.3 kg and 43.2-53.8 kg, respectively) (Pickering et al., 2012).

2.1.1. Comparative materials

Our comparative material includes extant human and *Pan* specimens, all lacking any macroscopic evidence of outer or inner alteration or obvious pathological changes.

The human sample used for quantitative analyses consists of 12 femora from adult individuals of South African origin (7 males and 5 females, aged 26-54 years) selected from the McGregor Museum of Kimberley (Morris, 1984), the Pretoria Bone Collection at the Department of Anatomy of the University of Pretoria (L'Abbé et al., 2005), and the R.A. Dart skeletal collection at the University of the Witwatersrand (Dayal et al., 2009). For qualitative comparative assessment of the trabecular systems variation (Aiello and Dean, 1990; Levangie and Norkin, 2005; Kapandji, 2011), we also used the digital X-ray radiographic record of 214 proximal femora sampling adult individuals of both sexes from the Imperial Roman osteological collection of Isola Sacra (Macchiarelli and Bondioli, 2000).

Here, *Pan* is represented by two adult femora from a *P. troglodytes* and a *P. paniscus* individuals stored at the Evolutionary Studies Institute of the University of the Witwatersrand, Johannesburg. For comparative descriptions, we also used the XCT-based records of seven adult *P. troglodytes* femora from the Primate Research Institute, Kyoto University (Digital Morphology Museum, KUPRI; http://dmm.pri.kyoto-u.ac.jp/dmm/WebGallery/index.html) and two *P. troglodytes* femora from the primate osteological collections of the Muséum national

d'Histoire naturelle, Paris, imaged in 2005 by SR-µXCT at the beamline ID 17 of the European Synchrotron Radiation Facility (ESRF) of Grenoble (350 µm isotropic voxel size).

2.2. Methods

2.2.1. Data acquisition and image processing

To detail their inner structural morphology, all specimens were imaged by X-ray micro-tomography (µXCT). SK 82, 97, 3121 and SWT1/LB-2 were scanned between 2014 and 2017 at the micro-focus X-ray tomography facility (MIXRAD) of the South African Nuclear Energy Corporation SOC Ltd (Necsa), Pelindaba, using a Nikon XTH 225 ST (Metris) equipment according to the following parameters: 100 kV (SK 3121 and SWT1/LB-2) and 190 kV (SK 82 and SK 97) tube voltage; 0.10 mA (SK 3121 and SWT1/LB-2) and 0.12 mA (SK 82 and 97) tube current; and an angular increment of 0.36° between each projection (for a total of 1000 projections). SKW 19 was scanned in 2015 at the micro-focus X-ray tomography facility at the Evolutionary Studies Institute of the University of the Witwatersrand, Johannesburg, using a Nikon metrology XT H225/320L industrial XCT system equipped with a micro focal X-ray tube according to the following parameters: 85 kV tube voltage, 0.10 mA tube current, and an angular increment of 0.12° (for a total of 3000 projections). The final volumes were reconstructed with an isotropic voxel size ranging from 20 µm (SKW 19) to 79 µm (SK 82), which is higher for all specimens but SKW 19 to the voxel dimensions used by Ryan et al. (2018) for scanning the *P. robustus* specimens included in their study (range: 20-21 µm).

Three extant human femora were also imaged at Necsa at resolutions ranging from 50 µm to 92 µm isotropic voxel size, while the remaining specimens forming the human reference sample and the two *Pan* femora stored in Johannesburg were scanned at the X-ray micro-tomography facility of the University of the Witwatersrand at resolutions ranging from 42 µm to 45 µm isotropic voxel size.

By using the more complete SK 82 and SK 97 specimens as reference guide, SK 3121, SKW 19 and SWT1/LB-2 were virtually rotated by Avizo© v.8.0.0. so that all were tentatively oriented in the same way. The images used to investigate the inner structural organisation of the femoral neck were taken perpendicular to the main neck axis. Independently from their original side, all extant comparative specimens were imaged as right femora. Repeated intra- and inter-observer tests ran for orientation accuracy provided differences of less than 4%.

2.2.2. Cancellous bone analyses

The specimens SK 82 and SK 97, which preserve the largest amount of outer anatomical information within the entire fossil assemblage, underwent a number of taphonomic and diagenetic changes which limited and constrained the analyses of the cancellous network (Fig. 2). Accordingly, we preferred to perform primarily a comparative assessment of the whole sample to describe inter-individual variation. Our analytical protocol for 3D data collection was specifically calibrated according to the variably preserved inner structure.

Differently from Ryan et al. (2018), our µXCT records did not allow the centre of the femoral head to be confidently sampled in all fossil specimens because of a punctually lower bone-matrix contrast in some specimens which could not be systematically overcome. After various attempts (Cazenave, 2015; Cazenave et al., 2015) and tests among independent observers, we identified in the infero-lateral portion of the femoral head a cubic volume of interest (hVOI) which delivered a sufficiently well-preserved amount of cancellous bone suitable for structural analysis across the vertical and arcuate trabecular bundles (Aiello and Dean, 1990) in all five fossil specimens. This tentatively homologous hVOI is positioned at a distance of: 37% of the antero-posterior diameter from the posterior aspect of the femoral head; 17% of the medio-lateral diameter from the lateral aspect; and 29% of the supero-inferior diameter from the inferior aspect (Fig. 3a). Its side corresponds to 20% of the medio-lateral head diameter and ranges in volume from 85 mm^3 to 173 mm^3, in SKW 19 and SWT1/LB-2, respectively, which is smaller than the cubic VOI extracted by Ryan et al. (2018; estimated approximate range: 857-1643 mm^3). In our extant human and *Pan* samples, hVOI ranges from 203 mm^3 to 576 mm^3 and from 97 mm^3 to 199 mm^3, respectively.

Similarly to the hVOI sampling the head, another homologous cubic VOI, the nVOI, was identified in SK 97, 3121 and SWT1/LB-2 near the inferior portion of the femoral neck. Set within the vertical bundle, this nVOI is located at 50% of the antero-posterior neck diameter (Fig. 3a). Even if SK 82 preserves a greater amount of trabecular bone compared to SK 97 (Fig. 2), a reliable assessment of its textural properties was not possible because of a rather noisy signal all around hVOI due to network discontinuities and matrix infilling the inter-trabecular spaces. The nVOI's side corresponds to c. 17% of the maximum supero-inferior height of the mid-neck, thus ranging from 39 mm^3, in SK 3121, to 145 mm^3, in SK 97. In our samples of extant humans and *Pan*, the nVOI ranges from 56 mm^3 to 278 mm^3 and from 31 mm^3 to 101 mm^3, respectively.

The hVOI and nVOI were binarised into bone and non-bone using the "Half Maximum Height" (HMH) quantitative iterative thresholding method (Spoor et al., 1993) and the region of interest protocol (ROI-Tb; Fajardo et al., 2002) by taking repeated measurements on different slices of the virtual stack by Avizo© v.8.0.0. and ImageJ© (Schneider et al., 2012). By using the star volume distribution (SVD) algorithm in Quant3D© (Ryan and Ketcham, 2002a), on each virtually extracted VOI we measured the following variables: (i) the trabecular bone volume fraction (BV/TV, in %), given as the ratio of the number of bone voxels to the total number of voxels; (ii) the trabecular thickness (Tb.Th., in mm), which is the mean thickness of the trabecular struts; and (iii) the degree of anisotropy (DA), a fabric characteristic of trabecular bone assessed following Ryan and Ketcham (2002a) by dividing the eigenvalue representing the relative magnitude of the primary material axe of the bone structure (τ_1) by the eigenvalue representing the relative magnitude of the tertiary material axe of the bone structure (τ_3) (see also Ryan and Walker, 2010; Shaw and Ryan, 2012). Intra- and inter-observer tests for measurement accuracy showed differences less than 5%.

Besides other difficulties in quantifying the structural properties in fossil cancellous bone (e.g., Gross et al., 2014; Bishop et al., 2017), Ryan et al. (2018) appropriately underlined the technical issue of the use of µXCT-based data obtained from different systems and scanning protocols implying variation in image resolution, which is of course the case of our study. We used the specimen SK 3121, whose femoral head core is relatively well preserved, to evaluate the extent of the differences for the BV/TV and the DA with respect to the measures performed by Ryan et al. (2018: 0.54 and 0.61, respectively; table 2). For the study conducted by Ryan et al. (2018), this specimen was scanned at the University of the Witwatersrand and reconstructed with an isotropic voxel size of 20 µm (Ryan et al., 2018: table 1), while we imaged it at Necsa (see above) at a resolution of 24 µm. Following the analytical protocol described by Ryan et al. (2018) and using a VOI of 857 mm^3 virtually extracted from its head centre, we obtained a BV/TV of 0.56 (vs. 0.54) and a DA of 0.66 (vs. 0.61), a result showing differences of 3.6% and 7.6%, respectively, which we consider satisfactory.

2.2.3. Cortical bone analyses

In SK 82, 97, SWT1/LB-2 and in all extant specimens used for comparison, the femoral neck was virtually delimited between the head-neck junction, medially, and its base, laterally, avoiding the superior flaring of the greater trochanter (Ruff and Higgins, 2013; Ruff et al., 2016). To extract its cortical shell, a semi-automatic threshold-based segmentation with manual

corrections (notably in the case of SK 82 and SWT1/LB-2) has been carried out (Spoor et al., 1993; see also the region-based segmentation approach based on topographic concepts, known as the watershed transform, in Meyer and Beucher, 1990; Roerdink and Meijster, 2000) by Avizo© v.8.0.0. In each specimen, an antero-posterior slice perpendicular to the longitudinal neck axis has been extracted for each voxel. In each slice, the highest and lowest pixel of cortical bone were used to delimit the most superior and most inferior limits of the cortex, respectively. A supero-inferior axis was defined as a line connecting the most superior and most inferior points (Ruff and Higgins, 2013). However, while in general we did not encounter serious difficulties in virtually extracting and assessing the neck cortex (Cazenave et al., 2017a), we could not reliably define the base of neck in SK 3121. Additionally, because of locally missing segments of bone and cracking (including across the lower endosteal border), the assessment of cortical bone thickness variation in SWT1/LB-2 was limited to its superior cortex and anterior neck wall.

Whenever possible, the superior (S) and inferior (I) cortical thicknesses and their ratio (S/I) have been measured across the entire neck length; however, to allow direct comparisons with the results from other similar studies (Ruff and Higgins, 2013; Ruff et al., 2016), the local thicknesses measured at the base of neck and at mid-neck were specifically considered (for methodology, see Ruff and Higgins, 2013). Additionally, to get a more comprehensive quantitative assessment of cortical bone topographic variation, in each antero-posterior slice perpendicular to the longitudinal axis of the virtually isolated femoral neck, the superior, inferior, anterior and posterior quadrants were delimited by two orthogonal lines set at 45° with respect to the supero-inferior axis, and the average cortical thickness thus measured for each quadrant (Fig. 3b). To automatically assess all measurements, we used an ad hoc routine created by J. Dumoncel (UMR 5288 AMIS CNRS, University of Toulouse III Paul Sabatier).

Within the investigated fossil sample, SK 82 preserves the best periosteal and endosteal neck surfaces. To provide a synthetic functional image of its cortical bone repartition through a planar representation of its topographic thickness variation, we virtually unzipped the portion between the base of neck and the head-neck junction along a predefined line of its inferior aspect, unrolled such portion and projected its local properties into a morphometric map (Bondioli et al., 2010; see also Bayle et al., 2011; Morimoto et al., 2011; Puymerail et al., 2012; Jashashvili et al., 2015; Zanolli et al., 2018). The map was generated by a custom routine developed in R v.3.4.4 (R Development Core Team, 2018) with the packages Momocs (Bonhomme et al., 2014), spatstat (Baddeley et al., 2015) and gstat (Pebesma, 2004). Cortical bone thickness values have been standardised between 0 and 1 and the morphometric map has

been set within a grid of 180 rows by 40 columns. To allow a comprehensive visual comparison between the structural signature characterising SK 82 and the maps summarising the variation expressed by our extant human (n=12) and *Pan* (n=2) comparative samples, by a custom routine developed in Scilab v.4.1.2 (The Scilab Consortium) we performed generalised additive models (GAM) of interpolation by merging the individual morphometric maps into single datasets to create consensus maps (Wood, 2006; Puymerail et al., 2012). Intra- and inter-observer tests for measurement accuracy showed differences less than 4%.

3. Results

3.1. Cancellous network architecture

As illustrated by a virtual coronal slice approximately crossing the femoral head centre, the degree of inner structural preservation and the cancellous bone architecture of the five fossil specimens from Swartkrans and extant human and *Pan* representatives are shown in Figure 2.

In SK 82, cancellous bone preservation varies across the head. There is a c. 3 mm large crack running nearly vertically while another crack courses posteriorly, near the head-neck junction. Variably sized lacunae and discontinuities are also present, and some struts are locally highly mineralised. However, at several sites the cancellous network is well preserved, including across the neck. In this specimen, the vertical, the arcuate and the trochanteric bundles (Aiello and Dean, 1990) are present. The vertical bundle arises from the superior aspect of the head and radiates infero-laterally towards the inferior cortex of the neck. The outline of its lower limit is slightly convex medially, where some thickened rod-like trabeculae locally result into plate-like structures (Gibson, 1985; Dalstra and Huiskes, 1995; Ding et al., 2002; Stauber and Müller, 2006). While not evident within the femoral head, a slightly inferiorly concave and relatively wide arcuate bundle is appreciable at the head-neck joint. This bundle moves laterally by crossing the superior portion of the neck, then bending inferiorly to join the lateral cortex of the upper shaft. With this respect, apart from its faint appearance within the head and a less arcuate outline, it fits the human condition. In its lateral portion, the trabeculae forming this bundle are thicker and well oriented. Lateral to the base of the neck, a more closed network of plate-like structures is noticeable. Inferiorly, the local impact of diagenetic changes accentuates the original condition of likely thickened cell walls. The area below and lateral to the crossing between the vertical and arcuate bundles, which in humans corresponds to the "Ward's triangle" (the so-called "zone of weakness"; Levangie and Norkin, 2005: 367), is filled by a looser

cancellous network but consisting of relatively thick struts. Because of local damages, the trochanteric bundle is poorly distinguishable. However, near the base of neck, the presence of thickened supero-inferiorly and latero-medially projecting trabeculae displaying an arched outline is compatible with a human-like so-called secondary compressive group bundle (Levangie and Norkin, 2005; Kapandji, 2011). Some elements of a bundle-like structure are also preserved within the greater trochanter, but the specimen is highly damaged in this area (Fig. 2).

Within the investigated fossil assemblage, the cancellous network of SK 97 revealed by our µXCT-based record is the least preserved. Consolidated matrix extensively fills the cells and locally replaces, or mimics, the struts, notably within the head. Cracking and wide lacunae are found across the neck. However, nearly intact cancellous bone is preserved in the inferior aspect of the head and around the inferior portion of the neck. In this specimen, the vertical and arcuate bundles are only partially preserved. As in SK 82, the vertical bundle crosses the head and courses towards the inferior neck cortex, where it uniquely consists of rod-like trabeculae; across the head, it shows a slightly medially-oriented convexity. The origin and first trait of the arcuate bundle are evident just below the fovea capitis. The arcuate bundle crosses the vertical bundle near the centre of the femoral head. Its preserved lateral extension goes through the superior portion of the neck. Despite extensive damage resulting in textural discontinuities or bone destruction, this bundle seems to terminate into the lateral diaphyseal cortex. The preserved network locally consists of relatively thick and well-oriented trabeculae. The trochanteric bundle is not appreciable; however, the greater trochanter is essentially filled by vacuolar-like cancellous bone (Fig. 2).

The inner structure of SK 3121 is relatively well preserved, with limited matrix infilling the inter-trabecular spaces. Indeed, compared to SK 82 and SK 97, the matrix-trabeculae contrast is less ambiguous. Yet, despite hand-assisted segmentation, densities do overlap at points and obscure the signal. In this specimen, a slightly medially convex vertical bundle is well distinguishable. Conversely, the arcuate bundle is less expressed, with only poor evidence an intersection between the two structures. Here, the origin of the arcuate bundle also seems confined to the infero-medial portion of the head, just below the fovea capitis, where its trabeculae are abundant and well-oriented (Fig. 2).

Trabecular bone preservation in SKW 19 is comparable to that of similarly small-sized specimen SK 3121. However, within the present sample of five *P. robustus* proximal femora, SKW 19 is anatomically the least informative specimen, as it uniquely consists of the head. Some matrix infill and isolated lacunae are punctually found, but the contrast bone-matrix is

usually distinct. In terms of degree of expression and topographic patterning, the preserved form of SK 19's vertical and arcuate bundles traces the condition seen in SK 3121. The arcuate bundle is thinner than the vertical one and mostly consists of oriented trabeculae essentially found in its infero-medial aspect (Fig. 2).

Compared to other fossil specimens investigated here, trabecular architecture is finely preserved in SWT1/LB-2. Though, some regions of the inferior head, neck, as well as the medial wall of the shaft, have been filled by glue and plaster for reconstructing and joining the two originally separated fragments. Some minor matrix spots are found within the lateral, anterior and inferior aspects of the head, but the contrast with the trabeculae is nearly universally unambiguous. At some supero-medial head sites, the struts show an increased degree of mineralisation. Network discontinuities exist within the neck and near the head-neck junction, where a medially convex break runs supero-inferiorly. Isolated lacunae are found across the entire specimen, although they are rare. Conversely, cracking and missing chunks of cortex are especially common in the inferior and superior portions of the neck. The posterior neck wall is also locally damaged. In this specimen, the vertical, the arcuate and the trochanteric bundles are well distinguishable. The vertical bundle is wide, rather dense and infero-medially convex to a greater extent than that observed in all other *P. robustus* specimens and commonly seen in extant humans. Inferiorly, it extends rather laterally, where the thickest struts merge into plates. The arcuate bundle also is well defined all along its regularly arched and human-like outline; it can be traced from the infero-medial aspect of the head, just below the fovea capitis, across the upper portion of the neck, until the diaphyseal lateral cortex (even if the latter is not preserved). Its trabeculae are nearly universally thick and oriented. Similarly to SK 82, the area below and lateral to the vertical-arcuate bundle crossing is the least dense and shows a loose trabecular network. However, in this case, the trochanteric bundle is apparently more structured than seen in SK 82 and consists of more distinct, thicker and oriented trabeculae. Conversely, because of local bone damage, the organisation and degree of structuration of the bundle-like structure of the greater trochanter is not fully appreciable, even if the region is clearly filled by a relatively dense but poorly organised cancellous network. SWT1/LB-2 is also the only fossil among those examined here preserving partial evidence of the so-called secondary tensile trabecular system (Levangie and Norkin, 2005: 367). Here, it is represented by relatively thick and obliquely-oriented trabeculae departing from the medial aspect of the upper shaft and oriented towards the lateral diaphyseal cortex (Fig. 2).

3.2. Cancellous network properties

Cancellous bone properties of the VOI sampling the infero-lateral portion of the femoral head (hVOI; Fig. 3) in all five fossil specimens from Swartkrans and in the extant human and *Pan* representatives are shown in Table 1. For bone volume fraction (BV/TV), the values in the fossil specimens range from 31.5%, in the likely female SKW 19, to 44.6%, in the likely male SWT1/LB-2; the values of the two other likely males, SK 82 and SK 97, also exceed that of SK 3121, the other presumably female represented in the assemblage. These density estimates correspond with values available for *Pan* (av.: 39.2%) and are, on average, slightly higher than our extant human sample (range: 17.5-37.7%). For trabecular thickness, the three likely male *P. robustus* (range: 0.19-0.23 mm) show the absolutely highest values measured in all fossil and extant specimens considered here, while the estimates of the two likely female *P. robustus* (0.14 and 0.16 mm) fall within the range expressed by extant humans (0.11-0.19 mm) and *Pan* (av.: 0.17 mm). Finally, the estimates of the degree of anisotropy (DA) overlap between *P. robustus* (range: 2.56-3.70) and extant humans (range: 2.28-5.97), while a slightly lower anisotropy is shown by the two *Pan* representatives (av.: 2.18).

Among the fossil specimens, cancellous bone properties of the volume of interest sampling the vertical bundle at the inferior mid-neck (nVOI; Fig. 3) have been assessed in the two likely males SK 97 and SWT1/LB-2 and in the likely female SK 3121. Together with the measures of extant humans and *Pan*, their values are shown in Table 2. For BV/TV, the estimates overlap among *P. robustus* (50.4-57.3%), extant humans (range: 33.4-63.4%) and *Pan* (av.: 56.1%). Compared to SK 97 and SWT1/LB-2, *Pan* tends to show slightly thinner struts (Tb.Th.) and a lower DA, the highest degree of anisotropy at this femoral neck site having been measured in extant human individuals. Among the three *P. robustus*, SK 3121 shows the lowest bone volume fraction and trabecular thickness, but a slightly higher degree of anisotropy (Table 2).

3.3. Cortical bone thickness variation

As detailed above, the femoral neck cortex is rather variably preserved within the *P. robustus* specimens examined here, with some spread cracking, damages or even local tissue removal. Conversely, the cortical bone shell enveloping the head is nearly universally well preserved. In all cases, it appears as a thin layer whose thickness does not differ from that shown by extant humans and *Pan* (Fig. 2).

Cortical bone thickness measures have been performed at the base of neck in SK 82, 97 and SWT1/LB-2 (only the upper cortex measured in the latter) and at mid-neck in SK 82, 97, 3121

and SWT1/LB-2 (again, only the upper cortex), respectively. The sections of the four fossil specimens available at these two sites are shown as Supplementary Online Material (SOM) Fig. S1. Whenever possible, on the same virtual slices we also assessed the mean cortical thickness of the geometrically-defined superior and inferior quadrants (Fig. 3b). The results are shown in Table 3, together with the XCT-based superior (S) and inferior (I) measurements previously performed on SK 82 and SK 97 by Ruff and Higgins (2013). Table 3 also shows the estimates obtained in our extant human and *Pan* comparative samples, as well as the µXCT-based cortex thicknesses and ratios of the *A. afarensis* "Lucy" (Ruff et al., 2016).

For SK 82 and SK 97, the differences between the µXCT-based (present study) and the XCT-based (Ruff and Higgins, 2013) measures vary between 0.54 mm (16.0%) and 1.12 mm (48.7%), at its base, and between 0.06 mm (2.1%) and 1.31 mm (46.6%), at mid-neck. In terms of polarity, those µXCT-based are higher (up to 1.12 mm) in 5/8 cases and lower (up to 0.58 mm) in the remaining three, with no topographic significance (Table 3). The impact of such differences on the S/I ratio of the two specimens is clear, as they imply distinctly less asymmetric cortices at the base of neck (0.76 vs. 0.47 and 0.68 vs. 0.42, in SK 82 and SK 97, respectively) and a closer signal between the two fossils for the mid-neck thickness ratio (0.86 vs. 1.05 and 0.96 vs. 0.68, in SK 82 and SK 97, respectively) than previously reported (Ruff and Higgins, 2013).

According to the present *P. robustus* estimates, the S/I cortical ratio varies from 0.68 (SK 97) to 0.76 (SK 82) at the base of neck, and from 0.71 (SK 3121) to 0.96 (SK 97) at mid-neck. Both mid-neck measures of the likely female specimen SK 3121 correspond to the absolutely thinnest cortices assessed within this fossil assemblage (no reliable measures available for SK 3121 at base of neck). For the S/I ratio at the base of neck, *P. robustus* is thus intermediate between the asymmetric values shared by extant humans (range: 0.10-0.54) and "Lucy" (0.34) and the higher values displayed by *Pan* (range: 1.11-1.52). At mid-neck, *P. robustus* more closely approximates *Pan* (range: 0.73-0.82) than the still asymmetric condition of extant humans (range: 0.15-0.76 vs. 0.71-0.96 in *P. robustus*) and "Lucy" (0.58) (for comparative evidence on extant apes and humans, see Ruff et al., 2016). A rather coherent picture with respect to the pattern shown by the punctual measures at base of neck and mid-neck is provided by the mean cortical thickness assessed in *P. robustus*, extant humans and *Pan* on the respective superior and inferior quadrants (Fig. 3b, Table 3). In such case, however, while the likely female SK 3121 again shows the thinnest average superior cortex at mid-neck, that of the lower quadrant is shown by the likely male SK 82 (Table 3).

For SK 82 and SK 97, the standardised latero-medial variation of the S/I ratio from the base of neck (0%) to the head-neck junction (100%) is shown in Fig. 4a and is compared to the variation expressed by extant humans (Fig. 4b) and *Pan* (Fig. 4c). As noted, SK 82 and SK 97 share higher values than measured in extant humans, i.e., less asymmetric cortices. Yet, they share a tendency for a latero-medial increase of the ratio, which in humans is especially accentuated across the medial half of the neck (Fig. 4b). A distinctly different pattern is shown by the two *Pan* individuals, which exhibit a marked latero-medial ratio decrease, i.e., a tendency towards thickness asymmetry inversion from the base of neck towards the femoral head.

We used quadrants to comparatively assess mean cortical thickness variation across the anterior and posterior walls (Fig. 3b). The results (Fig. 5) are shown for SK 82, SK 97 and SWT1/LB-2 (the latter uniquely considered for its anterior wall) and for the extant human and *Pan* samples. In the specific comparative context considered here, SK 82 and SK 97 distinctly evince thicker anterior and thinner posterior walls across the entire neck (Fig. 5a and b), while cortex asymmetry is nearly absent in extant humans (Fig. 5d, e) and only low in *Pan* (Fig. 5f, g). Differently from the S/I ratio (Fig. 4), the tendency in *P. robustus* and, to a lesser extent, in extant humans, is towards a latero-medial decrease of the average cortical thickness across both walls. Among the three fossil specimens, SWT1/LB-2 (Fig. 5c) shows, on average, the thickest anterior wall. It is notable that while both *P. troglodytes* and *P. paniscus* globally approximate the values expressed by *P. robustus*, thus largely exceeding the extant human estimates, they do not clearly express a latero-medial decrease pattern. Rather, they exhibit variation in the topographic distribution of cortical bone thickness across the neck, with both walls being, on average, slightly thicker in *P. paniscus* (Fig. 5f, g).

The standardised morphometric maps of the virtually projected cortical bone thickness of the SK 82's neck and the consensus cartographies generated for the extant human sample and the two *Pan* representatives are shown in Fig. 6. It should be noted that, similarly to the results provided in Fig. 4 for the S/I ratio and in Fig. 5 for the anterior vs. posterior wall thickness variation, the geometrically-defined quadrants are neck shape-dependent. Thus, the morphometric maps provide information derived from surfaces having slightly different proportions in each taxon. When compared to the average human condition, for example, the superior quadrant of *P. robustus* is longer and narrower, while its anterior wall is both latero-medially and supero-inferiorly more extended. In terms of both relative topographic distribution pattern and absolute cortex thickness, the contrast between SK 82 and the extant human map is especially marked, notably for the superior and anterior neck quadrants. Nonetheless, some relevant differences are also appreciable with respect to the map summarising the conditions

expressed by the two *P. troglodytes* and *P. paniscus* representatives used in this study, notably in terms of latero-medial thickness distribution. However, while globally showing a comparable pattern (with the exception of the very last medial portion of the posterior wall), the specimen sampling *P. paniscus* shows a slightly but universally thickened neck (SOM Fig. S2).

4. Discussion

For reconstructing actual, rather than potential, locomotor behaviours in fossil specimens, variation in trabecular structure of the appendicular skeleton is considered "the best source of morphological information that is preserved…, particularly when analysed in conjunction with cortical bone" (Kivell, 2016: 587). Indeed, the internal organisation of the proximal femoral structure is seen as intimately related to variation in hip joint loading (e.g., Ruff et al., 2016; Ryan et al., 2018), but the evidence extracted so far from the hominin fossil record remains limited (Lovejoy, 1988; Ohman et al., 1997; Lovejoy et al., 2002; Ruff and Higgins, 2013; Chirchir et al., 2015; Ruff et al., 2016; Ryan et al., 2018).

Using the entire Swartkrans assemblage of five proximal femora currently attributed to *P. robustus* (SK 82, 97, 3121, SKW 19 and SWT1/LB-2), we added complementary information to the data published by Ryan et al. (2018) on the trabecular bone textural properties of the head core. Furthermore, we extended the known trabecular record to the femoral neck. We also refined some local estimates of the degree of superior vs. inferior cortical bone thickness asymmetry of the neck performed by Ruff and Higgins (2013) and extended such analyses to the entire compartment. Major limitations were imposed by the incompleteness of the fossil specimens (notably, SK 3121 and SKW 19) and the heterogeneous preservation quality of their inner signal (notably, in SK 97). The very modest amount of specimens representing the extant reference samples were a factor which prevented the appropriate assessment of intra-taxic variation and currently limits the significance of inter-taxic comparisons (cf. Tsegai et al., 2018). Nonetheless, as the primary objective of this study is the investigation of the still poorly reported structural organisation of the proximal femur in *P. robustus*, the results provide a coherent picture of some unique features characterising this extinct hominin which have implications in the assessment of its hip joint loading conditions.

To face the complex set of postural and locomotion-related forces acting at the hip joint, in humans the upper femoral end displays a rather structured and topographically heterogeneous cancellous architecture, which is commonly described as consisting of two major and three minor systems (Aiello and Dean, 1990; Levangie and Norkin, 2005; Kapandji, 2011). The main

medial trabecular system consists of a vertical (or supporting) bundle which transmits the main compressive forces passing through the hip joint through the head and neck, while the main lateral system, which crosses the medial one forming the dense femoral head network, consists of an arcuate bundle transmitting the tensile forces at this region. Together with the action played by cortical bone in supporting the loads placed on the proximal femur (Lotz et al., 1995; Crabtree et al., 2001; Levangie and Norkin, 2005), these structures respond to the mostly tensile stresses acting on the superior aspect of the neck and to the mostly compressive stresses acting on its inferior aspect. Besides these two major systems, three secondary trabecular systems have been described: the secondary compressive trochanteric bundle, the secondary tensile system, and a bundle-like structure within the greater trochanter (Levangie and Norkin, 2005). The areas where such structures cross (e.g., the vertical and arcuate bundles within the femoral head) should provide the greatest resistance to stress and strain; however, special mechanical resistance is locally assured by the presence of plate-like shaped trabeculae which are especially adapted for withstanding higher compressive loads (Ding et al., 2002; Mittra et al., 2005; Djuric et al., 2010; Sinclair et al., 2013; Milanovic et al., 2017).

It is true that remarkable similarities exist among the extant hominoid proximal femoral ends in the basic distribution and directionality of trabecular bone (e.g., Lovejoy et al., 2002; Fajardo et al., 2007). Nonetheless, our µXCT-based 3D analytical perspective shows that trabecular bone architecture in *P. robustus* more closely resembles the extant human condition than the less organised, less topographically contrasted and globally denser configuration of *Pan*, where the poorly distinct trabecular systems (notably, those forming the so-called three minor, or accessory, systems) reveal a more homogeneous network organisation. Furthermore, *P. robustus* also shows some specificities in local textural arrangement and density absent or uncommon in extant humans. With this respect our record supports the warning that subtle differences in predominant trabecular direction may not be reliably imaged in 2D radiographs (Lovejoy et al., 2002: 118).

Nearly at all sites, the *P. robustus* cancellous network is denser and the struts, on average, thicker than in extant humans, especially in the three likely male specimens SK 82, 97 and SWT1/LB-2. In addition to trabecular thickening observed at some spots of the arcuate bundle along its supero-lateral neck portion, the presence of plate-like structures in the inferior neck trait of the vertical bundle and towards the diaphyseal medial cortex is common in *P. robustus*, while in humans it is rare and/or rather localised. This is in line with the prediction that a site-specific net increase in bone volume usually causes trabeculae to become quite plate-like (Mittra et al., 2005). In *Pan*, plate-like trabeculae are mostly confined to the superior neck

portion of the arcuate bundle. Interestingly, a configuration similar to that observed in *P. robustus* is also found in some *A. africanus* specimens (e.g., StW 99 and StW 479) imaged by Ryan et al. (2018: fig. 2). Conversely, while distinctly revealing a human-like trabecular pattern and, apparently, some thickened struts adjacent to the superior neck cortex, the X-ray film and the xeroradiograph of the partial femur MAK-VP-1/1 of *A. afarensis* from Maka, Ethiopia (Lovejoy et al., 2002: fig. 18) do not allow a reliable assessment of the presence and topographic distribution of plate structures.

Schematically, among other features found in the trabecular architecture of the proximal femoral ends of *P. robustus*, we note: (i) a variably marked medially convex (i.e., arched) vertical bundle, especially in its head portion, which is not expressed in extant humans but is present, for example, in the *A. africanus* StW 311 and StW 501 (Ryan et al., 2018); (ii) an origin of the arcuate bundle, also noticeable in *A. africanus* (Ryan et al. 2018), confined to the head portion below the fovea capitis, while in extant humans it can reach, or even exceed, the level of the depression; (iii) a looser appearance of the network in the so-called "Ward's triangle" below and lateral to the vertical and arcuate bundles crossing; however, differently from the extant human pattern where increasing bone loss in this area is appreciable even in young adults, at this site the struts of the trochanteric bundle are thickened and well-oriented in *P. robustus* (notably in SWT1/LB-2), a configuration also displayed by the *A. africanus* StW 479, for example (Ryan et al. 2018), which differs from the poorly organised vacuolar network of *Pan*; (iv) a greater trochanter cancellous infill of intermediate texture and density between the proportionally looser human network and the denser honeycomb pattern of *Pan*. Conversely, as testified, for example, by the *H. erectus* KNM-WT 15000 proximal femur (SOM Fig. S3), a vertical bundle which extends quite laterally along the inferior margin of the neck till the medial diaphyseal cortex is not a unique australopith feature (for *A. africanus*, see Ryan et al., 2018; for *A. afarensis*, see Lovejoy et al., 2002), but clearly correlates with the typically longer femoral neck shared by australopiths and early *Homo*. The possibility that a neck length-related distally extended vertical bundle is also mechanically associated to a more medially arched shape remains to be determined.

While it is certain that some inter-taxic differences in the structural arrangement of the hip joint cancellous network are functionally-related (i.e., contain a locomotor-specific functional signal) and reflect differences in site-specific loading conditions (i.e., the biomechanical environment), their immediate translation in terms of nature, direction, frequency, and magnitude of such loads is not granted (Tsegai et al., 2018). Especially the trabecular architecture of the human proximal femur, which has a complex developmental pattern (rev. in

Milovanovic et al., 2017), has been shown to not be fully consistent at all sites ("fields") with the basic tenets of the "trajectory hypothesis" (Lovejoy et al., 2002; Skedros and Baucom, 2007; Sinclair et al. 2013). Accordingly, it has been suggested that the cancellous organisation of the femoral neck in both humans and chimpanzee more likely reflects predominantly shear stresses, which are better accommodated by non-orthogonal asymmetric trabecular tracts (Skedros and Baucon, 2007). As regional trabecular architectural variation may lack sufficient sensitivity and specificity for interpreting habitual loads at the hip joint (Lovejoy et al. 2002; Skedros and Baucon, 2007; Sinclair et al. 2013; Milovanovic et al., 2017), other factors should also be taken into account. They include the role exerted by load-sharing cortical bone and other stress carrying elements (notably, ligaments and tendons), as well as the taxon-specific developmental schedules in variably shaping trabecular architecture in the different compartments of the proximal femur.

The task of unambiguously disentangling the genetically-driven developmental and metabolic imprint from the functionally-related component is still unaccomplished and the relationship between trabecular structure and behaviour in extant species is often unclear (Tsegai et al., 2018). However, studies having comparatively explored the trabecular organisation of the femoral head in primate taxa displaying different locomotor behaviours provide evidence for some structural differences in trabecular architecture across locomotor groups, where repetitive/stereotypical loading patterns are commonly associated with anisotropic networks and heterogeneous/variable patterns with isotropic trabecular patterns (e.g., Fajardo and Müller, 2001; MacLatchy and Müller, 2002; Ryan and Ketcham, 2002a, b, 2005; Ryan and Krovitz, 2006; Ryan and Walker, 2010; Saparin et al., 2011; Ryan and Shaw, 2012, 2015; Shaw and Ryan, 2012; Raichlen et al., 2015; Ryan et al., 2018; Tsegai et al., 2018).

As previously mentioned, Ryan et al. (2018) have investigated some cancellous network properties at the core of the femoral head in four of the five *P. robustus* specimens from Swartkrans considered in the present study, as well as in six *A. africanus* from Sterkfontein and in a comparative sample of extant catarrhines (*Pan*, *Gorilla*, *Pongo*, *Papio*) and Pleistocene and recent humans. Their results show that *P. robustus* has a more anisotropic trabecular structure compared to the non-human primates, closer to the human values, with principal strut orientation similar to that possessed by fossil and extant humans. However, such human-like properties are also associated with a non-human primate-like pattern of robust trabecular bone (Ryan et al., 2018). Interestingly, a human-like pattern of trabecular anisotropy and orientation in *P. robustus* has also been identified by Ryan et al. (2018) in *A. africanus*, leading to the suggestion that both fossil hominins walked with a broadly human-like hip kinematics

associated to a limited range of habitual hip joint postures (Ryan et al., 2018). Similarly, a pattern of higher BV/TV values than typical in humans also characterises the femoral head of *A. africanus*, suggesting in both taxa higher musculoskeletal loading than experienced by *Homo* (Ryan et al. 2018). The evidence of a cancellous pattern in *Paranthropus* globally combining a relatively high degree of anisotropy with a more robust and dense network than measured in humans also comes from other sites of the australopith postcranial skeleton (e.g., Macchiarelli et al., 1999; DeSilva and Devlin, 2012; Su et al., 2013; Chirchir et al., 2015; Skinner et al., 2015; Su and Carlson, 2017; Cazenave et al., 2018). However, following a recent work by Tsegai et al. (2018) comparing the systemic pattern of trabecular bone across the extant human and chimpanzee skeleton, bone volume fraction does not seem to systematically correspond to locomotor-based predictions of joint loading at different skeletal sites, and the variable relationship between articular surface area and joint mobility should also be taken into account (Ruff, 2002; Tsegai et al., 2018).

For methodological reasons, our estimates of the degree of anisotropy of the volume of interest sampling the infero-lateral portion of the femoral head (the hVOI) and the inferior portion of the neck (nVOI) are not directly comparable with the measures provided by Ryan et al. (2018). Nonetheless, in the head, they agree with a pattern of human-like anisotropy (Tables 1). In the same spot, our estimates also reveal, on average, a denser, ape-like cancellous network in *P. robustus*, but associated to slightly thicker struts than measured in *Pan*, especially in the likely male individuals. However, the signal from the inferior mid-neck spot sampled in our study (Table 2) is taxonomically less distinct compared to the signal from the head. Of course, the modest size of the bone volume extracted from the nVOI could explain such slightly lower structural heterogeneity, but we note that a modest sensitivity of the femoral neck trabecular architecture to load variation has been predicted or measured in a number of anthropoids, including humans (e.g., Carter et al., 1989; Lotz et al., 1995; Lovejoy et al., 2002; Fajardo et al., 2007; Skedros and Baucom, 2007, Sinclair et al., 2013). Nonetheless, to the best of our knowledge, no comparative study besides the present one has quantitatively assessed the textural properties of the so-called vertical and/or arcuate bundles within their neck portions in any fossil hominin, a lack of information which deserves integration in order to refine the related biomechanical interpretative models. In addition, while the trabecular organisation of the femoral neck might not fully reflect direct loadings, it is still possible that the trochanteric region, which remains unexplored in extant and extinct hominids, is sensitive to the relative development and action of the hip abductor muscles. In this perspective, the currently ongoing extensive topographic analysis of the cancellous organisation of the *P. robustus* specimen

SWT1/LB-2, displaying a nearly complete and relatively well-preserved inner architecture (Fig. 2), should provide comparative information on the hip joint loading distribution at different compartments still unavailable among fossil hominins.

Evidence from extant humans indicates only a modest to low degree of sexual dimorphism for trabecular density and trabecular thickness at the proximal femur (e.g., Chirchir et al., 2015; Saers et al. 2016), a condition also confirmed by similar results from the proximal humerus, the distal femur, and the proximal and distal tibia (e.g., Chirchir et al., 2015; Saers et al., 2016; but see Scherf et al., 2013, for the BV/TV of the proximal humerus). Such studies are still limited in primates, but measures performed on the proximal humerus did not reveal significant sex-related differences in *Pan* (Scherf et al., 2013). In *P. robustus*, all likely male specimens (SK 82, 97 and SWT1/LB-2) systematically show a higher BV/TV at the femoral head (av.: 40.3% vs. 32.3% in the likely females) also associated with thicker trabeculae (av.: 0.21 mm) than measured in the two likely females SK 3121 and SKW 19 (av.: 0.15 mm). This tendency is confirmed at the femoral neck, where SK 97 and SWT1/LB-2 again show higher values than the likely female SK 3121 (av. BV/TV: 55.9% vs. 50.4%; av. Tb.Th.: 0.36 mm vs. 0.31 mm). However, it should be noted that a higher BV/TV has not been measured by Ryan et al. (2018) at the femoral head centre in the two likely male *P. robustus* specimens included in their study (av. likely males: 0.52%; av. likely females: 0.53%; Ryan et al., 2018: table 2). In this respect, also in the perspective of testing the impact of body size intra- and interspecific variation on cancellous bone (e.g., Doube et al. 2011; Barak et al. 2013a; Fajardo et al. 2013; Ryan and Shaw, 2013; Tsegai et al., 2018) and the possible metabolic effects in *Paranthropus* of its suggested bimaturism growth pattern (Lockwood et al., 2007; see also Susman et al., 2001), additional information to be compared to increasingly available evidence from apes (e.g., Tsegai et al., 2018) is necessary from other sites of the fossil hominin postcranial skeleton.

Relevant evidence for assessing the biomechanical environment of the hip joint in *P. robustus* is derived from the analysis of cortex variation across the femoral neck, a compartment which in extant humans is estimated to carry from c. 50% to c. 96% of the loads at the mid-neck and base of the neck, respectively, i.e., considerably more than the subcapital region (c. 20%; Lotz et al. 1995). As noted, compared to the modern human condition, the australopith femoral neck is longer and supero-inferiorly expanded relative to the femoral head breadth (rev. in Ruff and Higgins, 2013). Asymmetry in cortical bone thickness distribution between the superior and inferior margins, the former being absolutely thinner, is considered a typical human structural feature developed as mechanical response to the more stereotypic loading pattern imposed by habitual bipedal locomotion and the action of the gluteal abductors muscles,

which is also variably expressed in australopiths (Lovejoy, 1988, 2005; Ohman et al., 1997; Rafferty, 1998; Lovejoy et al., 2002; Ruff and Higgins, 2013; Ruff et al., 2016). Our new set of higher resolution linear and surface measures at the base and mid-neck confirm that *P. robustus* displays a thicker inferior cortex, especially laterally, which supports the view of a human-like action of the gluteal abductors producing a compressive force counteracting the tensile strains in the superior cortex (Lovejoy et al., 2002; Ruff and Higgins, 2013). However, they also provide evidence for a lower degree of asymmetry than previously reported using an XCT-based record (Ruff and Higgins, 2013). These results tend to amplify the extent of the already documented differences between the condition assessed in *P. robustus* and the measures taken on two *A. afarensis* representatives (Maka and "Lucy"), whose femoral neck asymmetry pattern approaches the human condition (Ohman et al., 1997; Lovejoy et al., 2002; Ruff et al., 2016). On the other hand, *P. robustus* shows a human-like trend of latero-medial asymmetry decrease from the base of neck to the head-neck junction. Here again, the only likely female *P. robustus* specimen available for measurements at the base of neck and mid-neck (SK 3121) shows absolutely thinner cortices compared to the likely males (SK 82, 97 and SWT1/LB-2). However, as recorded at other sites of the postcranial skeleton (e.g., Ruff, et al., 1999; Bleuze, 2010; Dominguez-Rodrigo et al., 2013; Dowdeswell et al., 2016; Cazenave et al., 2017b), the cortical bone of the proximal femur is thicker in *P. robustus* than in humans.

While superior vs. inferior cortical bone distribution across the femoral neck has received attention in primate comparative anatomy and paleoanthropology, limited information is available on the differences between the anterior and posterior walls. According to Ohman et al. (1997), humans and African apes display generally uniform anterior and posterior cortical thicknesses along the neck and the cortices tend to slightly wear thin from the neck-shaft junction to the head, with little difference between the species. Our 2D (Fig. 5) and 3D (Fig. 6) analytical approaches confirm that cortical asymmetry is absent in the extant human sample used here (Fig. 5d, e, Fig. 6) and only low in *Pan* (Fig. 5f, g, Fig. 6). The latter shows a non-fully overlapping configuration between the two *P. troglodytes* and *P. paniscus* representatives (SOM Fig. S2), the meaning of which cannot be further assessed in this study. However, they also show a previously unreported evidence: while sharing with humans a tendency towards a latero-medial decrease in average cortical thickness across both walls, two *P. robustus* specimens (SK 82 and SK 97) reveal a distinctly thicker anterior wall (Fig. 5a, b, Fig. 6), and a third specimen, for which no reliable information is available for entirely assessing the posterior wall (SWT1/LB-2), shows the absolutely thickest anterior cortex in the analytical and comparative context of the present study (Fig. 5c).

Following Ruff and Higgins (2013), the condition of variably less asymmetric cortices in the australopith femoral neck compared to humans, which our study demonstrates being more accentuated in *P. robustus* than in *Australopithecus*, points to a relative increase in supero-inferior bending of the neck likely associated with a greater lateral displacement of the body centre of gravity over the stance limb during the support phase of gait. This condition engenders a more vertical hip joint reaction force and bending increase relative to the neck axial loadings (Ruff and Higgins, 2013). Such loading conditions are compatible with a supero-inferior, not an antero-posterior, extension of the femoral neck, which is a typical australopith feature. Accordingly, anterior and posterior strains in australopiths decline under a more vertical loading configuration (Ruff and Higgins, 2013: 521). The distinctly thicker anterior wall detected in *P. robustus*, lacking in humans and apes (Ohman et al., 1997, and present study), could precisely result from the unique australopith architecture combining a longer, supero-inferiorly expanded and antero-posteriorly relatively compressed femoral neck. In terms of quadrant proportions (Fig. 3b), compared to the extant human and ape patterns, the australopith conformation implies medio-laterally extended but narrower superior and inferior strips of cortical bone, a greater portion of compressive loads being thus absorbed through anterior cortex thickening. If so, it is expected that the still unreported structural neck conformation in *Australopithecus* resembles that of *P. robustus* in the degree of anterior vs. posterior wall thickness asymmetry. Alternatively, whenever the inner organisation of *Australopithecus* is closer to the human pattern, or even reveals another configuration, it would imply different hip joint loading conditions in the two extinct hominins likely resulting from non-fully overlapping locomotive modes.

5. Conclusive remarks

As suggested by previous research, Plio-Pleistocene hominins practiced different forms of terrestrial bipedality (e.g., Stern, 2000; Ward, 2002, 2013; Lovejoy et al., 2009; Haile-Selassie et al., 2012; Barak et al., 2013b; DeSilva et al., 2013; Harcourt-Smith, 2016; Ruff et al., 2016, 2018; Zeininger et al., 2016), likely implying slightly different gait kinematics (see Komza et al., 2018). Evidence for some variations between *A. africanus* and *Paranthropus* (*boisei* and *robustus*) has been provided by the study of the trabecular architecture of the talus (Su and Carlson, 2017), while no textural differences have been found between the two taxa at the femoral head (Ryan et al. 2018). However, at the base of its femoral neck *A. afarensis* shows a more human-like pattern of cortical asymmetry (Ruff et al., 2018) than *P. robustus* (present

study), suggesting possible hip joint loading differences. In this respect, we predict that, based on the µXCT records recently realised for *A. afarensis* (Ruff et al., 2016) and *A. africanus* (Ryan et al., 2018), a refined comparative assessment of the australopith inner structural organisation of the femoral neck has the potential to reveal gait-related subtle differences possibly distinguishing *Australopithecus* and *Paranthropus*.

Acknowledgements

For access to fossil and comparative materials, we are grateful to the curatorial staff of the Ditsong National Museum of Natural History, Pretoria; the Pretoria Bone Collection at the Department of Anatomy of the University of Pretoria; the Evolutionary Studies Institute at the University of the Witwatersrand; the McGregor Museum of Kimberley; and the Muséum national d'Histoire naturelle, Paris. We especially acknowledge B. Billing (Johannesburg), L. Kgasi (Pretoria), D. Morris (Kimberley), S. Potze (Pretoria) and B. Zipfel (Johannesburg). We also thank K. Jakata (Johannesburg) and L. Bam (Pelindaba) for X-ray micro-tomographies at Wits and Necsa, respectively. Special thanks for data sharing (SKW 19) to K. Carlson (Johannesburg). Acquisitions at the ESRF were performed by R.M. within the EC TNT project in coll. with A. Mazurier (Poitiers). The X-ray image of the KNM-WT 15000-G *H. erectus* femur from Nariokotome (SOM Fig. S3) has been realised in 2000 at the National Museums of Kenya, Nairobi, by R.M., Bondioli (Rome) and M. Rossi (Bologna) thanks to the kind collaboration of M.G. Leakey (Nairobi), A. Walker (State College) and C.V. Ward (Columbia) and the technical assistance of G. Abungu and F.M. Kirera (Nairobi). For the creation of an ad hoc analytical routine used in this study, we are grateful to J. Dumoncel (Toulouse). For scientific collaboration and availability to run independent measures for inter-observer error assessment, we thank A. Beaudet (Johannesburg), J. Dumoncel, A. Mazurier and C. Zanolli (Tolouse). For discussion, we thank A. Beaudet, L. Bruxelles (Johannesburg and Toulouse), K. Carlson, R.J. Clarke (Johannesburg), J. Dumoncel, T. Jashashvili (Johannesburg), D. Marchi (Pisa), C. Zanolli, B. Zipfel (Johannesburg). We acknowledge the DST-NRF for financial support (Grant # UID23456) to establish the MIXRAD micro-focus X-ray tomography facility at Necsa. M.C. was funded by the European Commission (EACEA), Erasmus Mundus programme, AESOP and AESOP+ consortia coordinated by J.B.

References

Aiello, L., Dean, C., 1990. An Introduction to human Evolutionary Anatomy. Academic Press, New York.

Baddeley, A., Rubak, E., Turner, R., 2015. Spatial Point Patterns: Methodology and Applications with R. Chapman and Hall/CRC Press, London.

Balter, V., Blichert-Toft, J., Braga, J., Telouk, P., Thackeray, F., Albarède, F., 2008. U-Pb dating of fossil enamel from the Swartkrans Pleistocene hominid site, South Africa. Earth and Planetary Science Letters 267, 236-246.

Barak, M.M., Lieberman, D.E., Hublin, J.J., 2011. A Wolff in sheep's clothing: Trabecular bone adaptation in response to changes in joint loading orientation. Bone 49, 1141-1151.

Barak, M.M., Lieberman, D.E., Hublin, J.J., 2013a. Of mice, rats and men: Trabecular bone architecture in mammals scales to body mass with negative allometry. Journal of Structural Biology 183, 123-131.

Barak, M.M., Lieberman, D.E., Raichlen, D., Pontzer, H., Warrener, A.G., Hublin, J.J., 2013b. Trabecular evidence for a human-like gait in *Australopithecus africanus*. PLoS ONE 8, e77687.

Barak, M.M., Sherratt, E., Lieberman, D.E., 2017. Using principal trabecular orientation to differentiate joint loading orientation in the 3rd metacarpal heads of humans and chimpanzees. Journal of Human Evolution 113, 173-182.

Bayle, P., Bondioli, L., Macchiarelli, R., Mazurier, A., Puymerail, L., Volpato, V., Zanolli, C., 2011. Three-dimensional imaging and quantitative characterization of human fossil remains. Examples from the NESPOS database. In: Macchiarelli, R., Weniger, G.-C. (Eds), Pleistocene Databases. Acquisition, Storing, Sharing, vol. 4. Wissenschaftliche Schriften des Neanderthal Museums, Mettmann, pp. 29-46.

Berge, C., Goularas, D., 2010. A new reconstruction of Sts 14 pelvis (*Australopithecus africanus*) from computed tomography and three-dimensional modeling techniques. Journal of Human Evolution 58, 262-272.

Bishop, P.J., Clemente, C.J., Hocknull, S.A., Barrett, R.S., Lloyd, D.G., 2017. The effects of cracks on the quantification of the cancellous bone fabric tensor in fossil and archaeological specimens: A simulation study. Journal of Anatomy 230, 461-470.

Bleuze, M.M., 2010. Cross-Sectional Morphology and Mechanical Loading in Plio-Pleistocene Hominins: Implications for Locomotion and Taxonomy. Ph.D. Dissertation, The University of Western Ontario, Ontario.

Bondioli, L., Bayle, P., Dean, C., Mazurier, A., Puymerail, L., Ruff, C., Stock, J.T., Volpato, V., Zanolli, C., Macchiarelli, R., 2010. Morphometric maps of long bone shafts and dental

roots for imaging topographic thickness variation. American Journal of Physical Anthropology 142, 328-334.

Bonewald, L.F., Johnson, M.L., 2008. Osteocytes, mechanosensing and Wnt signaling. Bone 42, 606-615.

Bonhomme, V., Picq, S., Gaucherel, C., Claude, J., 2014. Momocs: Outline Analysis Using R. Journal of Statistical Software 56, 1-24.

Carter, D.R., Orr, T.E., Fyhrie, D.P., 1989. Relationships between loading history and femoral cancellous bone architecture. Journal of Biomechanics 22, 231-244.

Cazenave, M., 2015. The Inner Structural Morphology of the Femoral Head of *Paranthropus robustus*. Master Thesis, Université Toulouse III - Paul Sabatier, Toulouse.

Cazenave, M., Braga, J., de Beer, F., Hoffman, J.W., Macchiarelli, R., Oettlé, A., Thackeray, J.F., 2017a. Site-specific cortical bone topographic variation across the whole neck assessed in two hominin proximal femora from Swartkrans Member 1, South Africa: SK 82 and SK 97. American Journal of Physical Anthropology 162, S64, 140.

Cazenave, M., Braga, J., de Beer, F., Hoffman, J.W., Macchiarelli, R., Thackeray, J.F., 2015. The inner structural morphology of the femoral head of *Paranthropus robustus*. Proceedings of the European Society for the Study of human Evolution 5, 68.

Cazenave, M., Braga, J., Oettlé, A., Thackeray, J.F., de Beer, F., Hoffman, J., Endalamaw, M., Engda Redae, B., Puymerail L., Macchiarelli, R., 2017b. Inner structural organization of the distal humerus in *Paranthropus* and *Homo*. In: Macchiarelli, R., Zanolli, C. (Eds), Hominin Biomechanics, Virtual Anatomy and Inner Structural Morphology: From Head to Toe. A Tribute to Laurent Puymerail. Comptes Rendus Palevol 16, 521-532.

Cazenave, M., Oettlé, A., Thackeray, J.F., Nakatsukasa, M., de Beer, F., Hoffman, J., Macchiarelli, R., 2018. The SKX 1084 hominin patella from Swartkrans Member 2, South Africa: An integrated analysis of its outer morphology and inner structure. Comptes Rendus Palevol (CRPALEVOL-D-18-00012, in review).

Chirchir, H., Kivell, T.L., Ruff, C.B., Hublin, J.-J., Carlson, K.J., Zipfel, B., Richmond, B.G., 2015. Recent origin of low trabecular bone density in modern humans. Proceedings of the National Academy of Sciences USA 112, 366-371.

Crabtree, N., Loveridge. N., Parker, M., Rushton, N., Power, J., Bell, K.L., Beck, T.J., Reeve, J., 2001. Intracapsular hip fracture and the region-specific loss of cortical bone: Analysis by peripheral quantitative computed tomography. Journal of Bone and Mineral Research 16, 1318-1328.

Curnoe, D., Grün, R., Taylor, L., Thackeray, F., 2001. Direct ESR dating of a Pliocene hominin from Swartkrans. Journal of Human Evolution 40, 379-391.

Dalstra, M., Huiskes, R., 1995. Load transfer across the pelvic bone. Journal of Biomechanics. 28, 715-724.

Dayal, M.R., Kegley, A.D.T., Štrkalj, G., Bidmos, M.A., Kuykendall, K.L., 2009. The history and composition of the Raymond A. Dart collection of human skeletons at the University of the Witwatersrand, Johannesburg, South Africa. American Journal of Physical Anthropology 140, 324-335.

Delson, E., 1988. Chronology of South African australopith site units. In: Grine, F.E. (Ed.), Evolutionary History of the "Robust" Australopithecines. Aldine de Gruyter, New York, pp. 317-324.

Demissie, S., Dupuis, J., Cupples, L.A., Beck, T., Kiel, D.P., Karasik, D., 2007. Proximal hip geometry is linked to several chromosomal regions: Genome-wide linkage results from the Framingham Osteoporosis Study. Bone 40, 743-750.

DeSilva, J.M., Devlin, M.J., 2012. A comparative study of the trabecular bony architecture of the talus in humans, non-human primates, and *Australopithecus*. Journal of Human Evolution 63, 536-551.

DeSilva, J.M., Holt, K., Churchill, S., Carlson, K., Walker, C., Zipfel, B., Berger, L., 2013. The lower limb and mechanics of walking in *Australopithecus sediba*. Science 340, 1232999.

Ding, M., Odgaard, A., Danielsen, C.C., Hvid, I., 2002. Mutual associations among microstructural, physical and mechanical properties of human cancellous bone. J. Bone Joint Surg. 84-B, 900-907.

Djuric, M., Djonic, D., Milovanovic, P., Nikolic, S., Marshall, R., Marinkovic, J., Hahn, M., 2010. Region-specific sex-dependent pattern of age-related changes of proximal femoral cancellous bone and its implications on differential bone fragility. Calcified Tissue International 86, 192-201.

Domínguez-Rodrigo, M., Pickering, T.R., Baquedano, E., Mabulla, A., Mark, D.F., Musiba, C., Pérez-González, A., 2013. First partial skeleton of a 1.34-million-year-old *Paranthropus boisei* from Bed II, Olduvai Gorge, Tanzania. PLoS ONE 8, e80347.

Doube, M., Klosowski, M.M., Wiktorowicz-Conroy, A.M., Hutchinson, J.R., Shefelbine, S.J., 2011. Trabecular bone scales allometrically in mammals and birds. Proceedings of the Royal Society B 278, 3067-3073.

Dowdeswell, M.R., Jashashvili, T., Patel, B.A., Lebrun, R., Susman, R.L., Lordkipanidze, D., Carlson, K.J., 2016. Adaptation to bipedal gait and fifth metatarsal structural properties in

Australopithecus, *Paranthropus*, and *Homo*. In: Macchiarelli, R., Zanolli, C. (Eds), Hominin Biomechanics, Virtual Anatomy and Inner Structural Morphology: From Head to Toe. A Tribute to Laurent Puymerail. Comptes Rendus Palevol 16, 585-599.

Fajardo, R.J., Desilva, J.M., Manoharan, R.K., Schmitz, J.E., Maclatchy, L.M., Bouxsei, M.L., 2013. Lumbar vertebral body bone microstructural scaling in small to medium-sized strepsirhines. Anatomical Record 296, 210-226.

Fajardo, R.J., Müller, R., 2001. Three-dimensional analysis of nonhuman primate trabecular architecture using micro-computed tomography. American Journal of Physical Anthropology 115, 327-336.

Fajardo, R.J., Müller, R., Ketcham, R.A., Colbert, M., 2007. Nonhuman anthropoid primate femoral neck trabecular architecture and its relationship to locomotor mode. The Anatomical Record 290, 422-436.

Fajardo, R.J., Ryan, T.M., Kappelman, J., 2002. Assessing the accuracy of high-resolution X-ray computed tomography of primate trabecular bone by comparisons with histological sections. American Journal of Physical Anthropology 118, 1-10.

Gibbon, R.J., Rayne, T., Sutton, M.B., Heaton, J.L., Kuman, K., Clarke, R.J., Brain, C.K., Granger, D.E., 2014. Quaternary geochronology cosmogenic nuclide burial dating of hominin-bearing Pleistocene cave deposits at Swartkrans, South Africa. Quaternary Geochronology 24, 10-15.

Gibson, L.J., 1985. The mechanical behaviour of cancellous bone. Journal of Biomechanics 18, 317-328.

Gosman, J.H., Stout, S.D., Larsen, C.S., 2011. Skeletal biology over the life span: A view from the surfaces. American Journal of Physical Anthropology 146, 86-98.

Grabowski, M.W., Roseman, C.C., 2015. Complex and changing patterns of natural selection explain the evolution of the human hip. Journal of Human Evolution 85, 94-110.

Grine, F.E., 1989. New hominid fossils from the Swartkrans formation (1979-1986 excavations): Craniodental specimens. American Journal of Physical Anthropology 79, 409-449.

Gross, T., Kivell, T.L., Skinner, M.M., Huynh Nguyen, N., Pahr, D.H., 2014. A CT-image-based framework for the holistic analysis of cortical and trabecular bone morphology. Palaeontologia Electronica 17, 33A, 1-13.

Gruss, L.T., Schmitt, D., 2015. The evolution of the human pelvis: Changing adaptations to bipedalism, obstetrics and thermoregulation. Philosophical Transactions of the Royal Society B 370, 20140063.

Haile-Selassie, Y., Saylor, B., Deino, A., Levin, N., Alene, M., Latimer, B., 2012. A new hominin foot from Ethiopia shows multiple Pliocene bipedal adaptations. Nature 483, 565-569.

Harcourt-Smith, W., 2016. Early hominin diversity and the emergence of the genus *Homo*. Journal of Anthropological Sciences 94, 19-27.

Harmon, E., 2009. Size and shape variation in the proximal femur of *Australopithecus africanus*. Journal of Human Evolution 56, 551-559.

Havill, L.M., Allen, M.R., Bredbenner, T.L., Burr, D.B., Nicolella, D.P., Turner, C.H., Warren, D.M., Mahaney, M.C., 2010. Heritability of lumbar trabecular bone mechanical properties in baboons. Bone 46, 835-840.

Havill, L.M., Mahaney, M.C., Binkley, T.L., Specker, B.L., 2007. Effects of genes, sex, age, and activity on BMC, bone size, and areal and volumetric BMD. Journal of Bone and Mineral Research 22, 737-746.

Herries, A.I.R., Curnoe, D., Adams, J.W., 2009. A multi-disciplinary seriation of early *Homo* and *Paranthropus* bearing palaeocaves in Southern Africa. Quaternary International 202, 14-28.

Huiskes, R., 2000. If bone is the answer, then what is the question? Journal of Anatomy 197, 145-56.

Jashashvili, T., Dowdeswell, M.R., Lebrun, R., Carlson, K.J., 2015. Cortical structure of hallucal metatarsals and locomotor adaptations in hominoids. PLoS ONE 10, e0117905.

Johansson, J., Nordström, A., Nordström, P., 2015. Objectively measured physical activity is associated with parameters of bone in 70-year-old men and women. Bone 81, 72-79.

Judex, S., Garman, R., Squire. M, Leah-Rae, D., Rubin, C., 2004. Genetically based influences on the site-specific regulation of trabecular and cortical bone morphology. Journal of Bone and Mineral Research 19, 600-606.

Kapandji, A.I., 2011. The Physiology of the Joints. Vol. 2. The Lower Limb. 6th ed. Elsevier, Edinburgh.

Kibii, J.M., Churchill, S.E., Schmid, P., Carlson, K.J., Reed, N.D., de Ruiter, D.J., Berger, L.R., 2011. A partial pelvis of *Australopithecus sediba*. Science 333, 1407-1411.

Kivell, T.L., 2016. A review of trabecular bone functional adaptation: What have we learned from trabecular analyses in extant hominoids and what can we apply to fossils? Journal of Anatomy 228, 569-594.

Komza, K., Kivell, T.L., Skinner, M.M., 2018. Unique forms of locomotion in Swartkrans hominins: An analysis of the trabecular structure of the first metatarsal. American Journal of Physical Anthropology 165, S66, 144.

L'Abbé, E.N., Loots, M., Meiring, J.H., 2005. The Pretoria Bone Collection: A modern South African skeletal sample. Homo 56, 197-205.

Lanyon, L., Skerry, T., 2001. Perspective: Postmenopausal osteoporosis as a failure of bone's adaptation to functional loading: A hypothesis. Journal of Bone and Mineral Research 16, 1937-1947.

Levangie, P.K., Norkin, C.C., 2005. Joint Structure and Function: A Comprehensive Analysis. F.A. Davis, Philadelphia.

Lieberman, D.E., Pearson, O.M., Polk, J.D., Demes, B., Crompton, A.W., 2003. Optimization of bone growth and remodeling in response to loading in tapered mammalian limbs. Journal of Experimental Biology 206, 3125-3138.

Lieberman, D.E., Polk, J.D., Demes, B., 2004. Predicting long bone loading from cross-sectional geometry. American Journal of Physical Anthropology 123, 156-171.

Lockwood, C.A., Menter, C.G., Moggi-Cecchi, J., Keyser, A.W., 2007. Extended male growth in a fossil hominin species. Science 318, 1443-1446.

Lotz, J.C., Cheal, E.J., Hayes, W.C., 1995. Stress distributions within the proximal femur during gait and falls: Implications for osteoporotic fracture. Osteoporosis International 5, 252-261.

Lovejoy, C.O., 1975. Biomechanical perspectives on the lower limb of early hominids. In: Tuttle, R.H. (Ed.), Primate Functional Morphology and Evolution. Mouton, Paris, pp. 291-326.

Lovejoy, C.O., 1988. Evolution of human walking. Scientific American 259, 118-125.

Lovejoy, C.O., 2005. The natural history of human gait and posture. Part 2. Hip and thigh. Gait & Posture 21, 113-124.

Lovejoy, C.O., Cohn, M.J., White, T.D., 1999. Morphological analysis of the mammalian postcranium: A developmental perspective. Proceedings of the National Academy of Sciences USA 96, 13247-13252.

Lovejoy, C.O., Heiple, K.G., Burstein, A.H., 1973. The gait of *Australopithecus*. American Journal of Physical Anthropology 38, 757-780.

Lovejoy, C.O., Meindl, R.S., Ohman, J.C., Heiple, K.G., White, T.D., 2002. The Maka femur and its bearing on the antiquity of human walking: Applying contemporary concepts of morphogenesis to the human fossil record. American Journal of Physical Anthropology 119, 97-133.

Lovejoy, C.O., Suwa, G., Spurlock, L., Asfaw, B., White, T., 2009. The pelvis and femur of *Ardipithecus ramidus*: The emergence of upright walking. Science 326, 71e1-71e6.

Macchiarelli, R., Bondioli, L., 2000. Multimedia dissemination of the "Isola Sacra" human paleobiological project: Reconstructing lives, habits, and deaths of the "ancient Roman people" by means of advanced investigative methods. In: Guarino, A. (Ed.), Proceedings of 2nd International Congress on Science and Technology for the Safeguard of Cultural Heritage in the Mediterranean Basin, vol. 2. Elsevier, Paris, pp. 1075-1080.

Macchiarelli, R., Bondioli, L., Galichon, V., Tobias, P.V., 1999. Hip bone trabecular architecture shows uniquely distinctive locomotor behaviour in South African australopithecines. Journal of Human Evolution 36, 211-232.

MacLatchy, L., Müller, R., 2002. A comparison of the femoral head and neck trabecular architecture of *Galago* and *Perodicticus* using micro-computed tomography (microCT). Journal of Human Evolution 43, 89-105.

McHenry, H.M., 1975. Biomechanical interpretation of the early hominid hip. Journal of Human Evolution 4, 343-355.

Meyer, F., Beucher, S., 1990. Morphological segmentation. Journal of Visual Communication and Image Representation 1, 21-46.

Milovanovic, P., Djonic, D., Hahn, M., Amling, M., Busse, B., Djuric, M., 2017. Region-dependent patterns of trabecular bone growth in the human proximal femur: A study of 3D bone microarchitecture from early postnatal to late childhood period. American Journal of Physical Anthropology 164, 281-291.

Mittra, E., Rubin, C., Qin, Y.X., 2005. Interrelationship of trabecular mechanical and microstructural properties in sheep trabecular bone. Journal of Biomechanics 38, 1229-1237.

Morimoto, N., Ponce de León, M.S., Zollikofer, C.P.E., 2011. Exploring femoral diaphyseal shape variation in wild and captive chimpanzees by means of morphometric mapping: A test of Wolff's Law. The Anatomical Record 294, 589-609.

Morris, A.G., 1984. Osteological Analysis Populations of the Cape and Western Africa. Ph.D. Dissertation, University of the Witwatersrand, Johannesburg.

Napier, J.R., 1964. The evolution of bipedal walking in the hominids. Archives de Biologie (Liege) 75, 673-708.

Ohman, J.C., Krochta, T.J., Lovejoy, C.O., Mensforth, R.P., Latimer, B., 1997. Cortical bone distribution in the femoral neck of hominoids: Implications for the locomotion of *Australopithecus afarensis*. American Journal of Physical Anthropology 104, 117-131.

O'Neill, M.C., Dobson, S.D., 2008. The degree and pattern of phylogenetic signal in primate long-bone structure. Journal of Human Evolution 54, 309-322.

Pearson, O.M., Lieberman, D.E., 2004. The aging of Wolff's "law": Ontogeny and responses to mechanical loading in cortical bone. Yearbook of Physical Anthropology 47, 63-99.

Pebesma, E.J., 2004. Multivariable geostatistics in S: The gstat package. Computers & Geosciences 30, 683-691.

Pickering, T.R., Heaton, J.L., Clarke, R.J., Sutton, M.B., Brain, C.K., Kuman, K., 2012. New hominid fossils from Member 1 of the Swartkrans formation, South Africa. Journal of Human Evolution 62, 618-628.

Pickering, R., Kramers, J.D., Hancox, P.J., de Ruiter, D.J., Woodhead, J.D., 2011. Contemporary flowstone development links early hominin bearing cave deposits in South Africa. Earth and Planetary Science Letters 306, 23-32.

Puymerail, L., Ruff, C.B., Bondioli, L., Widianto, H., Trinkaus, E., Macchiarelli, R., 2012. Structural analysis of the Kresna 11 *Homo erectus* femoral shaft (Sangiran, Java). Journal of Human Evolution 63, 741-749.

R Development Core Team, 2018. R: A Language and Environment for Statistical Computing (http://www.R-project.org).

Rafferty, K.L., 1998. Structural design of the femoral neck in primates. Journal of Human Evolution 34, 361-383.

Raichlen, D.A., Gordon, A.D., Foster, A.D., Webber, J.T., Sukhdeo, S.M., Scott, R.S., Gosman, J.H., Ryan, T.M., 2015. An ontogenetic framework linking locomotion and trabecular bone architecture with applications for reconstructing hominin life history. Journal of Human Evolution 81, 1-12.

Robinson, J.T., 1972. Early Hominid Posture and Locomotion. University of Chicago Press, Chicago.

Roerdink, J., Meijster, A., 2000. The watershed transform: Definitions, algorithm and parallelization strategies. Fundamenta Informaticae 41, 178-228.

Ruff, C.B., 1995. Biomechanics of the hip and birth in early *Homo*. American Journal of Physical Anthropology 98, 527-574.

Ruff, C.B., 2002. Long bone articular and diaphyseal structure in old world monkeys and apes. I: Locomotor effects. American Journal of Physical Anthropology 119, 305-342.

Ruff, C.B., 2010. Body size and body shape in early hominins. Implications of the Gona pelvis. Journal of Human Evolution 58, 166-178.

Ruff, C.B., 2017. Mechanical constraints on the hominin pelvis and the "obstetrical dilemma". The Anatomical Record 30, 946-955.

Ruff, C.B., Burgess, M.L., Ketcham, R.A., Kappelman, J., 2016. Limb bone structural proportions and locomotor behavior in AL 288-1 ("Lucy"). PLoS ONE 11, e0166095.

Ruff, C.B., Burgess, M.L., Squyres, N., Junno, J.A., Trinkaus, E., 2018. Lower limb articular scaling and body mass estimation in Pliocene and Pleistocene hominins. Journal of Human Evolution 115, 85-111.

Ruff, C.B., Higgins, R., 2013. Femoral neck structure and function in early hominins. American Journal of Physical Anthropology 150, 512-525.

Ruff, C.B., Holt, B.H., Trinkaus, E., 2006. Who's afraid of the big bad Wolff? Wolff's Law and bone functional adaptation. American Journal of Physical Anthropology 129, 484-498.

Ruff, C.B., McHenry, H.M., Thackeray, J.F., 1999. Cross-sectional morphology of the SK 82 and 97 proximal femora. American Journal of Physical Anthropology 109, 509-521.

Ryan, T.M., Carlson, K.J., Gordon, A.D., Jablonski, N. Shaw, C.N., Stock, J.T., 2018. human-like hip joint loading in *Australopithecus africanus* and *Paranthropus robustus*. Journal of Human Evolution, in press (https://doi.org/10.1016/j.jhevol.2018.03.008).

Ryan, T.M., Ketcham, R., 2002a. The three-dimensional structure of trabecular bone in the femoral head of strepsirrhine primates. Journal of Human Evolution 43, 1-26.

Ryan, T.M., Ketcham, R., 2002b. Femoral head trabecular bone structure in two omomyid primates. Journal of Human Evolution 43, 241-263.

Ryan, T.M., Ketcham, R.A., 2005. Angular orientation of trabecular bone in the femoral head and its relationship to hip joint loads in leaping primates. Journal of Morphology 265, 249-263.

Ryan, T.M., Krovitz, G.E., 2006. Trabecular bone ontogeny in the human proximal femur. Journal of Human Evolution 51, 591-602.

Ryan, T.M., Shaw, C.N., 2012. Unique suites of trabecular bone features characterize locomotor behavior in human and non-human anthropoid primates. PLoS ONE 7, 1-11.

Ryan, T.M., Shaw, C.N., 2013. Trabecular bone microstructure scales allometrically in the primate humerus and femur. Proceedings of the Royal Society of London B 280, 20130172.

Ryan, T.M., Shaw, C.N., 2015. Gracility of the modern *Homo sapiens* skeleton is the result of decreased biomechanical loading. Proceedings of the National Academy of Sciences USA 112, 372-377.

Ryan, T.M., Sukhdeo, S., 2016. KSD-VP-1/1: Analysis of the postcranial skeleton using high-resolution computed tomography. In: Haile-Selassie, Y., Su, D.E. (Eds), The Postcranial Anatomy of *Australopithecus afarensis*. Springer, Dordrecht, pp. 39-62.

Ryan, T.M., Walker, A., 2010. Trabecular bone structure in the humeral and femoral heads of anthropoid primates. The Anatomical Record 293, 719-729.

Saers, J.P.P., Cazorla-Bak, Y., Shaw, C.N., Stock, J.T., Ryan, T.M., 2016. Trabecular bone structural variation throughout the human lower limb. Journal of Human Evolution 97, 97-108.

Saparin, P., Scherf, H., Hublin, J.J., Fratzl, P., Weinkamer, R., 2011. Structural adaptation of trabecular bone revealed by position resolved analysis of proximal femora of different primates. Anatomical Record 294, 55-67.

Schneider, C.A., Rasband, W.S., Eliceiri, K.W., 2012. NIH Image to ImageJ: 25 years of image analysis. Nature Methods 9, 671-675.

Shaw, C., Ryan, T., 2012. Does skeletal anatomy reflect adaptation to locomotor patterns? Cortical and trabecular architecture in human and nonhuman anthropoids. American Journal of Physical Anthropology 147, 187-200.

Sinclair, K.D., Farnsworth, R.W., Pham, T.X., Knight, A.N., Bloebaum, R.D., Skedros, J.G., 2013. The artiodactyl calcaneus as a potential "control bone" cautions against simple interpretations of trabecular bone adaptation in the anthropoid femoral neck. Journal of Human Evolution 64, 366-379.

Skedros, J.G., Baucom, S.L., 2007. Mathematical analysis of trabecular "trajectories" in apparent trajectorial structures: The unfortunate historical emphasis on the human proximal femur. Journal of Theoretical Biology 244, 15-45.

Skerry, T.M., 2008. The response of bone to mechanical loading and disuse: Fundamental principles and influences on osteoblast/osteocyte homeostasis. Archives of Biochemistry and Biophysics 473, 117-123.

Skinner, M.M., Stephens, N.B., Tsegai, Z.J., Foote, A.C., Nguyen, N H., Gross, T., Dieter H. Pahr, D.H., Hublin, J.-J., Kivell, T.L., 2015. human-like hand use in *Australopithecus africanus*. Science 347, 395-399.

Spoor, F., Zonneveld, F., Macho, G., 1993. Linear measurements of cortical bone and dental enamel by computed tomography: Applications and problems. American Journal of Physical Anthropology 91, 469-484.

Stauber, M., Müller, R., 2006. Volumetric spatial decomposition of trabecular bone into rods and plates: A new method for local bone morphometry. Bone 38, 475-484.

Stern, J.T., 2000. Climbing to the top: A personal memoir of *Australopithecus afarensis*. Evolutionary Anthropology 9, 113-133.

Stern, J.T., Susman, R.L., 1981. Electromyography of the gluteal muscles in *Hylobates*, *Pongo*, and *Pan*: Implications for the evolution of hominid bipedality. American Journal of Physical Anthropology 55, 153-166.

Su, A., Carlson, K.J., 2017. Comparative analysis of trabecular bone structure and orientation in South African hominin tali. Journal of Human Evolution 106, 1-18.

Su, A., Wallace, I.J., Nakatsukasa, M., 2013. Trabecular bone anisotropy and orientation in an Early Pleistocene hominin talus from East Turkana, Kenya. Journal of Human Evolution 64, 667-677.

Susman, R.L., de Ruiter, D., Brain, C.K., 2001. Recently identified postcranial remains of *Paranthropus* and early *Homo* from Swartkrans Cave, South Africa. Journal of Human Evolution 41, 607-629.

Tague, R.G., Lovejoy, C.O., 1986. The obstetric pelvis of A.L. 288-1 (Lucy). Journal of Human Evolution 15, 237-255.

Tsegai, Z.J., Skinner, M.M., Pahr, D.H., Hublin, J.J., Kivell, T.L., 2018. Systemic patterns of trabecular bone across the human and chimpanzee skeleton. Journal of Anatomy 232, 641-656.

Vansickle, C., 2017. Measuring lateral iliac flare by different methods risks obscuring evolutionary changes in the pelvis. The Anatomical Record 300, 956-963.

Vrba, E.S., 1975. Some evidence of chronology and palaeoecology of Sterkfontein, Swartkrans and Kromdraai from the fossil Bovidae. Nature 254, 301-304.

Wallace, I.J., Tommasini, S.M., Judex, S., Garland, T., Demes, B., 2012. Genetic variations and physical activity as determinants of limb bone morphology: An experimental approach using a mouse model. American Journal of Physical Anthropology 148, 24-35.

Ward, C.V., 2002. Interpreting the posture and locomotion of *Australopithecus afarensis*: Where do we stand? American Journal of Physical Anthropology 119, 185-215.

Ward, C.V., 2013. Postural and locomotor adaptations of *Australopithecus* species. In: Reed, K.E., Fleagle, J.G., Leakey, R.E. (Eds), The Paleobiology of *Australopithecus*. Springer, Dordrecht, pp. 235-245.

Wood, B.A., Leakey, M., 2011. The Omo-Turkana basin fossil hominins and their contribution to our understanding of human evolution in Africa. Evolutionary Anthropology 20, 264-292.

Wood, S.N., 2004. Stable and efficient multiple smoothing parameter estimation for generalized additive models. Journal of the American Statistical Association 99, 673-686.

Wood, S.N., 2006. Generalized Additive Models: An Introduction with R. Chapman & Hall, Boca Raton.

Zanolli, C., Pan, L., Dumoncel, J., Kullmer, O., Kundrát, M., Liu, W., Macchiarelli, R., Mancini, L., Schrenk, F., Tuniz, C., 2018. Inner tooth morphology of *Homo erectus* from Zhoukoudian. New evidence from an old collection housed at Uppsala University, Sweden. Journal of Human Evolution 116, 1-13.

Zeininger, A., Patel, B.A., Zipfel, B., Carlson, K.J., 2016. Trabecular architecture in the StW 352 fossil hominin calcaneus. Journal of Human Evolution 97, 145-158.

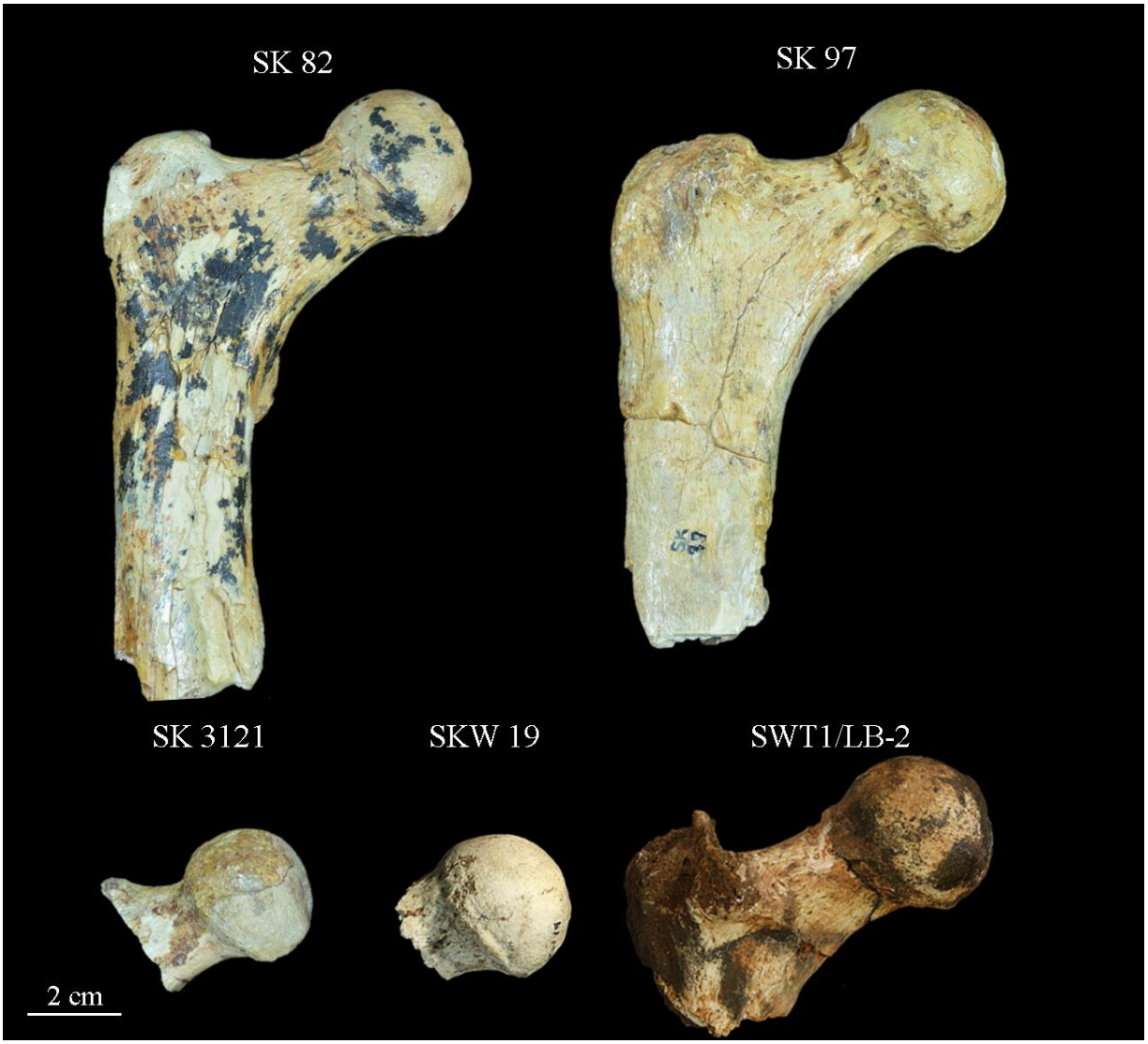

Figure 1. The five *P. robustus* proximal femoral ends from Swartkrans considered in this study (SK 82, SK 97, SK 3121, SKW 19 and SWT1/LB-2) in anterior view.

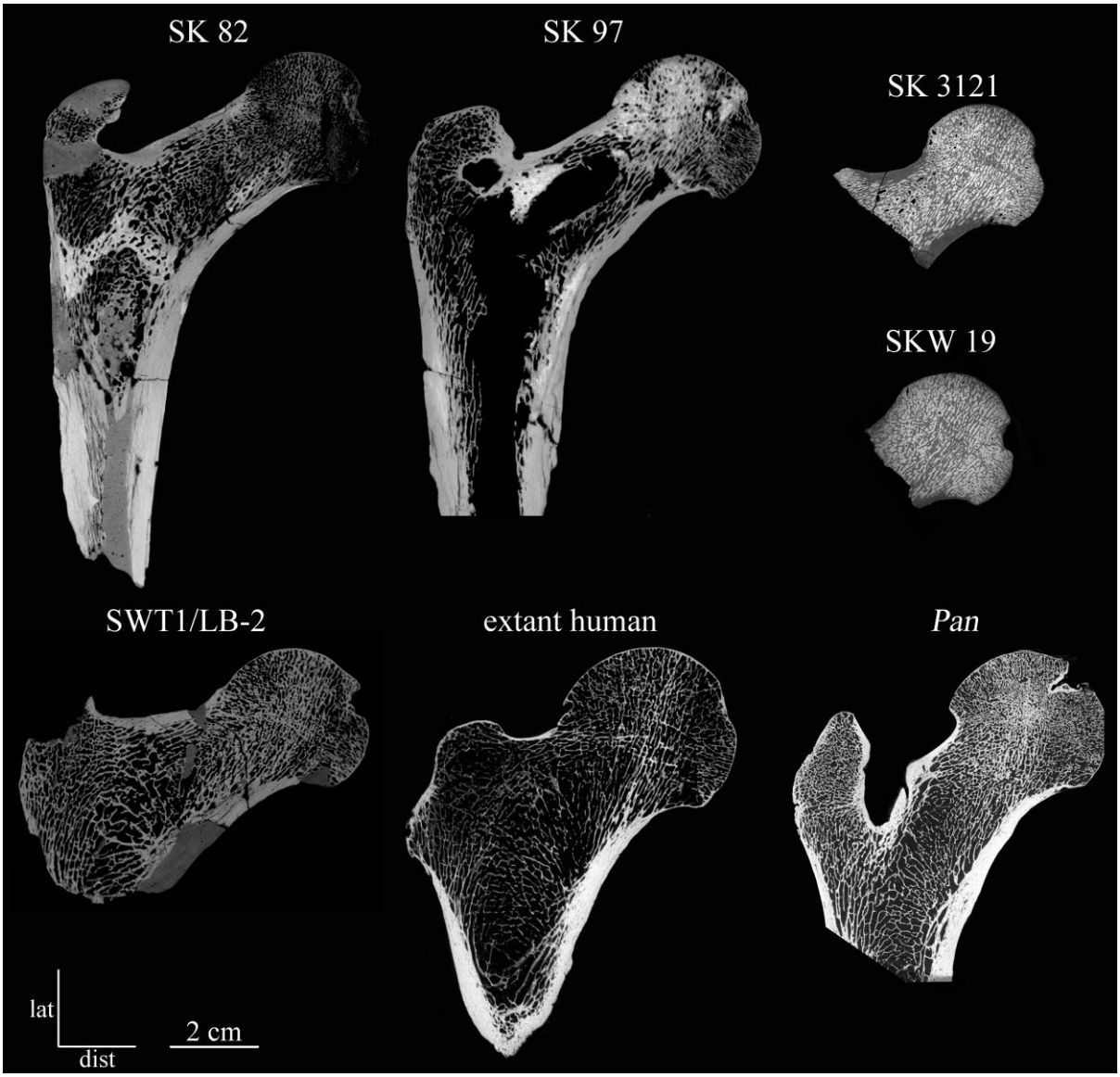

Figure 2. Micro-XCT-based virtual coronal sections through the femoral head centre showing the degree of inner preservation and structural organisation of the five *P. robustus* specimens from Swartkrans (SK 82, SK 97, SK 3121, SKW 19 and SWT1/LB-2) compared to the proximal femoral ends of an extant human and *Pan* (*P. troglodytes*) representatives.

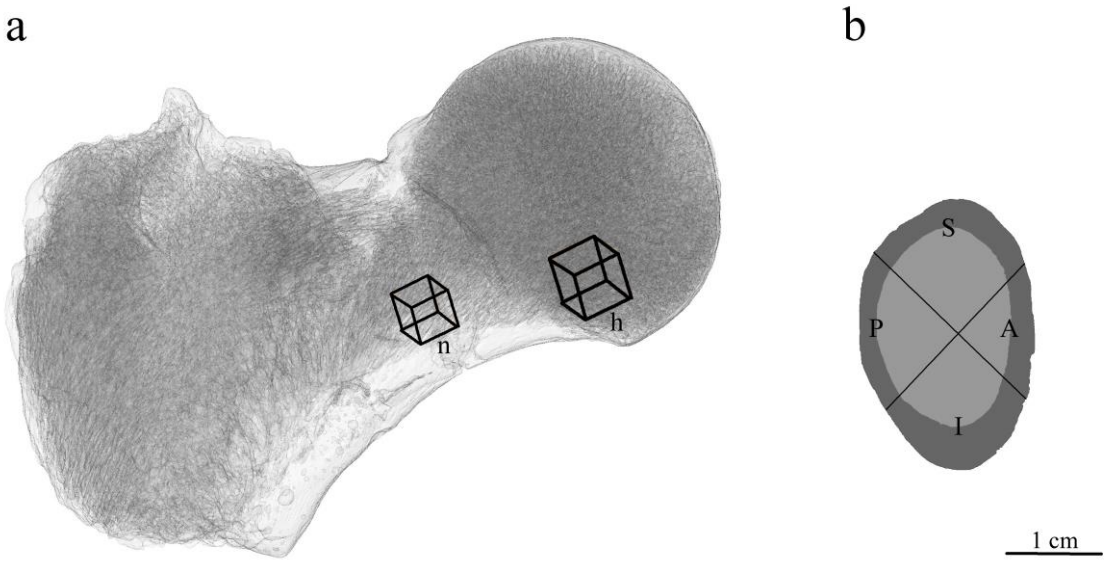

Figure 3. a) Position, orientation and proportions of the two cubic volume of interests (VOIs) virtually extracted for cancellous bone assessment from the infero-lateral portion of the femoral head (hVOI) and the inferior portion of the femoral neck (nVOI). The micro-CT-based image of the *P. robustus* specimen SWT1/LB-2 in semi-transparency is used as reference model. b) Antero-posterior virtual section across the longitudinal axis of the femoral neck illustrating the method used for delimiting the superior (S), inferior (I), anterior (A) and posterior (P) quadrants by two orthogonal lines set at 45° with respect to the supero-inferior neck axis. Thickness variation of the cortex is in dark grey.

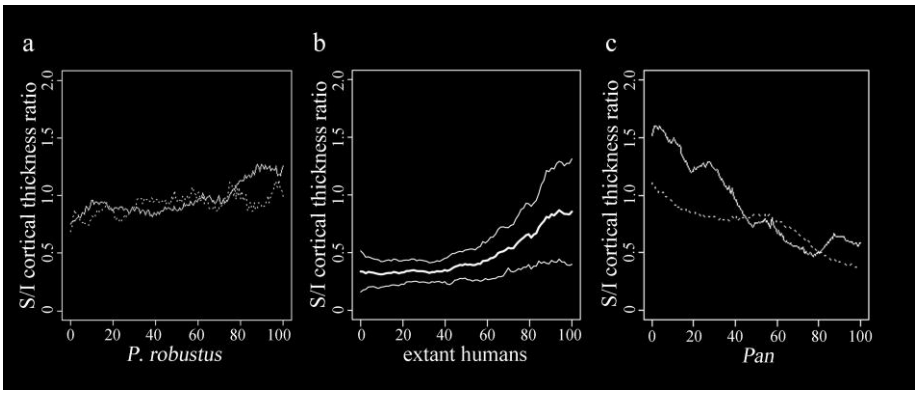

Figure 4. Latero-medial variation from the base of neck (0) to the head-neck junction (100%) of the S/I ratio between the superior (S) and inferior (I) cortical thicknesses in: a) *P. robustus* (SK 82: solid line; SK 97: dotted line), b) extant humans (mean ± 1 s.d.; n=12), c) *Pan* (*P. troglodytes*: solid line; *P. paniscus*: dotted line).

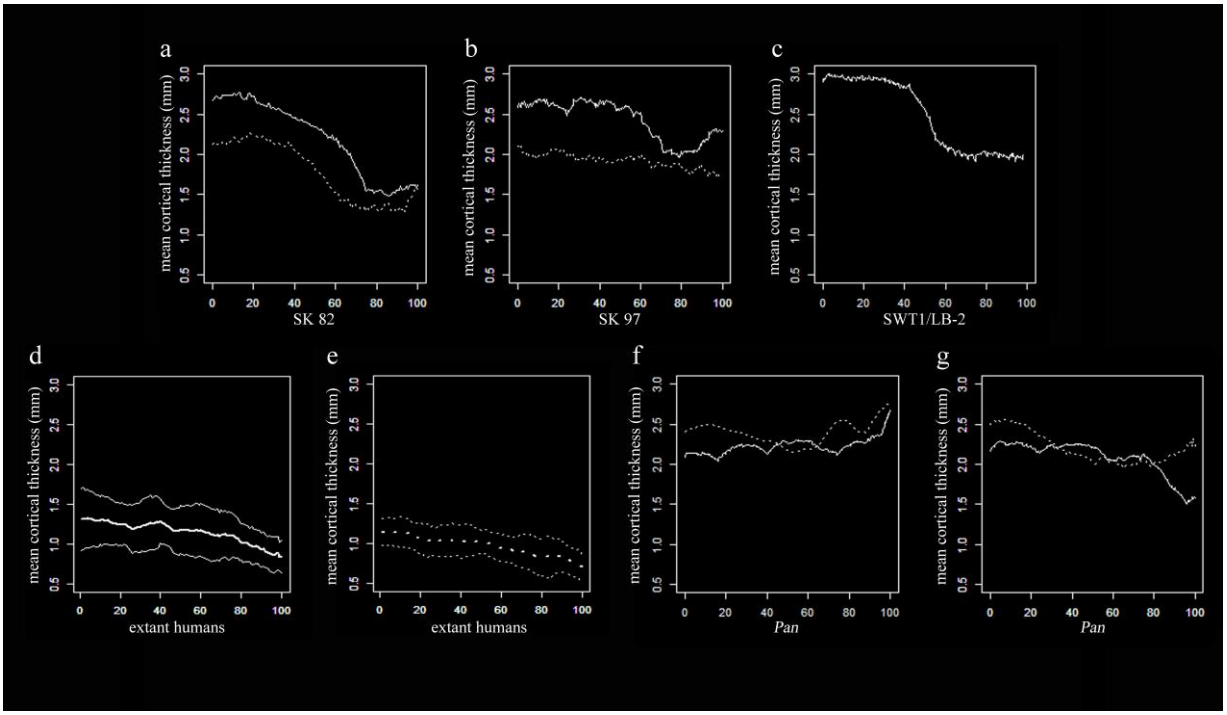

Figure 5. Latero-medial variation from the base of neck (0) to the head-neck junction (100%) of the mean cortical thickness (in mm) distinctly assessed for the anterior and posterior walls of the femoral neck in: a) SK 82 (anterior: solid line; posterior: dotted line), b) SK 97 (anterior: solid line; posterior: dotted line), c) SWT1/LB-2 (anterior), d) extant humans anterior (mean ± 1 s.d.; n=12), and e) extant humans posterior wall (mean ± 1 s.d.; n=12), f) *Pan* anterior (*P. troglodytes*: solid line; *P. paniscus*: dotted line) and g) *Pan* posterior wall (*P. troglodytes*: solid line; *P. paniscus*: dotted line).

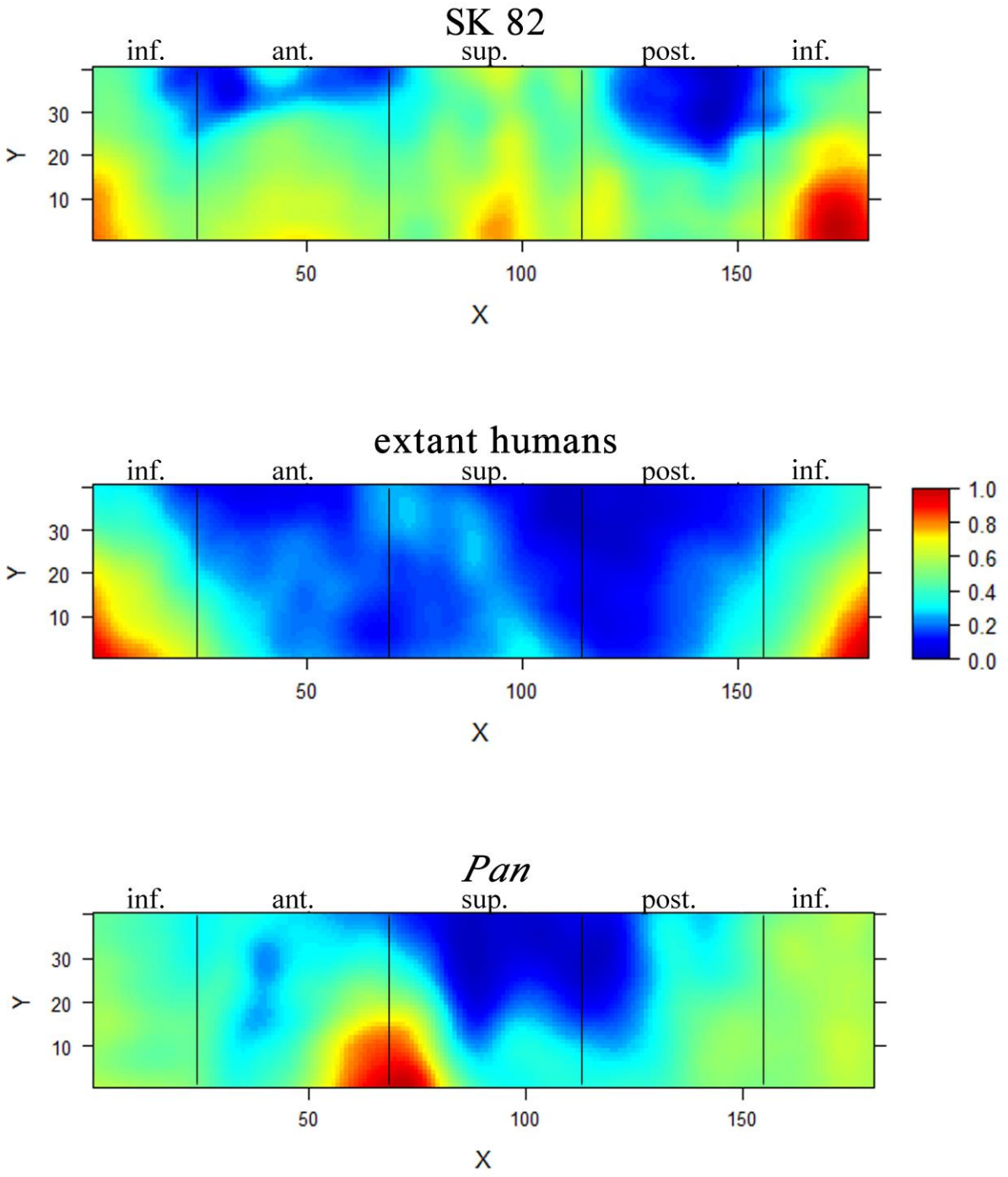

Figure 6. Micro-XCT-based standardised morphometric maps of the virtually unzipped, unrolled and projected cortical bone thickness of the *P. robustus* SK 82 neck from the base of neck (bottom Y-axis) to the head-neck junction (top Y-axis) compared to the consensus cartographies generated for the extant human sample (n = 12) and the two *Pan* representatives. Relative thickness is rendered by a pseudo-colour scale increasing from dark blue (0, thinner)

to red (1, thicker). inf., inferior quadrant; ant., anterior quadrant; sup., superior quadrant; post., posterior quadrant.

Table 1

Bone volume fraction (BV/TV, in %), trabecular thickness (Tb.Th., in mm), and degree of anisotropy (DA) of the volume of interest sampling the infero-lateral portion of the femoral head (hVOI; see Fig. 3a) assessed in *P. robustus* from Swartkrans (SK 82, SK 97, SK 3121, SKW 19 and SWT1/LB-2) and in two comparative samples of extant humans (n = 12; s.d., standard deviation) and *Pan* (n = 2).

Specimen/sample	BV/TV (%)	Tb.Th. (mm)	DA
SK 82	36.4	0.19	2.56
SK 97	39.9	0.23	3.48
SK 3121	33.1	0.16	3.55
SKW 19	31.5	0.14	3.70
SWT1/LB-2	44.6	0.22	2.86
Extant humans	27.5	0.16	3.46
(s.d.)	(7.3)	(0.02)	(1.29)
Pan	36.1-42.3	0.15-0.18	2.03-2.32

Table 2

Bone volume fraction (BV/TV, in %), trabecular thickness (Tb.Th., in mm), and degree of anisotropy (DA) of the volume of interest sampling the inferior portion of the femoral neck (nVOI; see Fig. 3a) assessed in *P. robustus* from Swartkrans (SK 97, SK 3121 and SKW 19) and in two comparative samples of extant humans (n = 12; s.d., standard deviation) and *Pan* (n = 2).

Specimen/sample	BV/TV (%)	Tb.Th. (mm)	DA
SK 97	54.5	0.37	4.68
SK 3121	50.4	0.31	4.99
SWT1/LB-2	57.3	0.35	3.39
Extant humans	50.9	0.31	7.34
(s.d.)	(11.4)	(0.07)	(3.47)
Pan	54.0-58.1	0.25-0.30	2.30-3.51

Table 3

Cortical bone thickness (in mm) of the superior (S) and inferior (I) cortices and S/I ratios assessed at the base of neck and at mid-neck, and mean cortical thickness (in mm) and S/I ratios assessed for the entire superior and inferior neck quadrants in *P. robustus* (SK 82, SK 97, SK 3121 and SWT1/LB-2) and in two comparative samples of extant humans (n = 12; s.d., standard deviation) and *Pan* (n = 2). For the punctual measures, the values available for the *A. afarensis* A.L. 288-1 femoral neck (from Ruff et al., 2016) are also shown. Italics indicates XCT-based measures (from Ruff and Higgins, 2013); all remaining values are micro-XCT-based data from the present study.

		Cortical Thickness						Mean Cortical Thickness					
		Base of neck			Mid-neck			Base of neck			Mid-neck		
Specimen	Taxon	Superior	Inferior	S/I	Superior	Inferior	S/I	Superior	Inferior	S/I	Superior	Inferior	S/I
SK 82	*P. robustus*	2.59[a]-*1.93*[b]	3.43[a]-*4.09*[b]	0.76[a]-*0.47*[b]	2.42[a]-*3.00*[b]	2.80[a]-*2.86*[b]	0.86[a]-*1.05*[b]	2.20[a]	2.84[a]	0.78[a]	2.32[a]	2.41[a]	0.96[a]
SK 97	*P. robustus*	2.30[a]-*1.18*[b]	3.37[a]-*2.83*[b]	0.68[a]-*0.42*[b]	2.81[a]-*1.50*[b]	2.94[a]-*2.20*[b]	0.96[a]-*0.68*[b]	1.83[a]	3.05[a]	0.60[a]	2.18[a]	2.87[a]	0.76[a]
SK 3121	*P. robustus*				1.80[a]	2.50[a]	0.71[a]				1.76[a]	2.64[a]	0.67[a]
SWT1/LB-2	*P. robustus*	1.99[a]			2.82[a]			2.45[a]			2.54[a]		
	Extant humans	1.06[a]	3.68[a]	0.30[a]	1.11[a]	2.65[a]	0.43[a]	0.93[a]	2.70[a]	0.37[a]	0.92[a]	2.08[a]	0.46[a]
	(s.d.)	(0.31)	(0.79)	(0.10)	(0.46)	(0.67)	(0.15)	(0.14)	(0.70)	(0.13)	(0.22)	(0.51)	(0.13)
	Pan	3.57-4.81[a]	3.22-3.16[a]	1.11-1.52[a]	2.18-2.40[a]	2.91-2.99[a]	0.73-0.82[a]	2.66-3.18[a]	2.84-3.00[a]	0.94-1.06[a]	2.11-2.15[a]	2.86-2.94[a]	0.72-0.73[a]
A.L. 288-1[c]	*A. afarensis*	1.20	3.50	0.34	1.50	2.60	0.58						

[a] Present study.
[b] Ruff and Higgins (2013).
[c] Ruff (2018, pers. comm.; see also Ruff et al., 2016: fig. 7).

Supplementary Online Material

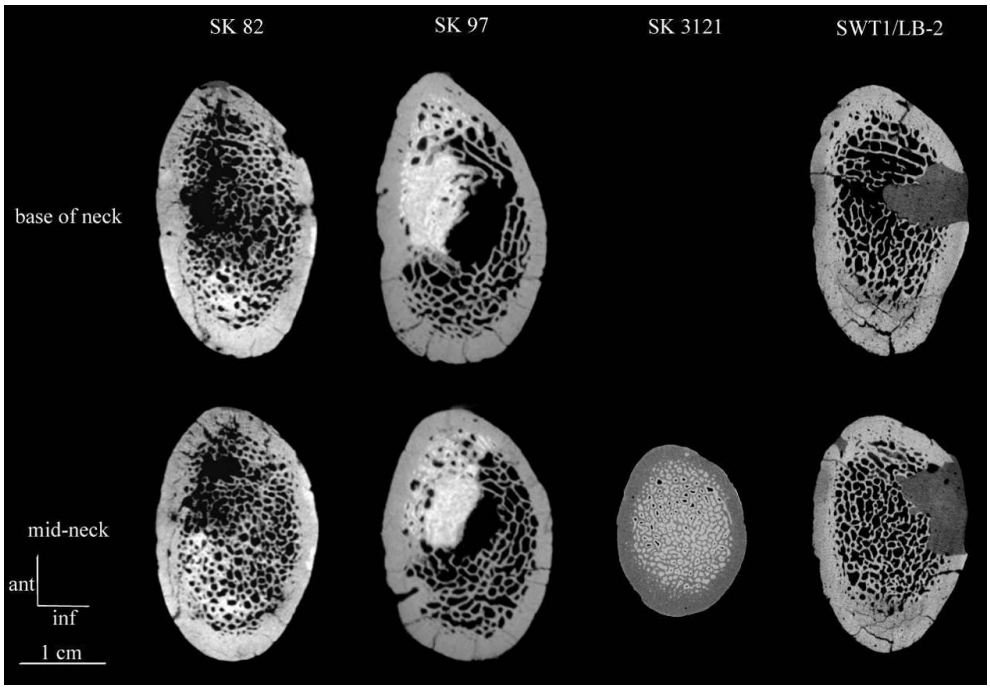

Figure S1. Micro-XCT-based antero-posterior virtual slices perpendicular to the longitudinal neck axis taken at the base of neck (upper) and at mid-neck (lower) in four *P. robustus* specimens from Swartkrans (SK 82, SK 97, SK 3121 and SWT1/LB-2).

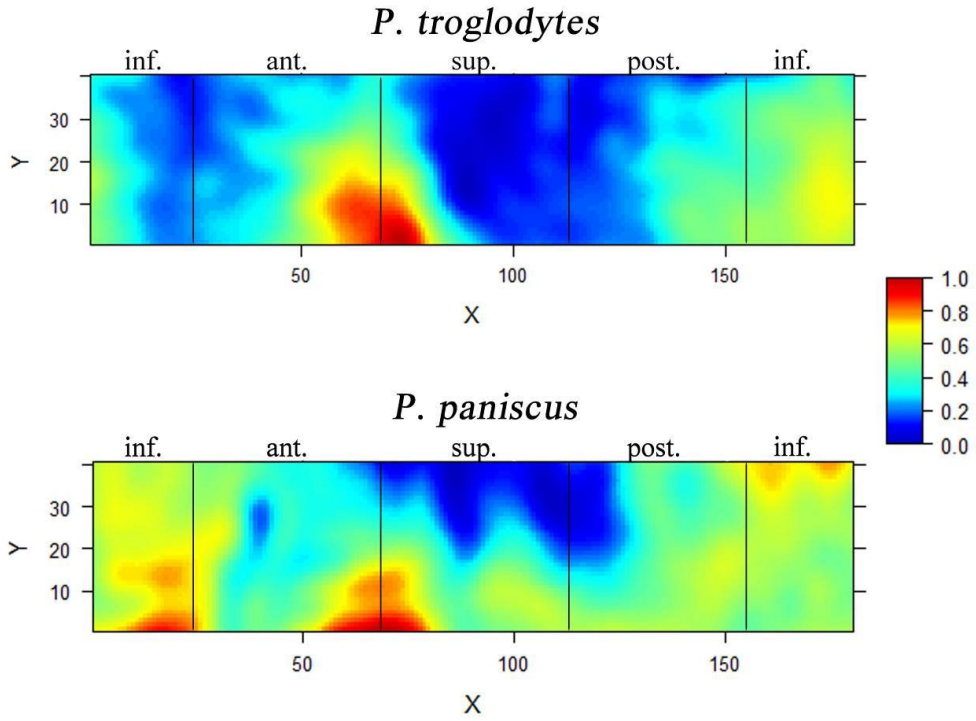

Figure S2. Micro-XCT-based standardised morphometric maps of the virtually unzipped, unrolled and projected cortical bone thickness of the femoral neck from the base of neck (bottom Y-axis) to the head-neck junction (top Y-axis) of two *P. troglodytes* (upper) and *P. paniscus* (lower) representatives. Their consensus map is shown in the main text as Fig. 6 (*Pan*). Relative thickness is rendered by a pseudo-colour scale increasing from dark blue (0, thinner) to red (1, thicker). inf., inferior quadrant; ant., anterior quadrant; sup., superior quadrant; post., posterior quadrant.

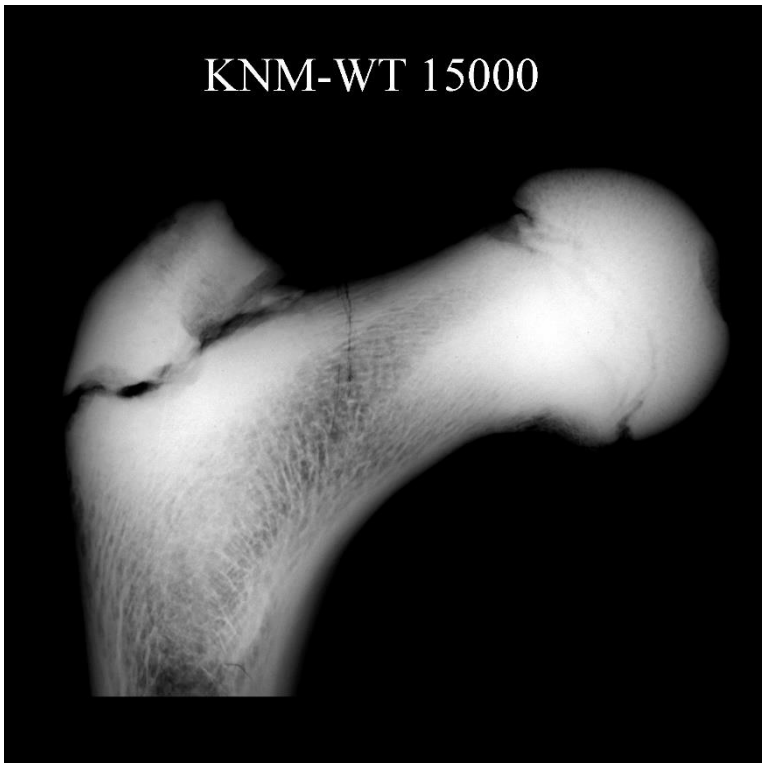

Figure S3. Digitally processed radiographic image of the proximal end of the *H. erectus* KNM-WT 15000-G left femur (Walker and Leakey, 1993: figs 7.125.-7.130.) in standard coronal view (original unpublished image). The image has been mirrored to make the direct comparison with the specimens from Swartkrans (main text) easier.

References

Walker, A., Leakey, R., 1993. The postcranial bones. In Walker, A., Leakey, R. (Eds), The Nariokotome *Homo erectus* Skeleton. Harvard University Press, Cambridge, MA, pp. 95-160.

3.2.2. Extended information

3.2.2.1. The extant human sample

MicroCT based virtual coronal sections of the 12 extant human specimens used in the study and discussed in the manuscript entitled "The inner structural organisation of the proximal femoral end in *Paranthropus robustus*: Implications for the assessment of the australopith hip joint loading conditions", under review in the *Journal of Human Evolution*, are presented in Fig. 3.2.2.1.A showing their structural organisation and the extent of variation among individuals. These specimens have been selected from the osteological collections of the McGregor Museum of Kimberley (Morris, 1984), the Pretoria Bone Collection at the Department of Anatomy of the University of Pretoria (L'Abbé et al., 2005) and the R.A. Dart skeletal collection at the University of the Witwatersrand (Dayal et al., 2009). Information regarding the sex and age of each individual is provided in Table 3.2.2.1.A.

In Figure 3.2.2.1.A, we can notice that the vertical, arcuate and trochanteric bundles (Aiello and Dean, 1990; Levangie and Norkin, 2005; Kapandji, 2011) are well distinguishable in all individuals. The width of the vertical bundle varies among the specimens but it always represents the densest bony area, especially in its inferior portion. In contrast with the condition expressed by *P. robustus*, the vertical bundle in extant Humans is never infero-medially convex and it does not extend laterally along the inferior margin of the neck to the medial diaphyseal border. The vertical bundle originates a few millimetres above the fovea capitis its orientation diverges ca 30° superiorly from the neck axis. Variations to this pattern included a slightly more vertical orientation compared to the neck axis (e.g., in EH 3, 6, 7), or a slightly more horizontal orientation (e.g., in EH 5, 12). The arcuate bundle is well defined all along its regularly arched outline; it can be traced from the infero-medial aspect of the head, across the upper portion of the neck, to the diaphyseal lateral cortex. Medially, while usually found below the fovea capitis, its origin varies and can reach, or even exceed, the level of the depression. The width of the arcuate bundle varies across the proximal femur, but it is proportionally large near the diaphyseal lateral cortex and relatively narrow in the upper portion of the neck. In the infero-medial aspect of the head, its development varies among the human femora investigated in this study. While it is well defined in EH 3 and 14, with well oriented and thick trabeculae, in EH 6, 7, 9, the infero-medial region of the head shows a more vacuolar network, which could even be poorly developed in some individuals.

In addition to these two bundles, it is worth noting that some human specimens display a crown-like appearance of more or less radially oriented trabeculae adjoining the cortical tissue all around the femoral head (e.g., EH 13, 14). It has been claimed that the forces applied to the femoral head converge to a central dense wedge and then to the junction of the neck and shaft. This crown-like cancellous network varies among the individuals in terms of density. Below and lateral to the vertical and arcuate bundles crossing in the neck, all human specimens show accentuated bone loss in the so-called "Ward's triangle", even though the extent and development of this structure varies between individuals (e.g., EH 2 vs. EH 12), notably (but not uniquely) depending on the age. The expression of the so-called secondary tensile trabecular system (Levangie and Norkin, 2005: 367) is variable among the specimens. This secondary tensile trabecular system varies from a poorly developed appearance consisting of a dense bundle represented by obliquely oriented trabeculae departing from the medial aspect of the upper shaft towards the lateral diaphyseal cortex. At this region, strut thickness varies among the individuals, but the presence of plate-like structures was never observed. Finally, the bundle-like structure of the greater trochanter is poorly organised and structured, and could be composed of sparse and very thin trabeculae, i.e., in Humans it consists of a much looser network compared to the condition displayed by *P. robustus*.

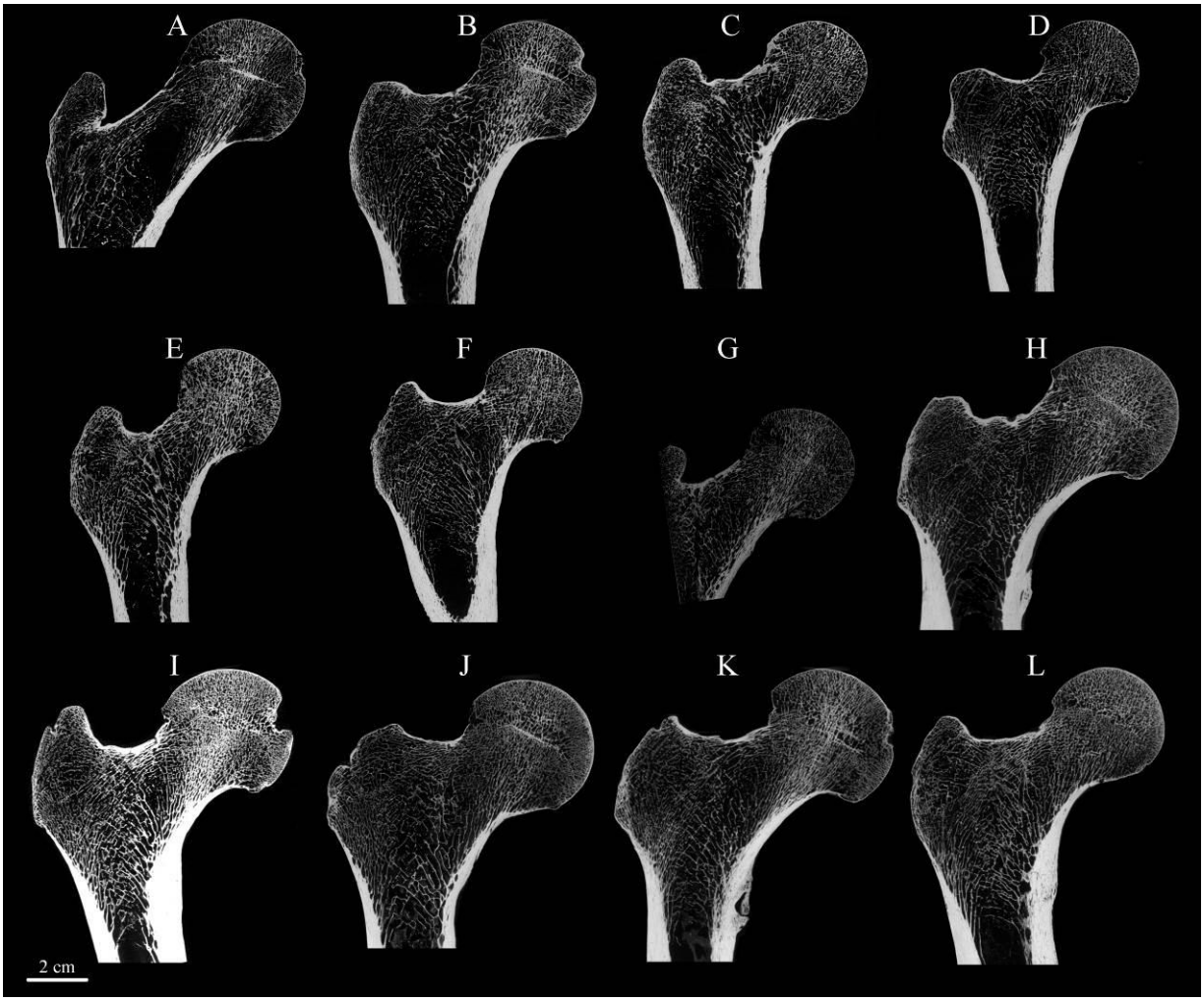

Fig. 3.2.2.1.A. µXCT-based virtual coronal sections extracted approximately across the centre of the proximal femoral end in the 12 extant human specimens used in the study under review in the *Journal of Human Evolution*. Upper row, from A to D: EH 2, 3, 5, 6; middle row, from E to H: EH 7, 8, 9, 11; lower row, from I to L: EH 12, 13, 14, 16. Information regarding the sex and age of each individual is provided in Table 3.2.2.1.A.

Table 3.2.2.1.A. Composition of the extant human sample of proximal femoral ends detailed using high resolution µXCT scanning.

specimen	sex	age (years)
EH 1	M	41
EH 2	M	40
EH 3	F	38
EH 4	M	40
EH 5	M	30-49

EH 6	F	44-54
EH 7	F	30's
EH 8	F	32-52
EH 9	F	30-47
EH 10	M	27
EH 11	M	26
EH 12	M	26
EH 13	M	27
EH 14	M	34
EH 15	M	45
EH 16	M	36
EH 17	M	26

Digital radiographs showing the structural organisation of the proximal femoral end in 8 adult individuals of both sexes selected from the Imperial Roman osteological collection of Isola Sacra (National Prehistoric Museum of Rome) can be noted in Fig. 3.2.2.1.B. These radiographs have been selected from a record available to document the condition of a total of 214 individuals (Macchiarelli and Bondioli, 2000). The analysis of this assemblage confirms that the vertical bundle presents the densest bony area of the proximal femur, especially in its inferior portion. Unlike *P. robustus*, this structure is never infero-medially convex. It is confined medially along the inferior margin of the neck and its orientation may vary. In addition, the radiographic record confirms the evidence that, while usually found below the fovea capitis, in Humans, the medial origin of the arcuate bunde varies and can reach the level of the depression (e.g., D, E, F).

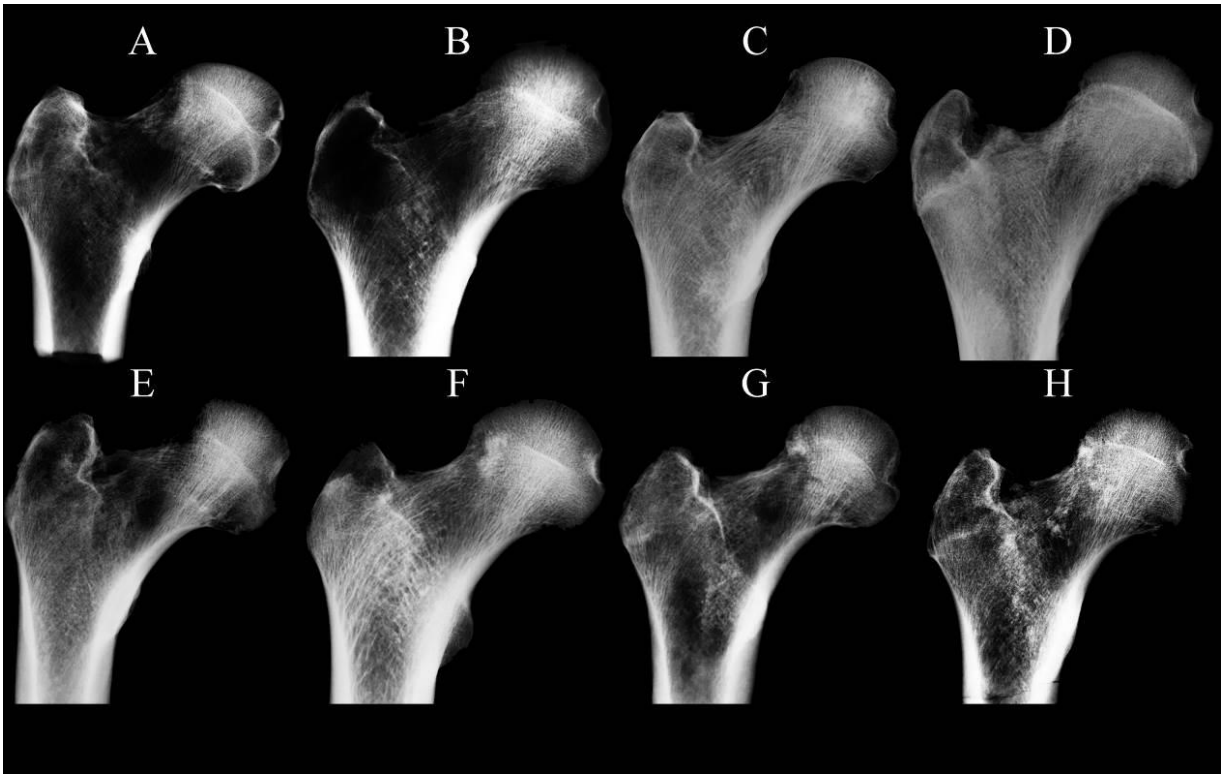

Fig. 3.2.2.1.B. Digital radiographs showing the structural organisation of the proximal femoral end in 8 adult individuals of both sexes.

Details of the results of the 12 extant human specimens in the study discussed in the manuscript entitled "The inner structural organisation of the proximal femoral end in *Paranthropus robustus*: Implications for the assessment of the australopith hip joint loading conditions" under review in the *Journal of Human Evolution*, are given in the three following tables (Table 3.2.2.1.B, Table 3.2.2.1.C, Table 3.2.2.1.D).

Table 3.2.2.1.B. Individual values and descriptive statistics of bone volume fraction (BV/TV, in %), trabecular thickness (Tb.Th., in mm), and degree of anisotropy (DA) of the volume of interest sampling the infero-lateral portion of the femoral head (hVOI; see supra section 3.2.1) measured in 12 extant Humans; s.d., standard deviation; min., minimum value; max., maximum value.

specimen	BV/TV (%)	Tb.Th. (mm)	DA
EH 1	17.5	0.11	5.83
EH 2	31.0	0.18	3.48
EH 3	37.7	0.18	4.52

EH 4	28.1	0.13	3.18
EH 5	24.9	0.18	2.58
EH 6	25.0	0.16	3.33
EH 7	35.4	0.17	2.28
EH 8	32.7	0.17	2.80
EH 9	37.1	0.16	2.33
EH 10	19.9	0.17	2.68
EH 11	22.6	0.19	5.97
EH 12	18.2	0.17	2.59
mean	27.5	0.16	3.46
s.d.	7.3	0.02	1.29
min.	17.5	0.11	2.28
max.	37.7	0.19	5.97

Table 3.2.2.1.C. Individual values and descriptive statistics of bone volume fraction (BV/TV, in %), trabecular thickness (Tb.Th., in mm), and degree of anisotropy (DA) of the volume of interest sampling the inferior portion of the femoral neck (nVOI; see Fig. 3a) measured in 12 extant Humans, but excluding the outliers indicated in italics; s.d., standard deviation; min., minimum value; max., maximum value.

specimen	**BV/TV (%)**	**Tb.Th. (mm)**	**DA**
EH 2	*17.3*	*0.19*	12.42
EH 3	51.1	0.27	4.68
EH 5	33.4	0.21	9.76
EH 6	34.6	0.21	13.00
EH 7	*72.3*	0.40	*2.52*
EH 8	*29.8*	*0.10*	*1.81*
EH 9	43.8	0.22	8.84
EH 13	51.9	0.33	5.89
EH 14	58.7	0.36	4.49
EH 15	59.7	0.39	4.33
EH 16	61.7	0.36	6.60
EH 17	63.4	0.36	3.39
mean	50.9	0.31	7.34
s.d.	11.4	0.07	3.47
min.	33.4	0.21	3.39
max.	63.4	0.40	13.00

Table 3.2.2.1.D. Individual values and descriptive statistics of cortical bone thickness (in mm) of the superior (S) and inferior (I) cortices and S/I ratios assessed at the base of neck and at mid-neck and S/I ratios assessed for the entire superior and inferior neck quadrants in 12 extant Humans; s.d., standard deviation; min., minimum value; max., maximum value.

	cortical thickness						cortical mean thickness					
	base of neck			mid-neck			base of neck			mid-neck		
specimen	**superior**	**inferior**	**S/I**	**superior**	**inferior**	**S/I**	**superior**	**inferior**	**S/I**	**superior**	**inferior**	**S/I**
EH 2	1.57	4.70	0.33	2.00	3.44	0.58	0.79	3.77	0.21	1.02	2.52	0.41
EH 3	0.91	3.15	0.29	1.06	2.29	0.46	1.12	2.48	0.45	0.90	1.99	0.45
EH 5	1.46	4.04	0.36	0.95	3.08	0.31	0.92	3.46	0.27	0.70	2.68	0.26
EH 6	1.00	3.29	0.30	0.91	2.12	0.43	0.94	2.17	0.43	0.86	1.83	0.47
EH 7	1.46	4.50	0.32	0.63	3.15	0.20	1.02	3.45	0.30	0.85	2.69	0.31
EH 8	0.98	4.27	0.23	1.54	3.69	0.42	1.09	2.78	0.39	1.33	2.78	0.48
EH 9	0.94	4.17	0.23	1.46	3.43	0.42	0.88	2.85	0.31	0.96	2.12	0.45
EH 13	0.84	2.29	0.37	0.70	1.95	0.36	0.93	1.57	0.59	0.93	1.43	0.65
EH 14	1.26	2.31	0.54	0.91	1.82	0.50	1.03	1.67	0.61	0.79	1.39	0.57
EH 15	0.84	3.71	0.23	1.75	2.31	0.76	0.96	2.63	0.36	1.32	1.81	0.73
EH 16	0.91	3.60	0.25	0.84	1.96	0.43	0.61	2.29	0.26	0.58	1.45	0.40
EH 17	0.56	4.14	0.14	0.63	2.59	0.24	0.84	3.25	0.26	0.75	2.30	0.33
mean	1.06	3.68	0.30	1.11	2.65	0.43	0.93	2.70	0.37	0.92	2.08	0.46
s.d.	0.31	0.79	0.10	0.46	0.67	0.15	0.14	0.70	0.13	0.22	0.51	0.13
min.	0.56	2.29	0.14	0.63	1.82	0.20	0.61	1.57	0.21	0.58	1.39	0.26
max.	1.57	4.70	0.54	2.00	3.69	0.76	1.12	3.77	0.61	1.33	2.78	0.73

Statistical analyses of the results discussed in the manuscript entitled "The inner structural organisation of the proximal femoral end in *Paranthropus robustus*: Implications for the assessment of the australopith hip joint loading conditions", under review in the *Journal of Human Evolution*, were conducted. A between-group principal component analysis (bgPCA) (Fig. 3.2.2.1.C) and two sample t-tests via Monte-Carlo permutations (Table 3.2.2.1.E) of the three variables (BV/TV, Tb.Th., DA) measured at the femoral head in the five *P. robustus* specimens (SK 82, 97, 3121, SKW 19, SWT1/LB-2) and in our recent human and *Pan* samples were first conducted. In the bgPCA, the two likely female *P. robustus* specimens (SK 3121 and SKW 19) cluster together with the Humans, while the three likely male *P. robustus* specimens (SK 82, SK 97 and SWT1/LB-2) are distinct from the human morphotype. By showing a proportionally denser cancellous network and thicker trabeculae, SK 82, SK 97 and SWT1/LB-2 fall in the positive space of bgPC1, whereas SK 3121 and SKW 19 and Humans, are mostly found in the negative space of bgPC1 because of their less robust cancellous bone. All specimens were not discriminated along bgPC2, except for one *Pan* specimen. The two sample t-tests via Monte-Carlo permutations confirm a significant difference for the BV/TV between the human and *P. robustus* specimens, while the DA significantly discriminate our *Pan* and human samples on one hand, and *Pan* and *P. robustus* samples on the other hand.

Secondly, a bgPCA analysis (Fig. 3.2.2.1.D) and two sample t-tests via Monte-Carlo permutations (Table 3.2.2.1.F) of the three variables (BV/TV, Tb.Th., DA) measured at the femoral neck in two *P. robustus* specimens (SK 97 and SWT1/LB-2) and in our recent human and *Pan* samples, were conducted. The results show no structural differences in the cancellous organisation at the inferior region of the mid-neck between the three taxa, but for the DA between *P. robustus* and *Pan*.

Finally, two-sample t-tests via Monte-Carlo permutation between the *P. robustus* specimens (SK 82, and SK 97) and the human and *Pan* samples for the superior (S) and inferior (I) cortical thicknesses ratio (S/I) assessed from the base of neck (0) to the head-neck junction, (100%) were conducted (Table 3.2.2.1.G). Significant differences of the cortical thickness ratio were found in the base of neck region between *P. robustus* and Humans on one hand, and *Pan* and Humans on the other hand.

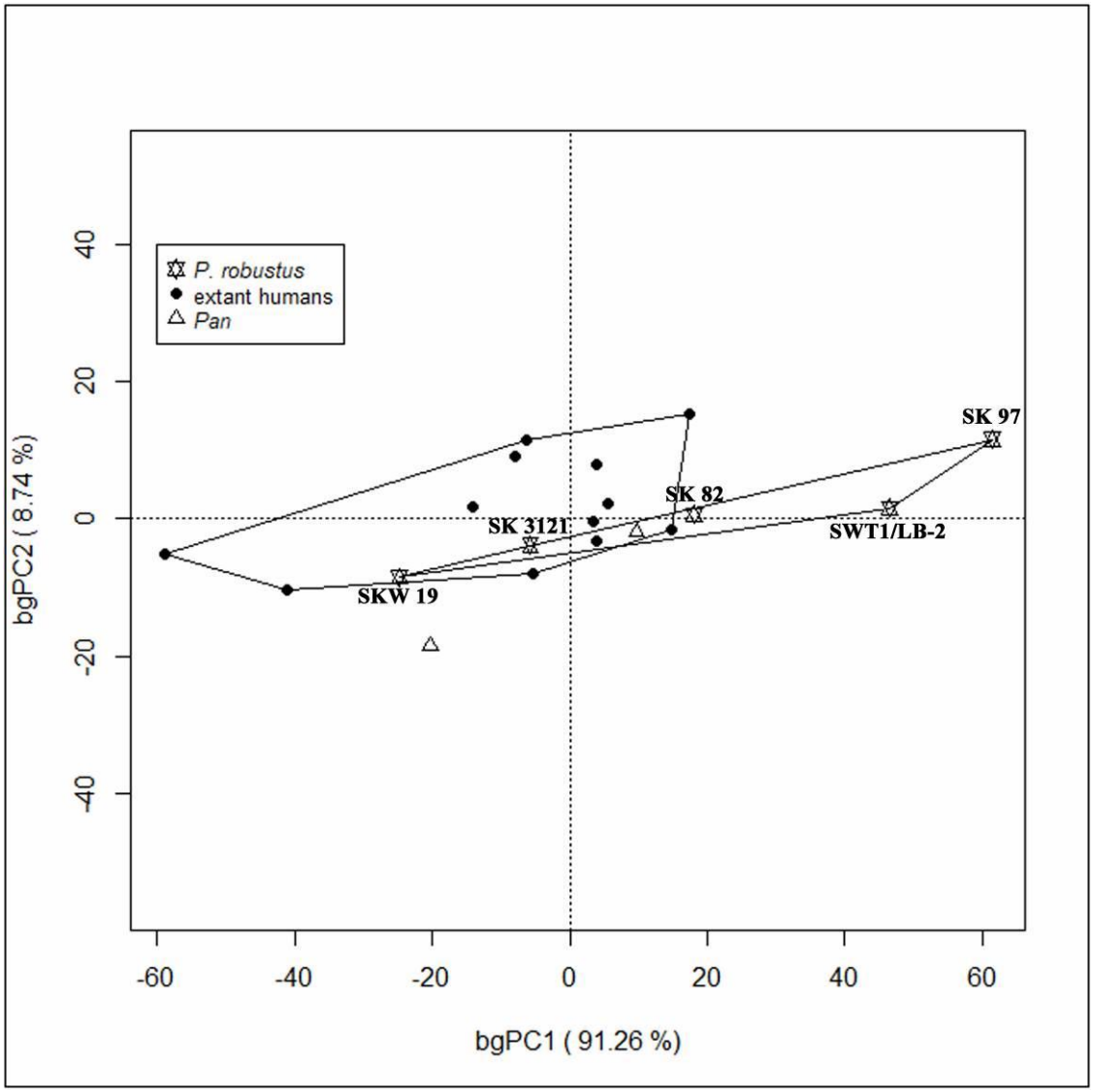

Fig. 3.2.2.1.C. Between-group principal component analysis (bgPCA) of the three variables (BV/TV, Tb.Th., DA) measured at the femoral head in the five *P. robustus* specimens (SK 82, 97, 3121, SKW 19, SWT1/LB-2), in recent Humans (n = 12), and in *Pan* (n = 2).

Table 3.2.2.1.E. Two-sample t-test via Monte-Carlo permutation between the *P. robustus* specimens (SK 82, 97, 3121, SKW 19, SWT1/LB-2), the extant human (n = 12) and *Pan* (n = 2) samples for bone volume fraction (BV/TV, in %), trabecular thickness (Tb.Th., in mm), and degree of anisotropy (DA) of the femoral head. Significant differences are shown in bold.

	taxa	**human**	***Pan***
BV/TV	*P. robustus*	**p = 0.019**	p = 0.617
	human	-	p = 0.055
Tb.Th.	*P. robustus*	p = 0.105	p = 0.428

	human	-	p = 0.782
DA	*P. robustus*	p = 0.0755	**p = 0.048**
	human	-	**p = 0.034**

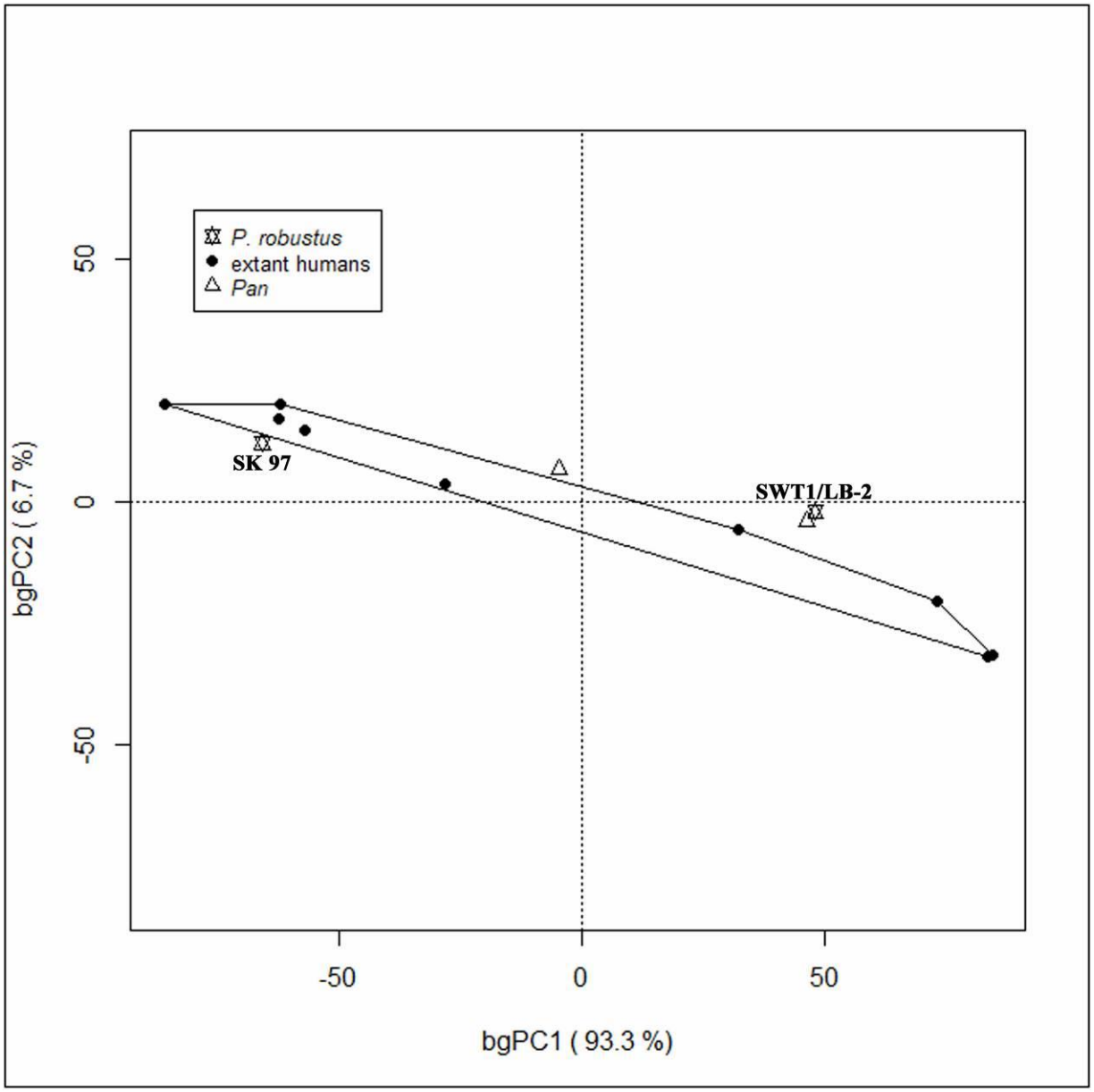

Fig. 3.2.2.1.D. Between-group principal component analysis (bgPCA) of the three variables (BV/TV, Tb.Th., DA) measured at the femoral neck in two *P. robustus* specimens (SK 97 and SWT1/LB-2), in recent Humans (n = 12), and in *Pan* (n = 2). In this analysis, the three samples cluster together, showing no structural differences in the cancellous organisation at the inferior region of the mid-neck.

Table 3.2.2.1.F. Two-sample t-test via Monte-Carlo permutation between the *P. robustus* specimens (SK 97, and SWT1/LB-2), the human (n = 12) and *Pan* (n = 2) samples for BV/TV, Tb.Th. and DA of the femoral neck. Significant differences are shown in bold.

	taxa	**Human**	***Pan***
BV/TV	*P. robustus*	p = 0.827	p = 0.617
	human	-	p = 0.668
Tb.Th.	*P. robustus*	p = 0.832	p = 0.428
	human	-	p = 0.604
DA	*P. robustus*	p = 0.502	**p = 0.048**
	human	-	p = 0.056

Table 3.2.2.1.G. Two-sample t-test via Monte-Carlo permutation between the *P. robustus* specimens (SK 82, and SK 97), the human (n = 12) and *Pan* (n = 2) samples for the superior (S) and inferior (I) cortical thicknesses ratio (S/I) assessed from the base of neck (0) to the head-neck junction (100%). Significant differences are shown in bold.

	taxa	**human**	***Pan***
S/I	*P. robustus*	**0-61%: p < 0.05** 61%-100%: p > 0.05	0-100%: p > 0.05
	human	-	**0-56%: p < 0.05** 56%-100%: p > 0.05

We used the specimen SK 3121 and SWT1/LB-2, whose femoral head core is relatively well preserved, to evaluate the extent of the differences for the BV/TV and the DA with respect to the measures performed by Ryan et al. (2018) for SK 3121. The results are presented in Table 3.2.2.1.H. Following the analytical protocol described by Ryan et al. (2018) and using a VOI of 857 mm3 virtually extracted from its head centre, we obtained a result for SK 3121 showing differences of 3.6% and 7.6%, respectively, which we consider satisfactory.

Table 3.2.2.1.H. Bone volume fraction (BV/TV, in %) and degree of anisotropy (DA) of the volume of interest sampling the centre of the femoral head extracted following the protocol established by Ryan et al. (2018), measured using BoneJ and Quant3D and assessed in the two *P. robustus* specimens SWT1/LB-2 and SK 3121 from Swartkrans in comparison to the measurements performed by Ryan et al. (2018) shown in italic.

specimen	**BoneJ**	**Quant3D**

	BV/TV	DA	BV/TV	DA
SWT1/LB-2	0.57	0.57	0.60	3.70
SK 3121	0.56-*0.54*	0.66-*0.61*	0.58	3.96

3.2.2.2. The human hip complex: Influence of soft tissues on the inner structural organisation of the proximal femoral end

The internal architecture of the human proximal femur reveals the interaction between mechanical stresses and structural bony adaptation related to the dissipation of forces acting at the hip joint (e.g., Lovejoy, 1988, 2005; Aiello and Dean, 1990; Ohman et al., 1997; Rafferty, 1998; Demes et al., 2000; Lovejoy et al., 2002; Levangie and Norkin, 2005; Kapandji, 2011). Trabeculae, notably when incorporated within a thin shell of compact bone, are normally disposed along the lines of greatest stress and form systems that adapt to stress requirements (Aiello and Dean, 1990; Levangie and Norkin, 2005; Kapandji, 2011; Kivell, 2016 and references therein). At this skeletal site, cortical tissue is also distributed across the femoral neck in response to the variation of multiple forces acting on the joint (Lovejoy, 1988, 2005; Ohman et al., 1997; Rafferty, 1998; Lovejoy et al., 2002; Ruff and Higgins, 2013; Ruff et al., 2016).

In Humans, when standing or during upright weight bearing activities, at least half of the weight of the head, arms and trunk passes down through the pelvis to the femoral head, whereas the ground reaction force travels up the shaft. These two forces, nearly parallel but acting in opposite directions, create a force couple with a moment arm, thus a bending moment (or a set of shear stress) across the femoral neck. The bending stress generates a tensile force on the superior aspect of the femoral neck and a compressive stress on the inferior wall (Levangie and Norkin, 2005). Two major and three minor trabecular systems, as well as the cortical bone distribution at the femoral neck, mechanically respond to the requirements of this loading environment (Lovejoy, 1988; Aiello and Dean, 1990; Levangie and Norkin, 2005; Kapandji, 2011; Ruff and Higgins, 2013). However, the whole complex of muscles inserted in the lateral region of the proximal femur, the connective tissues directly acting on the bone (i.e., ligaments, cartilage) and the articulating contact pressures between the femoral head and the acetabulum, all play a mechanical role in the loading environment at this joint which is not fully/necessarily recorded by the inner bony structure, but that should be taken into account in paleobiomechanics (Lovejoy et al., 2002).

In the femoral head articulating with the acetabulum (lunate surface) is covered by articular cartilage, except in the attachment area of the ligamentum teres. Cartilage thickness of the femoral head is maximal antero-laterally, which corresponds to the principal load-bearing area within the joint. A strong and dense capsule also covers the proximal femur. It originates from the acetabulum, extends laterally to surround the femoral head and neck and attaches at four sites: (i) anteriorly to the intertrochanteric line; (ii) superiorly to the base of the femoral neck; (iii) posteriorly, 1 cm supero-medially to the intertrochanteric crest; and (iv) inferiorly to the femoral neck, near the lesser trochanter. The capsule is thicker antero-superiorly, where maximal stresses occur. Its capsule is also strengthened anteriorly by the iliofemoral and pubofemoral ligaments, and posteriorly by the ischiofemoral ligament. The apex of the iliofemoral ligament is attached to the anterior inferior iliac spine, and the two arms of the Y fan out to attach along the intertrochanteric line of the femur. The superior band of the iliofemoral ligament represents the strongest and thickest among the hip joint ligaments. The pubofemoral ligament is also anteriorly located, arising from the anterior aspect of the pubic ramus and passing to the anterior surface of the intertrochanteric fossa. The ischiofemoral ligament attaches to the posterior surface of the acetabular rim and the acetabulum labrum. Some of its fibres spiral around the femoral neck and blend with the circumferential fibres of the capsule. Other fibres are arranged horizontally and attach to the inner surface of the greater trochanter. There is evidence that the anterior ligaments are stronger than the ischiofemoral ligament. The posteriorly located ischio-femoral ligament has been suggested to be primarily related to medial rotation of the hip regardless of the hip position in flexion or extension. On the anterior side of the hip joint, the pubofemoral ligament controls the lateral rotation in an extended position. The joint capsule is surrounded by muscles, primary abductors or rotators, from the gluteal region (Levangie and Norkin, 2005; Standring, 2008; Kapandji, 2011). Under normal circumstances, the human hip joint, its capsule and ligaments routinely support two thirds of the body weight represented by the head, the arms, and the trunk.

The gluteus minimus, an abductor muscle contributing to the expansion of the capsule, arises from the outer surface of the ilium, between the anterior and inferior gluteal lines, and, behind, from the margin of the greater sciatic notch. It then converges below to the deep surface of an aponeurosis that ends in a tendon, which is attached to an antero-lateral ridge on the greater trochanter. It is covered by two other muscles from the abductor and extensor group, respectively: the gluteus medius and the gluteus maximus (Table 3.2.2.3.A) (Levangie and Norkin, 2005; Standring, 2008; Kapandji, 2011). In Humans, the gluteus maximus is hypertrophic compared to *Pan* and serves as the major propulsive muscle in upright walking,

as well as the stabilising muscle of the pelvis. It also prevents the trunk from pitching forward when running (Lovejoy, 1988, 2005; Bramble and Lieberman, 2004). With each step, the action of the gluteus medius and gluteus minimus prevent the pelvis and the trunk to tip towards the unsupported side causing rapid fatigue, while in *Pan* both are powerful hip extensors during quadrupedal locomotion (Lovejoy, 1988, 2005). In the *A. afarensis* "Lucy" (A.L. 288-1), it has been suggested that the three muscles approach the human condition in proportions and attachment topography (Lovejoy, 1988, 2005). The rotator muscles of the gluteal region reinforcing the capsule and ligaments are the piriformis, the obturator internus, the obturator externus, the gemellus inferior, the gemellus superior and the quadratus femoris (Table 3.2.2.2.A). From the iliac region and the thigh, respectively, the iliopsoas and the rectus femoris, which are preliminary flexor muscles, also expand the capsule (Table 3.2.2.2.A) (Levangie and Norkin, 2005; Standring, 2008; Kapandji, 2011). In Humans, the role of the iliopsoas is to alternatively contract or tug the limb forwards, as an extended leg has a large moment of inertia and requires powerful muscle impulses to start and stop its swing (Lovejoy, 1988, 2005). The flexor group of muscles also includes the sartorius and the other muscles of the quadriceps femoris (vastus medialis, vastus medialis obliquus, vastus lateralis and vastus intermedius) (Table 3.2.2.2.A) (Lovejoy, 1988, 2005). The pectinus also strengthens the capsule, and similarly to the gracilis, the adductor longus, the adductor brevis, and the adductor magnus is an adductor muscle (Table 3.2.2.2.A) (Levangie and Norkin, 2005; Standring, 2008; Kapandji, 2011). Finally, the extensor muscles are also present in the hip region: the semitendinosus, the semimembranosus and the biceps femoris, which are also referred to as the harmstring muscles (Table 3.2.2.2.A) (Levangie and Norkin, 2005; Standring, 2008; Kapandji, 2011). In Humans, the morphology of the ischium permits torque production specific to the hip extensor muscles at full hip extension (180° angle between the trunk and leg), improving walking economy for straight-legged gait. However, the mechanical advantage of these muscles is reduced in Humans relative to apes and other non-human primates, especially in the flexed-hip postures. The morphology of the ischium in *Australopithecus* shows a human-like pattern, suggesting reduced power in hip extension and an increased range of hip hyperextension (Kozma et al., 2018). In this regard, it should be noted that the condition characterising *Paranthropus*, remains less defined.

Table 3.2.2.2.A. Muscles of the gluteal and thigh region in extant Humans and information about their origin(s) and attachment(s) according to their principal function (Standring, 2008; Levangie and Norkin, 2005).

muscles	origin(s)	insertion(s)
abductors		
Gluteus minimus	- outer surface of the ilium, between the anterior and inferior gluteal line - margin of the greater sciatic notch	- antero-lateral ridge on the greater trochanter
Gluteus medius	- outer surface of the ilium, between the iliac crest and the posterior gluteal line - anterior gluteal line -fascia superficial to its upper part	- ridge that slants downwards and forwards on the lateral surface of the greater trochanter
rotators		
Piriformis	- anterior surface of the sacrum by three digitations - gluteal surface of the ilium near the posterior inferior iliac spine - capsule of the adjacent sacroiliac joint - upper part of the pelvic surface of the sacro-tuberous ligament	- medial side of the upper border of the greater trochanter of the femur
Obturator internus	- internal surface of the antero-lateral wall of the lesser pelvic cavity	- inferior ramus of the pubis - the ischial ramus - pelvic surface of the hip bone below and behind the pelvic brim - upper part of the greater sciatic foramen above and behind - obturator foramen below and in front
Obturator externus	- antero-medial two-thirds of the external surface of the obturator membrane	- trochanteric fossa

	- adjacent bone of the pubic and ischial rami	
Gemellus inferior	- upper part of the lateral surface of the ischial tuberosity	- medial surface of the greater trochanter
Gemellus superior	- dorsal surface of the ischial spine	- medial surface of the greater trochanter
Quadratus femoris	- upper part of the external aspect of the ischial tuberosity	- small tubercle a little above the middle of the trochanteric crest -bone for a short distance below
flexors		
Iliopsoas	- anterior surfaces and lower borders of the transverse processes of all the lumbar vertebrae including five digitations	- lesser trochanter of the femur
Rectus femoris	- anterior inferior iliac spine - groove above the acetabulum - fibrous capsule of the hip joint	- base of the patella
Sartorius	- anterior superior iliac spine - upper half of the notch below the iliac spine	- proximal part of the medial surface of the tibia (in front of gracilis and semitendinosus)
Vastus medialis & Vastus medialis obliquus	- lower part of the intertrochanteric line - spiral line - medial lip of the linea aspera - proximal part of the medial supracondylar line - tendons of adductor longus and magnus - medial intermuscular septum	- medial border of the patella and quadriceps tendon
Vastus lateralis	- upper part of the intertrochanteric line - anterior and inferior borders of the greater trochanter - lateral lip of the gluteal tuberosity - proximal half of the lateral lip of the linea aspera	- base and lateral border of the patella (and blends into the compound quadriceps femoris tendon)
Vastus intermedius	- anterior and lateral surfaces of the upper two-thirds of the femoral shaft	- lateral border of the patella - lateral condyle of the tibia

	- lower part of the lateral intermuscular septum	
adductors		
Pectinus	- pecten pubis - bone in front of it between the iliopubic ramus and the pubic tubercle - fascia on its own anterior surface	- a line from the lesser trochanter to the linea aspera
Gracilis	- medial margins of the lower half of the body of the pubis - whole of the inferior pubic ramus - adjoining part of the ischial ramus	- upper part of the medial surface of the tibia, just below the condyle (part of the pes anserinus)
Adductor longus	- front of the pubis in the angle between the crest and the symphysis	- into the linea aspera in the middle third of the femur, between vastus medialis and adductors magnus and brevis
Adductor brevis	- external aspect of the body and inferior ramus of the pubis, between gracilis and obturator externus	- along a line from the lesser trochanter to the linea aspera, - upper part of the linea immediately behind pectineus - upper part of adductor longus
Adductor magnus	- small part of the inferior ramus of the pubis - the conjoined ischial ramus - the infero-lateral aspect of the ischial tuberosity	- linea aspera and the proximal part of the medial supracondylar line - lower third of the thigh in a rounded tendon proximal to its attachment to the adductor tubercle on the medial condyle of the femur - medial supracondylar line
extensor		
Gluteus maximus	- posterior gluteal line of the ilium - aponeurosis of erector spinae - dorsal surface of the lower part of the sacrum and the side of the coccyx - sacrotuberous ligament	- iliotibial tract of the fascia lata - gluteal tuberosity (between vastus lateralis and adductor magnus)

	- fascia (gluteal aponeurosis) which covers gluteus medius	
Semitendinosus	- infero-medial impression on the upper area of the ischial tuberosity by a tendon it shares with the long head of biceps femoris - aponeurosis connecting the adjacent surfaces of the two muscles for 7.5 cm from their common origin	upper part of the medial surface of the tibia behind the attachment of sartorius and distal to that of gracilis
Semimembranosus	- impression on the ischial tuberosity	- tubercle (sometimes called the tuberculum tendinis) on the posterior aspect of the medial tibial condyle -medial margin of the tibia, immediately behind the medial collateral ligament - series of slips to the medial margin of the tibia, immediately behind the medial collateral ligament - thin fibrous expansion to the fascia over popliteus - cord-like tendon to the inferior lip and adjacent part of the groove on the back of the medial tibial condyle, deep to the medial collateral ligament - strong expansion which passes obliquely upwards to the femoral intercondylar line and lateral femoral condyle and forms much of the oblique popliteal ligament of the knee joint
Biceps femoris	- infero-medial impression on the upper area of the ischial tuberosity - lateral lip of the linea aspera, between adductor magnus and vastus lateralis	- head of the fibula - fusion with the fibular collateral ligament - lateral condyle of the tibia

3.2.2.3. Internal structure of the proximal femoral end in *Gorilla* and *Papio*

In a complementary comparative study of the internal structural organisation of the upper femoral end not included in the paper under review in the *Journal of Human Evolution*, the same 2-3D techniques of virtual imaging have been applied to assess the condition of two male *Gorilla* femora (one from the right side and one from the left side) from the R.A. Dart skeletal collection of the University at the Witwatersrand, and of four *Papio* femora (all from the right side) curated at the Pretoria Bone Collection stored in the Department of Anatomy at the University of Pretoria. All six specimens lack any macroscopic evidence of outer or inner alteration and obvious pathological changes. They were scanned between 2015 and 2017 at the micro-focus X-ray tomography facility (MIXRAD) of the South African Nuclear Energy Corporation (Necsa), Pelindaba, at resolutions ranging from 59 µm to 92 µm isotropic voxel size. For obvious reasons dealing with data comparison, the same protocol and methodology established for the study of proximal femoral ends of *P. robustus* (see supra section 3.2.1). A cubic volume of interest (hVOI) in the infero-lateral portion of the femoral head across the vertical and the arcuate trabecular bundles were firstly extracted in order to measure (i) the trabecular bone volume fraction (BV/TV, in %), (ii) the trabecular thickness (Tb.Th., in mm), and (iii) the degree of anisotropy (DA). The superior (S) and inferior (I) cortical thicknesses and their ratio (S/I) were also quantified across the entire neck length. In each antero-posterior slice perpendicular to the longitudinal axis, the superior, inferior, anterior and posterior quadrants were delimited by two orthogonal lines set at 45° with respect to the supero-inferior axis and the average cortical thickness thus measured for each quadrant. Finally, a synthetic functional image of its cortical bone repartition through a planar representation of its topographic thickness variation by virtually unzipping the portion between the base of neck and the head-neck junction along a predefined line of its inferior aspect and then unrolling such portion and projecting its local properties into a morphometric map was provided (Bondioli et al., 2010; see also Bayle et al., 2011; Morimoto et al., 2011; Puymerail et al., 2012; Jashashvili et al., 2015; Zanolli et al., 2018). The map was generated by a custom routine developed in R v.3.4.4 (R Development Core Team, 2017) with the packages Momocs (Bonhomme et al., 2014), spatstat (Baddeley et al., 2015) and gstat (Pebesma, 2004). More information about the methodology is provided in section 3.2.1.

As revealed by a virtual coronal slice approximately crossing the femoral head centre, the cancellous bony architectures of a *Gorilla* and a *Papio* representative are shown in Figure 3.2.2.3.A. As previously noted by some authors, it is true that similarities exist among some

extant primate femoral ends in the basic distribution and directionality of the trabecular bundles (e.g., Lovejoy et al., 2002; Fajardo et al., 2007). Nonetheless, this µXCT-based 3D rendering shows that trabecular bone architecture in *Gorilla* more closely resembles the *P. robustus* and extant human conditions (see supra section 3.2.1) than the less organised, less topographically contrasted and globally denser configuration of *Pan* and *Papio*, where the poorly distinct trabecular systems (notably, those forming the so-called three minor, or accessory systems) reveal a more homogeneous network organisation. As observed in our study on *P. robustus*, the cancellous network in the *Gorilla* is denser at nearly all sites, and the struts, on average, thicker than in extant Humans. However, while the absence in *Gorilla* of a *P. robustus*-like trabecular thickening at some spots of the arcuate bundle along its supero-lateral neck portion was noticed, the presence of plate-like structures in the inferior neck trait of the vertical bundle and towards the diaphyseal medial cortex is shared by *P. robustus* and *Gorilla*, while in Humans it is rare and/or rather localised. In *Papio*, the presence of plate-like structures in the inferior portion of the vertical bundle and towards the diaphyseal medial cortex is associated with a trabecular thickening of more oriented trabeculae compared to the vacuolar-shaped structure of other regions of the proximal femur, which apparently might be very dense in the upper portion of the vertical bundle in the superior portion of the head. As opposed to *P. robustus* and Humans, the former displaying a widely denser bundle, the arcuate bundle is poorly developed in *Gorilla*, where it is composed of: (i) few but thick trabeculae adjacent to the infero-medial surface of the femoral head; (ii) few trabeculae in the superior region of the neck parallel to the surface; and (iii) very thin and oriented trabeculae in the upper lateral shaft portion. Schematically, among other features of the femoral end trabecular architecture in *Gorilla*, the following were noted: (i) a wide and rather dense vertical bundle as seen in *P. robustus*, but not anteriorly convex; (ii) an origin of the arcuate bundle confined to the head portion below the fovea capitis, as seen in *P. robustus*, while in extant Humans it can reach, or even exceed, the level of the depression; (iii) a looser appearance of the network in the so-called "Ward's triangle" below and lateral to the vertical and arcuate bundle crossing comparable to the human condition, while at this site, the struts of the trochanteric bundle are thickened and well-oriented in *P. robustus*, the latter clearly different from the poorly organised vacuolar network observed in *Pan* and *Papio*; (iv) a greater trochanteric cancellous infill of intermediate texture and density, similar to that recorded in *P. robustus*, somehow intermediate between the proportionally looser human network and the denser honeycomb pattern of *Pan* and *Papio* (Fig. 3.2.2.3.A).

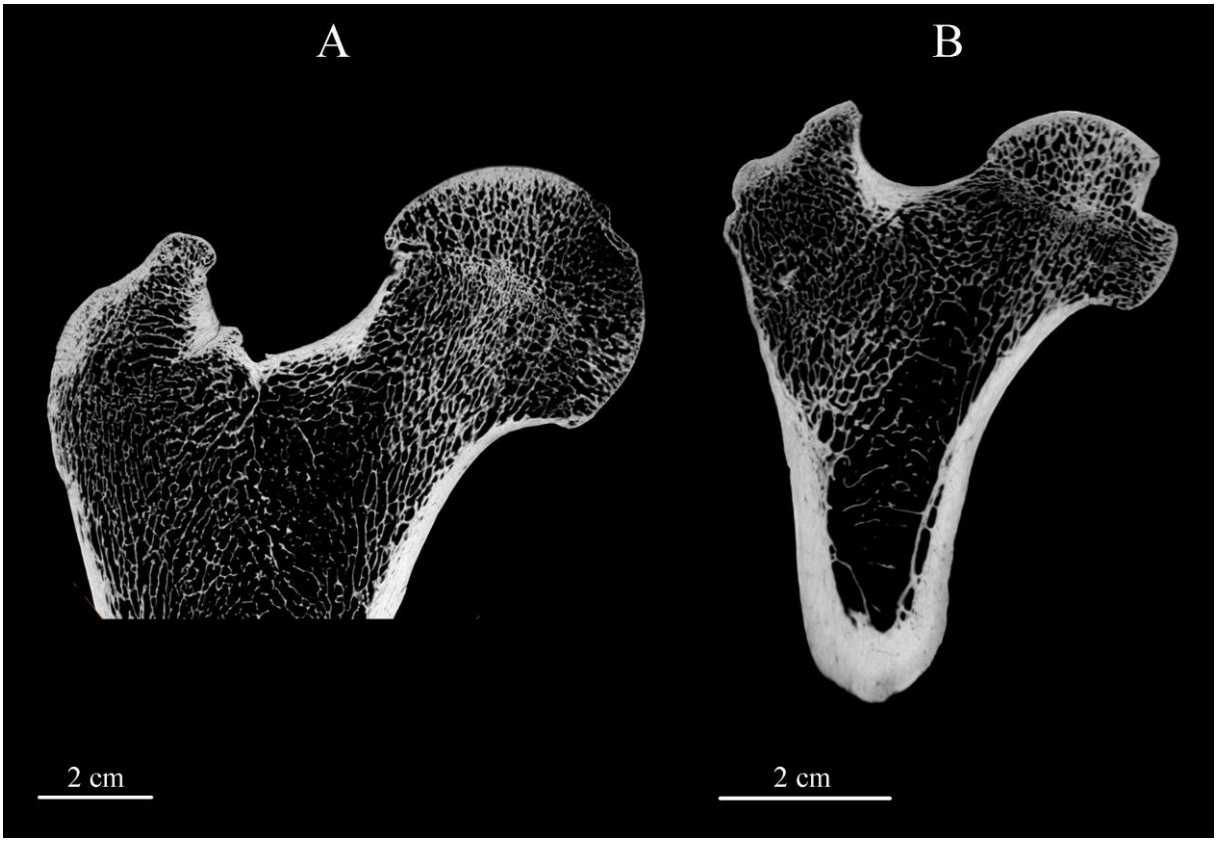

Fig. 3.2.2.3.A. µXCT-based virtual coronal sections extracted approximately across the centre of the proximal femoral end showing the structural organisation in *Gorilla* (A) and *Papio* (B).

The analyses reveal a similar degree of cancellous density in *Gorilla* as measured in *P. robustus* and *Pan*, which is characterised by thicker struts compared to *Homo*. However, the more robust condition associated with dense trabecular bone and thick trabeculae, was found also in *Papio*. Finally, the estimates show that *Gorilla* has a slightly more anisotropic trabecular structure compared to *Pan*, but lower than measured in *P. robustus* and in Humans, while *Papio* shows the lowest degree of anisotropy (Table 3.2.2.3.A).

Table 3.2.2.3.A. Bone volume fraction (BV/TV, in %), trabecular thickness (Tb.Th., in mm), and degree of anisotropy (DA) of the volume of interest sampling the infero-lateral portion of the femoral head (hVOI) assessed in *P. robustus* from Swartkrans (SK 82, SK 97, SK 3121, SKW 19 and SWT1/LB-2), in extant Humans (n = 12; s.d., standard deviation), *Pan* (n = 2), *Gorilla* (n = 2) and *Papio* (n = 4).

specimen/sample	BV/TV (%)	Tb.Th. (mm)	DA

SK 82	36.4	0.19	2.56
SK 97	39.9	0.23	3.48
SK 3121	33.1	0.16	3.55
SKW 19	31.5	0.14	3.70
SWT1/LB-2	44.6	0.22	2.86
Extant Humans (s.d.)	27.5 (7.3)	0.16 (0.02)	3.46 (1.29)
Pan	36.1-42.3	0.15-0.18	2.03-2.32
Gorilla	33.2-37.3	0.25-0.33	2.40-2.76
Papio (range)	53.1 (190.6-227.5)	0.21 (0.49-0.56)	1.72 (1.50-2.02)

As previously mentioned (see section 3.2.1), Ryan et al. (2018) have investigated some cancellous network properties on a volume of interest extracted from the core of the femoral head of four of five *P. robustus* specimens from Swartkrans considered in this study, as well as from six *A. africanus* from Sterkfontein and from a comparative sample of extant catarrhines (*Pan*, *Gorilla*, *Pongo*, *Papio*), as well as fossil and recent Humans. Differently from the signal provided by the two individuals used in the present study, the *Gorilla* specimen imaged by Ryan et al. (2018: fig. 2) shows a vacuolar-shaped homogeneous cancellous network at the head, with one spot of trabecular thickening in the inferior neck trait of the barely discernable vertical bundle. Also, while revealing some structural similarities, the condition shown by the *Papio* individuals forming this comparative sample, slightly differs from the pattern revealed by the *Papio* specimen imaged by Ryan et al. (2018: fig. 2), the latter showing a well-defined vertical bundle in its inferior portion and a distinct arcuate bundle, especially along its supero-lateral neck portion as seen in hominins. The results of trabecular bone density and degree of anisotropy shown by Ryan et al. (2018) confirm such disparities. Indeed, they show that, in contrast to the pattern of highly anisotropic bone observed in hominins and papionins, the three ape groups (*Pan, Gorilla* and *Pongo*) have more isotropic femoral head trabecular bone.

These discrepancies between the two studies could be explained by different factors. First, for methodological reasons, our estimates of the degree of anisotropy of the VOI sampling the infero-lateral portion of the femoral head (the hVOI) are not directly comparable with the measures provided by Ryan et al. (2018), as the position and size of the investigated region differ. Additionally, no information is available about the origin(s) of the *Gorilla* individuals and their possible wild vs. captive status. It is well documented that *Gorilla* is predominantly a terrestrial taxon, but that the degree of arboreal component in its locomotor repertoire varies according to species, origin, age, sex (Fleagle, 2013; Ruff et al., 2018b), but it also depends on the natural vs. artificial environment. For instance, *G. gorilla* is more arboreal than *G. beringei*

and females and juveniles normally feed and rest in trees (Remis, 1995; Doran, 1997; Mehlman and Doran., 2002; Fleagle, 2013; Ruff et al., 2018b), while mountain gorillas show a preference for secondary and herbaceous forests and are among the most terrestrial of all primates (Fleagle, 2013; Ruff et al., 2018b). In fact, adult mountain gorillas rarely climb trees, and they prepare their nest on the ground (Schaller, 1963; Rothman et al., 2006). Similarly, the degree of arboreality in the locomotor behaviour of *Papio* varies according to the region, which can be extremely different among species (Fleagle, 2013). In this study, wild *P. ursinus* from South Africa was included. In general, the intraspecific locomotor differences are not negligible within *Papio* and might also be responsible for different inner structural arrangements at the femoral head. No specific study has yet quantified such variation between taxa.

Regarding the 2D and 3D original analytical approaches for assessing cortical distribution along the femoral neck, for the *Gorilla* and *Papio* representatives, the standardised latero-medial variation of the S/I ratio from the base of neck (0%) to the head-neck junction (100%) is shown in Fig. 3.2.2.3.B. As seen in *Pan*, the two *Gorilla* individuals share higher values than measured in extant Humans, i.e., less asymmetric cortices, together with a tendency for marked latero-medial decrease of the ratio, while, according to this study, in Humans, there is a tendency towards thickness asymmetry reversal, extending from the base of neck towards the femoral head. A distinctly different pattern is shown by the four *Papio* individuals, sharing human-like asymmetric cortices and a neck-head tendency towards latero-medial increase of the ratio. Accordingly, the results of this study support the observations of previous findings (e.g., Ohman et al., 1997; Rafferty, 1998; Pina et al., 2011, 2012) indicating that extant non-human hominoids display a more homogeneous distribution of cortical bone in the femoral neck compared to Humans and most monkeys, except *Ateles* and *Alouatta*. It thus appears that asymmetrical cortical bone distribution may not solely be related to a human-like gluteal abductor action, but that extant apes may be the outliers in this respect, with their more symmetrical distributions possibly resulting from less stereotyped loadings across the hip than typical in most primates (Rafferty, 1998). Both generalised quadrupedal and bipedal taxa display a thinner superior cortex indicating a predominantly unidirectional (verticalised) pattern of weight transmission at the hip joint resulting into a concentration of loading stresses on the inferior side of the femoral neck. This can be functionally related to the predominance of adducted positions of the femur in these taxa, where the hind limbs move predominantly along the parasagittal plane (Rafferty, 1992; Pina et al., 2011, 2012). In contrast, both knuckle-walkers and specialised suspensory taxa display a thicker superior cortex, resulting in a more homogeneous distribution of cortical bone in the femoral neck. In other words, taxa with a

significant orthograde, suspensory and/or vertical-climbing component, display nonspecific loading distribution patterns at the femoral neck. It does not matter whether they are specialised suspensory taxa (such as hylobatids and *Pongo*), or whether they combine arboreal climbing and/or suspension with knuckle-walking, such as the African apes.

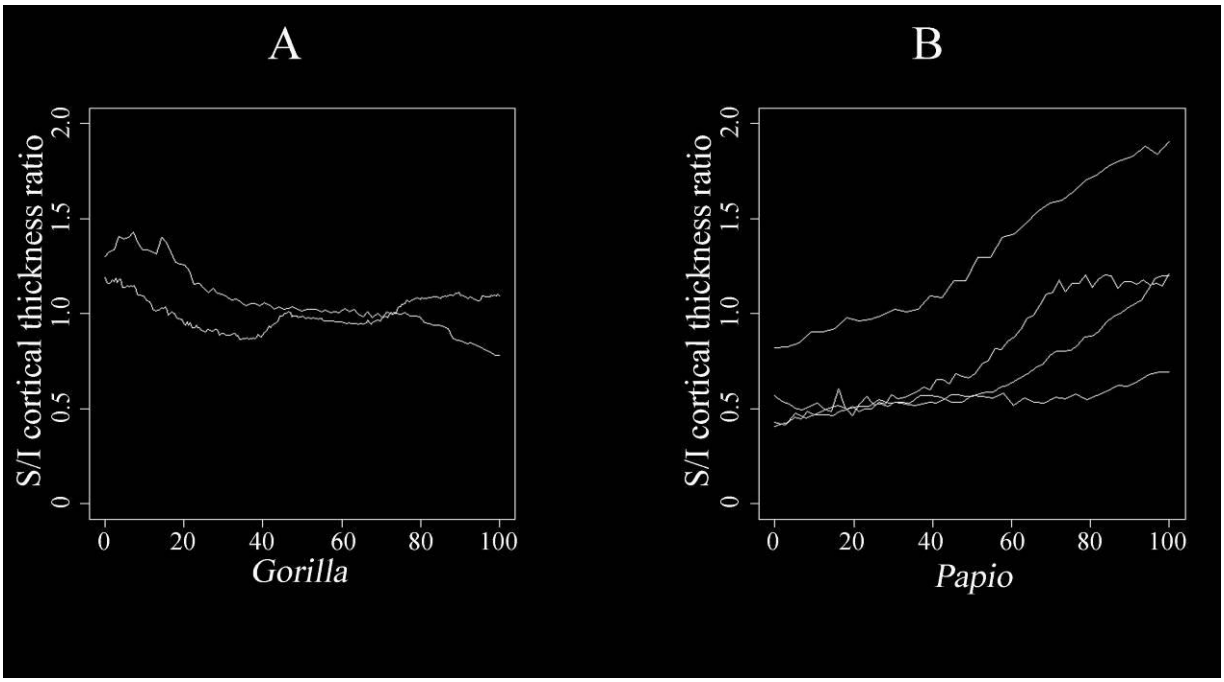

Fig. 3.2.2.3.B. Latero-medial variation from the base of neck (0) to the head-neck junction (100%) of the S/I ratio between the superior (S) and inferior (I) cortical thicknesses in *Gorilla* (A; n = 2) and *Papio* (B; n = 4).

The quadrant system previously assessed to detail the inner arrangement of the femoral neck in *P. robustus*, was used to comparatively evaluate mean cortical thickness variation across the anterior and posterior walls in *Gorilla* and *Papio*. The results are shown in Fig. 3.2.2.3.C. In the comparative context considered here, it is noticeable that anterior vs. posterior cortex asymmetry is almost absent in *Gorilla* (similar to Humans and *Pan*). As a whole, the conditions displayed by *Gorilla* and *Pan* are in line with the claim for nonspecific loading distribution patterns at the femoral neck. Conversely, as seen in *P. robustus*, the generalised quadrupedal *Papio* displays a thicker anterior and a thinner posterior wall across the entire neck length (Fig. 3.2.2.3.C, Fig. 3.2.2.3.D), which is compatible with a predominantly horizontally directed pattern of force transmission at the hip joint, resulting in the concentration of loading stresses on the anterior side of the femoral neck. Differences between Humans, *P. robustus* and

Pan in the action, size and morphology of the muscles situated on the anterior region of the proximal femur, might be responsible for the anterior cortical reinforcement eminent in *P. robustus*, and now also in *Papio*, but absent in Humans. More specifically, the action of the shared tendon insertion of the gemellus superior, gemellus inferior and the obturator internus muscles parallel to the head and neck of the femur, might create a variation of compressive force inducing cortical reinforcement at the anterior neck wall. In addition, in Humans the iliofemoral and pubofemoral ligaments reinforce the capsule anteriorly. Variation in this connective tissues between Humans, *P. robustus* and *Papio* might thus play a role in the loading environment at this joint.

Further investigation and lager sample sizes, including subadult individuals, are necessary to clarify the relative impact of the soft tissues on the endostructural bony arrangement at the joint site.

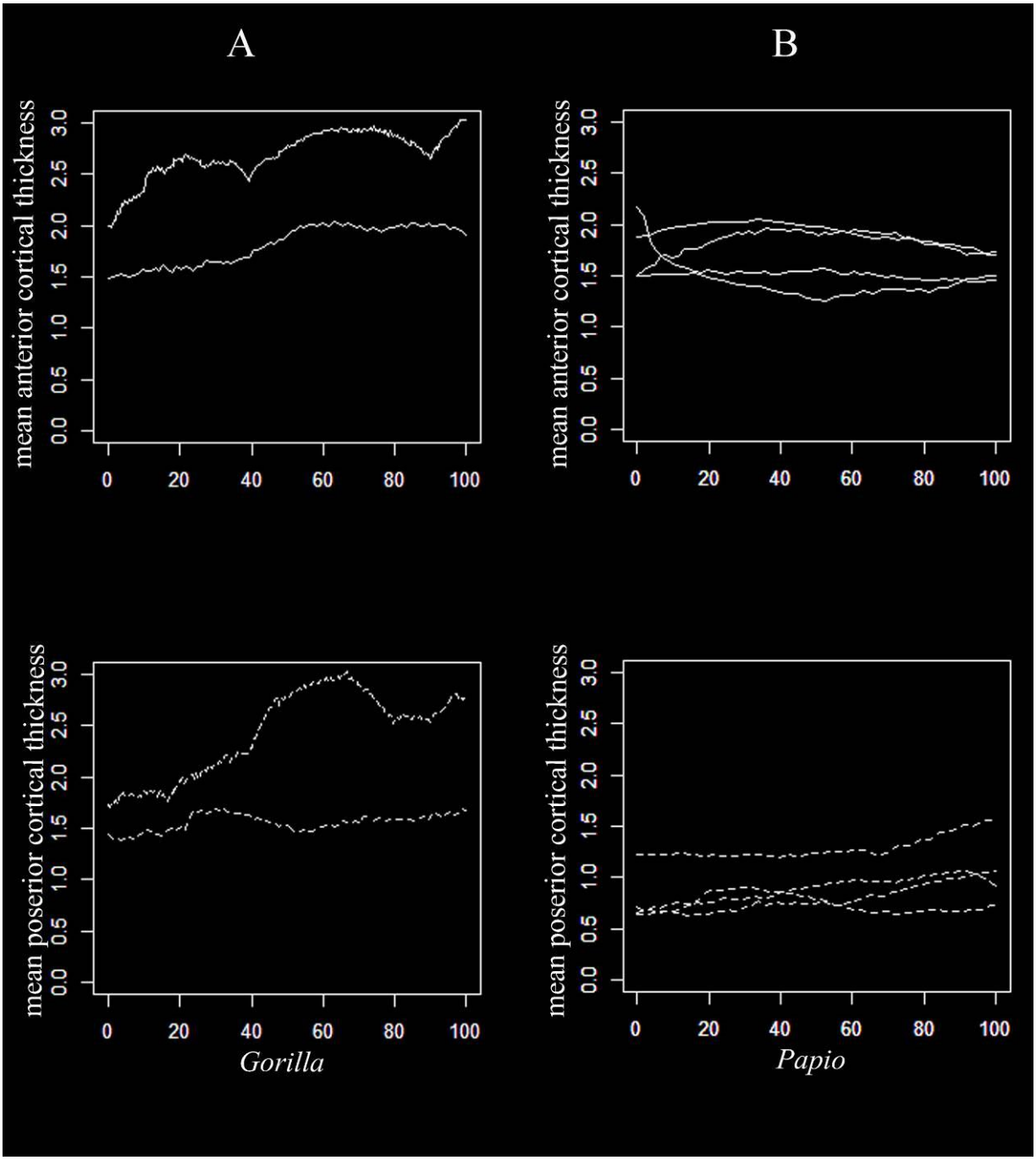

Fig. 3.2.2.3.C. Latero-medial variation from the base of neck (0) to the head-neck junction (100%) of the mean cortical thickness (in mm), distinctly assessed for the anterior and posterior walls of the femoral neck in *Gorilla* (A; anterior: solid line; posterior: dotted line; n = 2) and *Papio* (B; anterior: solid line; posterior: dotted line; n = 4).

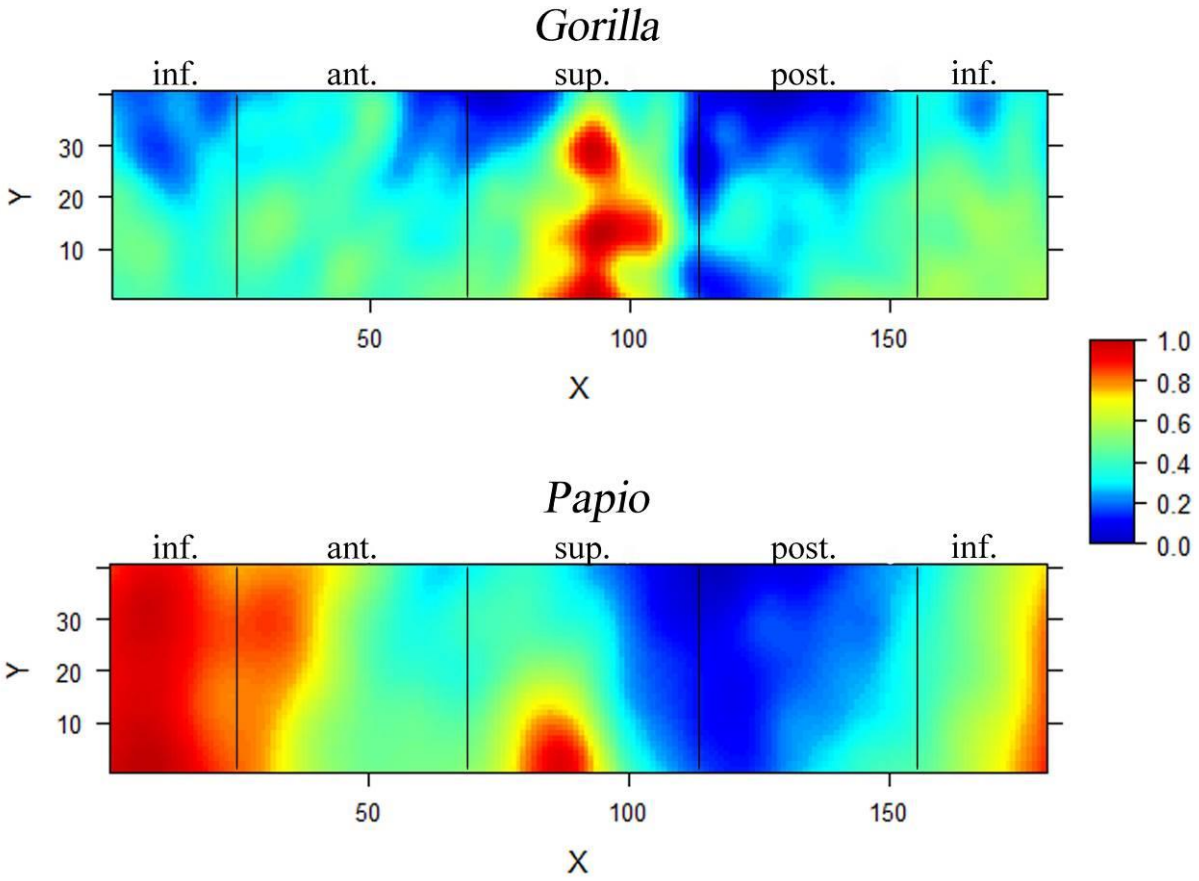

Fig. 3.2.2.3.D. µXCT-based standardised consensus morphometric maps of the virtually unzipped, unrolled and projected cortical bone thickness of the femoral neck from the base of neck (bottom Y-axis) to the head-neck junction (top Y-axis) of two *Gorilla* (upper) and four *Papio* (lower) individuals. Relative thickness is rendered by a pseudo-colour scale increasing from dark blue (0, thinner) to red (1, thicker). inf., inferior quadrant; ant., anterior quadrant; sup., superior quadrant; post., posterior quadrant.

3.2.2.4. Allometry

As discussed in the manuscript included in section 3.2.1, the mechanosensitive bone tissues remodel during life to adjust to the loading environment (e.g., Huiskes, 2000; Layon and Skerry, 2001; Lieberman et al., 2003, 2004; Pearson and Lieberman, 2004; Mittra et al., 2005; Ruff et al., 2006; Skerry, 2008; Barak et al., 2011, 2017; Gosman et al., 2011; Raichlen et al., 2015; rev. in Kivell, 2016). In fact, cross-sectional diaphyseal shape and cortical bone distribution have been shown to be particularly responsive to mechanical loading environments

(Trinkaus et al., 1994). Both body mass (BM) and body shape, which result from the distribution of body mass, affect the mechanical loadings of weight-bearing skeletal elements (i.e., resistance of the skeleton to gravity). Hence, strong relationships between BM and long bone shaft cross-sectional properties have been documented for many vertebrate taxa (Biewener, 1982; Ruff, 1988; Selker and Carter, 1989; Anyonge, 1993; Biknevicius, 1993; Demes and Jungers, 1993; Jungers and Burr, 1994). This observation is actually part of a more general issue regarding allometry, or size-shape relationships, within long bones, first broached centuries ago (Galilei, 1638; among others, see also Schultz, 1953; McMahon, 1973; Alexander et al., 1979). In that perspective, many researchers acknowledged that, when distinguishing the effects of specific postural, locomotor and mobility behaviour on limb bone structure, it is necessary to account for the effects of both body size and body shape on the absolute measures of bone strength (e.g., Ruff, 2008b; Sparacello and Marchi, 2008; Shaw and Stock, 2009; Carlson and Marchi, 2014).

While adjustments in the amount and distribution of cortical bone can significantly alter the strength and stiffness of the structure, trabecular bone tissue also contributes to the mechanical properties of bone as a whole (Brodetti and Hirsch, 1956; Pennycuick, 1967; Rockoff et al., 1969; Werner et al., 1988; Rogers and LaBarbera, 1993; Barak et al., 2008, 2010; Kivell, 2016). Most analyses of trabecular microarchitecture in mammals have focused on the functional significance of interspecific variation. However, only a few studies provide insights into the allometric scaling relationships between trabecular bone microstructure and body size across taxa (Swartz et al., 1998; Cotter et al., 2009; Doube et al., 2011; Barak et al., 2013b; Fajardo et al, 2013; Ryan and Shaw, 2013).

Analyses were performed to comparatively assess whether the interspecific variations observed for the microarchitectural cortical and trabecular features of the proximal femur, scale with BM in samples of five *P. robustus*, 12 Humans, two *Pan*, two *Gorilla* and four *Papio*. However, given the modest size of the samples, cortical and cancellous textures scaling with BM by exclusively using the present data, could not be reliably addressed. Similar to this study, the cross-sectional area of the femoral mid-neck, the punctual cortical thickness of the superior and inferior aspects and their ratio (superior thickness vs. inferior thickness), have been previously measured by Rafferty (1998) in a study using a sample of 231 individuals representing 21 non-human primate species. The results of this study were combined with the data provided by Rafferty (1998). By using the BM estimates for Humans, *Pan*, *Papio* and *Gorilla* provided in her study (Rafferty, 1998) and those recently proposed by Ruff et al.

(2018a) for *P. robustus* based on the specimens SK 82, SK 97 and SKWT1/LB-2, scaling of each variable to BM could be analysed.

Rafferty (1998) found an isometric relation between cortical area and BM. Combined results show that the superior and inferior cortical thicknesses and the cortical area at the femoral mid-neck exhibit a significant positive correlation with BM ($r = 0.729$ and $p < 0.01$ for the superior thickness [Fig. 3.2.2.4.A]; $r = 0.819$ and $p < 0.01$ for the inferior thickness [Fig. 3.2.2.4.B]; $r = 0.934$ and $p < 0.01$ for the cortical area [Fig. 3.2.2.4.C]), while the superior vs. inferior cortical thickness ratio is independent of BM ($r = 0.379$ and $p > 0.01$). Since slopes smaller than 0.33, or larger than -0.33 in cases of negative correlation, are significantly below the expectations of isometry, superior cortical thickness (slope = 0.44) and cortical area (slope = 0.63) show a positive allometry with BM, while inferior cortical thickness (slope = 0.27) scales to BM with a negative allometry. With special reference to the hominoids, the superior and inferior cortical thicknesses scale negatively to BM (0.33 and 0.26 respectively), while the cortical area scales positively (0.65). The inferior and superior cortical thicknesses in *P. robustus* are higher than expected by the allometric regressions for similar BM within the hominoid samples, and are outside the residual variation about the regression lines and closer to *P. troglodytes*. While cortical area in *P. robustus* is slightly higher than expected for similar BM by the allometric regressions for the primate and hominoid samples, it falls within the residual variation about the regression lines and is similar to the *Ateles paniscus* and *Propithecus dialema* and close to the *P. troglodytes* condition. *Gorilla* representatives in this study show thinner inferior cortex, thicker superior cortex and a slightly lower cortical area than expected by the allometric regressions for similar BM, while *Papio* shows slightly thicker superior and inferior cortex and a slightly inferior area. In this comparative context, a higher superior and inferior thicknesses in *P. robustus* thus appear as biomechanically-related, as they should have faced more important loads acting at the superior and inferior aspects of the femoral mid-neck.

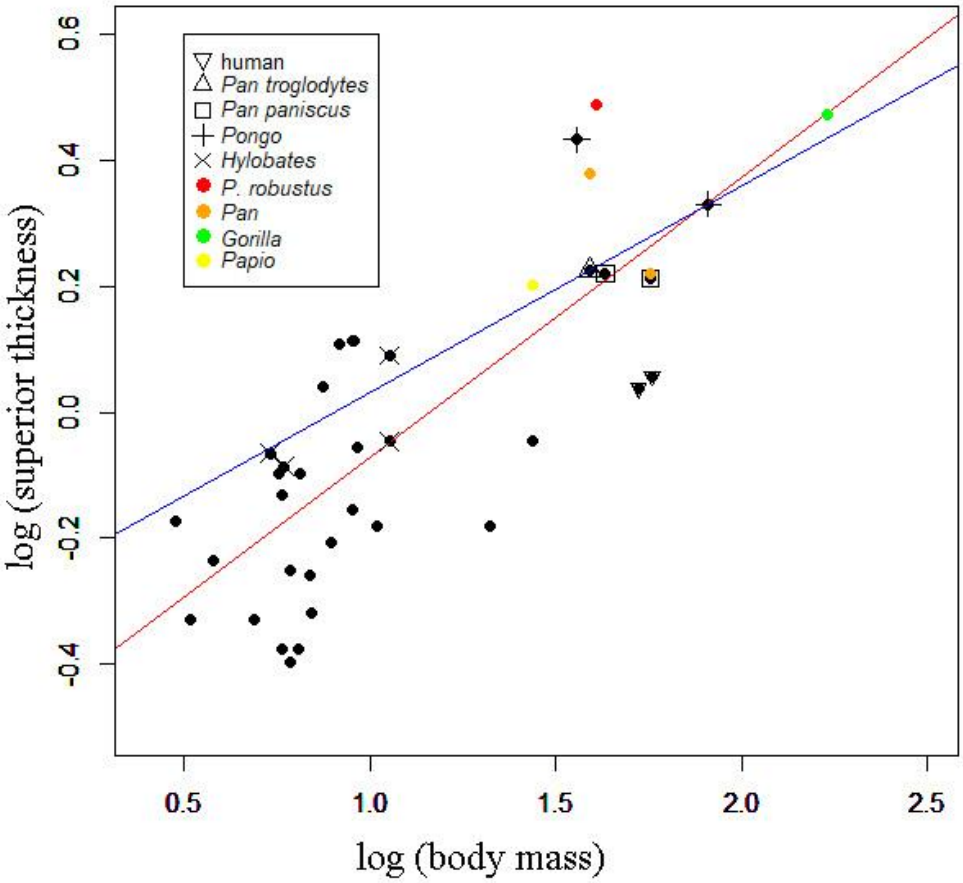

Fig. 3.2.2.4.A. Log-transformed scaling relationships between body mass (BM) and superior thickness measured at the femoral mid-neck for all species included in Rafferty (1998) and in this primate sample (colour solid dots), and regression lines for the hominoid (blue line) and the entire primate samples (red line).

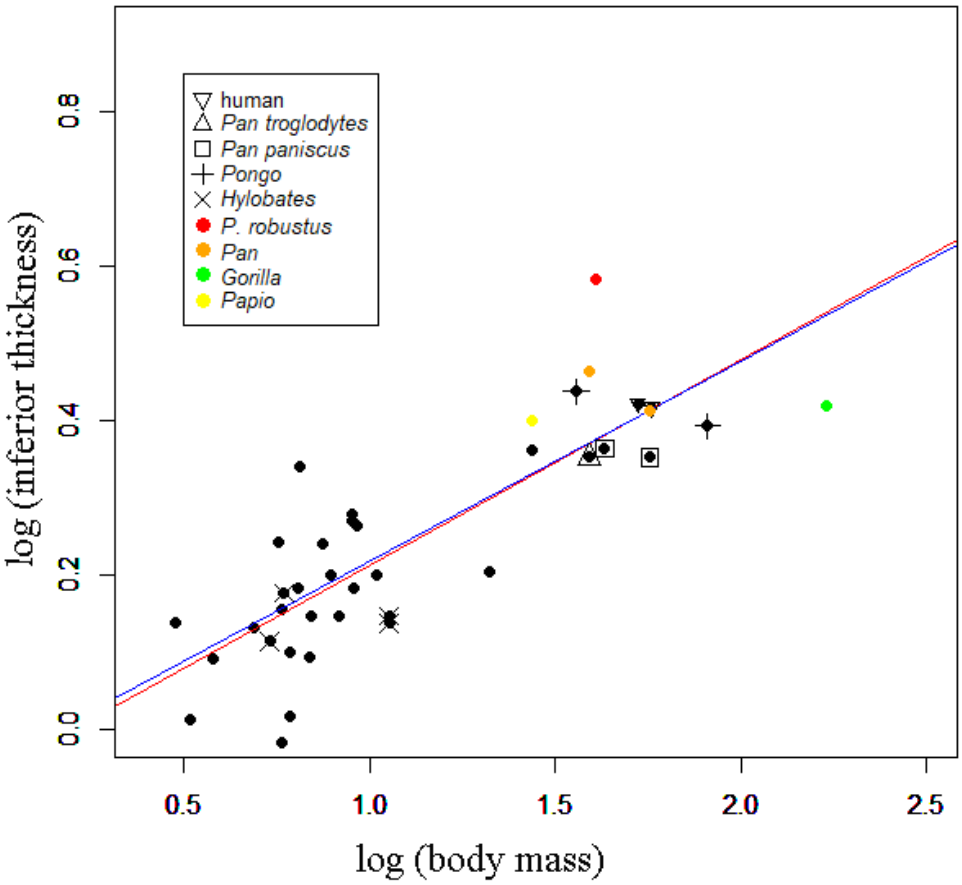

Fig. 3.2.2.4.B. Log-transformed scaling relationships between body mass (BM) and inferior thickness measured at the femoral mid-neck for all species included in Rafferty (1998) and in this primate sample (colour solid dots), and regression lines for the hominoid (blue line) and the entire primate samples (red line).

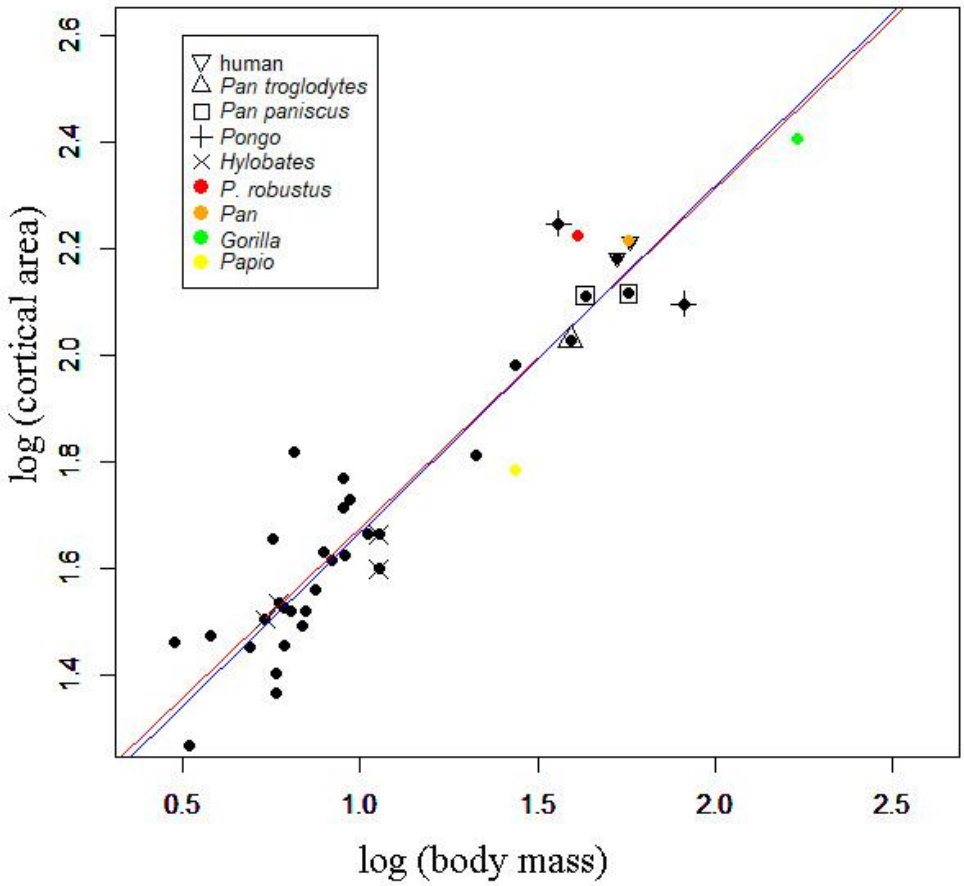

Fig. 3.2.2.4.C. Log-transformed scaling relationships between body mass (BM) and cortical area measured at the femoral mid-neck for all species included in Rafferty (1998) and in this primate sample (colour solid dots), and regression lines for the hominoid (blue line) and the entire primate samples (red line).

In this comparative analysis of the cancellous organisation of the femoral head in *P. robustus*, the selected volumes of interest have been extracted according to a shared size and position depending on the preservation conditions of the fossils. Accordingly, to the same extent, the calibrated protocol in this study is 'specific' and the results cannot be directly compared to any similar previous study using extant primates. As discussed in the manuscript in section 3.2.1, although trabecular thickness (Tb.Th.) has been shown to be strongly correlated with body size (Doube et al., 2011; Barak et al., 2013b; Fajardo et al., 2013; Ryan and Shaw, 2013), given that the three taxa *P. robustus*, extant Humans and *Pan* have a widely similar BM (Ruff et al., 2018a), the findings of modest or no differences in trabecular thickness among

these taxa confirm what has been observed in previous studies (Cotter et al., 2009; Scherf et al., 2013; Ryan and Shaw, 2015; Zeininger et al., 2016; Tsegai et al., 2018; but see Barak et al., 2013a; Su and Carlson, 2017).

3.3. Patella

The mammalian knee is an especially complex joint because of its implications in locomotion and weight bearing (Lovejoy, 2007; Masourus et al., 2010). Comparative research has documented the differences between the human and the ape knee joint configurations as part of a suite of traits intimately related to habitual postural and locomotion modes (e.g., Aiello and Dean, 1990; Tardieu, 1999; Lovejoy, 2007; Zipfel and Berger, 2009; Mazurier et al., 2010; Sylvester, 2013; Frelat et al., 2017). However, while the knee joint has been intensively studied in Humans, notably in a clinical context, non-human extant and fossil primate (including fossil hominins) knee shape and biomechanics still need additional investigation (e.g., Preuschoft, 1970; Badoux, 1974; Kumakura, 1989; Aiello and Dean, 1990; Preuschoft and Tardieu, 1996; Lovejoy, 2007; Diogo et al., 2012, 2013; Pina et al., 2014; Ingham et al., 2015; Pina, 2016).

Although the patella has an important role in knee biomechanics, its analysis has frequently been limited to a few features compared to the more detailed studies commonly conducted on the distal femur and the proximal tibia (e.g., Lague, 2002; Mazurier et al., 2010; Tallman, 2013, 2016; Frelat et al., 2017). In (palaeo)anthropology, the principal studies on the patella concern its outer proportions and shape and the differences between Humans and apes in the quadriceps complex (smaller in the latter, where flexion prevails) and in the vastus medialis (which in apes does not insert onto its extreme medial edge) (Mariani et al., 1978; Aiello and Dean, 1990; Taylor et al., 2004; Lovejoy, 2007; Standring, 2008; Masouros et al., 2010; Marchi et al., 2017). Only a few studies focused on providing a detailed biomechanical perspective of the differences in patellar shape among the living and fossil primate taxa, including hominids (e.g., Ward et al., 1995; DeSilva et al., 2013; Pina et al., 2014; Pina, 2016).

It has been pointed out that "variation in trabecular structure is our best source of morphological information that is preserved in the fossil record, particularly when analysed in conjunction with cortical bone, for reconstructing actual, rather than potential, behaviours in fossil hominoids and hominins" (Kivell, 2016: 587; see also section 1.5). However, from the rich literature available on the inner structural organisation of the proximal femur (rev. in Ryan et al., 2018), to the best of our knowledge, no study comparatively assessing cortical thickness distribution and cancellous bone organisation of the patella has been performed in extant and/or fossil hominids apart from essential clinical work developed on extant Humans (e.g., Raux et al., 1975; Townsend et al., 1975, 1977; Katoh et al., 1996; Toumi et al., 2006, 2012).

The lack of functional-related endostructural analyses of the patella and of its implications in terms of knee biomechanics is especially evident for the hominin fossil record, where Plio-

Early Pleistocene patellar specimens are rare and so far only reported for their external morphology (e.g., Carretero et al., 1999; Alemseged et al., 2006; Lordkipanidze et al., 2007; Harrison and Kweka, 2011; DeSilva et al., 2013; Martín-Francés et al., 2016). In this quantitatively poor comparative context, it is noteworthy that only one patella has so far been attributed to the taxon *P. robustus*: the isolated incomplete specimen SKX 1084 from Swartkrans Member 2 (Susman, 1988, 1989).

Given the topographic context of the hominin knee joint (Aiello and Dean, 1990; Lovejoy, 2007) and the documented ability of bone tissues to adjust structurally to the loading environments (e.g., Lieberman et al., 2004; Pearson and Lieberman, 2004; Ruff et al., 2006; Gosman et al., 2011; Wallace et al., 2012; Carlson and Marchi, 2014; Kivell, 2016), the still unexplored combined signals from the outer and the inner patellar structure have the potential to provide critical functional-related information. Accordingly, in our study of the specimen SKX 1084, we integrated and extended the available record on its outer conformation. We also comparatively assessed its unreported inner characteristics by using a recent human sample, a Neanderthal specimen and two *Pan* representatives. The aim of this exploratory study is to provide a first qualitative and quantitative 3D record, potentially useful for the future assessment of isolated hominin patellar remains.

Preliminary results of the study of the *P. robustus* patella have been presented to the *85th Annual Meeting of the American Association of Physical Anthropologists* (Atlanta, 12-16/4/2016): Cazenave M., Beaudet A., Braga J., Oettlé A., Thackeray J.F., Hoffman J., de Beer F. & Macchiarelli R. - The inner structural organization of a (likely) *Paranthropus* patella from Swartkrans Member 2 (SKX 1084): human- and non-human-like features. *American Journal of Physical Anthropology* 159, suppl. S62: 111 (https://onlinelibrary.wiley.com/doi/abs/10.1002/ajpa.22955). The methods of data acquisition and the results *in extenso* of this study are detailed in the paper "The SKX 1084 hominin patella from Swartkrans Member 2, South Africa: An integrated analysis of its outer morphology and inner structure", currently in press in the journal *Comptes Rendus Palevol* (ms. CRPALEVOL-D-18-00012R1) and provided in the section 3.3.1.

3.3.1. Manuscript CRPALEVOL-D-18-00012R1 in press in the journal Comptes Rendus Palevol

The SKX 1084 hominin patella from Swartkrans Member 2, South Africa: An integrated analysis of its outer morphology and inner structure

La patelle hominine SKX 1084 du Membre 2 de Swartkrans en Afrique du Sud: analyse intégrée de sa morphologie externe et de sa structure interne

Marine Cazenave[a,b],* Anna Oettlé[a,c], John Francis Thackeray[d], Masato Nakatsukasa[e], Frikkie de Beer[f], Jakobus Hoffman[f], Roberto Macchiarelli[g,h]

[a] *Department of Anatomy, University of Pretoria, Pretoria, South Africa*

[b] *Computer-assisted Palaeoanthropology Team, UMR 5288 CNRS-Université Paul Sabatier, Toulouse, France*

[c] *Department of Anatomy and Histology, Sefako Makgatho Health Sciences University, Ga-Rankuwa, Pretoria, South Africa*

[d] *Evolutionary Studies Institute and School of Geosciences, University of the Witwatersrand, Johannesburg, South Africa*

[e] *Laboratory of Physical Anthropology, Department of Zoology, Graduate School of Science, Kyoto University, Kyoto, Japan*

[f] *South African Nuclear Energy Corporation, Pelindaba, South Africa*

[g] *UMR 7194 CNRS-Muséum national d'Histoire naturelle, Musée de l'Homme, Paris, France*

[h] *Unité de Formation Géosciences, Université de Poitiers, Poitiers, France*

* Corresponding author. Computer-assisted Palaeoanthropology Team, UMR 5288 CNRS-Université Paul Sabatier, Toulouse, France.

E-mail address: marine.cazenave4@gmail.com (M. Cazenave)

ABSTRACT

SKX 1084 is an isolated partial patella from Swartkrans Member 2, South Africa, attributed to a small-bodied *Paranthropus robustus*. This study provides complementary information on its outer conformation and, for the first time for a fossil hominin patella, documents its inner structure in the perspective of adding biomechanically-related evidence to clarify its identity. We used X-ray micro-tomography to investigate SKX 1084 and to extract homologous information from a sample of 12 recent human, one Neanderthal, and two adult *Pan* patellae. We used geometric morphometrics to compare the outer equatorial contours. In SKX 1084, we identified two cancellous bony spots suitable for textural assessment (trabecular bone volume fraction, trabecular thickness, degree of anisotropy) and two related virtual slices for measuring the maximum cortico-trabecular thickness (CTT) of the articular surface. SKX 1084 shows a more complex articular shape than that for *Pan*, but still simpler than typical in *Homo sapiens*. At all sites, its CTT is thinner compared to *Pan* and approaches the condition in humans. This is also true for the expanded volume of the cancellous network. However, at both investigated spots, SKX 1084 is systematically intermediate between *Homo* and *Pan* for trabecular bone volume fraction and trabecular thickness, a pattern already shown in previous analyses on other *Paranthropus* postcranial remains. In the absence of any structural signal from patellae unambiguously sampling *Paranthropus*, as well as of comparable evidence extracted from specimens representing early *Homo*, our results do not allow rejection of the original taxonomic attribution of SKX 1084.

RÉSUMÉ

SKX 1084 est une patelle isolée incomplète du Membre 2 de Swartkrans, en Afrique du Sud, attribuée à un individu *Paranthropus robustus* de petite taille. La présente étude apporte des informations complémentaires sur sa conformation externe. Elle dévoile également, pour la première fois chez un hominine fossile, des caractéristiques de sa structure interne permettant d'extraire des informations biomécaniques pour clarifier son identité. Nous avons utilisé la microtomographie à rayons X pour étudier SKX 1084 et extraire des informations homologues à partir d'un échantillon composé de 12 patelles humaines récentes, un Néanderthalien et deux chimpanzés et appliqué la morphométrie géométrique pour comparer leurs contours externes. Nous avons identifié deux régions dans le tissu trabéculaire de SKX 1084 qui sont adaptées à l'évaluation texturale (densité osseuse, épaisseur trabéculaire, degré d'anisotropie) et nous avons

extrait deux coupes virtuelles pour mesurer l'épaisseur cortico-trabéculaire maximale (CTT) de la surface articulaire. SKX 1084 présente une forme articulaire plus complexe que celle des chimpanzés, mais plus simple que celle de *Homo sapiens*. Son CTT est partout moins épais par rapport à *Pan* et se rapproche de la condition humaine. Ceci est également vrai pour le volume global du réseau trabéculaire. Cependant, pour les deux régions étudiées, SKX 1084 montre une densité osseuse et une épaisseur trabéculaire intermédiaire entre *Homo* et *Pan*, une tendance déjà observée dans de précédentes analyses d'autres restes post-crâniens de *Paranthropus*. En l'absence de toute information du signal structural d'autres patelles de *Paranthropus*, ainsi que d'éléments comparables issues des premiers représentants du genre *Homo*, nos résultats ne permettent pas de rejeter l'attribution taxonomique originale de SKX 1084.

Keywords: Fossil hominins, knee joint, cortical bone, cancellous network, X-ray micro-tomography
Mots clés: Hominines fossiles, articulation du genou, os cortical, réseau trabéculaire, micro-tomographie à rayons X

1. Introduction

The discovery of isolated fragmentary hominin remains from the axial and appendicular skeleton in the Plio-Pleistocene South African cave deposits is a rather frequent occurrence which complicates the task of confidently assessing diversity in contexts where *Australopithecus*, *Paranthropus* and early *Homo* may have co-existed (Berger et al., 2010; Braga et al., 2016; Cazenave et al., 2017; Grine and Susman, 1991; Keyser et al., 2000; Lague, 2015; McHenry, 1975; McHenry et al., 2007; Moggi-Cecchi et al., 2010; Schwartz and Tattersall, 2003; Susman and Brain, 1988; Susman and de Ruiter, 2004; Susman et al., 2001). An example of such difficulties is represented by the specimen SKX 1084, an isolated partial patellar bone from Swartkrans Member 2 commonly attributed to a small-bodied *P. robustus* individual (Susman, 1988, 1989). However, the estimated chronology of Swartkrans Member 2 (1.36-1.1 Ma) (Balter et al., 2008; Delson, 1988; Gibbon et al., 2014; Herries et al., 2009; Vrba, 1975) is also compatible with the presence in the area of representatives of the genus *Homo*, whose percentage in the Swartkrans Members 1-3 hominin assemblage has been estimated to 9% (Pickering et al., 2012).

Rare Pliocene-Early Pleistocene hominin patellar specimens are usually reported for their size and outer gross morphology (e.g., Alemseged et al., 2006; Carretero et al., 1999; DeSilva et al., 2013; Harrison and Kweka, 2011; Lordkipanidze et al., 2007; Martín-Francés et al., 2016). However, given the topographic context of the hominin knee joint (Aiello and Dean, 1990; Lovejoy, 2007) and the documented ability of bone tissues to adjust structurally to the loading environments (e.g., Carlson and Marchi, 2014; Gosman et al., 2011; Kivell, 2016; Lieberman et al., 2004; Pearson and Lieberman, 2004; Ruff et al., 2006; Wallace et al., 2012), the so far unexplored combined signals from the outer and the inner patellar structure have the potential to provide subtle functionally-related information. Indeed, the differences between the human and ape knee joint configurations are part of a suite of traits intimately related to habitual postural and locomotion modes (e.g., Aiello and Dean, 1990; Frelat et al., 2017; Lovejoy, 2007; Mazurier et al., 2010; Sylvester, 2013; Tardieu, 1999; Zipfel and Berger, 2009). With regard to the patella, such differences do not only concern its outer proportions and shape and the extension and insertion topography of the quadriceps complex (smaller in the latter, where flexion prevails) and of the vastus medialis (which in apes does not insert onto its extreme medial edge) (Aiello and Dean, 1990; Lovejoy, 2007; Mariani et al., 1978; Masouros et al., 2010; Standring, 2008; Taylor et al., 2004), but should also be expressed in terms of regional variation of the patellar subchondral bone thickness and structural arrangement of the

underlying cancellous network (for the human patella, see Katoh et al., 1996; Raux et al., 1975; Toumi et al., 2012; Toumi et al., 2006; Townsend et al., 1975; Townsend et al., 1977).

Following Kivell, (2016: 587), "variation in trabecular structure is our best source of morphological information that is preserved in the fossil record, particularly when analysed in conjunction with cortical bone, for reconstructing actual, rather than potential, behaviours in fossil hominoids and hominins". However, while the outer aspect of SKX 1084 has been the object of description and comparative morphological analysis (Ramirez and Pontzer, 2015; Susman, 1988, 1989; Susman et al., 2001), its inner structural organization remains unreported (Cazenave et al., 2016).

By assuming that the patella bears a functionally-related signal and that the *Paranthropus* inner structural signature should be somehow distinct from the human one (for the proximal femur, for example, see Chirchir et al., 2015; Ryan et al., 2018), in this exploratory study we use imaging techniques applied to an X-ray micro-tomographic record of SKX 1084 (i) to integrate and comparatively assess its outer conformation and (ii) to detail and preliminarily compare its inner characteristics to homologous features extracted from a recent human sample, a Neanderthal individual and two *Pan* representatives. Given the current lack of similar combined information extracted from the patellar bone of any pre-modern human and extant and fossil non-human hominid, the present exploratory study represents a first qualitative and quantitative three-dimensional (3D) glimpse useful for the future assessment of isolated hominin patellar remains.

2. Materials and methods

2.1. Materials

SKX 1084 represents the superior two-thirds of an undistorted, relatively well-preserved while incomplete left patella (Fig. 1). Its ossification, general morphology and degree of development of some longitudinal markings on its anterior surface (likely related to the quadriceps tendon) indicate it comes from an adult individual, even if surface rugosity may have been locally accentuated by mineral matrix dissolution. The specimen preserves the entire base, which slopes antero-inferiorly from behind; however, its cortical shell is chipped all along the superior posterior margin, approximately at the insertion of the vastus intermedius tendon, thus revealing an underlying trabecular network partially filled by sediment. The lateral border is nearly intact, but the specimen lacks the apex and almost entirely its medial border, uniquely

represented by its uppermost portion. Posteriorly, the articular portion which contacts the lateral lip of the femoral trochlea is virtually intact. As a whole, this specimen shows an only modest degree of mineralization. While its maximum height cannot be assessed, SKX 1084 has a medio-lateral breadth of 30.2 mm (Susman, 1989) and an antero-posterior thickness near its centre of 13.0 mm (original measure).

SKX 1084 was previously curated at the Ditsong National Museum of Natural History, Pretoria. Since 2016 the specimen has been integrated into the fossil hominin collections of the Evolutionary Studies Institute at the University of the Witwatersrand, Johannesburg.

The comparative material used in this study consists of human and chimpanzee adult patellae, all lacking macroscopic evidence of alteration or pathological change. The recent human specimens come from six individuals of African ancestry (4 males and 2 females aged 24-29 years) selected from the Pretoria Bone Collection at the Department of Anatomy of the University of Pretoria (L'Abbé et al., 2005), and from six individuals (2 likely males and 4 likely females whose estimated age at death ranges between 30 and 50 years) from the Imperial Roman graveyard of Velia, Italy, stored at the National Prehistoric Museum of Rome (rev. in Beauchesne and Agarwal, 2017). The fossil human representative is the perfectly preserved left patella from the OIS 4 Neanderthal partial skeleton Regourdou 1, from the homologous rock shelter in Dordogne, France, stored at the Musée d'Art et d'Archéologie du Périgord, Périgueux (Bayle et al., 2011; Maureille et al., 2015). We also studied two female chimpanzee patellae from the Mahale skeletal collection stored at the Japan Monkey Centre of Inuyama, Japan.

2.2. Methods

All specimens were imaged by X-ray micro-tomography. SKX 1084 was scanned in 2015 at the South African Nuclear Energy Corporation (Necsa), Pelindaba, using a Nikon XTH 225 ST equipment with an isotropic voxel size of 16.2 µm. The human patellae from the Pretoria Bone Collection were also recorded at Necsa, in 2016, with an isotropic voxel size ranging from 24.0 µm to 29.0 µm, while the archaeological specimens from Velia were scanned in 2012 at the Multidisciplinary Laboratory of the International Centre for Theoretical Physics (ICTP) of Trieste, Italy (Tuniz et al., 2013), at an isotropic voxel size ranging from 26.5 µm to 33.1 µm. The Neanderthal Regourdou 1 was imaged in 2004 by SR-µCT at the beamline ID 17 of the European Synchrotron Radiation Facility (ESRF) of Grenoble, France, at an isotropic spatial resolution of 45.5 µm (Bayle et al., 2011). Finally, the two chimpanzee patellae were recorded in 2017 at the Laboratory of Physical Anthropology, Kyoto University, using a ScanXmate

A080s (Comscan co.) equipment with an isotropic voxel size of 48.5 µm. Following acquisition, a virtual transformation of each dataset was necessary to coherently orient the specimens by using Avizo© v.8.0.0. (Visualization Sciences Group Inc.).

The articular (posterior) surface of the patella presents distinct differences in extant and extinct hominids (Aiello and Dean, 1990; Lovejoy, 2007; Masouros et al., 2010; Pina et al., 2014; Pritchard, 1980; Standring, 2008; Ward et al., 1995; for a review, see Pina, 2016). Accordingly, before detailing its inner structure, we virtually extracted the transverse section of SKX 1084 at its maximum medio-lateral breadth and performed a comparative geometric morphometric (GM) analysis of its unsmoothed outer equatorial contour with respect to the outlines extracted from the comparative material used in this study. However, because of local bony discontinuities on the anterior surface of the South African specimen (Fig. 1), the anterior portion of its cross-section was reconstructed by two independent observers by using the preserved contours of the antero-lateral and medial regions as a guide. Accordingly, three outer outlines of SKX 1084 displaying an increasing degree of anterior convexity were generated (see Supporting information, Fig. S1). On each virtually reconstructed outline (a to c), 100 semilandmarks were placed following the sectional contour using the B-spline module in Avizo© v.8.0.0. Using the package Morpho v.2.5.1 (Schlager, 2017) for R v.3.4.0 (R Development Core Team, 2018), a generalized Procrustes analysis (GPA) and a weighted between-group principal component analysis (bgPCA) based on the Procrustes shape residuals (Mitteroecker and Bookstein, 2011) were then performed to compare the three reconstructed versions of SKX 1084 and the human and chimpanzee shapes. Allometry was tested on the landmark-based analyses using the coefficient of determination (R^2) of a multiple regression (Bookstein, 1991), in which the explicative variable is the centroid size and the dependent variables are the bgPC scores (Mitteroecker et al., 2013).

Relatively well preserved cancellous network spots in SKX 1084 were found in the central and medial posterior areas; however, the amount of cemented matrix infill permeating the network increased towards its outer surface, especially laterally and anteriorly. Accordingly, we firstly identified in the inner central and medial upper portion of SKX 1084 two cubic volumes of interest (Ryan and Ketcham, 2002a, b), aVOI and bVOI, respectively, suitable for textural properties assessment (Fig. 2). Both had an edge length equal to 11% of the medio-lateral breadth (i.e., 3.32 mm in SKX 1084, which corresponds to a volume of 36.6 mm^3). The centre of aVOI was placed midway between 50% of the medio-lateral diameter and its most distant point on the upper margin along an axis perpendicular to the breadth. The bVOI was positioned medially to the aVOI, the distance between the two centres corresponding to 25%

of the medio-lateral diameter (i.e., 7.6 mm in SKX 1084). The same analytical protocol was systematically applied to the specimens used for comparison. In extant humans the VOIs range in size from 70.2 mm^3 to 151.9 mm^3 and from 13.8 mm^3 to 15.6 mm^3 in *Pan*.

At two sites of the articular surface topographically related to the VOIs defined above, we measured the maximum thickness of the cortico-trabecular complex (CTC, in mm), i.e., the subchondral component which includes the cortical shell (lamina) and the intimately related adjoining portions of the supporting trabecular network, which mostly consists of plate-like structures (Supporting information, Fig. S2; Beaudet et al., 2013; Mazurier, 2006; Mazurier et al., 2006, 2010; Volpato, 2007). The maximum cortico-trabecular thickness (CTT) was measured by the routine MPSAKv2.9© (in Dean and Wood, 2003) on two sagittal virtual slices set perpendicular to the posterior face of each VOI and crossing their centre (Fig. 2). To facilitate comparisons, in each specimen such measures (aCTT and bCTT) were standardized with respect to the medio-lateral diameter of the patella. Unfortunately, in SKX 1084 we could not similarly assess the anterior CTT, as in this specimen the cortical shell was not preserved and some matrix infill obscured the boundaries.

The cubic VOIs were binarized into bone and non-bone using the "Half Maximum Height" (HMH) quantitative iterative thresholding method (Spoor et al., 1993) and the region of interest protocol (ROI-Tb; Fajardo et al., 2002) by taking repeated measurements on different slices of the virtual stack (Coleman and Colbert, 2007) using Avizo© v.8.0.0. and ImageJ© (Schneider et al., 2012). Because of local matrix infill, segmentation of the specimen SKX 1084 required manual interventions. By using the star volume distribution (SVD) algorithm in Quant3D© (Ryan and Ketcham, 2002a, b), on each virtually extracted VOI we measured the following variables: (i) the trabecular bone volume fraction (BV/TV, in %), given as the ratio of the number of bone voxels to the total number of voxels; (ii) the trabecular thickness (Tb.Th., in mm), which is the mean thickness of the trabecular struts; and (iii) the degree of anisotropy (DA), a fabric characteristic of trabecular bone assessed following Ryan and Ketcham (2002a; see also Ryan and Walker, 2010; Shaw and Ryan, 2012) by dividing the eigenvalue representing the relative magnitude of the primary material axe of the bone structure (τ_1) by the eigenvalue representing the relative magnitude of the tertiary material axe of the bone structure (τ_3).

For all variables, a number of intra- and inter-observer tests for accuracy run by three independent observers revealed differences less or equal to 5%.

3. Results

For the medio-lateral breadth and the antero-posterior thickness, SKX 1084 fits the proportions shown by *H. floresiensis* (Jungers et al., 2009) and *A. sediba* (DeSilva et al., 2013), and also approaches those of the slightly thicker *H. naledi* (Berger et al., 2015; Marchi et al., 2017) and the slightly smaller male and female chimpanzee patellae (Aiello and Dean, 1990; Pina, 2016; Pina et al., 2014; Pritchard, 1980; Ward et al., 1995). Conversely, SKX 1084 is systematically smaller compared to *H. erectus* (*georgicus*) from Dmanisi (Lordkipanidze et al. 2007; T. Jashawili, pers. comm.), *H. antecessor* (Carretero et al., 2001), the Neanderthals (Radovčić et al., 1988; Trinkaus, 1983; Vandermeersch, 1981; and original data), as well as to the extant human figures (Baldwin and House, 2005; Dayal and Bidmos, 2005; Irampur et al., 2008; Kemkes-Grottenthaler, 2005; Olateju et al., 2013; Yoo et al., 2007) (Fig. 3 and Supporting information Table S1).

The bgPCA based on the Procrustes shape coordinates of the three reconstructed outer outlines of the transverse section at the maximum medio-lateral breadth of SKX 1084 (a to c; see Supporting information Fig. S1) are shown in Fig. 4 together with those of the human and chimpanzee specimens. The first two components (bgPC1 and bgPC2) show no allometric signal ($R^2 = 0.02$) and no size-dependent shape variation ($R^2 = 0.01$). In the analysis, the three reconstructed equatorial profiles of the South African fossil patella cluster together and are distinct from both the human and chimpanzee morphotypes. Specifically, by showing a proportionally more ovoid outline, SKX 1084 and the two *Pan* used in this analysis fall in the negative space of bgPC1, whereas all human specimens, including the Neanderthal Regourdou 1, are mostly found in the positive space of bgPC1 because of their more complex articular shape showing concave articular facets and a convex vertical ridge. The three contours of SKX 1084 and the two *Pan* representatives were discriminated along bgPC2, the fossil specimen exhibiting a more rounded shape compared to the flatter chimpanzee shape (Fig. 4).

In terms of volume and spatial organization, the cancellous network preserved in SKX 1084 is globally closer to the human than to the *Pan* condition, even if in coronal view the specimen from Swartkrans and *Pan* show a slightly more honeycomb-like, vacuolar appearance of the cancelli in respect to the human pattern (Fig. 5). Specifically, despite its incompleteness, SKX 1084 shares with humans a larger proportional volume of trabecular bone compared to *Pan*, a denser area at the supero-lateral margin (likely related to the attachment of the quadriceps), and a higher number of radially oriented trabeculae at the medial and superior peripheral areas. In sagittal view, a typically human vertically oriented anterior bundle (Standring, 2008), also appreciable in transversal view, is noticeable in SKX 1084 (where it is anyhow incompletely

preserved inferiorly), while *Pan* displays at all sites a relatively and absolutely thicker cortical shell and much less expanded but denser spongy bone.

For both relative (%) values of the maximum cortico-trabecular thickness (CTT) measured at the central (aCTT) and medial (bCTT) spots of the posterior surface (Fig. 6), SKX 1084 fits the recent human estimates and is distinct from the thicker *Pan* condition (Table 1). In this context, the proportionally thinnest cortico-trabecular complex was found at the bVOI of the Regourdou 1 Neanderthal specimen.

As measured in both central and medial VOIs (Table 2), SKX 1084 shows a relative bone volume fraction (BV/TV) intermediate between the human and the chimpanzee estimates, *Pan* being over twice denser than observed in all human specimens used in this study, including the Neanderthal representative. An intermediate position is again shown by SKX 1084 for the average trabecular thickness (Tb.Th.), all humans systematically displaying thinner struts. For the degree of anisotropy (DA), the South African fossil specimen closely fits the modern human estimates for the central aVOI, while for the medial bVOI it is intermediate between the higher human values and the generalized lower degree of anisotropy displayed by the chimpanzee patella. Interestingly, for all variables considered here, the Neanderthal specimen always falls within the extant human range, which is not the case for SKX 1084 but for the DA of the aVOI (Table 2).

4. Discussion

This exploratory study aimed at tentatively adding previously unreported biomechanically-related evidence to clarify the common allocation of the SKX 1084 patella from Swartkrans to the taxon *Paranthropus* (e.g., Jungers, 1988; Marchi et al., 2017; McHenry, 1991; Ramirez and Pontzer, 2015; Susman, 1988, 1989, 2004; Susman and Brain, 1988; Susman and de Ruiter, 2004; Susman et al., 2001; Sylvester et al., 2011). Besides the incomplete preservation of this specimen and its limited amount of subchondral and cancellous bone spots preserved for reliable quantitative assessment, the major limiting factor in this study is the lack of comparative information on the inner structural organization characterizing any nonhuman fossil hominin patella (including in *Australopithecus*) and, of course, that of any specimen confidently representing early *Homo*. Nonetheless, we consider that some results obtained from the present analyses may deserve attention in similar future studies.

Ramirez and Pontzer (2015) have suggested that patellar dimensions can be used in extant primate and fossil hominin taxa as proxy for the physiological cross-sectional area of the

quadriceps, the primary extensor of the knee (see also Pina et al., 2014; Trinkaus, 1983, and the review in Pina, 2016). While the maximum height cannot be measured in SKX 1084, its medio-lateral breadth and antero-posterior thickness fit the dimensions of diminutive *H. floresiensis* and of *A. sediba*, and more closely approaches those of *Pan* and *H. naledi* than the size of any other human patella reported so far. The patellar antero-posterior thickness and supero-inferior height (the latter unknown in SKX 1084), but not the medio-lateral breadth, appear to play a major role in the length of the patellar tendon moment arm and in the lever arm length associated with the quadriceps, respectively (Pina, 2016; Pina et al., 2014; Ward et al., 1995). Accordingly, whenever the conclusions by Ramirez and Pontzer (2015) are correct, the relatively small-sized fossil hominin patellae considered here, including SKX 1084 (Fig. 3 and Supporting information Table S1), should represent taxa having experienced a limited home range size compared to that expected for *Homo* (Antón, 2013; Antón et al., 2014; Ramirez and Pontzer, 2015).

Comparative research on structural anatomy and functional morphology supports the view that the mammalian knee is an especially complex joint (Lovejoy, 2007: 326), including in primates, where shape variation of the patellar articular surface plays a key functional role. In humans, where the patella tends to have the thickest articular cartilage in the entire body (Masouros et al., 2010; Standring, 2008), its smaller medial facet contacts the antero-lateral portion of the medial femoral condyle and the wider lateral facet contacts the anterior part of the lateral condyle only in full flexion, while in extension the patellar-femoral contact is limited to the lowest portions of both facets (Aglietti and Menchetti, 1995; Goodfellow et al., 1976; Lovejoy, 2007; Pina, 2016). Compared to the multifaceted human patella bearing several distinctly angulated planes, a simpler articular morphology is found in *Pan*, where the posterior surface is relatively smooth and casts the similarly flatter trochlear surface (patellar groove) of the distal femur (Aiello and Dean, 1990; Lovejoy, 2007). With this respect, while necessarily limited to the equatorial contour, our GM-based shape analysis confirms such distinction in articular complexity between *Homo* and *Pan* and also reveals that the SKX 1084 outline occupies a somehow intermediate morphospace. Additional research work is needed to relate such differences in the outer conformation of the hominid patellar bone to locomotion-related differences in knee joint kinematics.

Especially when assessed in fossil remains, the inner boundaries of the so-called cortico-trabecular complex (CTC) are locally difficult to define (e.g., Mazurier, 2006; Mazurier et al., 2006, 2010; Volpato, 2007; Supporting information, Fig. S2). Nonetheless, compared to the human condition, the chimpanzee patella unambiguously shows at all sites a relatively thicker

and denser CTC, notably expressed by a distinctly thicker anterior lamina which, in both individuals used in this study, is about twofold as thick as measured in our human comparative sample (Supporting information, Fig. S3 and Table S2). Interestingly, relatively and absolutely higher values of cortico-trabecular thickness in *Pan* are also found at both medial and lateral condyles of the tibial plateau compared to the human condition (Mazurier, 2006; Mazurier et al., 2010). In the small-sized chimpanzee patella, this greater proportional amount of subchondral bone is associated to a relatively and absolutely reduced volume of vacuolar spongy bone. To the contrary, the human patella displays a proportionally thinner shell and a relatively and absolutely higher volume of locally more structured cancellous bone, thus behaving as a kind of "sandwich" construction combining high strength with relatively low density (Dalstra and Huiskes, 1995; Huiskes, 2000). As subchondral bone tends to respond to loading of the complementary joint surface, while cancellous bone primarily responds to forces traveling through the bone itself (Su, 2011; Zeininger et al., 2011), the gross structural solutions distinguishing the human and chimpanzee patellae reflect two ways of dealing with different patterns of mechanical stresses at the joint, those acting on the human patella being greater medially and centrally than laterally (Toumi et al., 2006, 2012). With this respect, while cortico-trabecular thickness variation across the anterior surface cannot be assessed in SKX 1084, thickness measured at two sites beneath its articular surface fits the human figures, as also does its proportion of spongy bone.

In terms of textural properties assessed at two cancellous volumes of interest selected because of the quality of their signal, our results show that, apart from a relatively honeycomb-like appearance and a slightly less structured medial aspect, the inner organization of SKX 1084 more closely resembles the human than the *Pan* condition. Whereas SKX 1084 displays a denser cancellous network and relatively thicker struts than measured in our recent human sample and in the Neanderthal representative, the South African fossil specimen and humans are more gracile compared to *Pan*.

According to recent interpretations based on the comparative analysis of the cancellous network properties assessed in the femoral head of extinct and extant hominids, humans and australopiths share a higher degree of anisotropy than typical in extant apes as response to the more stereotypic loading conditions at the hip joint imposed by habitual bipedal locomotion (Ryan et al., 2018). Similarly, the distinctly human-like signal from at least the more centrally-placed aVOI detected in this study in SKX 1084, which is higher than measured in *Pan*, is compatible with the model of a limited range of habitual knee joint motion, i.e., with a human-

like gait kinematics. However, given the limited number of cases investigated so far, this hypothesis remains to be tested on more representative hominid samples.

A number of studies having investigated the structural features in some postcranial hominin remains show that, compared to the typically human figures (e.g., Chirchir et al., 2015, 2017; Ryan and Shaw, 2015), *Paranthropus* commonly possesses a thicker cortex and a denser, thicker and less anisotropic cancellous network, but also that its conformation is globally closer to the human than to the ape pattern (Bleuze, 2010; Cazenave et al., 2017; Chirchir et al., 2015; DeSilva and Devlin, 2012; Dominguez-Rodrigo et al., 2013; Dowdeswell et al., 2016; Macchiarelli et al., 1999, 2001; Ruff and Higgins, 2013; Ruff et al., 1999; Skinner et al., 2015; Su and Carlson, 2017; Su et al., 2013; Ryan et al., 2018). With this respect, as the condition characterizing early *Homo* is still unknown, the endostructural signal preserved in SKX 1084 is compatible with what is expected for *Paranthropus*. However, depending on the investigated regions, more human- or chimpanzee-like textural features have been observed at site-specific level in both *Paranthropus* and *Australopithecus* (Barak et al., 2013; DeSilva and Devlin, 2012; Macchiarelli et al., 1999; Su, 2011; Su and Carlson, 2017; Su et al., 2013; Zeininger et al., 2016; Ryan et al. 2018).

5. Conclusions

Patellar remains are rare in the hominin fossil record. In the comparative context considered in this study, the coupled signals from what is preserved and suitable for analysis of the outer morphology and inner structural arrangement of the Early Pleistocene patella SKX 1084 from Swartkrans Member 2, South Africa, indicate that it belonged to an adult small-bodied hominin (Susman, 1989) likely equipped for exploiting a limited home range size (Ramirez and Pontzer, 2015). Its habitual postural- and locomotion-related charges at the knee joint appear compatible with, but not fully overlapping the human condition as represented by the Late Pleistocene and Holocene comparative materials examined so far. When compared to what is currently known on the structural bony characteristics of the postcranial skeleton in fossil hominins, the inner features assessed in SKX 1084 (i.e., thickness of the cortical shell and cancellous bone textural properties) globally fit the general australopith pattern (cf. Ryan et al., 2018). In the absence of any signal from patellae unambiguously attributed to *Paranthropus*, as well as of comparable evidence extracted from specimens representing early *Homo* (the patella D3418 from Dmanisi; Lordkipanidze et al., 2007), the attribution of SKX 1084 to the taxon *P. robustus* (Susman,

1988, 1989; Susman et al., 2001) cannot be rejected, and still represents a reasonable assessment.

Acknowledgements

For access to fossil and comparative materials, we are grateful to the curators of the Ditsong National Museum of Natural History, Pretoria; the Pretoria Bone Collection at the Department of Anatomy of the University of Pretoria; and the Evolutionary Studies Institute at the University of the Witwatersrand. For the realization at the ICTP Multidisciplinary Lab. of Trieste of scans of comparative human material stored at the National Museum "L. Pigorini" of Rome, we acknowledge F. Bernardini, L. Bondioli, C. Tuniz, and C. Zanolli; we also acknowledge M. Nakamura (Kyoto) and Y. Shintaku (Inuyama) for access to the *Pan* specimens used in this study. For their kind contribution during various analytical phases (including the intra- and inter-observer tests), we are especially grateful to A. Beaudet (Johannesburg) and C. Zanolli (Toulouse). For collaboration and discussion, we also thank L. Bam (Pelindaba), J. Braga (Toulouse & Johannesburg), L. Bruxelles (Toulouse and Johannesburg), R.J. Clarke (Johannesburg), J. Dumoncel (Toulouse), J. Heaton (Birmingham and Johannesburg), T. Jashashvili (Johannesburg), L. Kgasi (Pretoria), K. Kuman (Johannesburg), D. Marchi (Pisa), T. Pickering (Madison and Johannesburg), S. Potze (Pretoria), B. Zipfel (Johannesburg). The comments from two reviewers significantly enhanced the quality of the first version of this study. We acknowledge the DST-NRF for the financial support (Grant # UID23456) to establish the MIXRAD micro-focus X-ray tomography facility at Necsa. M.C. is funded by the European Commission (EACEA), Erasmus Mundus programme, AESOP and AESOP+ consortia coordinated by J. Braga (Toulouse).

References

Aglietti, P., Menchetti, P.P.M., 1995. Biomechanics of the patellofemoral joint. In: Scuderi, G.R. (Ed.), The patella. Springer, New York, pp. 25-48.

Aiello, L., Dean, C., 1990. An introduction to human evolutionary anatomy. Academic Press, New York.

Antón, S.C., 2013. *Homo erectus* and related taxa. In: Begun, D.R. (Ed.), A Companion to Paleoanthropology. Blackwell Publ., Chichester, pp. 497-516.

Antón, S.C., Potts, R., Aiello, L.C., 2014. Evolution of early *Homo*: An integrated biological perspective. Science 345, 45-58.

Alemseged, Z., Spoor, F., Kimbel, W.H., Bobe, R., Geraads, D., Reed, D., Wynn, J.G., 2006. A juvenile early hominin skeleton from Dikika, Ethiopia. Nature 443, 296-301.

Baldwin, J.L., House, C.K., 2005. Anatomic dimensions of the patella measured during total knee arthroplasty. J. Arthroplasty 20 250-257.

Balter, V., Blichert-Toft, J., Braga, J., Telouk, P., Thackeray, F., Albarède, F., 2008. U-Pb dating of fossil enamel from the Swartkrans Pleistocene hominid site, South Africa. Earth Planet. Sc. Lett. 267, 236-246.

Barak, M.M., Lieberman, D.E., Raichlen, D., Pontzer, H., Warrener, A.G., Hublin, J.-J., 2013. Trabecular evidence for a human-like gait in *Australopithecus africanus*. PLoS ONE 8, 1-9.

Bayle, P., Bondioli, L., Macchiarelli, R., Mazurier, A., Puymerail, L., Volpato, V., Zanolli, C., 2011. Three-dimensional imaging and quantitative characterization of human fossil remains. Examples from the NESPOS database. In: Macchiarelli, R., Weniger, G.-C. (Eds.), Pleistocene databases. Acquisition, storing, sharing. Wissenschaftliche Schriften des Neanderthal Museums 4, Mettmann, pp. 29-46.

Beauchesne, P., Agarwal, S.C., 2017. A multi-method assessment of bone maintenance and loss in an Imperial Roman population: Implications for future studies of age-related bone loss in the past. Am. J. Phys. Anthropol. 164, 41-61.

Beaudet, A., Bernardini, F., Cazenave, M., Mazurier, A., Radovčić, D., Radovčić, J., Tuniz C., Volpato V., Macchiarelli, R., 2013. The Neanderthal patella: Topographic bone distribution and inner structural organization. Proc. Europ. Soc. Study Hum. Evol. 2, 41.

Berger, L.R., de Ruiter, D.J., Churchill, S.E., Schmid, P., Carlson, K.J., Dirks, P.H.G.M., Kibii, J.M., 2010. *Australopithecus sediba*: A new species of *Homo*-like australopith from South Africa. Science 328, 195-204.

Berger, L.R., Hawks, J., de Ruiter, D.J., Churchill, S.E., Schmid, P., Delezene, L.K., Kivell, T.L., Garvin, H.M., Williams, S.A., DeSilva, J.M., Skinner, M.M., Musiba, C.M., Cameron, N., Holliday, T.W., Harcourt-Smith, W., Ackermann, R.R., Bastir, M., Bogin, B., Bolter, D., Brophy, J., Cofran, Z.D., Congdon, K.A., Deane, A.S., Dembo, M., Drapeau, M., Elliott, M.C., Feuerriegel, E.M., Garcia-Martinez, D., Green, D.J., Gurtov, Al, Irish, J.D., Kruger, A., Laird, M.F., Marchi, D., Meyer, M.R., Nalla, S., Negash, E.W., Orr, C.M., Radovcic, D., Schroeder, L., Scott, J.E., Throckmorton, Z., Tocheri, M.W., VanSickle, C., Walker, C.S., Wei, P., Zipfel, B., 2015. *Homo naledi*, a new species of the genus *Homo* from the Dinaledi Chamber, South Africa. eLife 4, 1-35.

Bleuze, M. M., 2010. Cross-sectional morphology and mechanical loading in Plio-Pleistocene hominins: Implications for locomotion and taxonomy. (PhD dissertation). The University of Western Ontario, Ontario.

Bookstein, F.L., 1991. Morphometric tools for landmark data: Geometry and biology. Cambridge University Press, Cambridge.

Braga, J., Fourvel, J.-B., Lans, B., Bruxelles, L., Thackeray, J.F., 2016. The Kromdraai hominins revised with an updated portrayal of differences between *Australopithecus africanus* and *Paranthropus robustus*. In: Braga, J., Thackeray, J.F. (Eds.), Kromdraai, a birthplace of *Paranthropus* in the Cradle of Humankind. Sun Press, Johannesburg, pp. 49-68.

Carlson, K.J., Marchi, D., 2014. Reconstructing mobility. Environmental, behavioral, and morphological determinants. Springer, New York.

Carretero, J.M., Lorenzo, C., Arsuaga, J.L., 1999. Axial and appendicular skeleton of *Homo antecessor*. J. Hum. Evol. 37, 459-499.

Carretero, J.M., Lorenzo, C., Arsuaga, J.L., 2001. Restes post-crâniens du niveau TD6 du site en grotte du Pleistocène inférieur de Gran Dolina, Sierra de Atapuerca, Espagne. L'Anthropol. 105, 179-202.

Cazenave, M., Beaudet, A., Braga, J., Oettlé, A., Thackeray, J.F., Hoffman, J., de Beer F., Macchiarelli, R., 2016. The inner structural organization of a (likely) *Paranthropus* patella from Swartkrans Member 2 (SKX 1084): Human- and nonhuman-like features. Am. J. Phys. Anthropol. 159, suppl. 62 111-112.

Cazenave, M., Braga, J., Oettlé, A., Thackeray, J.F., de Beer, F., Hoffman, J., Endalamaw, M., Redae, B.E., Puymerail, L., Macchiarelli, R., 2017. Inner structural organization of the distal humerus in *Paranthropus* and *Homo*. In: Macchiarelli, R., Zanolli, C. (Eds.), Hominin biomechanics, virtual anatomy and inner structural morphology: From head to toe. A tribute to Laurent Puymerail. C.R. Palevol 16, pp. 521-532.

Chirchir, H., Kivell, T.L., Ruff, C.B., Hublin, J.-J., Carlson, K.J., Zipfel, B., Richmond, B.G., 2015. Recent origin of low trabecular bone density in modern humans. Proc. Nat. Acad. Sc. USA. 112, 366-371.

Chirchir, H., Ruff, C.B., Junno, J.A., Potts, R., 2017. Low trabecular bone density in recent sedentary modern humans. Am. J. Phys. Anthropol. 162, 550-560.

Chirchir, H., Zeininger, A., Nakatsukasa, M., Ketcham, R.A., Richmond, B.G., 2016. Does trabecular bone structure within the metacarpal heads of primates vary with hand posture? In: Macchiarelli, R., Zanolli, C. (Eds.), Hominin biomechanics, virtual anatomy and inner

structural morphology: From head to toe. A tribute to Laurent Puymerail. C.R. Palevol 16, pp. 533-544.

Coleman, M.N., Colbert, M.W., 2007. Technical note: CT thresholding protocols for taking measurements on three-dimensional models. Am. J. Phys. Anthropol. 133, 723-725.

Dalstra, M., Huiskes, R., 1995. Load transfer across the pelvic bone. J. Biomech 28, 715-724.

Dayal, M.R., Bidmos, A.B., 2005. Discriminating sex in South African blacks using patella dimensions. J. Foren. Sc. 50, JFS2004306-4.

Dean, M.C., Wood, B.A., 2003. A digital radiographic atlas of great ape skull and dentition. In: Bondioli, L., Macchiarelli, R. (Eds.), Digital archives of human paleobiology. 3. Museo Nazionale "L. Pigorini", Rome.

Delson, E., 1988. Chronology of South African australopith site units. In: Grine, F.E. (Ed.), Evolutionary history of the "robust" australopithecines. Aldine de Gruyter, New York, pp. 317-324.

DeSilva, J.M., Devlin, M.J., 2012. A comparative study of the trabecular bony architecture of the talus in humans, non-human primates, and *Australopithecus*. J. Hum. Evol. 63, 536-551.

DeSilva, J.M., Holt, K.G., Churchill, S.E., Carlson, K.J., Walker, C.S., Zipfel, B., Berger, L.R., 2013. The lower limb and mechanics of walking in *Australopithecus sediba*. Science 340, 54-78.

Domínguez-Rodrigo, M., Pickering, T.R., Baquedano, E., Mabulla, A., Mark, D.F., Musiba, C., Pérez-González, A., 2013. First partial skeleton of a 1.34-million-year-old *Paranthropus boisei* from Bed II, Olduvai Gorge, Tanzania. PLoS ONE 8, e80347.

Dowdeswell, M.R., Jashashvili, T., Patel, B.A., Lebrun, R., Susman, R.L., Lordkipanidze, D., Carlson, K.J., 2016. Adaptation to bipedal gait and fifth metatarsal structural properties in *Australopithecus*, *Paranthropus*, and *Homo*. In: Macchiarelli, R., Zanolli, C. (Eds.), Hominin biomechanics, virtual anatomy and inner structural morphology: From head to toe. A tribute to Laurent Puymerail. C.R. Palevol 16, pp. 585-599.

Fajardo, R.J., Ryan, T.M., Kappelman, J., 2002. Assessing the accuracy of high-resolution X-ray computed tomography of primate trabecular bone by comparisons with histological sections. Am. J. Phys. Anthropol. 118, 1-10.

Frelat, M.A., Shaw, C.N., Sukhdeo, S., Hublin, J.-J., Benazzi, S., Ryan, T.M., 2017. Evolution of the hominin knee and ankle. J. Hum. Evol. 108, 147-160.

Gibbon, R.J., Pickering, T.R., Sutton, M.B., Heaton, J.L., Kuman, K., Clarke, R.J., Brain, C.K., Granger, D.E., 2014. Cosmogenic nuclide burial dating of hominin-bearing Pleistocene cave deposits at Swartkrans, South Africa. Quat. Geochron. 24, 10-15.

Goodfellow J., Hungerford D.S., Zindel M., 1976. Patello-femoral joint mechanics and pathology. J. Bone Joint Surg. 58, 287-90.

Gosman, J.H., Stout, S.D., Larsen, C.S., 2011. Skeletal biology over the life span: A view from the surfaces. Am. J. Phys. Anthropol. 146, 86-98.

Grine, F.E., Susman, R.L., 1991. Radius of *Paranthropus robustus* from Member 1, Swartkrans Formation, South Africa. Am. J. Phys. Anthropol. 84, 229-248.

Harrison, T., Kweka, A., 2011. Paleontological localities on the Eyasi Plateau, including Laetoli. In: Harrison, T. (Ed.), Paleontology and geology of Laetoli: Human evolution in context: volume 1: geology, geochronology, paleoecology and paleoenvironment. Springer, Dordrecht, pp. 17-45.

Herries, A.I.R., Curnoe, D., Adams, J.W., 2009. A multi-disciplinary seriation of early *Homo* and *Paranthropus* bearing palaeocaves in southern Africa. Quat. Int. 202, 14-28.

Huiskes, R., 2000. If bone is the answer, then what is the question? J. Anat. 197, 145-156.

Iranpour, F., Merican, A.M., Amis, A.A., Cobb, J.P., 2008. The width: Thickness ratio of the patella. Clin. Orthop. Related Res. 466, 1198-1203.

Jungers, W.L., 1988. New estimates of body size in australopithecines. In: Grine, F.E. (Ed.), The evolutionary history of the "robust" australopithecines. Aldine de Gruyter, New York, pp. 115-125.

Jungers, W.L., Larson, S.G., Harcourt-Smith, W., Morwood, M.J., Sutikna, T., Awe, R.D., Djubiantono, T., 2009. Descriptions of the lower limb skeleton of *Homo floresiensis*. J. Hum. Evol. 57, 538-554.

Katoh, T., Griffin, M.P., Wevers, H.W., Rudan, J., 1996. Bone hardness testing in the trabecular bone of the human patella. J. Arthroplasty 11, 460-468.

Kemkes-Grottenthaler, A., 2005. Sex determination by discriminant analysis: an evaluation of the reliability of patella measurements. For. Sc. Int. 147, 129-133.

Keyser, A., Menter, C.G., Moggi-Cecchi, J., Pickering, T.R., Berger, L.R., 2000. Drimolen: A new hominid-bearing site in Gauteng, South Africa. South Afr. J. Sc. 96, 193-197.

Kivell, T.L., 2016. A review of trabecular bone functional adaptation: What have we learned from trabecular analyses in extant hominoids and what can we apply to fossils? J. Anat. 228, 569-594.

L'Abbé, E.N., Loots, M., Meiring, J.H., 2005. The Pretoria bone collection: A modern South African skeletal sample. Homo 56, 197-205.

Lague, M.R., 2015. Taxonomic identification of Lower Pleistocene fossil hominins based on distal humeral diaphyseal cross-sectional shape. PeerJ 3, e1084.

Lieberman, D.E., Polk, J.D., Demes, B., 2004. Predicting long bone loading from cross-sectional geometry. Am. J. Phys. Anthropol. 123, 156-171.

Lordkipanidze, D., Jashashvili, T., Vekua, V., Ponce de Leon, M.S., Zollikofer, C.P.E., Rightmire, G.P., Pontzer, H., Ferring, R., Oms, O., Tappen, M., Bukhsianidze, M., Agusti, J., Kahlke, R., Kiladze, G., Martinez-Navarro, B., Mouskhelishvili, A., Nioradze, M., Rook, L., 2007. Postcranial evidence from early *Homo* from Dmanisi, Georgia. Nature 449, 305-310.

Lovejoy, C.O., 2007. The natural history of human gait and posture: Part 3. The knee. Gait & Post. 25, 325-341.

Macchiarelli, R., Bondioli, L., Galichon, V., Tobias, P.V., 1999. Hip bone trabecular architecture shows uniquely distinctive locomotor behaviour in South African australopithecines. J. Hum. Evol. 36, 211-232.

Macchiarelli, R., Rook, L., Bondioli, L., 2001. Comparative analysis of the iliac trabecular architecture in extant and fossil primates by means of digital image processing techniques: Implications for the reconstruction of fossil locomotor behaviours. In: de Bonis, L., Koufos, G., Andrews, P. (Eds.), Hominoid evolution and climatic change in Europe. Vol. 2. Phylogeny of the Neogene hominoid primates of Eurasia. Cambridge University Press, Cambridge, pp. 60-101.

Marchi, D., Walker, C.S., Wei, P., Holliday, T.W., Churchill, S.E., Berger, L.R., DeSilva, J.M., 2017. The thigh and leg of *Homo naledi*. J. Hum. Evol. 104, 174-204.

Mariani, P.P., Puddu, G., Ferretti, A., 1978. Jumper's knee. Ital. J. Orthopaed. Traumat. 4, 85-93.

Martín-Francés, L., Martinón-Torres, M., Gracia-Téllez, A., Bermúdez de Castro, J.M., 2016. Evidence of trauma in a ca. 1-million-year-old patella of *Homo antecessor*, Gran Dolina-Atapuerca (Spain). C.R. Palevol 15, 1011-1016.

Masouros, S.D., Bull, A.M.J., Amis, A.A., 2010. Biomechanics of the knee joint. Orthopaed. Trauma 24, 84-91.

Maureille, B., Gómez-Olivencia, A., Couture-Veschambre, C., Madelaine, S., Holliday, T., 2015. Nouveaux restes humains provenant du gisement de Regourdou (Montignac-sur-Vézère, Dordogne, France). Paléo 26, 117-138.

Mazurier, A., 2006. Relations entre comportement locomoteur et variation cortico-trabéculaire du plateau tibial chez les Primates: analyse quantitative noninvasive à haute réolution (SR-μCT) et applications au registre fossile. (PhD dissertation). Université de Poitiers, Poitiers.

Mazurier, A., Nakatsukasa, M., Macchiarelli, R., 2010. The inner structural variation of the primate tibial plateau characterized by high-resolution microtomography. Implications for the reconstruction of fossil locomotor behaviours. C.R. Palevol 9, 349-359.

Mazurier, A., Volpato, V., Macchiarelli, R., 2006. Improved noninvasive microstructural analysis of fossil tissues by means of SR-microtomography. Appl. Phys. A, Mat. Sc. Process. 83, 229-233.

McHenry, H.M., 1975. A new pelvic fragment from Swartkrans and the relationship between the robust and gracile australopithecines. Am. J. Phys. Anthropol. 43, 245-262.

McHenry, H.M., 1991. Petite bodies of the "robust" australopithecines. Am. J. Phys. Anthropol. 86, 445-454.

McHenry, H.M., Brown, C.C., McHenry, L.J., 2007. Fossil hominin ulnae and the forelimb of *Paranthropus*. Am. J. Phys. Anthropol. 134, 209-218.

Mitteroecker, P., Bookstein, F.L., 2011. Linear discrimination, ordination, and the visualization of selection gradients in modern morphometrics. Evol. Biol. 38, 100-114.

Mitteroecker, P., Gunz, P., Windhager, S., Schaefer, K., 2013. A brief review of shape, form, and allometry in geometric morphometrics, with applications to human facial morphology. Hystrix 24, 59-66.

Moggi-Cecchi, J., Menter, C., Boccone, S., Keyser, A., 2010. Early hominid dental remains from the Plio-Pleistocene site of Drimolen, South Africa. J. Hum. Evol. 58, 374-405.

Olateju, O.I., Philander, I., Bidmos, M.A., 2013. Morphometric analysis of the patella and patellar ligament of South Africans of European ancestry. South Afr. J. Sc. 109, 01-06.

Pearson, O.M., Lieberman, D.E., 2004. The aging of Wolff's law: Ontogeny and responses to mechanical loading in cortical bone. Yearb. Phys. Anthropol. 47, 63-99.

Pickering, T.R., Heaton, J.L., Clarke, R.J., Sutton, M.B., Brain, C.K., Kuman, K., 2012. New hominid fossils from Member 1 of the Swartkrans formation, South Africa. J. Hum. Evol 62, 618-628.

Pina, M., 2016. Unravelling the positional behaviour of fossil hominoids: Morphofunctional and structural analysis of the primate hindlimb. (PhD dissertation). Universidad Autònoma de Barcelona, Barcelona.

Pina, M., Almécija, S., Alba, D.M., O'Neill, M.C., Moyà-Solà, S., 2014. The middle Miocene ape *Pierolapithecus catalaunicus* exhibits extant great ape-like morphometric affinities on its patella: Inferences on knee function and evolution. PLoS One 9, e91944.

Pritchard, J.L., 1980. An osteometric analysis of the patella and femur in *Pan*, *Gorilla* and *Homo*. (PhD dissertation). School of The Ohio State University, Colombus.

Radovčić, J., Smith, F.H., Trinkaus, E., Wolpoff, M.H., 1988. The Krapina hominids. An illustrated catalog of skeletal collection. Croatian Natural History Museum, Zagreb.

Ramirez, K.R., Pontzer, H., 2015. Estimates of fossil hominin quadriceps physiological cross sectional area from patellar dimensions. Am. J. Phys. Anthropol. 156, 261.

Raux, P., Townsend, P.R., Miegel, R., Rose, R.M., Radin, E.L., 1975. Trabecular architecture of the human. J. Biomech. 8, l-7.

Ruff, C.B., Higgins, R., 2013. Femoral neck structure and function in early hominins. Am. J. Phys. Anthropol. 150, 512-525.

Ruff, C.B., Holt, B., Trinkaus, E., 2006. Who's afraid of the big bad Wolff?: Wolff's law and bone functional adaptation. Am. J. Phys. Anthropol. 129, 484-498.

Ruff, C.B., McHenry, H.M., Thackeray, J.F., 1999. Cross-sectional morphology of the SK 82 and 97 proximal femora. Am. J. Phys. Anthropol. 109, 509-521.

Ryan, T.M., Carlson, K.J., Gordon, A.D., Jablonski, N. Shaw, C.N., Stock, J.T., 2018. Human-like hip joint loading in *Australopithecus africanus* and *Paranthropus robustus*. J. Hum. Evol. (https://doi.org/10.1016/j.jhevol.2018.03.008).

Ryan, T.M., Ketcham, R., 2002a. The three-dimensional structure of trabecular bone in the femoral head of strepsirrhine primates. J. Hum. Evol. 43, 1-26.

Ryan, T.M., Ketcham, R., 2002b. Femoral head trabecular bone structure in two omomyid primates. J. Hum. Evol. 43, 241-263.

Ryan, T.M., Shaw, C.N., 2015. Gracility of the modern *Homo sapiens* skeleton is the result of decreased biomechanical loading. Proc. Nat. Acad. Sc. USA 112, 372-377.

Ryan, T.M., Walker, A., 2010. Trabecular bone structure in the humeral and femoral heads of anthropoid primates. Anat. Rec. 293, 719-729.

Schlager, S., 2017. Morpho: Calculations and visualizations related to geometric morphometrics. R package version 2.5.1.

Schneider, C.A., Rasband, W.S., Eliceiri, K.W., 2012. NIH Image to ImageJ: 25 years of image analysis. Nature Meth. 9, 671-675.

Schwartz, J.H., Tattersall, I., 2003. The human fossil record. Vol. 2. Craniodental morphology of genus *Homo* (Africa and Asia). Wiley-Liss, New York.

Shaw, C., Ryan, T., 2012. Does skeletal anatomy reflect adaptation to locomotor patterns? Cortical and trabecular architecture in human and nonhuman anthropoids. Am. J. Phys. Anthropol. 147, 187-200.

Skinner, M.M., Stephens, N.B., Tsegai, Z.J., Foote, A.C., Nguyen, N.H., Gross, T., Pahr, D.H., Hublin, J., Kivell, T.L., 2015. Human-like hand use in *Australopithecus africanus*. Science 347, 395-399.

Spoor, F., Zonneveld, F., Macho, G., 1993. Linear measurements of cortical bone and dental enamel by computed tomography: applications and problems. Am. J. Phys. Anthropol. 91, 469-484.

Standring, S., 2008. Gray's anatomy: The anatomical basis of clinical practice. Elsevier Health Sciences, UK.

Su, A., 2011. The functional morphology of subchondral and trabecular bone in the hominoid tibiotalar joint. (PhD dissertation). Stony Brook University, New York.

Su, A., Carlson, K.J., 2017. Comparative analysis of trabecular bone structure and orientation in South African hominin tali. J. Hum. Evol. 106, 1-18.

Su, A., Wallace, I.J., Nakatsukasa, M., 2013. Trabecular bone anisotropy and orientation in an Early Pleistocene hominin talus from East Turkana, Kenya. J. Hum. Evol. 64, 667-677.

Susman, R.L., 1988. New postcranial remains from Swartkrans and their bearing on the functional morphology and behavior of *Paranthropus robustus*. In: Grine, F.E. (Ed.), The evolutionary history of the ‘"robust" australopithecines. Aldine de Gruyter, New York, pp. 149-172.

Susman, R.L., 1989. New hominid fossils from the Swartkrans formation (1979-1986 excavations): Craniodental specimens. Am. J. Phys. Anthropol. 79, 451-474.

Susman, R.L., 2004. Swartkrans; a cave's chronicle of early man. Hominid postcranial remains from Swartkrans. Transv. Mus. Monogr. 8, Pretoria.

Susman, R.L., Brain, T.M., 1988. New first metatarsal (SKX 5017) from Swartkrans and the gait of *Paranthropus robustus*. Am. J. Phys. Anthropol. 77, 7-15.

Susman, R.L., de Ruiter, D.J., 2004. New hominin first metatarsal (SK 1813) from Swartkrans. J. Hum. Evol. 47, 171-181.

Susman, R.L., de Ruiter, D., Brain, C.K., 2001. Recently identified postcranial remains of *Paranthropus* and early *Homo* from Swartkrans Cave, South Africa. J. Hum. Evol. 41, 607-629.

Sylvester, A., 2013. A geometric morphometric analysis of the medial tibial condyle of African hominids. Anat. Rec. 296, 1518-1525.

Sylvester, A.D., Mahfouz, M.R., Kramer, P.A., 2011. The effective mechanical advantage of AL 129-1a for knee extension. Anat. Rec. 294, 1486-1499.

Tardieu, C., 1999. Ontogeny and phylogeny of femoro-tibial characters in humans and hominid fossils: Functional influence and genetic determinism. Am. J. Phys. Anthropol. 110, 365-377.

Taylor, W.R., Heller, M.O., Bergmann, G., Duda, G.N., 2004. Tibio-femoral loading during human gait and stair climbing. J. Orthop. Res. 22, 625-632.

Toumi, H., Higashiyama, I., Suzuki, D., Kumai, T., Bydder, G., McGonagle, D.D., Emery, P., Fairclough, J., Benjamin, M., 2006. Regional variations in human patellar trabecular architecture and the structure of the proximal patellar tendon enthesis. J. Anat. 208, 47-57.

Toumi, H., Larguech, G., Filaire, E., Pinti, A., Lespessailles, E., 2012. Regional variations in human patellar trabecular architecture and the structure of the quadriceps enthesis: A cadaveric study. J. Anat. 220, 632-637.

Touraine, S., Bouhadoun, H., Engelke, K., Laredo, J.D., Chappard, C., 2017. Influence of meniscus on cartilage and subchondral bone features of knees from older individuals: A cadaver study. PLoS ONE 12, e0181956.

Townsend, P.R., Raux, P., Rose, R.M., Miegel, R.E., Radin, E.L., 1975. The distribution and anisotropy of the stiffness of cancellous bone in the human patella. J. Biomech. 8, 363-367.

Townsend, P.R., Rose, R.M., Radin, E.L., Raux, P., 1977. The biomechanics of the human patella and its implications for chondromalacia. J. Biomech. 10, 403-407.

Trinkaus, E., 1983. The Shanidar Neandertals. Academic Press, New York.

Tuniz, C., Bernardini, F., Cicuttin, A., Crespo, M.L., Dreossi, D., Gianoncelli, A., Mancini, L., Mendoza Cuevas, A., Sodini, N., Tromba, G., Zanini, F.,, Zanolli., C., 2013. The ICTP-Elettra X-ray laboratory for cultural heritage and archaeology. Nucl. Instr. Meth. Phys. Res. A: Acceler., Spectrom., Detect. Ass. Equipm. 711, 106-110.

Vandermeersch, B., 1981. Les hommes fossiles de Qafzeh (Israel). CNRS, Paris.

Volpato, V., 2007. Morphogenèse des propriétés texturales du tissu osseux et environnement biomécanique. Caractérisation non invasive du réseau trabéculaire et de l'os cortical du squelette appendiculaire de mammifères actuels et fossiles, hominidés inclus. (PhD dissertation). Université de Poitiers, Poitiers.

Vrba, E.S., 1975. Some evidence of chronology and palaeoecology of Sterkfontein, Swartkrans and Kromdraai from the fossil Bovidae. Nature 254, 301-304.

Wallace, I.J., Tommasini, S.M., Judex, S., Garland, T. Jr., Demes, B., 2012. Genetic variations and physical activity as determinants of limb bone morphology: An experimental approach using a mouse model. Am. J. Phys. Anthropol. 148, 24-35.

Ward, C.V., Ruff, C.B., Walker, A., Teaford, M.F., Rose, M.D., Nengo, I.O., 1995. Functional morphology of *Proconsul* patellas from Rusinga Island, Kenya, with implications for other Miocene-Pliocene catarrhines. J. Hum. Evol. 29, 1-19.

Yoo, J.H., Yi, S.R., Kim, J.H., 2007. The geometry of patella and patellar tendon measured on knee MRI. Surg. Rad. Anat. 29, 623-266.

Zeininger, A., Patel, B.A., Zipfel, B., Carlson, K.J., 2016. Trabecular architecture in the StW 352 fossil hominin calcaneus. J. Hum. Evol. 97, 145-158.

Zeininger, A., Richmond, B.G., Hartman, G., 2011. Metacarpal head biomechanics: A comparative backscattered electron image analysis of trabecular bone mineral density in *Pan troglodytes*, *Pongo pygmaeus,* and *Homo sapiens*. J. Hum. Evol. 60, 703-710.

Zipfel, B., Berger, L.R., 2009. Partial hominin tibia (StW 396) from Sterkfontein, South Africa. Palaeont. Afr. 44, 71-75.

Tables

Table 1
Maximum thickness of the cortico-trabecular complex (in mm) standardized by the medio-lateral breadth of the patella (% values) measured from the articular surface in correspondence of the central (aCTT) and medial (bCTT) volumes of interest (see Fig. 2) in SKX 1084, recent humans (n = 12), a Neanderthal (Regourdou 1), and *Pan* (n = 2); s.d., standard deviation.
Tableau 1
Epaisseur maximale du complexe cortico-trabéculaire (en mm) standardisée par la largeur médio-latérale de la patella (%) mesurée à partir de la surface articulaire en correspondance avec les volumes d'intérêt central (aCTT) et médial (bCTT) (voir Fig. 2) pour SKX 1084, les humains récents (n = 12), un Néandertalien (Regourdou 1) et *Pan* (n = 2); s.d., déviation standard.

specimens/samples	aCTT (%)	bCTT (%)
SKX 1084	9.6	7.2
recent humans	8.7	7.1
(s.d.)	(1.4)	(1.7)
Neanderthal	8.0	4.6
Pan	12.4-12.7	9.3-10.8

Table 2
Bone volume fraction (BV/TV, in %), trabecular thickness (Tb.Th., in mm), and degree of anisotropy (DA) of the central (aVOI) and medial (bVOI) volumes of interest of the patella (see Fig. 2) assessed in SKX 1084, recent humans (n = 12), a Neanderthal (Regourdou 1), and *Pan* (n = 2); s.d., standard deviation.
Tableau 2
Volume osseux (BV/TV, en %), épaisseur trabéculaire (Tb.Th., en mm) et degré d'anisotropie (DA) des volumes d'intérêt central (aVOI) et médial (bVOI) de la patella (voir Fig. 2) mesurée pour SKX 1084, les humains récents (n=12), un Néandertalien (Regourdou 1) et *Pan* (n = 2); s.d., déviation standard.

specimens/ samples	aVOI			bVOI		
	BV/TV (%)	Tb.Th. (mm)	DA	BV/TV (%)	Tb.Th. (mm)	DA
SKX 1084	40.4	0.20	3.83	38.6	0.19	2.73
recent humans	30.5	0.15	3.87	26.5	0.14	4.92
(s.d.)	(6.5)	(0.03)	(1.46)	(5.7)	(0.03)	(1.52)
Neanderthal	34.5	0.15	4.44	30.3	0.13	5.81
Pan	65.1-79.1	0.23-0.27	2.73-2.87	67.8-81.2	0.23-0.24	1.88-1.94

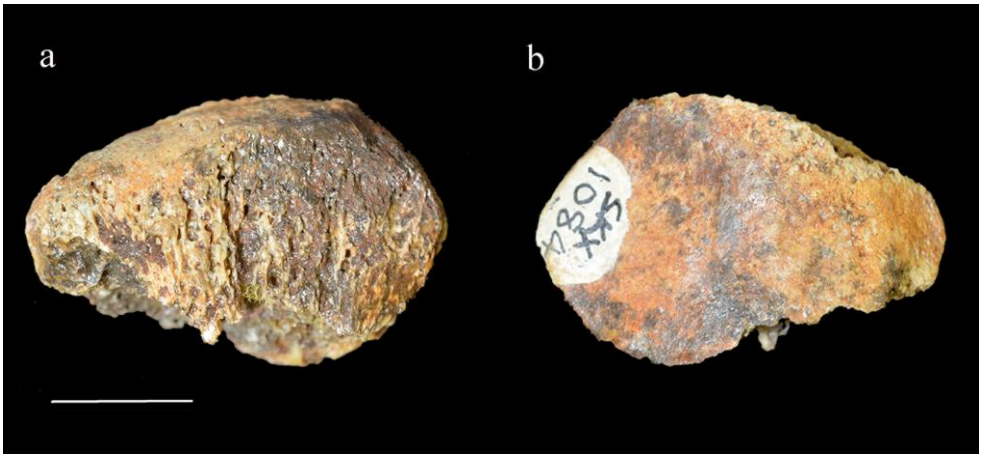

Fig. 1. The left patella SKX 1084 from Swartkrans, South Africa, in anterior (a) and posterior (b) views. Scale bar, 10 mm.
Fig. 1. La patelle gauche SKX 1084 de Swartkrans, en Afrique du Sud, en vues antérieure (a) et postérieure (b). Barre d'échelle, 10 mm.

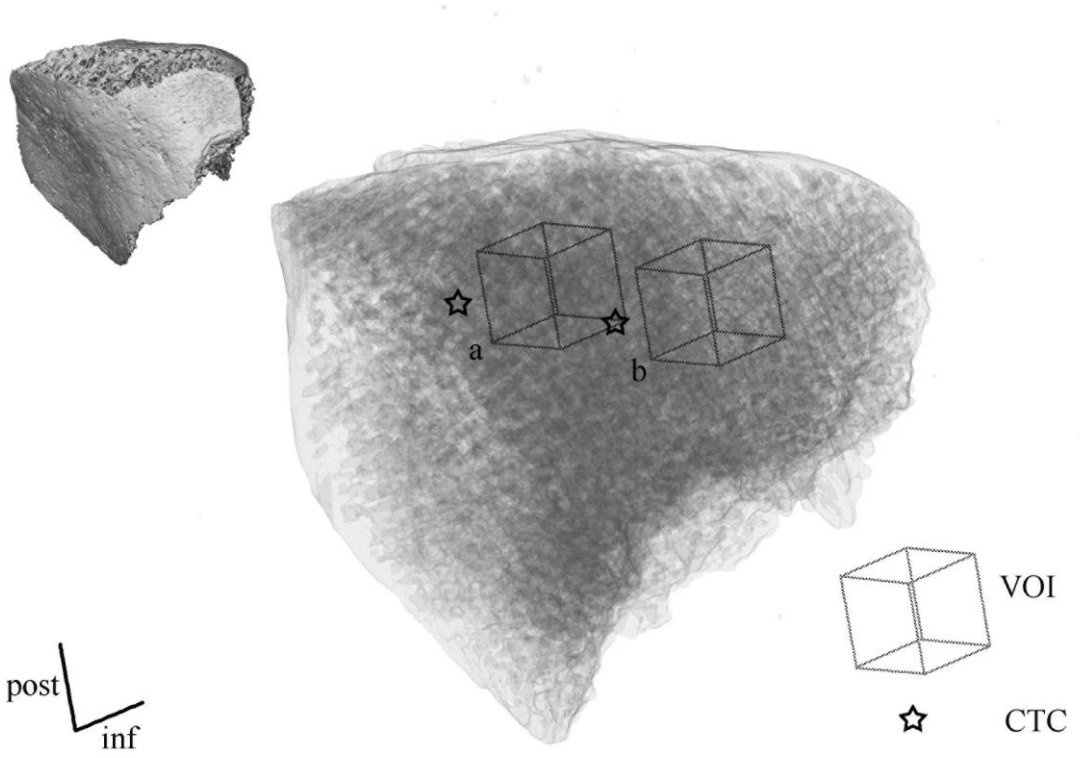

Fig. 2. 3D tomographic oblique posterior view of SKX 1084 in semi-transparency showing the position of the central (a) and medial (b) cubic volumes of interest (VOI) extracted for assessing cancellous bone properties and the two topographically related slices (aCTC and bCTC) sampling the cortico-trabecular complex of the articular surface. The virtual reconstruction of the outer surface of the specimen (not to scale) is only provided for orientation.
Fig. 2. Rendu 3D virtuel en vue postérieure oblique de SKX 1084 montrant par semi-transparence la position des volumes cubiques d'intérêt (VOI) central (a) et médial (b) extraits pour analyser les propriétés de l'os trabéculaire et les deux coupes topographiquement liées (aCTT et bCTT) échantillonnant le complexe cortico-trabéculaire de la surface articulaire. La

reconstruction virtuelle de la surface externe du spécimen (pas à l'échelle) est simplement donnée pour orientation.

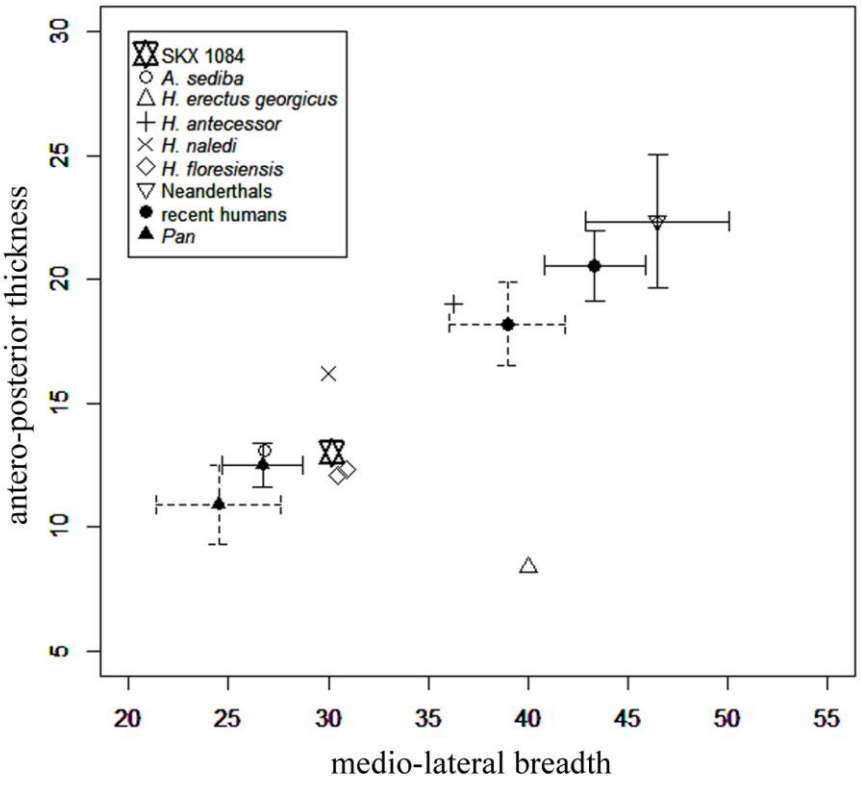

Fig. 3. Medio-lateral breadth and antero-posterior thickness of SKX 1084 compared to those of: *Australopithecus sediba* (DeSilva et al., 2013), *Homo erectus georgicus* (Lordkipanidze et al. 2007; T. Jashawili, pers. comm.), *H. antecessor* (Carretero et al., 2001), *H. naledi* (Berger et al., 2015; Marchi et al., 2017), *H. floresiensis* (Jungers et al., 2009), Neanderthals (n = 12; pooled specimens from Krapina: Radovčić et al., 1988 and original data; Regourdou 1, Tabun 1, La Ferassie 2, La Chapelle aux Saints, Spy II: Vandermeersch, 1981 and original data; Shanidar: Trinkaus, 1983), recent humans (n = 60 males and 60 females; Dayal and Bidmos, 2005), *Pan* (n = 14 males and 20 females; Pritchard, 1980). For the Neanderthal, recent human and *Pan* samples, the average value ± 1 s.d. is shown; in the human and *Pan* samples, the dashed lines correspond to the female, that continuous to the male estimates.

Fig. 3. Largeur médio-latérale et épaisseur antéro-postérieure de SKX 1084 par rapport à celles de: *Australopithecus sediba* (DeSilva et al., 2013), *Homo erectus georgicus* (Lordkipanidze et al. 2007; T. Jashawili, comm. pers.), *H. antecessor* (Carretero et al., 2001), *H. naledi* (Berger et al., 2015; Marchi et al., 2017), *H. floresiensis* (Jungers et al., 2009), Néandertaliens (n = 12; spécimens de Krapina: Radovčić et al., 1988 et données originales; Regourdou 1, Tabun 1, La Ferassie 2, La Chapelle, Spy II: Vandermeersch, 1981 et données originales; Shanidar: Trinkaus, 1983), humains récents (n = 60 hommes and 60 femmes; Dayal and Bidmos, 2005), *Pan* (n = 14 mâles and 20 femelles; Pritchard, 1980). Pour les échantillons des Néandertaliens, des humains récents et des chimpanzés, la valeur moyenne ± 1 d.s. est donnée. Pour les humains et les chimpanzés, la ligne en pointillés correspond aux estimations des femelles et celle en continue aux estimations des mâles.

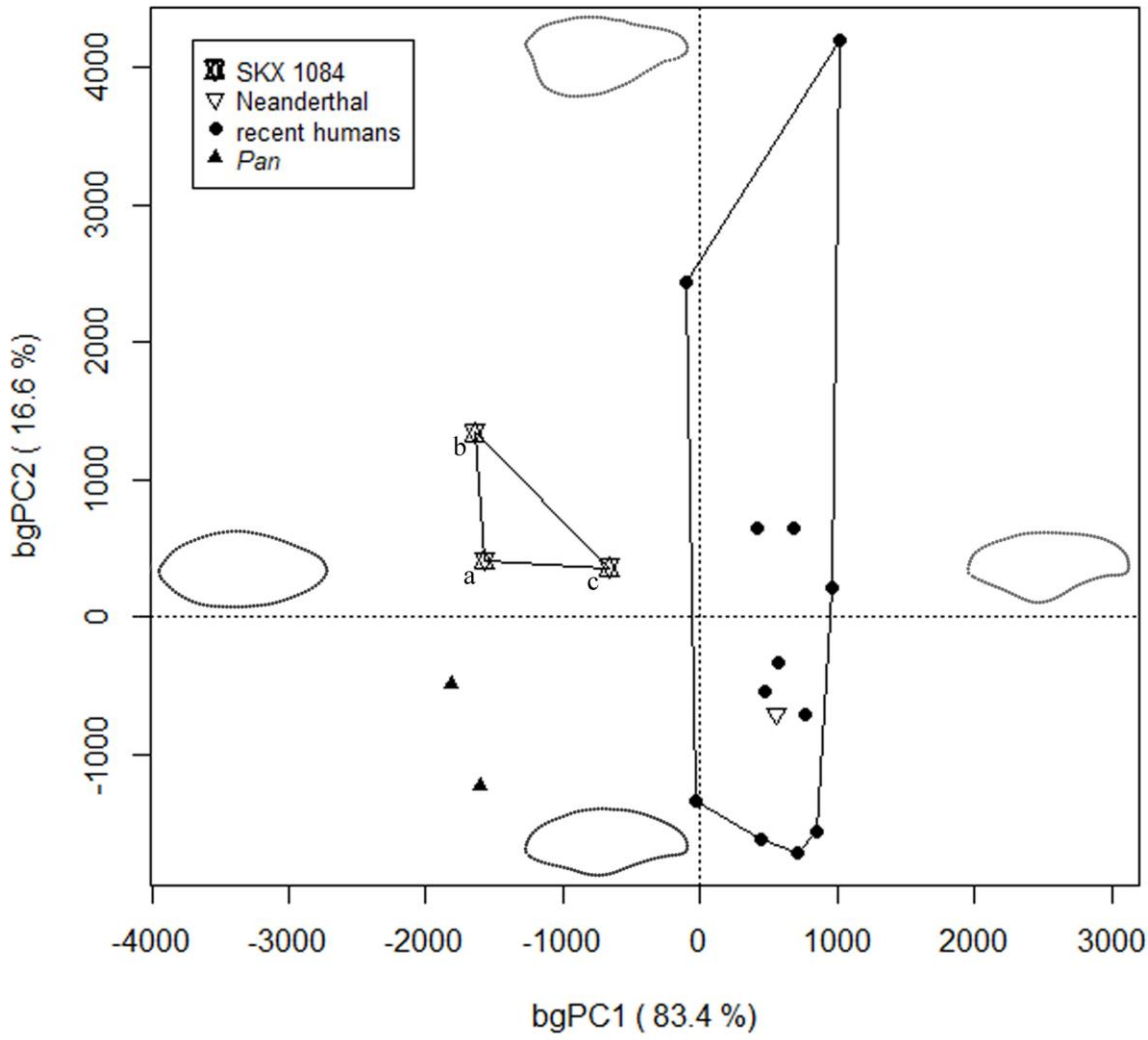

Fig. 4. Between-group principal component analysis (bgPCA) of the Procrustes shape coordinates of the three reconstructions of the outer outline of the transverse section across the maximum medio-lateral breadth of SKX 1084 (a, b, c), a Neanderthal (Regourdou 1), recent humans (n = 12), and *Pan* (n = 2).

Fig. 4. Analyse en composantes principales intergroupe réalisée à partir des coordonnées Procrustes de trois reconstructions du contour externe de la section transversale extraite au niveau de la largeur médio-latérale maximale de SKX 1084 (a, b, c) comparées à un Néandertalien (Regourdou 1), des humains récents (n = 12) et *Pan* (n = 2).

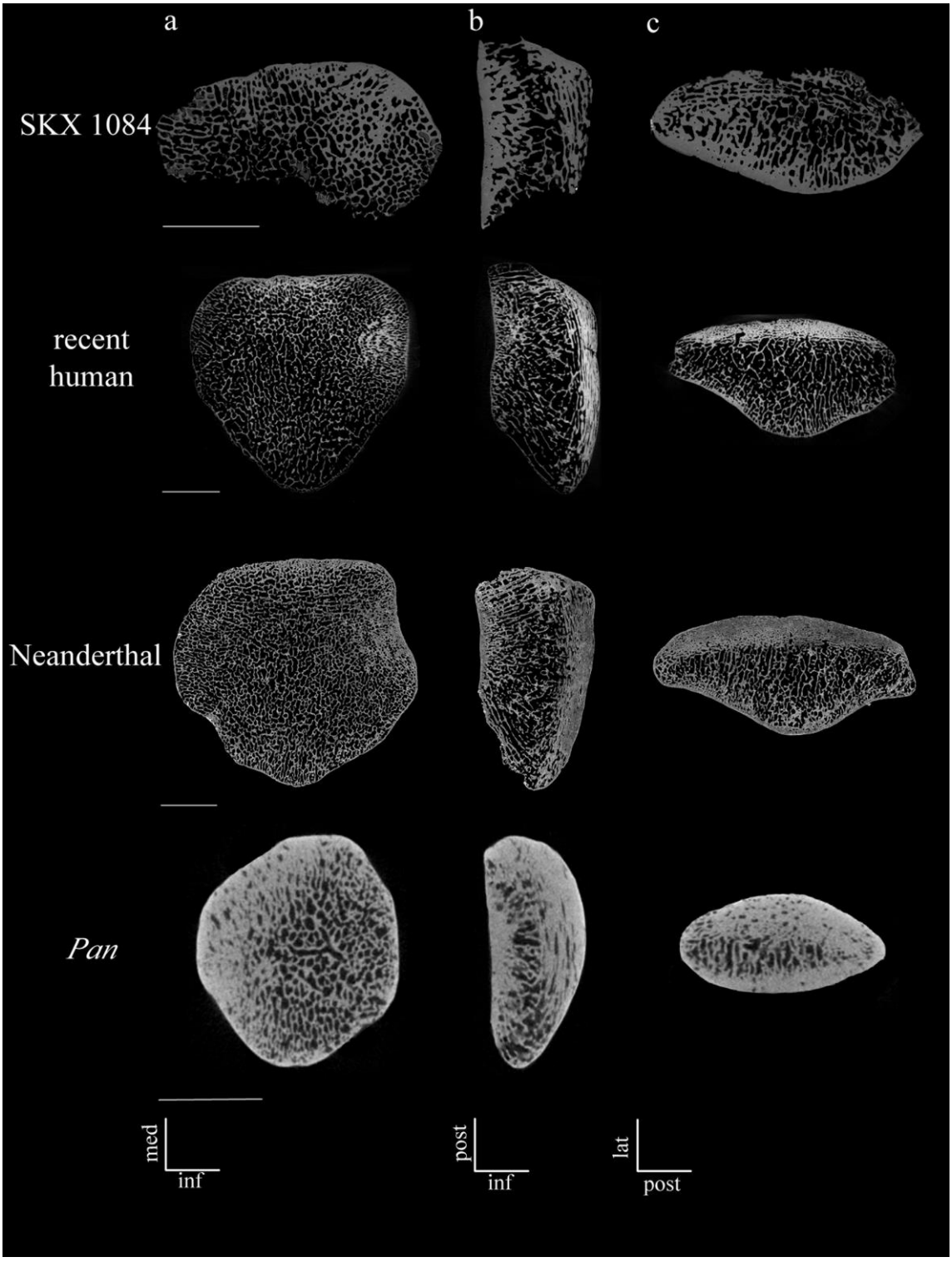

Fig. 5. Coronal (a), parasagittal (b) and transversal (c) virtual sections from 3D tomographic view approximately across the centre of the patella in SKX 1084, a recent human (male, 26 years old), a Neanderthal (Regourdou 1), and a female chimpanzee (M09). Scale bars, 10 mm.
Fig. 5. Sections virtuelles coronale (a), parasagittale (b) et transversale (c) extraites à partir de vues tomographiques 3D approximativement au centre de la patelle SKX 1084, d'un humain récent (homme, 26 ans), d'un Néandertalien (Regourdou 1) et d'une femelle chimpanzé (M09). Barre d'échelle, 10 mm.

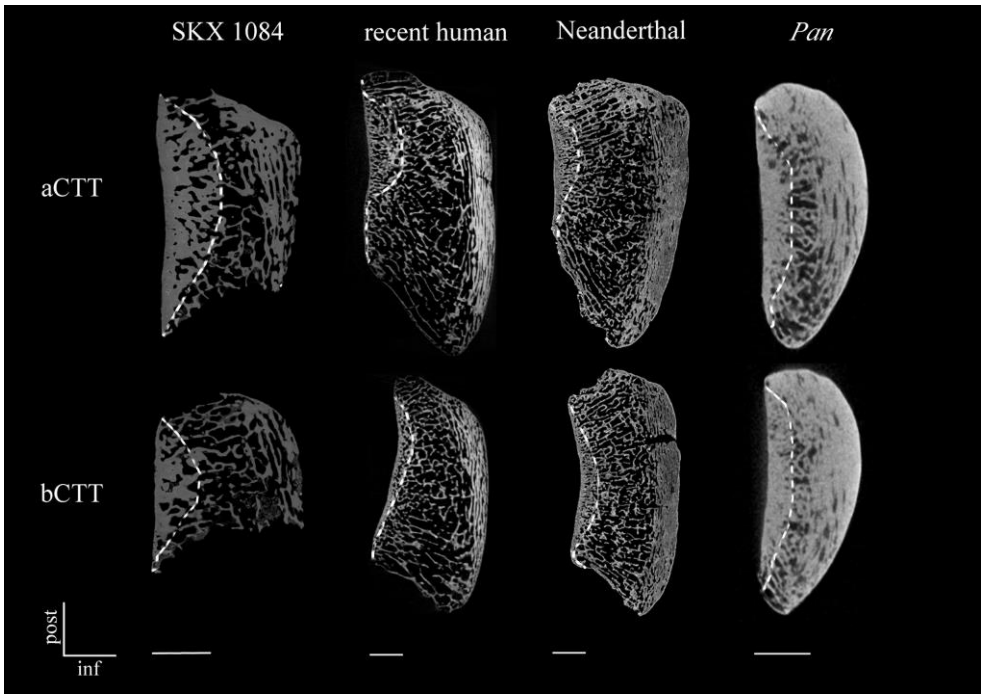

Fig. 6. Transversal sections across the central (aVOI) and medial (bVOI) 3D tomographic volumes of interest of the patella (see Fig. 2) in SKX 1084, a recent human (male, 26 years old), a Neanderthal (Regourdou 1), and a female chimpanzee (M09); in each section, the dashed line delimits the cortico-trabecular complex measured for its maximum thickness (aCTT and bCTT, respectively) from the articular surface. Scale bars, 5 mm.

Fig. 6. Sections transversales extraites au centre des volumes d'intérêts central (aVOI) et médial (bVOI) de la patelle (voir Fig. 2) de SKX 1084, d'un humain récent (homme, 26 ans), d'un Néandertalien (Regourdou 1) et d'une femelle chimpanzé (M09). Pour chaque section la ligne en pointillés délimite le complexe cortico-trabéculaire mesuré pour son épaisseur maximale (respectivement, aCTT et bCTT) au niveau de la surface articulaire. Barre d'échelle, 5 mm.

Supporting information

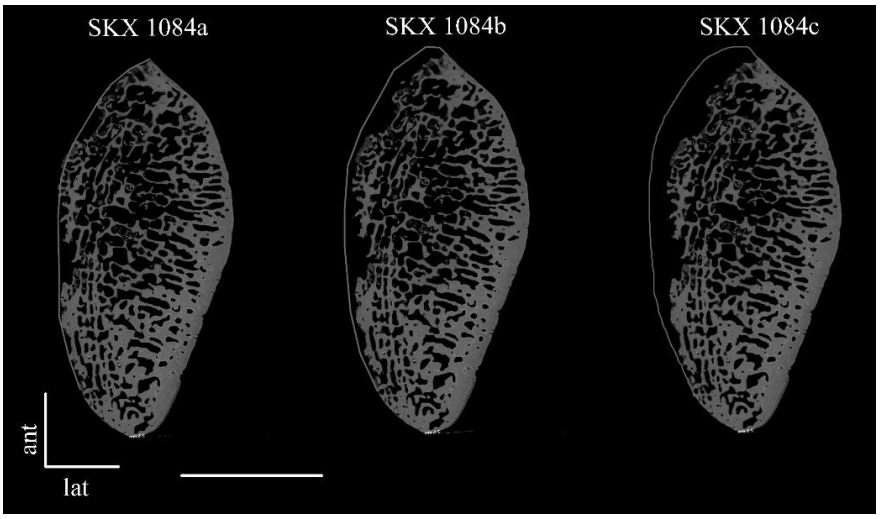

Fig. S1. Three reconstructions (a, b, c) of the anterior portion of the outer contour of the transverse section of SKX 1084 virtually taken across its maximum medio-lateral breadth displaying an increasing degree of anterior convexity. The three outlines, generated by two independent observers (M.C. and C. Zanolli) for integrating the local anterior bony discontinuities, were used in the GM-based comparative analysis shown in Fig. 4 (main text). Scale bar, 10 mm.

Fig. S1. Trois reconstructions (a, b, c) du contour externe de la portion antérieure de la section transversale de SKX 1084 virtuellement extraite au niveau de la largeur médio-latérale maximale présentant une augmentation du degré de convexité antérieure. Les trois reconstructions, générées par deux observateurs indépendants (M.C. et C. Zanolli) intégrant les discontinuités locales de l'os au niveau antérieur, ont été utilisées pour l'étude morphométrie géométrique comparative présentée en Fig. 4 (texte principal). Barre d'échelle, 10 mm.

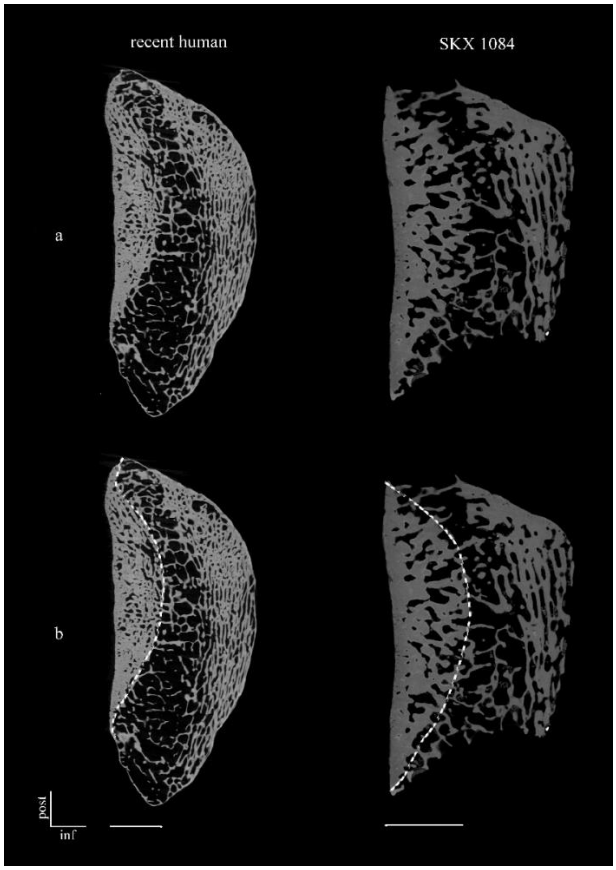

Fig. S2. Transversal virtual sections of a recent human patella (female, 24 years old) and of SKX 1084 (a) showing the difficulties of accurately assessing the limits of the cortico-trabecular complex (left to the dashed line, in b), i.e., of the portion consisting of the lamina and the adjoining plate-like structures forming the supporting trabecular network (cf. Mazurier et al., 2010). Scale bars, 5 mm.

Fig. S2. Sections transversales virtuelles d'une patella d'un humain récent (femme, 24 ans) et de SKX 1084 (a) présentant les difficultés dans la définition des limites du complexe cortico-trabéculaire (à gauche de la ligne en pointillés, en b), i.e., de la partie constituée de la fine couche d'os cortical et des structures en forme de plaques attenantes constituant le réseau trabéculaire immédiatement sous-jacent (cf. Mazurier et al., 2010). Barre d'échelle, 5 mm.

Table S1

Medio-lateral breadth and antero-posterior thickness of SKX 1084 compared to those of: *Australopithecus sediba* (DeSilva et al., 2013), *Homo erectus georgicus* (Lordkipanidze et al. 2007; T. Jashawili, pers. comm.), *H. antecessor* (Carretero et al., 2001), *H. naledi* (Berger et al., 2015; Marchi et al., 2017), *H. floresiensis* (Jungers et al., 2009), Neanderthals (n = 12; pooled specimens from Krapina: Radovčić et al., 1988 and original data; Regourdou 1, Tabun 1, La Ferassie 2, La Chapelle aux Saints, Spy II: Vandermeersch, 1981 and original data; Shanidar: Trinkaus, 1983), recent humans (n = 60 males and 60 females; Dayal and Bidmos, 2005), *Pan* (n = 14 males and 20 females; Pritchard, 1980); s.d., standard deviation.

Tableau S1

Largeur médio-latérale et épaisseur antéro-postérieure de SKX 1084 par rapport à celles de: *Australopithecus sediba* (DeSilva et al., 2013), *Homo erectus georgicus* (Lordkipanidze et al. 2007; T. Jashawili, comm. pers.), *H. antecessor* (Carretero et al., 2001), *H. naledi* (Berger et al., 2015; Marchi et al., 2017), *H. floresiensis* (Jungers et al., 2009), Néandertaliens (n = 12; spécimens de Krapina: Radovčić et al., 1988 et données originales; Regourdou 1, Tabun 1, La

Ferassie 2, La Chapelle, Spy II: Vandermeersch, 1981 et données originales; Shanidar: Trinkaus, 1983), humains récents (n = 60 hommes and 60 femmes; Dayal and Bidmos, 2005), *Pan* (n = 14 mâles and 20 femelles; Pritchard, 1980); s.d., déviation standard.

specimens/samples	medio-lateral breadth (mm)	antero-posterior thickness (mm)	sources
SKX 1084	30.2	13.0	Susman, 1989 and original data
Australopithecus sediba U.W. 88-79+U.W.88-100	26.8	13.1	DeSilva et al., 2013
Homo erectus georgicus D3418	40.0	8.4	Lordkipanidze et al. 2007; T. Jashawili, pers. comm.
H. antecessor			
ATD6-22	36.3	19.0	Carretero et al., 2001
ATD6-56	36.1	19.4	Carretero et al., 2001
H. naledi U.W. 101-1404	30.0	16.2	Berger et al., 2015; Marchi et al., 2017
H. floresiensis			
B 10	30.5	12.1	Jungers et al., 2009
LB 11	30.9	12.3	Jungers et al., 2009
Neanderthals	46.0	21.6	
(s.d.)	(4.5)	(3.0)	
Krapina (n = 4)	50.1	25.1	Radovčić et al., 1988 and original data
Regourdou 1	44.7	21.0	Vandermeersch, 1981 and original data
Tabun 1	39	17	Vandermeersch, 1981
La Ferassie 2	42	19	Vandermeersch, 1981
La Chapelle	46	21	Vandermeersch, 1981
Spy II	51.5	23.0	Vandermeersch, 1981
Shanidar (n = 3)	48.5	25.0	Trinkaus, 1983
recent human males (n = 60)	43.3	20.6	Dayal and Bidmos, 2005
(s.d.)	(2.5)	(1.4)	
recent human females (n = 60)	39.0	18.2	Dayal and Bidmos, 2005
(s.d.)	(2.9)	(1.7)	
Pan males (n = 14)	26.7	12.5	Pritchard, 1980
(s.d.)	(2.0)	(0.9)	
Pan females (n = 20)	24.5	10.9	Pritchard, 1980
(s.d.)	(3.1)	(1.6)	

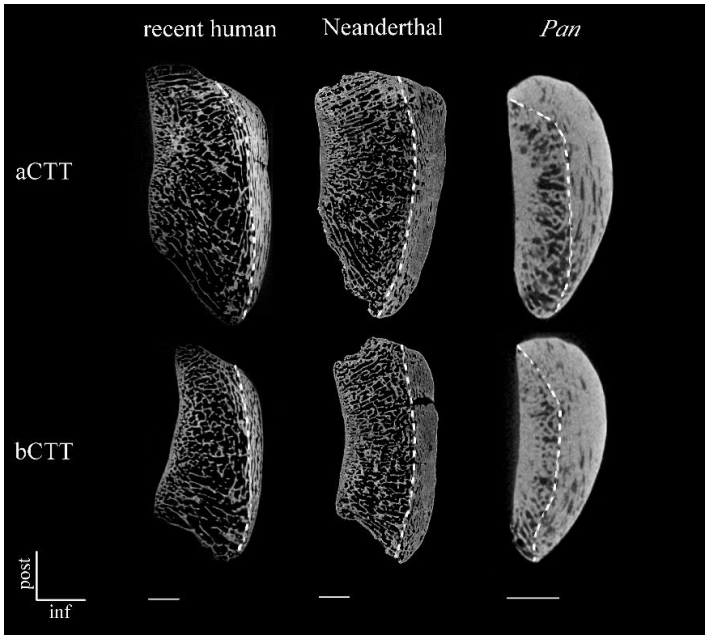

Fig. S3. Transversal virtual sections across the central (aVOI) and medial (bVOI) 3D tomographic volumes of interest of the patella (see Fig. 2) in a recent human (male, 26 years old), a Neanderthal (Regourdou 1), and a female chimpanzee (M09); in each section, the dashed line delimits the cortico-trabecular complex measured for its maximum thickness (aCTT and bCTT, respectively) from the anterior surface. Note that this measure is not available in SKX 1084. Scale bars, 5 mm.

Fig. S3. Sections transversales virtuelles extraites au centre des volumes d'intérêts central (aVOI) et médial (bVOI) de la patelle (voir Fig. 2) d'un humain récent (homme, 26 ans), d'un Néandertalien (Regourdou 1) et d'une femelle chimpanzé (M09). Pour chaque section la ligne en pointillés délimite le complexe cortico-trabéculaire mesuré pour son épaisseur maximale (respectivement, aCTT et bCTT) au niveau de la surface antérieure. Noter que cette mesure n'est pas disponible pour SKX 1084. Barre d'échelle, 5 mm.

Table S2

Maximum thickness of the cortico-trabecular complex standardized by the medio-lateral breadth of the patella (% values) measured from the anterior surface in correspondence of the central (aCTT) and medial (bCTT) volumes of interest (see Fig. 2) in recent humans (n = 12), a Neanderthal (Regourdou 1), and *Pan* (n = 2); s.d., standard deviation. Note that this measure is not available in SKX 1084.

Tableau S2

Epaisseur maximale du complexe cortico-trabéculaire standardisée par la largeur médio-latérale de la patella (%) mesurée à partir de la surface antérieure en correspondance avec les volumes d'intérêt central (aCTT) et médial (bCTT) (voir Fig. 2) pour les humains récents (n = 12), un Néandertalien (Regourdou 1) et *Pan* (n = 2); s.d., déviation standard. Noter que cette mesure n'est pas disponible pour SKX 1084.

specimens/samples	aCTT (%)	bCTT (%)
recent humans	8.9	7.3
(s.d.)	(3.1)	(1.6)
Neanderthal	14.7	8.3
Pan	19.8-19.9	14.6-21.8

3.3.2. Extended information

3.3.2.1. The extant human sample

Table 3.3.2.1.A. Composition of the recent human sample of patellae detailed using high resolution µXCT scanning.

specimens	sex	age (years)
RH 1	F	40-50
RH 2	M	40-50
RH 3	F	50
RH 4	F	40-50
RH 5	M	30-40
RH 6	F	40-50
RH 7	M	27
RH 8	M	27
RH 9	M	29
RH 10	F	24
RH 11	F	26
RH 12	M	28

Table 3.3.2.1.B. Individual data and descriptive statistics of the maximum thickness of the cortico-trabecular complex (in mm) standardised by the medio-lateral breadth of the patella (% values) measured from the articular surface in correspondence to the central (aCTT) and medial (bCTT) volumes of interest in a comparative sample of 12 recent Humans; s.d., standard deviation; min., minimum value; max., maximum value.

specimens	aCTT (%)	bCTT (%)
RH 1	10.9	6.2
RH 2	8.6	5.9
RH 3	6.3	5.7
RH 4	7.1	8.7
RH 5	10.5	6.5
RH 6	8.2	4.7
RH 7	9.0	9.5
RH 8	9.1	-
RH 9	8.1	9.5
RH 10	10.7	6.1
RH 11	8.6	7.2

RH 12	7.8	8.4
mean	8.7	7.1
s.d.	1.4	1.7
min.	6.3	4.7
max.	10.9	9.5

Table 3.3.2.1.C. Individual data and descriptive statistics of the bone volume fraction (BV/TV, in %), trabecular thickness (Tb.Th., in mm), and degree of anisotropy (DA) of the central (aVOI) and medial (bVOI) volumes of interest of the patella assessed in a comparative sample of 12 recent Humans, but excluding the outliers indicated in italics; s.d., standard deviation; min., minimum value; max., maximum value.

specimens	**aVOI**			**bVOI**		
	BV/TV (%)	**Tb.Th. (mm)**	**DA**	**BV/TV (%)**	**Tb.Th. (mm)**	**DA**
RH 1	29.0	0.14	3.05	27.6	0.12	6.43
RH 2	15.0	0.10	4.82	21.1	0.12	3.06
RH 3	28.7	0.16	6.11	27.1	0.17	7.19
RH 4	39.8	0.15	4.13	19.4	0.10	2.40
RH 5	32.0	0.15	5.44	31.0	0.14	6.00
RH 6	27.3	0.15	1.57	13.8	0.12	5.88
RH 7	33.2	0.17	2.22	27.1	0.14	5.29
RH 8	38.2	0.14	4.42	33.3	0.15	5.17
RH 9	32.5	0.19	4.87	27.6	0.16	5.48
RH 10	29.1	0.19	1.85	31.5	0.20	2.87
RH 11	30.7	0.14	4.70	29.4	0.14	5.44
RH 12	*46.8*	*0.25*	3.25	29.4	0.16	3.81
mean	30.5	0.15	3.87	26.5	0.14	4.92
s.d.	6.5	0.03	1.46	5.7	0.03	1.52
min.	15.0	0.10	1.57	13.8	0.10	2.40
max.	39.8	0.19	6.11	33.3	0.20	7.19

Table 3.3.2.1.D. Descriptive statistics of the cortico-trabecular complex standardised by the medio-lateral breadth of the patella (% values) and bone density (BV/TV in %) measured from the anterior surface in correspondence to the central (aCTT) volumes of interest in recent Humans (n = 12), a Neanderthal representative (Regourdou 1), *Pan* (n = 2) and *Papio* (n = 6); s.d., standard deviation. Note that this specific measurement is not available for SKX 1084.

specimens/samples	**aCTT (%)**	**BV/TV (%)**
recent Humans	8.9	78.3
(s.d.)	(3.1)	(8.7)
Neanderthal	14.7	89.9

Pan	19.8-19.9	95.7-96.2
Papio	18.8 (2.1)	94.3 (4.5)

3.3.2.2. Cancellous organisation of the Neanderthal patellae from Krapina, Croatia

In a complementary comparative study of the cancellous organisation of the patella not included in the paper under review in the *Journal of Human Evolution*, the same 2-3D techniques of virtual imaging have been applied to assess the condition of three adult European Neanderthals represented by two right (Pa1 and Pa3) and one left (Pa5) patellae from the OIS 5 Croatian site of Krapina, stored at the Croatian Natural History Museum, Zagreb (Radovčić et al., 1988).

In terms of volume and spatial organisation, the characteristics of the cancellous network of the three patellae from Krapina examined in our research project (Pa 1, Pa 3 and Pa 5; Radovčić et al., 1988), fit the extant human condition. Compared to *Pan*, the fossil specimens show a proportional larger volume of trabecular bone, a denser area at the supero-lateral margin (probably related to the attachment of the quadriceps) and a higher number of radially oriented trabeculae at the medial and superior peripheral areas (Fig. 3.3.2.2.A). As seen in SKX 1084, extant Humans and the later French Neanderthal patella Regourdou 1 (Fig. 2 ms. section 3.3.1), the core of the Croatian specimens shows a looser cancellous network of poorly organised trabeculae, while the trabeculae tend to radiate perpendicularly towards the outer surface (Fig. 3.3.2.2.A). The patellae from Krapina also show the typically human vertically oriented anterior bundle (Standring, 2008). As seen in Regourdou 1 and, to a lesser extent, in modern Humans (Fig. 2 ms. section 3.3.1), especially in the specimen Pa 1, a horizontal cancellous bundle of thick and plate-like trabeculae can be identified near the base (Fig. 3.3.2.2.A), while this feature is absent in *Pan*. Similarly, all Croatian patellae, show the typically human (including in Regourdou 1) inferior bundle arising from the articular surface towards the anterior surface and parallel to the outer surface of the apex (Fig. 3.3.2.2.A). Conversely, compared to Regourdou 1, the patellae from Krapina show a globally less dense and larger-meshed network consisting of more rod-like trabeculae, than more commonly found in extant Humans (Fig. 3.3.2.2.A).

For data comparison, the same protocol and methodology applied to investigate the cancellous network in the study of the SKX 1084 hominin patella from Swartkrans Member 2 (see section 3.3.1 above), were followed. Indeed, the bone volume fraction (BV/TV, in %), trabecular thickness (Tb.Th., in mm), and degree of anisotropy (DA) were quantified at a central

(aVOI) and medial (bVOI) volumes of interest virtually extracted from the patella (for details see section 3.3.1 above). The results are presented in Table 3.3.2.2.A. As a whole, the three patellae show a slightly denser cancellous network associated with thicker trabeculae and a higher degree of anisotropy than Regourdou 1, but their estimates are closer to the human than the *Pan* pattern.

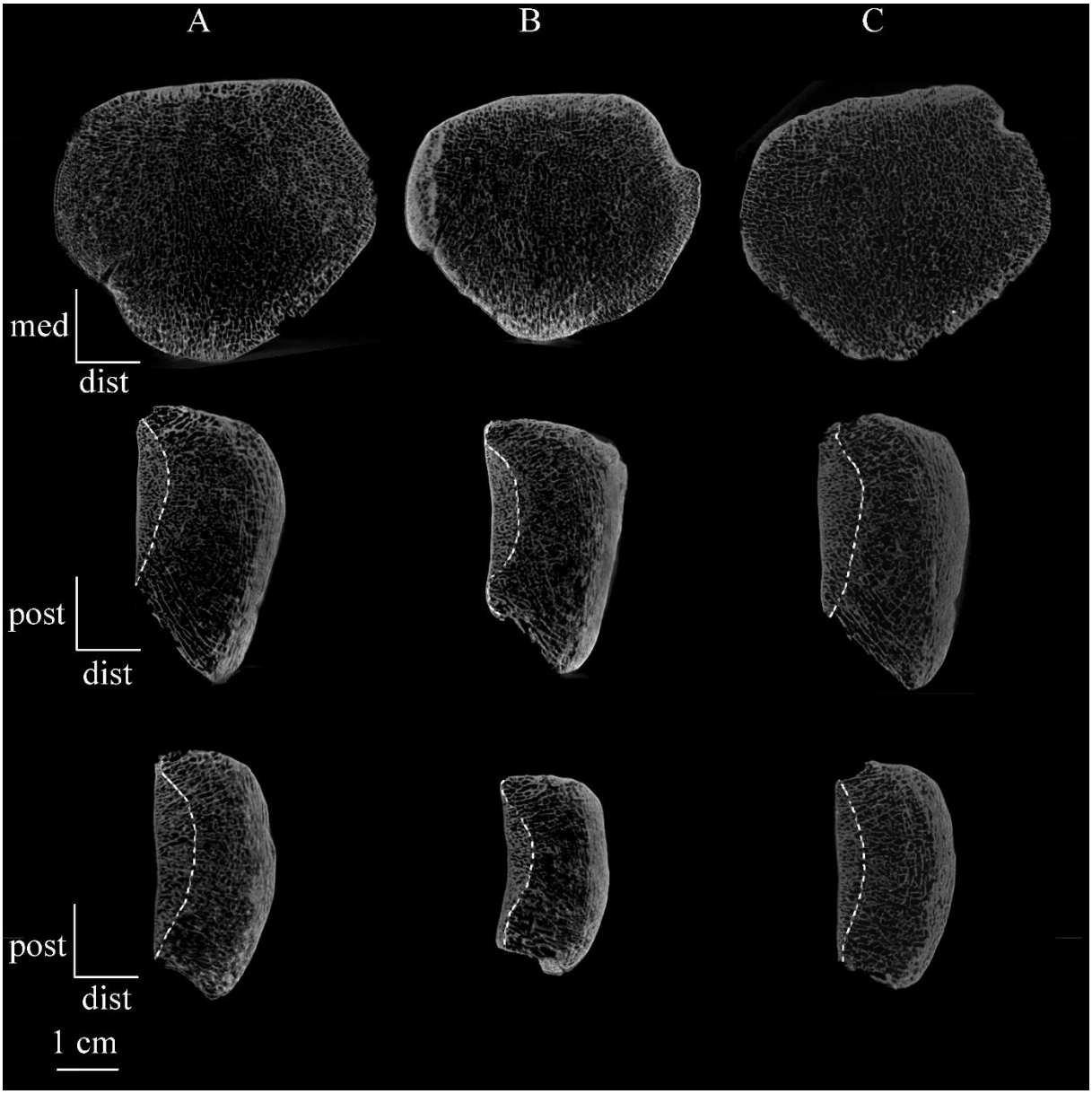

Fig. 3.3.2.2.A. µCT-based coronal sections (upper row) approximately across the centre of the patella and transversal sections (middle and lower rows) across the central VOI (aVOI, middle row) and the medial VOI (bVOI; lower row) in the sample of Neanderthal patellae from Krapina (Croatia), including specimens Pa 1 (A), Pa 3 (B) and Pa 5 (C). In each virtual section the

dashed line delimits the cortico-trabecular complex measured for its maximum thickness from the articular surface (aCTT and bCTT, respectively). Pa 5 is mirrored to be right.

Table 3.3.2.2.A. Bone volume fraction (BV/TV, in %), trabecular thickness (Tb.Th., in mm), and degree of anisotropy (DA) of the central (aVOI) and medial (bVOI) volumes of interest of the patella, assessed in a sample of recent Humans (n = 12), a Neanderthal sample consisting of Regourdou 1 and three specimens from Krapina (Pa 1, Pa 3, Pa 5), and in a *Pan* sample; s.d., standard deviation.

specimens	**aVOI**			**bVOI**		
	BV/TV (%)	**Tb.Th. (mm)**	**DA**	**BV/TV (%)**	**Tb.Th. (mm)**	**DA**
recent Humans (s.d.)	30.5 (6.5)	0.15 (0.03)	3.87 (1.46)	26.5 (5.7)	0.14 (0.03)	4.92 (1.52)
Regourdou 1	34.5	0.15	4.44	30.3	0.13	5.81
Pa 1	31.7	0.16	3.80	41.9	0.23	7.52
Pa 3	35.4	0.19	4.31	28.0	0.17	5.56
Pa 5	38.3	0.20	6.09	39.9	0.19	5.04
Pan	65.1-79.1	0.23-0.27	2.73-2.87	67.8-81.2	0.23-0.24	1.88-1.94

3.3.2.3. Patellar biomechanics during knee flexion: Humans vs. apes

The human patella is embedded within the ligaments and muscles of the quadriceps complex, as well as in the most extensive and complex joint synovial membrane in the body (Platzer, 2008; Standring, 2008). The articular cartilage is the thickest in the human body, thus reflecting the magnitude of the stresses to which the joint is commonly subjected (Standring, 2008). The quadriceps femoris, which is divided into four parts (rectus femoris, vastus medialis, vastus lateralis and vastus intermedius), is attached to the superior surface of the patella, except near its posterior margin. The attachment thus extends distally onto the anterior surface. The attachment of the rectus femoris at the base of the patella lies antero-inferior to that of the vastus intermedius. Rough markings can be traced around the periphery of the patella from its antero-superior surface to the deep surface of the apex, inferiorly. The markings at the lateral and medial borders relate to the attachments of the lateral and medial vasti, and those at the apex represent the attachment of the patellar tendon. The vastus lateralis is mainly inserted into the lateral retinaculum, rather than directly on the patella. However, the oblique fibres of vastus medialis attach directly to the medial border of the patella. In this position, they prevent the

bone from laterally dislocating when the quadriceps femoris (including the vastus medialis) extends the knee (Aiello and Dean, 1990; Standring, 2008). In this respect it is noteworthy that, in chimpanzee, the vastus medialis does not insert onto its extreme medial edge (Aiello and Dean, 1990; Lovejoy, 2007).

During locomotion, the contact area between the articular surface of the posterior side of the patella, and that on the anterior side of the femur (patellar groove), varies depending on the degree of knee flexion. Naturarly, the articular surface of the patella fits that of the distal femur. In Humans, the ‘odd' facet on the articular patellar surface articulates with the antero-lateral aspect of the medial femoral condyle in full flexion, when the highest lateral patellar facet makes contact with the anterior part of the lateral femoral condyle. As the knee extends, the middle patellar facets come in contact with the lower half of the femoral surface, while the lowest patellar facets come in contact with the femur only in full extension. In summary, in flexion, the patellofemoral contact point moves proximally (Nisell, 1985; Aglietti and Menchetti, 1995; Masouros et al., 2010; Schindler and Scott, 2011).

The different stages of flexion and extension are responsible for the multifaceted surface of the human patella which bears several distinct and angulated planes. This subdivision of the patellar surface reduces patella-femoral contact when the joint is in a greater degree of flexion (Goodfellow et al., 1976), but results into higher patella-femoral stresses than would occur if the patellar surface were more uniformly-shaped. The human knee is thus tibial-dominant (Aiello and Dean, 1990; Lovejoy, 2007; Standring, 2008). Furthermore, during knee flexion, the patella tilts latero-medially around a longitudinal axis (proximal to distal through the patella), shifts laterally in the frontal plane, and spins or rotates around an anteroposterior axis (perpendicular to the patella) (Standring, 2008). This movement implies that the contact area between the articular surface of the femur and the patella changes, moving to the lateral side of the patellar articular surface and becoming more discontinuous proximally (when the knee is completely axed; Standring, 2008; Masouros et al., 2010; Schindler and Scott, 2011). In *Pan*, the articulated surface of the patella is much simpler, more uniform, and mirrors the equally uncomplicated surface of the distal femur. This assures high patella-femoral congruity during the propulsion and ground contact phases of the quadrupedal cycle and thereby reduces joint stress under flexion conditions. The chimpanzee knee is thus patellar-dominant (Aiello and Dean, 1990; Lovejoy, 2006; Standring, 2008). In *A. afarensis*, the morphology of the femoral condyle suggests that the knee joint, as in Humans, is also tibial-dominant (Lovejoy, 2007).

In Humans, forces on the patellofemoral joint are influenced by the action of the quadriceps muscle and the angle of flexion of the knee (Levangie and Norkin, 2005; Schindler

and Scott, 2011). The most superficial parts of the patella are in tension due to the action of two opposite forces: that of the quadriceps muscle and that of the patellar ligament (Oxnard, 1971; Nisell, 1985). The compression of the femur against the patella during knee flexion generates a reaction force that increases progressively (Nisell, 1985; Levangie and Norkin, 2005; Lovejoy, 2007; Masouros et al., 2010).

The patellar antero-posterior thickness and supero-inferior height, but not the medio-lateral breadth, appear to play a major role in the length of the patellar tendon moment arm, and in the lever arm length associated with the quadriceps, respectively (Ward et al., 1995; Pina et al., 2014; Pina, 2016). In modern Humans, peak contact forces at the knee have been measured in vivo at 2.1 times the body weight (Taylor et al., 2004) and the patellar cancellous organisation has been seen to respond to the biomechanical demands. Indeed, microradiographic-based studies of the patellar trabecular organisation in Humans reveal that the essential elements in the structure are oriented sheets interconnecting laterally with rod-shaped elements (Raux et al., 1975; Townsend et al., 1977). A radiological study by Toumi et al. (2006) showed that, at the upper portion of the patella, the quantity of bone and the trabecular thickness are greatest medially, while in the lateral part, there are fewer trabeculae orientated either antero-posteriorly or superiorly inferiorly. Following such results, the mechanical stresses at the proximal patella appear as asymmetrically distributed, i.e., greater on the medial than on the lateral side. Consequently, the relative paucity of bone laterally at the proximal pole of the patella should reflect the lack of any direct muscle insertion in this region (Toumi et al., 2006). However, a more recent study from the same research team based on histological slices of cadaveric patellar bones showed that the trabeculae are thicker in the central and lateral parts than in the medial region (Toumi et al., 2012). The authors concluded that the mechanical stresses at the proximal quadriceps tendon enthesis is higher laterally and centrally, compared to the medial aspect, a result which is consistent with a lateral patellar translation (Toumi et al., 2012). In addition, it has been shown that the patella experiences a significant reduction of bone hardness with depth, and that proximal and central regions demonstrate higher bone hardness than the distal region (Katoh et al., 1996).

3.4. Skeletal maturation of *P. robustus*

In 1938, R. Broom reported the discovery of three postcranial elements found in the same matrix and nearby the holotype of *P. robustus*, composed of a calvarium (TM 1517a), an associated right mandibular corpus (TM 1517b) and several isolated teeth (TM 1517c) (Broom, 1938a), an assemblage which, according to Broom, might be "almost certainly that of a young female" (Broom, 1938b: 898). The three postcranial elements represent the distal end of a right humerus (TM 1517g), part of a proximal end of a right ulna (TM 1517e), and a toe phalanx (TM 1517o) (Broom 1938b).

In his report, Broom (1938b) declared being certain that the distal humerus (TM 1517g) belonged to the *Paranthropus* type individual as "in the caves at Sterkfontein and Kromdraai between 3,000 and 4,000 specimens have been collected and no tooth or bone of man has so far been discovered, and as this distal humerus was found close to the skull of *Paranthropus*, which in a number of points of structure is nearly man" (Broom, 1938b: 897). More recently, Thackeray et al. (2001) suggested that TM 1517g articulates with the proximal ulna TM 1517e, an evaluation also acknowledged by Skinner et al. (2013).

Within the framework of a geochemical analysis of the trace element content of the breccia directly associated with the *P. robustus* type specimen, performed to pinpoint the area where TM 1517 was originally discovered, a humeral diaphysis (KB 5522), claimed to represent the same individual as the distal humerus TM 1517g, has been discovered in close proximity of the sample associated with the holotype at ca 15 cm, in easterly coordinates, 10 cm, in northerly coordinates, and approximately at the same depth (relative to datum) of the geochemically most similar breccia (Thackeray et al., 2005; Braga et al., 2013). According to such new evidence, the distal humerus TM 1517g, the proximal ulna TM 1517e, the humeral shaft KB 5522 and the cranial assemblage TM 1517a, b, c should all be associated. However, the exact circumstances of the discovery of the *P. robustus* holotype at KB remain somehow unclear (Broom, 1938a, b; Braga et al., 2016a).

Some time after the discovery of the *P. robustus* holotype, Broom (1942, 1943) reported the discovery of several isolated hand and foot bones (TM 1517 h, i, j, l, m, n), as well as of another toe bone currently considered as a distal phalanx of the hallux (TM 151k). These specimens were recovered from a spot in the immediate vicinity of the toe bone described in 1938 (TM 1517o). R. Broom furthermore reported the discovery of a right talus (TM 1517d). All were from the same matrix of the *P. robustus* holotype. However, since their initial description (Broom, 1942, 1943), most of these elements are now considered as either more

likely representing baboon individuals, or not belonging to the same individual as the type specimen.

At present, the postcranial elements reported as more likely associated with individual TM 1517, include the distal humerus TM 1517g, the proximal ulna TM 1517e, the distal hallucial phalanx TM 1517k and the humeral diaphysis KB 5522, while the association with the talus TM 1517d remains uncertain.

Unfortunately, at the best of our knowledges, no detailed information on the precise stratigraphic provenance of these remains exists. However, Bruxelles et al. (2016) recently suggested that the so called "holotype block", i.e., the block where the *Paranthropus* holotype was found, is a conglomerate of breccia from Members 5 and 6, while Braga et al. (2016a) suggest a possible origin of all postcranial elements from Member 5.

Although the holotype skull (cranium + partial mandible + isolated teeth) has been reported to represent a young adult (Broom, 1938a) or a late adolescent individual (Braga et al., 2016b), since their early description, no analysis has documented the presence, or lack, of any remnant of still growing bone on the likely associated postcranial remains. Using high-resolution microCT (μCT) scanning, we performed a study aimed at characterising the inner structure of the distal humerus TM 1517g, the proximal ulna TM 1517e and the distal hallucial phalanx TM 1517k, specifically to tentatively detect any trace of a recent, or an even still incomplete, epiphyseal closure. Whenever available, such evidence would corroborate the suggested association of craniodental and postcranial remains and would provide, for the first time, information on the skeletal growth patterning in *P. robustus* derived from odontoskeletal remains, sampling a dentally immature individual (Broom, 1938b, 1942, 1943; Thackeray et al., 2001, 2005; Braga et al., 2013, 2016a, b; Skinner et al., 2013). However, since the trace of epiphyseal fusion of the talus is *a priori* unlikely to be identified, as it may not always be present (Cunninghan et al., 2016), we did not consider the right talus TM 1517d in our study.

In the hominin fossil record there are few postcranial remains of immature individuals unequivocally associated with craniodental specimens, an essential condition for accurately assessing the taxon-specific timing and patterns of odontoskeletal maturation. The discovery, in 2008, of *A. sediba* at Malapa, South Africa, including the remains of a juvenile male labelled MH1 dated at 1.98 Ma (Berger et al., 2010), showed some synchrony in skeletal maturation with respect to both the human and chimpanzee reference models, but a globally more chimpanzee-like pattern (Cameron et al., 2017). The 1.8 Ma immature individual from Dmanisi, Georgia, assigned to *H. erectus georgicus*, includes a skull with permanent dentition revealing a newly erupting M3 (Vekua et al., 2002) and some associated postcranial remains consisting

of completely fused phalanges, metatarsal IV and most distal elements of the distal humerus, incompletely fused metatarsal I, and still unfused medial epicondyle and proximal end of the distal humerus (Lordkipanidze et al., 2007). According to this assemblage, the Georgian specimen, showing a slightly more advanced fusion of the foot bones compared to *Pan* at a similar stage of dental development, but also a slightly less advanced humeral fusion, may represent a shift towards a non-ape-like skeletal union sequence (Kelley and Bolter, 2013). For the 1.6 Ma nearly-complete *H. erectus/ergaster* skeleton labelled KNM-WT 15000 from Nariokotome, Kenya (Walker and Leakey, 1993), a chimpanzee model of skeletal growth and dental maturity provided concordant age estimates (Smith, 1993). Even though the possibility of a more human pattern of growth and development has been suggested for this individual (Clegg and Aiello, 1999), because of the histologically-based revised dental age-at-death estimate now constrained within 7.6 and 8.8 years rather than previously established at approximately 11 years (Dean and Smith, 2009), the stages of skeletal development and stature of this individual do not fall within the ranges of variation documented in modern Humans. A recent study using dental age and femoral diaphysis length to predict development relative to the extant human condition shows that, in KNM-WT 15000, when both age and femoral diaphysis length are used as explanatory variables, the predicted dental development values for all teeth, but the M2, match the observed values (Šešelj, 2017). Therefore, given the likely age range of 7.6-8.8 years and rates of skeletal growth, dental development in KNM-WT 15000 does not exceed over what would be expected in a modern human individual of that age and femoral diaphysis length (Šešelj, 2017). Accordingly, the author concluded that "advanced dental formation in Nariokotome, given his chronological age, may simply be a reflection of his faster rates of skeletal growth, and not necessarily the result of independent evolutionary forces affecting dental development" (Šešelj, 2017: 8).

Based on the evidence of life history traits and skeletal maturation patterns of the available Pliocene and Early Pleistocene hominins (e.g., Dean and Smith, 2009; Schwartz, 2012; Kelley and Bolter, 2013; Cameron et al., 2017), for TM 1517, we may expect some synchrony with both the chimpanzee and the human reference profiles, as well as a pattern of odontoskeletal maturation in *P. robustus*, which more closely approaches an ape-like model.

3.4.1. Materials

As mentioned before, among the elements possibly associated with the type specimen of *P. robustus*, we selected and non-invasively detailed, at high resolution the distal right humerus

TM 1517g, the proximal right ulna TM 1517e and the distal hallucial phalanx TM 1517k. Details about these specimens are provided in section 2.1.3.

For comparative purposes, we used an extant human sample of subadult individuals consisting of five humeri, six ulnae and six distal hallucial phalanges selected from the R.A. Dart Collection at the University of the Witwatersrand, Johannesburg (Dayal et al., 2009). For each bone, we tentatively composed a comparative sample including three male and three female immature individuals. However, given the lack in the reference collection of a young female showing traces of recent fusion, no distal humerus could be included in this category. Accordingly, for each element and for each sex, excluding the distal humerus, our extant human comparative sample included one specimen showing the epiphysis not fused, one specimen revealing faint traces (remnants) of a recent epiphyseal fusion and one specimen where the corresponding epiphysis fused recently. Information on this assemblage is summarised below in Table 3.4.1.A.

Table 3.4.1.A. Composition and degree of epiphyseal fusion of the extant human subadult sample from the R.A. Dart Collection (University of the Witwatersrand, Johannesburg) used in the comparisons with the TM 1517-labelled postcranial elements representing *P. robustus*.

bone	sex	degree of epiphyseal fusion	age (years)
distal humerus	M	not fused	15
=	M	traces of recent fusion	16
=	M	just fused	17
=	F	not fused	12
=	F	just fused	14
proximal ulna	M	not fused	16
=	M	traces of recent fusion	16
=	M	just fused	17
=	F	not fused	13
=	F	traces of recent fusion	13
=	F	just fused	14
distal hallucial phalanx	M	not fused	15
=	M	traces of recent fusion	16
=	M	just fused	17
=	F	not fused	12
=	F	traces of recent fusion	13
=	F	just fused	14

3.4.2. Methods

Before scanning, the outer surfaces of all investigated fossil elements were systematically inspected using an Olympus SZ40 microscope (magnification up to × 40). The impact on the outer aspect of abiotic processes was recorded with respect to the following variables: degree of manganese invasion, weathering stage (following Behrensmeyer, 1978), water abrasion; chemical dissolution, presence/absence of matrix concretions, and degree of decalcification (if any). Following the method proposed by Val and Stratford (2015), five stages in the extent of precipitated manganese dioxide on the bone surface were recognized: none, slight (only a few spots), slight to moderate (abundant, spots covering less than 50% of the surface), moderate (> 50% of the surface covered) and heavy (whole surface covered). Various types of damages caused by biotic agents (root etching, carnivore and rodent gnawing, mammalian and/or avian digestion and insect boring and gnawing) were also investigated. Whenever possible, information available in the literature on carnivore damage (e.g., Maguire et al., 1980; Brain, 1981; Shipman and Rose, 1983; Val et al., 2014; Val and Stratford, 2015), rodent damage (Maguire et al., 1980; Brain, 1981; Shipman and Rose, 1983) and insect bony damage (Britt et al., 2008; Backwell et al., 2012; Parkinson, 2016) were also used for comparative purposes.

In order to detect, if any, traces of a recent epiphyseal fusion preserved in the three selected fossil specimens from Kromdraai likely associated with the *P. robustus* holotype, we detailed their inner structure by means of high resolution micro-focus X-ray tomography (μCT). The fossil specimens were scanned between 2015 and 2017 at the micro-focus X-Ray tomography facility (MIXRAD) of the South African Nuclear Energy Corporation (Necsa), Pelindaba, using a Nikon XTH 225 ST (Metris) scanner according to the following parameters: 125 kV tube voltage, 0.11 mA tube current, and a projection each 0.36° (for a total of 1000 projections) for the distal right humerus TM 1517g; 100 kV tube voltage, 0.10 mA tube current, and a projection each 0.36° (for a total of 1000 projections) for the proximal right ulna TM 1517e; and 100 kV tube voltage, 0.10 mA tube current, and a projection each 0.18° (for a total of 2000 projections) for the distal hallucial phalanx TM 1517k. The final volumes were reconstructed with an isotropic voxel size of 35 μm, 23 μm and 8.7 μm for the distal humerus, the proximal ulna and the distal hallucial phalanx, respectively.

All specimens forming the comparative human sample of known sex and age at death selected from the R.A. Dart Collection, were scanned at Necsa in 2017, at resolutions ranging from 12 μm to 77 μm isotropic voxel size.

3.4.3. Results

The microscopic investigation of the outer aspect of the distal humerus TM 1517g and the proximal ulna TM 1517e revealed a well preserved surface, nearly free from subaerial weathering alterations (stages 0 to 1; Behrensmeyer, 1978), with minial traces associated with initial superficial cracks only on the lateral facet of both specimens. Conversely, the distal hallucial phalanx TM 1517k is less preserved, especially at its dorsal surface, and its analysis is thus less probatory. Manganese coating is widely distributed over the distal humerus and the proximal ulna, but with only a few dots on the lateral aspect of both specimens (stage 1; Val and Stratford, 2015). Some completely covered areas (stage 4; Val and Stratford, 2015) obscuring the possible presence of previous bone surface modifications exist on the trochlea and capitulum of the distal humerus, as well as on the postero-medial surface of the anterior articular facet of the proximal ulna. Conversely, the phalanx TM 1517k demonstrates only a few dots of manganese dioxide staining. Interestingly, among other modifications, bore holes, similar in size and structure and likely representing insect damage, are present in the posterior surface of the lateral epicondyle of the distal humerus and in the supero-lateral aspect of the proximal ulna. In addition, pits with a diameter < 1 mm are present in the posterior part of the distal humerus, in the lateral and superior surfaces of the proximal ulna and on the most distal and proximal parts of the plantar surface of the distal hallucial phalanx. No external traces of a recent fusion of the epiphysis are noticeable on any of the bones (Fig. 3.4.3.A).

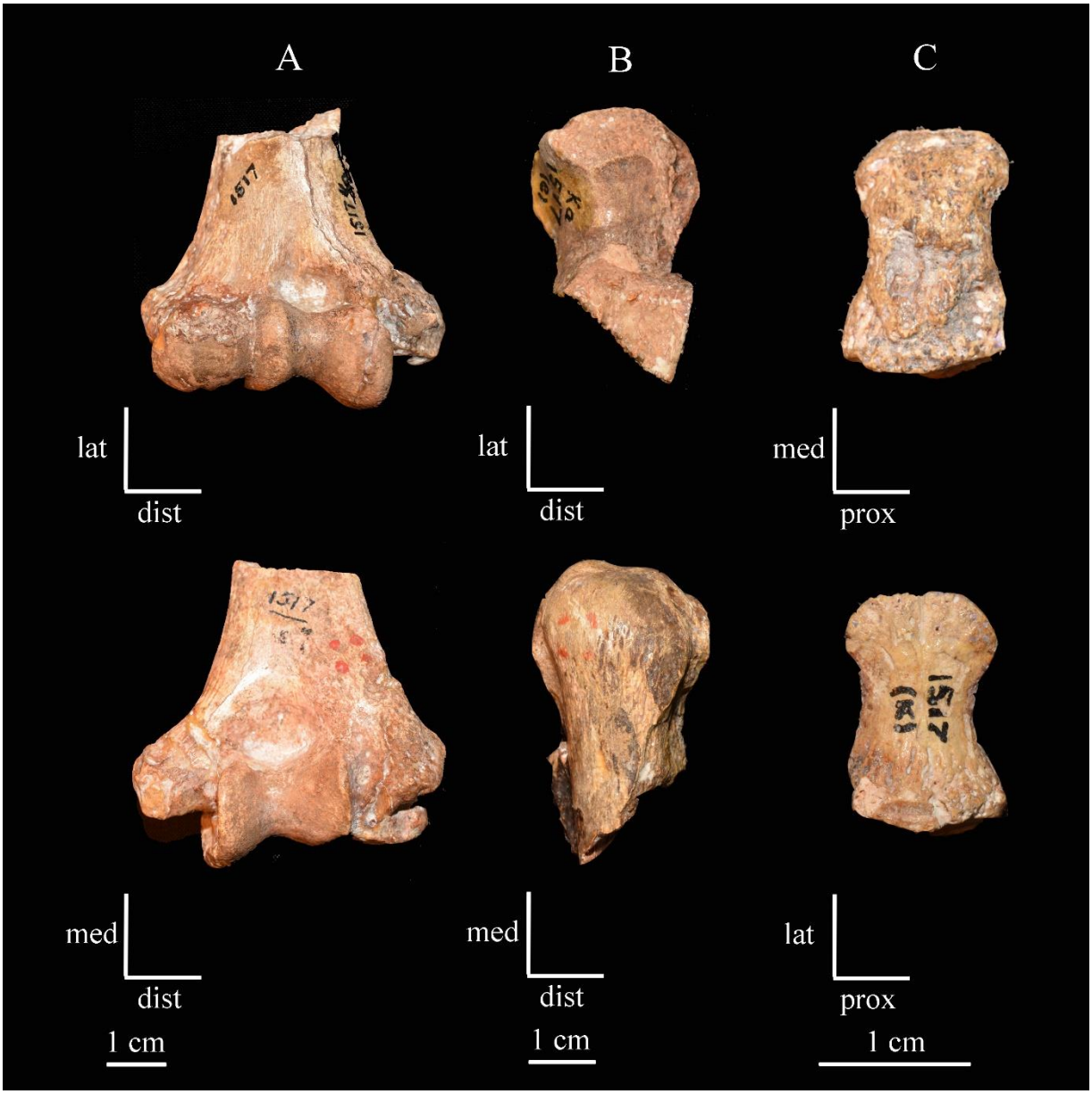

Figure 3.4.3.A. Anterior (upper row) and posterior (lower row) views of the distal right humerus TM 1517g (A) and of the proximal right ulna TM 1517e (B) and dorsal (upper row) and plantar (lower row) views of the distal hallucial phalanx TM 1517k (C).

Among the three fossils, the inner structure of TM 1517g is the least preserved. It is noteworthy that a sediment of similar density as the matrix is also found in the proximal ulna TM 1517e, where it extensively fills most of its cancellous network without replacing or mimicking the trabeculae. Cracking is most often found along both epicondyles, where lacunae can also be observed.

In our comparative human sample of immature humeri, variably extended sub-horizontal traces of incomplete distal epiphyseal fusion are evident from the most lateral part of the lateral epicondyle - which is unfortunately not well preserved in TM 1517g, where the region is characterised by some missing chunks of bone - to the most medial part of the capitulum and, horizontally, from the most lateral part of the trochlea to the junction between the medial epicondyle and the trochlea. However, such fusion marks are not unambiguously detectable in TM 1517g (Figure 3.4.3.B), where the sub-vertical "lines" visible between the lateral epicondyle and the capitulum, and in the medial epicondyle certainly correspond to physical cracks penetrating the bone from the outer surface (see Figure 3.4.3.A). In sum, our µCT record does not provide any evidence of an even faint remnant of distal epiphyseal fusion in TM 1517g.

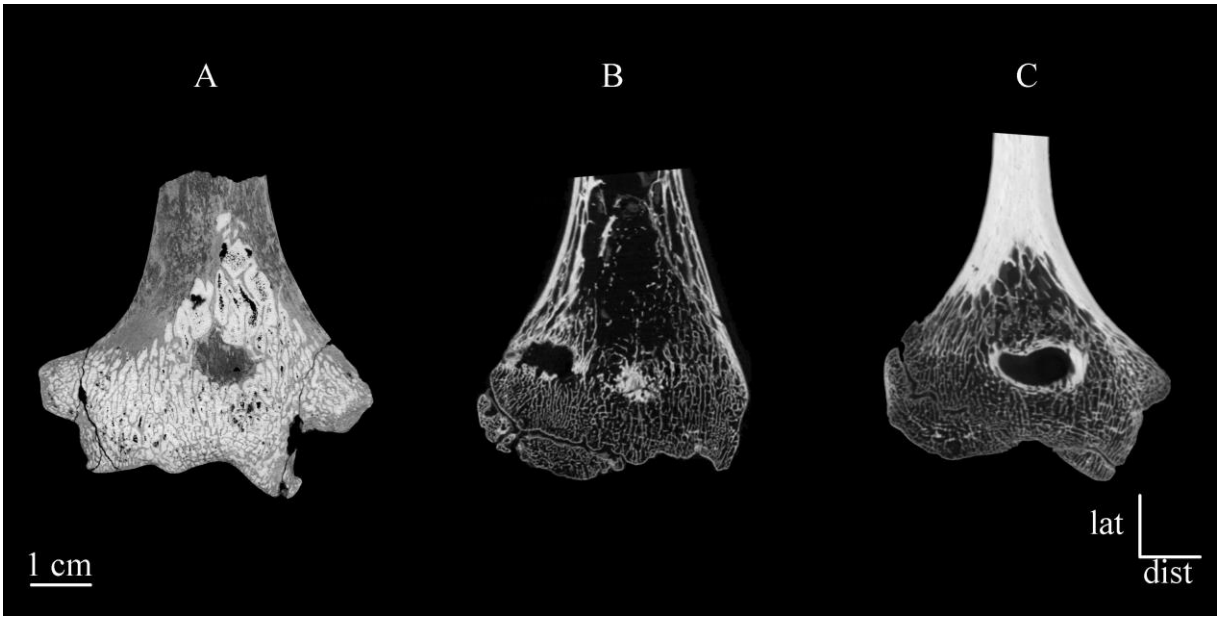

Figure 3.4.3.B. µCT-based coronal slices extracted at the centre of the maximum antero-posterior diameter in the distal humerus TM 1517g (A) and in two human humeri representing a 15 year old male (B) and a 12 year old female (C), showing still incomplete epiphyseal closure.

The inner structure of the proximal ulna TM 1517e is relatively well preserved and its high resolution microtomographic record can be confidently used to reliably assess the presence/absence of epiphyseal fusion traces. In this fossil, sediment extensively fills most of the cancellous network, but it does not replace or mimic the trabecular walls. Therefore, the original arrangement of the cancellous struts, as a whole, can be distinctly appreciated, even if

the matrix punctually veils some cell boundaries. Furthermore, no invasive cracks damaging the cortical bone and/or the cancellous network of this ulna can be noticed. A remnant of epiphyseal fusion, directly comparable to the marks found in the extant human immature ulnae used for comparison, is unambiguously traceable in TM 1517e, even if only faintly expressed because of the fossilisation fading effect (Fig. 3.4.3.C). This transverse remnant is present in the superior part of the specimen, where it runs from the most lateral point of the trochlear notch, laterally, to the most medial point of the medial trochlear notch.

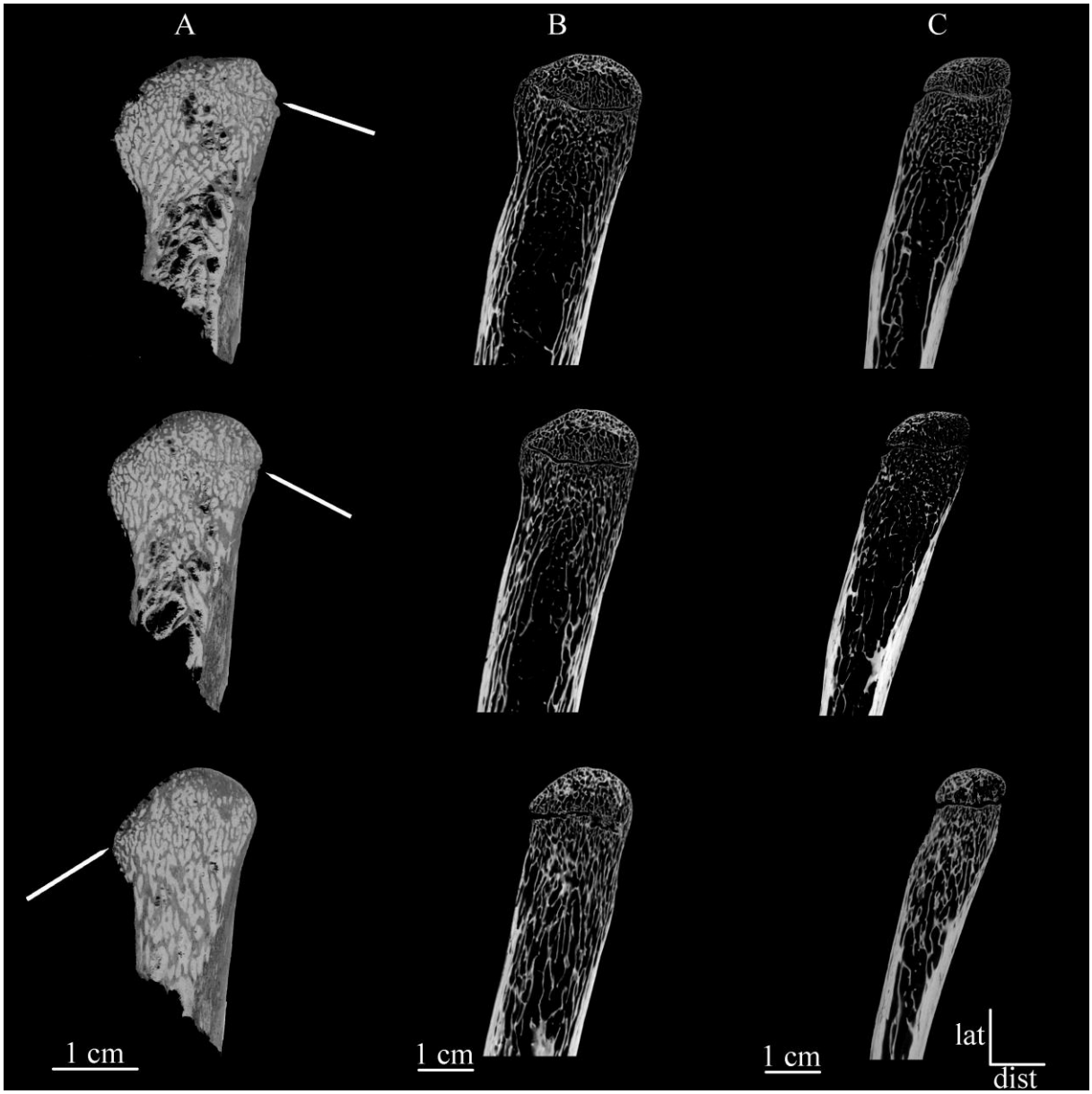

Figure 3.4.3.C. Coronal µCT-based anterior slices extracted at 9%, 25% and 50% of the maximum antero-posterior diameter of the proximal ulna TM 1517e (A) and two ulnae

representing a 16 year old male (B) and a 13 year old female (C) showing still incomplete epiphyseal closure. The white arrows indicate the faint preserved traces of recent fusion in TM 1517e.

Similar to the other specimens, a matrix extensively fills most of the cancellous network of the distal hallucial phalanx TM 1517k, but without affecting the trabecular organisation. Conversely, cracking is mostly found along its lateral and medial cortices and the whole outer aspect is affected by taphonomic damages (see above). In this specimen, while we cannot observe the well-defined mediolateral traces of an incomplete epiphyseal closure, as are evident in a variable degree in the immature extant human specimens used for comparison, we do note some traces of cortex separation across the entire proximal end of the distal hallucial phalanx, where the limits of the so-called cortico-trabecular complex - i.e., the subchondral component including the lamina and the immediately adjoining trabecular network essentially made of plate-like structures (Mazurier, 2006) - are well discernible (Figure 3.4.3.D).

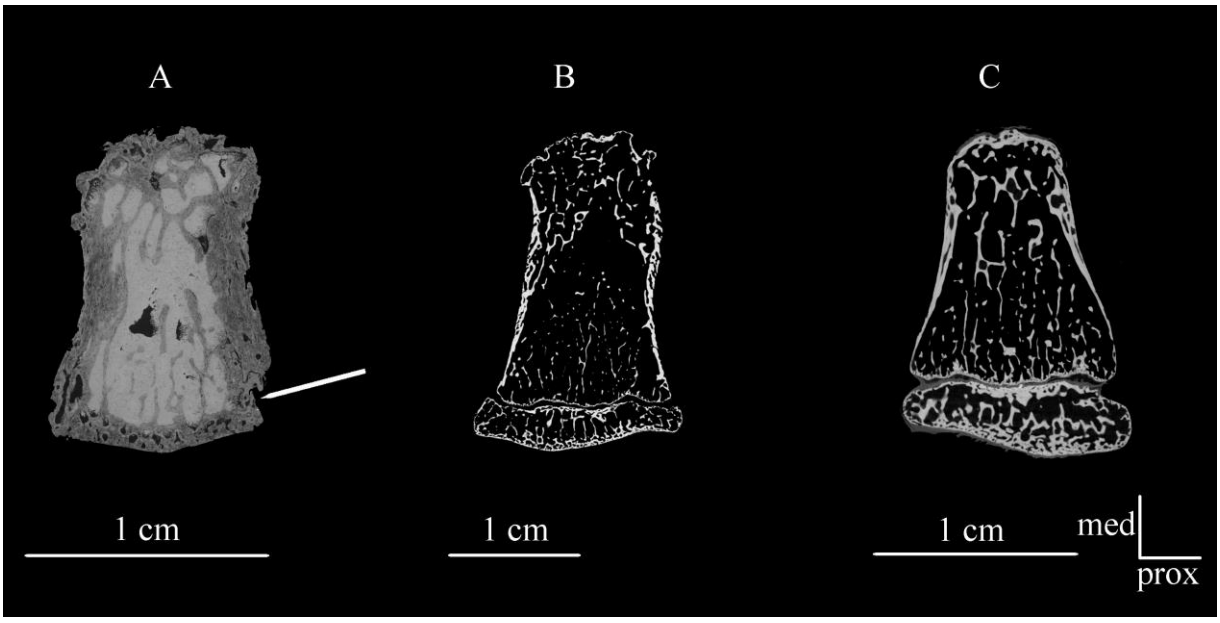

Figure 3.4.3.D. µCT-based transversal slices extracted at the centre of the maximum dorso-plantar diameter in the distal hallucial phalanx TM 1517k (A) and in two human hallucial phalanges representing a 15 year old male (B) and a 12 year old female (C) showing still incomplete epiphyseal closure.

3.4.4. Discussion

While the so called "holotype block" at Kromdraai, which appears to be the block where the *Paranthropus* holotype was found, could be a conglomerate of breccia from different Members (Bruxelles et al., 2016), the study of the outer preservation of the distal humerus TM 1517g, the proximal ulna TM 1517e, and the distal hallucial phalanx TM 1517K reveals similar outer damages consistent with the possibility that the remains were subject to comparable taphonomic conditions and thus shared a close original location during the fossilisation process. This new evidence does not allow rejection, but rather strengthens, the anatomically-based suggestion that TM 1517g and TM 1517e form an articulate elbow joint from a single individual (Thackeray et al., 2001; Skinner et al., 2013; Braga et al., 2016a, b).

Relying on high resolution µCT data, our 2-3D virtual reconstructions show that the distal humerus TM 1517g was likely completely fused, while the proximal ulna and the distal hallucial phalanx still display a remnant of fusion. Together with the anatomically-based evidence of an articulating unit between TM 1517g and TM 1517e, our new endostructural record supports the original suggestion that the three postcranial specimens TM 1517g, TM 1517e and TM 1517k, as well as the holotype skull (TM 1517a, b, c) sample a single still growing *P. robustus* individual (Broom, 1938b, 1942, 1943; Thackeray et al., 2001, 2005; Braga et al., 2013, 2016 a, b; Skinner et al., 2013).

The TM 1517 holotype skull has been described as a late adolescent-young adult (Broom, 1938a; Braga et al., 2016a, b). The degree of dental development of the permanent teeth of the right mandibular corpus TM 1517b, which preserves the C-M3 tooth row, was scored (by J. Braga) on the basis of a µCT record using the 14-stage coding system of Moorrees et al. (1963) (J. Braga, pers. comm.). While the C, P3 and M1 show a complete root apical closure (A_c), the P4 and M2 show nearly, but still not fully closed apices ($A_{1/2}$), and the M3 shows a root formation stage between half and three-quarters completed (scored as stage $R_{1/2}$-$R_{3/4}$ according to Moorrees et al., 1963).

Based on the London Atlas of Human Tooth Development and Eruption compiled by AlQahtani et al. (2010) using the Moorrees et al. (1963) dental scoring system applied to a sample of 704 extant human individuals of known age between 28 weeks in utero to 23 years, the age at death estimate of TM 1517b from its observed dental development is about 16.5 ± 3 years (Table 3.4.4.A.). For the elements of the TM 1517 postcranial skeleton examined here, the fusion of the distal humerus and proximal ulna in extant human males occurs within the age interval 14-18 years and between 14 and 16 years for the distal hallucial phalanx (Cunningham

et al., 2016). In extant human female individuals, the fusion of the distal humerus occurs between 11 and 15 years, that of the proximal ulna between 12 and 15 years, and that of the distal hallucial phalanx between 11 and 13 years (Cunningham et al., 2016). Therefore, based on a modern human skeletal maturity model, the estimated age at death of the TM 1517 assemblage ranges between 14 and 18 years for a male individual and between 11 and 15 years for a female individual (Table 3.4.4.A.).

By using the radiographs of the lower dentition of 80 chimpanzees (*P. troglodyte*s) and 34 bonobos (*P. paniscus*) ranging in age between 7.01 and 10.5 years, Boughner et al. (2012) established a dental development system divided in 12 scores for assessing crypt, crown and root formation (see also Dean and Wood, 1981). According to this system, the lower C, P3 and M1 of TM 1517b are scored as 12 (Rc/Ac), the P4 and M2 are scored as 11 (Rc/Ao), and the M3 is scored as 9-10 (R1/2-R3/4), a configuration corresponding to the "older juvenile" group defined by Boughner et al. (2012) (Table 3.4.4.A.). For the postcranial elements, it is reported that in *Pan*, the elbow is fused between 7.95 and 13.5 years (Zilhman et al., 2007; Bolter and Zilhman, 2012; Cameron et al., 2017), while the distal phalanx is fused at ca 9.45 years (Brimacombe et al., 2015). More precisely, in the so-called "Juvenile III" group of the chimpanzee subsample composed of 5 individuals from total of 22 immatures forming the sample from the Taï National Park studied by Zilhman et al. (2007), the humerus and the ulna fuse between 10.5 and 13.5 years in males (n = 2) and between 10.5 and 12.5 years in females (n = 3). In the study of Bolter and Zilhman (2012) of a *P. troglodytes* sample from the same area composed of 9 individuals, the distal humeral fusion occurs in individuals aged between 7.96 and 10 years. In a study by Cameron et al. (2017) of a sample of 9 cadaveric specimens of wild chimpanzees from the Taï National Forest and the Gombe Reserve, the humerus has just fused and the ulna partially fused in the only individual aged between 12 and 13 years. Finally, to the best of our knowledge, the only study that also takes into account the age-related development of the distal hallucial phalanx is that by Brimacombe et al. (2015) on 155 subadult *P. troglodyte*s (91 females and 64 males). In this work, the estimated chronological age of epiphyseal fusion at this site, assessed by using the Kuykendall's (1996) regression equation, is of ca 9.45 years. Therefore, based on the estimates available for skeletal maturity in *Pan*, the age at death of the TM 1517 assemblage should range between 7.95 and 13.5 years (Table 3.4.4.A.). However, it is worth noting that, in the same study by Brimacombe et al. (2015), among the individuals showing a dental development directly comparable to that observed in TM 1517b, the humerus is completely fused in only 25% of cases, while the proximal ulna and the distal phalanges of the foot are systematically fused in all individuals.

Table 3.4.4.A. Dental and skeletal age estimates based on extant human and *Pan* reference models for the dental development condition shown by the right hemi-mandible TM 1517b (J. Braga, pers. comm.) and the maturation indicators of the distal humerus, proximal ulna and distal hallucial phalanx forming the TM 1517 fossil assemblage; M =male; F= female.

model	dental age estimates (years)	references	skeletal age estimates	references
human	16.1 ± 3	AlQahtani et al., 2010	14-18 (M)/ 11-15 (F)	Cunningham et al., 2016
chimpanzee	7.01-10.5	Boughner et al., 2012	7.95-13.5	Zilhman et al., 2007; Bolter and Zilhman, 2012; Brimacombe et al., 2015; Cameron et al., 2017

The results of our study suggest that the skeletal maturation schedule of TM 1517 shows some synchrony with both the human and chimpanzee male reference data, but that its pattern is closer to the ape condition (Table 3.4.4.B). This is in line with the skeletal developmental pattern assessed in *A. sediba* (Cameron et al., 2017) (different from *A. afarensis*; see Kivell et al., 2018b). In *A. sediba*, the assessed age-at-death for the MH1 individual ranges from 9 to 11 years, based on the chimpanzee schedules, and at around 13 years, based on the human references. The human age estimate based on the third molar crown calcification of 10.5-11.5 years would place MH1 about 1.5-2.5 years younger than the skeletal estimate, although the degree of normal variation in skeletal maturation in modern Humans from childhood onwards is generally taken as ± 2 years, i.e., SD ± 1.0 year (Cameron et al., 2017). Conversely, a dental age < 10.5-11.5 years based on an ape model, is within the predicted skeletal maturity age of 9-11 years.

A relevant point here is that, while in Humans the fusion of the distal hallucial phalanx on average slightly precedes that of the distal humerus (Cunningham et al., 2016), in chimpanzees, the distal humerus tends to fuse earlier, followed by the distal hallucial phalanx and the proximal ulna (Birmacombe et al., 2014; Cameron et al., 2017), thus according to a pattern which more closely fits the evidence provided by the TM 1517 postcranial assemblage investigated in this study. With its completely fused distal humerus and the remnant of a recent fusion still discernible at the proximal ulna and the distal hallucial phalanx, the skeletal

maturational sequence of TM 1517 appears more ape-like in terms of patterning (Table 3.4.4.B).

Table 3.4.4.B. Extant human and chimpanzee ages corresponding to the observed maturational condition of the permanent teeth of the right mandible TM 1517b (belonging to the *P. robustus* type specimen) and those of the distal humerus TM 1517g, the proximal ulna TM 1517e and the distal hallucial phalanx TM 1517k.

***P. robustus* TM 1517 assemblage condition**	**corresponding extant human age (years)[1]**	**corresponding chimpanzee age (years)[1]**	**references**
TM 1517b C A_c	14.5 - 16.5	> 10.5	AlQahtani et al., 2010; Boughner et al., 2012
TM 1517b P3 A_c	13.5 - 15.5	7.01 - 10.5	AlQahtani et al., 2010; Boughner et al., 2012
TM 1517b P4 $A_{1/2}$	13.5 - 14.5	7.01 - 10.5	AlQahtani et al., 2010; Boughner et al., 2012
TM 1517b M1 A_c	8.5 - 12.5	7.01 - 10.5	AlQahtani et al., 2010; Boughner et al., 2012
TM 1517b M2 $A_{1/2}$	13.5 - 16.5	7.01 - 10.5	AlQahtani et al., 2010; Boughner et al., 2012
TM 1517b M3 $R_{1/2}$-$R_{3/4}$	15.5 - 19.5	7.01 - 10.5	AlQahtani et al., 2010; Boughner et al., 2012
TM 1517g distal end fused	11.0 - 18.0	7.96 - 13.5	Zilhman et al., 2007; Bolter and Zilhman, 2012; Cunningham et al., 2016; Cameron et al., 2017
TM 1517e remnant upper end fusion	12.0 - 18.0	10.5 - 13.5	Zilhman et al., 2007; Cunningham et al., 2016; Cameron et al., 2017
TM 1517k remnant proximal end fusion	11.0 - 16.0	9.45	Brimacombe et al., 2015; Cunningham et al., 2016

[1] Sexes pooled.

Although Broom (1938a) stated that "the type skull is almost certainly that of a young female", the still uncertain sex attribution of TM 1517 presents a complicating factor to confirm the *P. robustus* odontoskeletal maturation timing, especially because it has been suggested that male *Paranthropus* should experience some prolonged growth, i.e., a slower rate compared to females of the same taxon, possibly compatible with a bimaturational growth pattern (Lockwood et al., 2007). In addition, it is important to consider that the tooth methods employed here provide only very broad age ranges and, mostly, that the age estimates of epiphyseal fusion used for the extant Humans (Cunningham et al., 2016) rely upon observations performed on the

outer bone morphology, not on the inner structure. Accordingly, it is possible that our estimates of the maturational timing and patterning in TM 1517, based on the developmental human reference standards, are slightly underestimated.

Preliminary results of the study of the *P. robustus*' maturational pattern have been presented to the *5th International Palaeontological Congress* (Paris, 9-13/8/2018): Cazenave M. - The skeletal maturation of *Paranthropus robustus* (https://ipc5.sciencesconf.org/data/IPC5_Abstract_Book.pdf).

4. Summary

By means of high resolution X-ray micro-tomography techniques and two- and three-dimensional quantitative analyses, in this PhD research project we characterised the patterns of topographic thickness variation of the cortical shell and the site-specific textural properties of the cancellous network in a number of postcranial remains commonly, or tentatively, attributed to *P. robustus*. The investigated specimens consisted of the distal humerus (see supra section 3.1), the proximal ulna (section 3.4), the proximal femur (section 3.2), the patella (section 3.3), and the distal hallucial phalanx (section 3.4). On a comparative ground, we aimed at (i) identifying some endostructural bony features characteristic of *P. robustus*, if any, thus tentatively providing a reference framework for the attribution of isolated fossil specimens from commingled assemblages; (ii) deconstructing the biomechanical (loading) environment that shaped the cortical and cancellous bone arrangement at the elbow, the hip, and the knee joints; (iii) assessing variation and, whenever possible, sex- and age-related differences in this taxon.

It should first be noted that, in *P. robustus*, a more robust cortex and cancellous bone than typically measured in extant Humans, at all skeletal sites, is consistent with the process of general skeletal gracilisation and trabecular bone density reduction that recently occurred in late human evolution (Chirchir et al., 2015, 2017; Ryan and Shaw, 2015).

At all investigated sites, the inner bony structural organisation of *P. robustus* predominantly reveals human-like features, but also some *Pan*-like characteristics. For instance, at the femoral neck, our new set of linear and surface measurements taken at the base of the neck and at mid-neck shows that *P. robustus* displays a thinner superior cortex (av. 2.45 mm at the base of neck and 2.46 mm at mid-neck) than the proportionally thicker inferior cortex (av. 3.40 mm at the base of neck and 2.75 mm at mid-neck), especially laterally, as observed in Humans (av. superior thickness 1.06 mm and inferior thickness 3.68 mm at the base of neck, av. superior thickness 1.11 mm and inferior thickness 2.65 mm at mid-neck). This feature is also associated with a human-like tendency towards a latero-medial decrease in average cortical thickness across both the inferior and superior regions of the femoral neck. In the likely *P. robustus* SKX 1084 patella, the medio-lateral breadth (30.2 mm) and the antero-posterior thickness (13.0 mm) closely approaches the *Pan* proportions (av. 25.6 mm vs. 11.7 mm). The maximum relative thickness of the cortico-trabecular complex - i.e., the subchondral

component, including the lamina and the immediately adjoining trabecular network, essentially made of plate-like structures (Mazurier et al., 2010; Cazenave et al., 2018) - measured at two sites beneath its articular surface (i.e., 9.6 % and 7.2 %), fits the human condition (av. 8.7 % and 7.1 %), as does its proportion of spongy bone.

Besides cortex asymmetry at the neck, trabecular bone architecture at the proximal femur in *P. robustus* widely resembles the extant human condition. Features shared with the human condition include an organised and topographically contrasted trabecular configuration. The distinct trabecular systems (notably those forming the so-called three minor or accessory systems) reveal a heterogeneous network organisation, including a looser appearance of the network in the so-called "Ward's triangle", the area infero-lateral to the vertical and arcuate bundles crossing. Similarly, the inner organisation of the *P. robustus* patella SKX 1084 more closely resembles the human than the *Pan* condition. Indeed, SKX 1084 shows a human-like larger proportional volume of trabecular bone compared to *Pan*, a denser area at the supero-lateral margin (probably related to the attachment of the quadriceps femoris muscle), and a higher number of radially oriented trabeculae at the medial and superior peripheral areas. In sagittal view, SKX 1084 displays a typical human, vertically oriented anterior bundle (Standring, 2008), also appreciable in transverse view. Trabecular anisotropy measured in *P. robustus* at the proximal femoral head (av. 3.23) and at two spots sampling the medial and central regions of the patella (i.e., 3.83 and 2.73) confirms a human-like degree of trabecular orientation (av. 3.46 in the femoral head, 3.87 and 4.92 in the patella). On the contrary, the femoral head in *P. robustus* shows, on average, a denser ape-like cancellous network (but associated with slightly thicker struts than measured in *Pan*) (av. BV/TV of 37.1 % in *P. robustus* and 39.2 % in *Pan*; av. Tb.Th. of 0.19 mm in *P. robustus* vs. 0.17 mm in *Pan*), than the human condition (av. BV/TV of 27.5 % and av. Tb.Th. of 0.16 mm). Similarly, the cancellous network of the *Paranthropus* patellar bone is denser (BV/TV of 40.4 % and 38.6 %) and possesses thicker struts (Tb.Th. of 0.20 mm and 0.19 mm) than measured in our comparative human sample (av. BV/TV of 30.5 % and 26.5 % and av. Tb.Th. of 0.15 mm and 0.14 mm), but is more gracile compared to *Pan* (av. BV/TV of 72.1 % and 74.5 % and av. Tb.Th. of 0.25 mm and 0.24 mm). A more robust cancellous network in *P. robustus* compared to Humans, is also found at the distal humerus, where the struts are invariably thicker in the fossil specimens considered in our research (av. 0.48 mm) than our extant human humeri sample (av. 0.35 mm).

Besides the similarities with the human condition in bony inner structural arrangement, *P. robustus* also displays some unique features. Compared to Humans, at the distal humeral diaphysis, *P. robustus* shows an elliptical (proportionally flatter) outline of the medullary cavity, thicker cortices (%CA of 75.7 % in TM 1517, vs. 63.2 % in Humans) and a looser connection between the antero-posterior vs. medio-lateral second moments of area (Ix/Iy of 0.43 in TM 1517 and av. of 0.92 in Humans), as well as a higher maximum vs. minimum second moments of area (Imax/Imin of 2.43 in TM 1517 and av. of 1.94 in Humans). At the proximal femur, *P. robustus* also provides evidence for a lower degree of supero-inferior asymmetry of the femoral neck (av. S/I ratio of 0.72 at the base of neck and 0.91 at mid-neck) than in Humans (av. S/I ratio of 0.30 at the base of neck and 0.43 at mid-neck), and, importantly, reveals a uniquely thicker anterior wall. The outline of the patella SKX 1084 occupies a somehow intermediate morphospace compared to the multifaceted human patella, which bears several distinctly angulated planes, and the simpler articular morphology found in *Pan*, where the posterior surface is relatively smooth.

In *P. robustus*, some specificities are also found in the local textural arrangement and density of the trabecular network which are lacking, or are very uncommon, in both Humans and chimpanzees. At the distal epiphysis of the humerus, medio-lateral structural features in the South African fossil assemblage imply a denser medial bundle compared to a vertical lateral bundle, characterised by well oriented thin and long struts, while the trabecular pattern is more homogeneous between the two sides. At the proximal femur, in addition to trabecular thickening observed at some spots along the supero-lateral neck portion of the arcuate bundle, the presence of plate-like structures in the inferior neck trait of the vertical bundle and towards the diaphyseal medial cortex is common in *P. robustus*, while in Humans, it is rather localised, also contrasting with the homogenous organisation observed in *Pan*. Specifically, at the proximal femur we identified the following unique features in *P. robustus*: (i) a variably medially arched vertical bundle, notably in its head portion, absent in both Humans and *Pan*; (ii) an origin of the arcuate bundle systematically set below the fovea capitis, while in extant Humans it usually reaches, or even exceeds, the level of the depression (the condition in *Pan* remains to be assessed); (iii) a vertical bundle which extends quite laterally along the inferior margin of the neck to the medial diaphyseal cortex, which seems to correlate with the typically longer femoral neck shared by australopiths and early *Homo*; (iv) a greater trochanter cancellous infill of intermediate density between the proportionally looser human network and the denser honeycomb pattern typical of *Pan*; (v) thickened and well-oriented struts of the trochanteric bundle, while the extant human pattern typically shows increasing bone loss in this

area, including in young adults. In the patella SKX 1084, the relatively honeycomb-like appearance of the cancellous bone and the slightly less structured medial aspect, have not been observed in our comparative human and ape samples.

Given some uncertainties concerning the identity of isolated postcranial remains from the South African fossil hominin-bearing caves, we predict that the list of features identified in this study - which should be refined and extended by additional research - may contribute to their identification, notably with respect to the alternative taxonomic allocation to early *Homo* or *Australopithecus* representatives. Our results provide unambiguous evidence of a lower degree of cortex asymmetry at the femoral neck in *P. robustus* (av. S/I of 0.72 at the base of neck and 0.91 at mid-neck) than previously reported using an XCT-based record (Ruff and Higgins, 2013; av. S/I of 0.45 at the base of neck and 0.87 at mid-neck). This result amplifies the extent of the already documented differences between the less asymmetric condition of *P. robustus* and the highly asymmetric pattern measured in *A. afarensis*, whose condition is hardly distinguishable from the recent human one (Ohman et al., 1997; Lovejoy et al., 2002; Ruff et al., 2016). However, the general cancellous configuration at the femoral head in some *A. africanus* specimens imaged by Ryan et al. (2018; e.g., StW 99 and StW 479: fig. 2) is similar to that observed in *P. robustus*. The variably medially convex vertical bundle, especially in its head portion, seen in *P. robustus* but not expressed in Humans nor in *Pan*, is present in StW 311 and StW 501 (Ryan et al., 2018). An origin of the arcuate bundle confined below the fovea capitis and a looser appearance of the network in the so-called "Ward's triangle" area is also noticeable in *A. africanus* (Ryan et al., 2018). Thicker and well-oriented struts within the trochanteric bundle, lacking in Humans and *Pan*, are another shared feature in *P. robustus* and *A. africanus* (e.g., StW 479; Ryan et al., 2018). Finally, a human-like pattern of trabecular anisotropy and orientation in *P. robustus* has also been identified by Ryan et al. (2018) in *A. africanus* (av. DA of 0.61). Similarly, a pattern of higher BV/TV values than typical in Humans also characterises the femoral head of *A. africanus* (Ryan et al., 2018; av. BV/TV of 0.59% in *A. africanus* vs. 0.39 % in Humans).

According to our results, and supported by some information available in the literature, the following features at the distal humerus distinguish *P. robustus* from early *Homo* (as represented in our study by the *H. erectus*-like specimen GOM IB from Melka Kunture, Ethiopia): (i) a distinctly elliptically-shaped medullary cavity, while in *Homo*, the medio-lateral vs. antero-posterior diameter ratio more closely approaches the extant human condition; (ii) a lower percent of cortical area (%CA of 75.7 % in TM 1517 and 89.7% in GOMB IB); (iii) a

lower variation in the ratio of antero-posterior vs. medio-lateral second moments of area (Ix/Iy of 0.43 in TM 1517 and 0.51 in GOMB IB), even if a dominant maximum rigidity in the medio-lateral plane is shown by all specimens; (iv) a pattern of proximo-distal thinning in cortical bone distribution, while the opposite has been measured in the early *Homo* representative used in our study (-42% in SKX 10924 and -66% in SKX 34805 vs. +61% in GOMB IB); (v) a less developed and thinner lateral supracondylar crest than GOM IB (but we still ignored if this feature is sex- and/or body-size dependent). It should also be pointed out that, at the distal humeral shaft, the three fossil specimens from South Africa, show numerous and absolutely thicker trabeculae compared to the *H. erectus*-like representative. *H. erectus* displays fewer and less projecting struts mostly confined to the far distal end, likely in association with its narrower lumen resulting from a thicker cortex. In this respect, it is noticeable that, as seen in *P. robustus*, the medullary cavity of the OH 80-10 distal humerus fragment from the *P. boisei* partial skeleton of Olduvai Gorge, Tanzania, is also filled by trabecular bone (Dominguez-Rodrigo et al., 2013). A more oblique orientation component of the maximum rigidity at the humeral distal shaft, i.e., a less stereotyped medio-lateral maximum rigidity at the humero-ulnar joint than in Humans, characterises *P. robustus*, which also reveals a less developed m. brachioradialis than seen in early *Homo* (GOMB IB). This may be relevant in comparatively assessing biomechanical behaviour, as the m. brachioradialis in *P. robustus* is responsible for flexion of the forearm, pronation of a supine forearm, and supination of a prone forearm, while in Humans this muscle is associated with differences in flexion to extension movement patterns at the elbow (Rhodes and Knüsel, 2005).

It appears increasingly evident that Plio-Pleistocene hominins displayed a variety of skeletal adaptations for habitual terrestrial bipedalism (e.g., Stern, 2000; Ward, 2002, 2013; Ruff et al., 2016). However, various aspects of their taxon-specific gait kinematics, including in *Paranthropus*, remain unresolved, or are controversial (e.g., DeSilva et al., 2013, 2018; Ruff and Higgins, 2013; Harcourt-Smith, 2016; Hatala et al., 2016; Su and Carlson, 2017). In this context, the results of the present research project provide support for some previous conclusions concerning the locomotor-related biomechanical environment of *P. robustus*, but also adds new information.

As previously noted, cortical bone distribution at the femoral neck indicates that *P. robustus* and *A. africanus* walked with broad human-like hip kinematics associated with a limited range of habitual hip joint postures (Ryan et al., 2018). This observation is supported by the relatively small patella SKX 1084, close to the *A. sediba* proportions, as well as by its

trabecular arrangement, which suggests a response to more stereotypic loading conditions. According to previous results, *P. robustus* experienced a greater lateral displacement of the body centre of gravity over the stance limb during the support phase of gait, a condition engendering a more vertical hip joint reaction force and bending increase relative to the neck axial loadings (Ruff and Higgins, 2013). Similar to *A. africanus*, *P. robustus* also supported higher musculoskeletal loading at the hip joint than likely experienced by *Homo* (Ryan et al., 2018). However, anterior and posterior strains would decline in the mechanical condition of a more vertical hip joint reaction force and bending would increase relative to the neck axial loadings, likely characterising the *P. robustus* femoral neck. Therefore, the distinctly thicker anterior wall detected in this study in *P. robustus* (av. 2.72 mm), absent in both Humans (av. 1.31 mm) and *Pan* (av. 2.25 mm) (Ohman et al., 1997, but see the results of our *Papio* specimens in section 3.2.2.3), could result from the unique australopith architecture combining a longer, supero-inferiorly expanded and antero-posteriorly relatively compressed femoral neck. Whenever the antero-posterior asymmetry in *Australopithecus* is closer to the human pattern, or even reveals another configuration, it would imply different hip joint loading conditions in the two extinct hominins, probably resulting from non-fully overlapping locomotor modes. Finally, while the trabecular organisation of the femoral neck might not fully reflect direct loadings, it is still possible that the trochanteric region, which remains unexplored in extant and extinct hominids, is sensitive to the relative development and action of the hip abductor muscles.

As a whole, our results provide information of both palaeomechanical and palaeobiological potential interest regarding the taxon *P. robustus*. At the femoral head and neck, all likely male specimens show a higher BV/TV ratio (av. 40.3% vs. 32.3% in the likely females), also associated with thicker trabeculae (av. 0.21 mm) than measured in the two likely female individuals represented in our sample (av. 0.15 mm). In addition, the only likely female *P. robustus* specimen available for measurements at mid-neck, shows much thinner cortices compared to the likely males (superior thickness of 1.80 mm and inferior thickness of 2.50 mm vs. av. 2.68 mm and 2.87 mm in the likely male individuals). However, it should be noted that a higher BV/TV has not been measured by Ryan et al. (2018) at the femoral head centre in the two likely male *P. robustus* specimens included in their study. In this respect and also in the perspective of testing the impact of intra- and interspecific body size variation on cancellous bone (e.g., Doube et al., 2011; Barak et al., 2013a; Fajardo et al., 2013; Ryan and Shaw, 2013; Tsegai et al., 2018) and the possible metabolic effects in *Paranthropus* of its suggested

bimaturism growth pattern (Lockwood et al., 2007; see also Susman et al., 2001), additional information is necessary from other sites of the fossil hominin postcranial skeleton to be compared to the evidence available from extant apes (e.g., Tsegai et al., 2018).

Besides corroborating the original suggestion that the three postcranial specimens TM 1517g, TM 1517e and TM 1517k and the holotype skull TM 1517a, b, c represent a single still growing *P. robustus* individual (Broom, 1938b, 1942, 1943; Thackeray et al., 2001, 2005; Braga et al., 2013, 2016a, b; Skinner et al., 2013), our detailed analysis of the distal humerus, the proximal ulna and the distal hallucial phalanx labelled as TM 1517 provides original information on the odontoskeletal maturation pattern in *P. robustus*. Indeed, the results suggest that the skeletal maturation schedule of TM 1517 shows some synchrony with both the human and chimpanzee male reference data. The inner structure of the three elements, with a completely fused distal humerus, but the remnant of a recent fusion still discernible at the proximal ulna and the distal hallucial phalanx, indicates that the sequence of epiphyseal fusion in TM 1517 is slightly closer to the *Pan* condition than to the human pattern. In Humans, fusion of the distal hallucial phalanx, on average, slightly precedes that of the distal humerus (Cunningham et al., 2016), while in chimpanzees, the distal humerus tends to fuse earlier, followed by the distal hallucial phalanx and the proximal ulna (Birmacombe et al., 2014; Cameron et al., 2017).

Table 4.A. Summary of the cortico-trabecular condition/features observed at various postcranial sites in *Australopithecus*, early *Homo* (including *erectus*-like), Neanderthals, extant Humans, *Pan*, *Gorilla*, and *Papio* with respect to the reference condition/features expressed in *Paranthropus robustus*. << : sensibly lower value; < : lower value; -- : sensibly less developed/expressed; - : slightly less developed/expressed; ≅: comparable/similar; > : higher value; >> : sensibly higher value; + : slightly more developed/expressed; ++ : sensibly more developed/expressed; ≠ : different condition; ? : uncertain condition; n.a. : not available information.

***P. robustus* condition**	***Australopithecus***	**early *Homo***	**Neanderthals**	**extant Humans**	***Pan***	***Gorilla***	***Papio***
DISTAL HUMERUS							
CORTICAL BONE							
percent of cortical area (%CA): 72.4-75.7%	n.a.	>	n.a.	<	n.a.	n.a.	n.a.
antero-posterior vs. medio-lateral second moments of area (Ix/Iy): 0.35-0.43	n.a.	>	n.a.	>>	n.a.	n.a.	n.a.
maximum vs. minimum second moments of area (Imax/Imin): 2.43-2.94	n.a.	<	n.a.	<<	n.a.	n.a.	n.a.
proximo-distal cortical thinning (generalised)	n.a.	≠ (thickening)	n.a.	variable condition	n.a.	n.a.	n.a.
marked proximo-distal amount of cortical variation (generalised)	n.a.	>	n.a.	variable condition	n.a.	n.a.	n.a.
amount of proximo-distal cortical variation across the anterior aspect > posterior	n.a.	≅	n.a.	≅	n.a.	n.a.	n.a.
thinnest cortex: at the disto-lateral portion of the posterior aspect	n.a.	anteriorly, antero-laterally and along the mid-third of the posterior aspect	n.a.	anteriorly, antero-laterally and along the mid-third of the posterior aspect	n.a.	n.a.	n.a.

thickest cortex: at the postero-medial and proximal parts of the anterior aspect	n.a.	at the disto-lateral portion of the posterior surface	n.a.	at the disto-lateral portion of the posterior surface	n.a.	n.a.	n.a.
cortex at the medial crest: relatively thin	n.a.	≠ (relatively thick)	n.a.	≅	n.a.	n.a.	n.a.
TRABECULAR BONE							
trabecular thickness at the distal shaft: 0.41-0.61 mm	n.a.	≅	n.a.	<<	n.a.	n.a.	n.a.
numerous projecting trabeculae across the shaft	n.a.	<<	n.a.	<<	n.a.	n.a.	n.a.
presence of a medial bundle-like structure extending from the upper towards the lower portion of the olecranon fossa	n.a.	n.a.	≅	n.a.	n.a.	n.a.	n.a.
thick rod-like trabeculae forming the medial bundle-like structure of the distal epiphysis	n.a.	n.a.	--	n.a.	n.a.	n.a.	n.a.
presence of a lateral bundle-like structure extending from the upper portion of the lateral epicondyle towards the lower portion of the olecranon fossa	n.a.	n.a.	≅	n.a.	n.a.	n.a.	n.a.
thin, long and well-oriented trabeculae forming the lateral bundle-like structure of the distal epiphysis	n.a.	n.a.	--	n.a.	n.a.	n.a.	n.a.

PROXIMAL FEMUR							
CORTICAL BONE							
S/I cortical thickness ratio at the base of neck: 0.68-0.76	<< (1-3)	n.a.	n.a.	<< (1-4)	>> (1-4)	>> (1-4)	≅
average S/I cortical thickness ratio at the base of neck: 0.60-0.78	n.a.	n.a.	n.a.	<<	>>	n.a.	n.a.
S/I cortical thickness ratio at mid-neck: 0.71-0.96	</<< (1,2)	n.a.	n.a.	<< (1,2,4)	≅ (1,2,4,5)	>> (4)	≅ (5)
average S/I cortical thickness ratio at mid-neck: 0.67-0.96	n.a.	n.a.	n.a.	<<	≅	n.a.	n.a.
latero-medial S/I ratio increase across the neck	n.a.	n.a.	n.a.	≅	≠ (decrease)	≠ (decrease)	≅
cortical thickness of the anterior aspect > posterior	n.a. (but see 4)	n.a.	n.a.	- (4)	- (4)	- (4)	≅
latero-medial decrease in cortical thickness across the anterior and posterior walls	n.a.	n.a.	n.a.	≅	-	--	-
(likely) degree of sexual dimorphism in cortical thickness: - superior thickness at mid-neck: M = 2.68 mm, F = 1.80 mm - average superior thickness at mid-neck: M = 2.34 mm, F = 1.76 mm	n.a.	n.a.	n.a.	<<	n.a.	n.a.	n.a.

- inferior thickness at mid-neck: M = 2.87 mm, F = 2.50 mm - average inferior thickness at mid-neck: M = 2.64 mm, F = 2.64 mm - S/I cortical thickness at mid-neck: M = 0.91 mm, F = 0.71 - average S/I cortical thickness at mid-neck: M = 0.86, F = 0.67 mm							
TRABECULAR BONE							
topographic heterogeneity of the network across the whole epiphysis	≅ (6)	n.a.	n.a.	≅ (6)	-- (6)	? (6)	? (6)
thickest struts at the supero-lateral neck							
head: - bone density: 31.5-44.6%	≅ (6)			< (6)	≅/> (6)	≅ (6)	> (6)
- strut thickness: 0.14-0.23 mm	n.a.	n.a.	n.a.	</≅	</≅	>	≅
- degree of anisotropy: 2.56-3.70	≅ (6)			≅ (6)	< (6)	< (6)	? (6)
neck: - bone density: 50.4-57.3%				≅	≅		
- strut thickness: 0.31-0.37 mm	n.a.	n.a.	n.a.	≅	<	n.a.	n.a.
- degree of anisotropy: 3.39-4.99				>	</≅		
medial vertical bundle:		n.a.	n.a.				
- distinct	≅ (6)			≅ (6)	-- (6)	-/? (6)	-/? (6)
- infero-medially convex	≅ (6)			≠ (6)	≠ (6)	≠ (6)	≠ (6)

- extended laterally to the medial diaphyseal cortex	≅ [1,6]			≅ [6]	≅ [6]	≅ [6]	≅ [6]
- presence of plate-like structures	≅ [6]			++ [6]	+ [6]	? [6]	? [6]
lateral arcuate bundle:							
- distinct	≅ [6]			≅ [6]	-- [6]	-/? [6]	-/? [6]
- origin adjacent/below the *fovea capitis*	≅ [6]	n.a.	n.a.	≠ (it can reach, or even exceed, the upper rim of the depression) [6]	≅/? [6]	≅/? [6]	≅/? [6]
- extended to the lateral diaphyseal cortex	n.a.			≅	≅	≅/?	≅/?
trochanteric bundle:							
- distinct				≅	-		
- latero-medially projecting trabeculae displaying an arched outline	n.a.	n.a.	n.a.	≅	-	?	?
- relatively thick trabeculae				-	+		
- relatively well-oriented trabeculae				≅	-		
greater trochanteric bundle-like structure:							
- distinct	n.a.	n.a.	n.a.	≅	?	?	?
- dense network				-	?	?	?
Ward's triangle:							
- loose	n.a.	n.a.	n.a.	≅	-	- [6]	?
- thick trabeculae				-	≅	≅ [6]	
(likely) degree of sexual dimorphism in bone density of the head: M = 40.3%, F = 32.3%	n.a.	n.a.	n.a.	<<	n.a.	n.a.	n.a.
(likely) degree of sexual dimorphism in bone density of the neck:	n.a.	n.a.	n.a.	<<	n.a.	n.a.	n.a.

M = 55.9%, F = 50.4%							
(likely) degree of sexual dimorphism in trabecular thickness of the head: M = 0.21 mm, F = 0.15 mm	n.a.	n.a.	n.a.	<<	n.a.	n.a.	n.a.
(likely) degree of sexual dimorphism in trabecular thickness of the neck: M = 0.36 mm, F = 0.31 mm	n.a.	n.a.	n.a.	<<	n.a.	n.a.	n.a.
PATELLA							
CORTICAL BONE							
cortico-trabecular complex relative thickness: 7.2-9.6%	n.a	n.a	≅	≅	>>	n.a.	n.a.
TRABECULAR BONE							
honeycomb-like appearance of the network	n.a	n.a	-	-	+	n.a.	n.a.
topographic heterogeneity across the whole bone	n.a	n.a	≅	≅	-	n.a.	n.a.
trabecular bone volume > cortical bone volume	n.a	n.a	≅	≅	--	n.a.	n.a.
denser area at the supero-lateral margin	n.a	n.a	≅	≅	≠	n.a.	n.a.
radially-oriented trabeculae around the patellar margin in coronal view	n.a	n.a	≅	≅	≠	n.a.	n.a.
vertically-oriented anterior bundle	n.a	n.a	≅	≅	≠	n.a.	n.a.
bone density:	n.a	n.a	<	<<	>>	n.a.	n.a.

38.6-40.4%							
strut thickness: 0.19-0.20 mm	n.a	n.a	<	<	>	n.a.	n.a.
degree of anisotropy: 2.73-3.83	n.a	n.a	≅/>	≅/>	<	n.a.	n.a.
SKELETAL GROWTH							
when (C A_c, P3 A_c, P4 $A_{1/2,}$ M2 $A_{1/2}$) M3 $R_{1/2}$-$R_{3/4}$: - no remnant of the epiphyseal line of the distal humerus - medial remnant of the epiphyseal line of the proximal ulna - faint remnant of the proximal epiphyseal line of the distal hallucial phalanx	n.a.	n.a.	n.a.	- distal humerus completely or nearly fused - upper end ulna completely or nearly fused - proximal end distal hallucial phalanx fused	- distal humerus completely or nearly fused - upper end ulna in fusion - proximal end distal hallucial phalanx fused or in fusion	n.a.	n.a.
epiphyseal fusion chronological sequence: - distal humerus > distal hallucial phalanx > proximal ulna	n.a.	n.a.	n.a.	- distal hallucial phalanx < distal humerus	≅	n.a.	n.a.

[1] Lovejoy et al., 2002
[2] Ruff and Higgins, 2013
[3] Ruff et al., 2016
[4] Ohman et al., 1997
[5] Rafferty, 1998
[6] Ryan et al., 2018

5. Perspectives

The results presented and discussed in this PhD dissertation on the inner structural organisation of the elbow (see supra section 3.1), the hip (section 3.2) and the knee joints (section 3.3) of *Paranthropus robustus* have provided new qualitative and quantitative evidence contributing to the assessment of the functional requirements having shaped the cortical and cancellous bone conformation at these skeletal sites. A number of features/characteristics of potential taxonomic significance for the identification of isolated and fragmented hominin remains from commingled fossil assemblages have been revealed. From the results, the hypothesis that *Australopithecus* (at least, *A. afarensis*) and *Paranthropus* (notably, *P. robustus*) likely practiced different forms of terrestrial bipedality because of differences in cortical bone distribution at the femoral neck compartment, and of other subtle details in trabecular organisation at the proximal femoral end (compare the body of evidence from Lovejoy et al., 2002; Ruff and Higgins, 2013; Ruff et al, 2016; Ryan et al., 2018 to the results presented in the section 3.2) has been proposed. However, our analyses mainly focussed on just one component of the hip joint only, being the proximal femur, and did not integrate the iliac component. In addition, a possible heterogeneity in the functional meaning of the structural information across different regions of the proximal femoral end, remains to be explored in greater detail.

5.1. Topographic structural variation across the proximal femur

As mentioned throughout the present manuscript, both cortical and trabecular bone is sensitive to loadings. Whenever appropriately decoded, their local structural arrangement can thus be used as a kind of litmus test for reconstructing biomechanical behaviour in early hominins through the analysis of their fossil remains. However, the ability to meaningfully interpret variation in the inner bony morphology of a functional structure - such as a joint - depends on the extent to which bone properties - notably those of the cancellous network - locally vary in response to topographic loading variation. By means of a number of uniaxial compressive and tensile mechanical tests applied to the human lumbar spine, the femoral greater trochanter, the femoral neck and the proximal tibia, Morgan and Keaven showed already in 2001, that the yield strains of the human trabecular bone are site-dependent. More recently, by comparing trabecular bone structure throughout the lower limb between a group of highly

mobile foragers and two groups of sedentary agriculturalists, Saers et al. (2016) revealed a similar pattern of trabecular proximo-distal limb tapering, with a bone volume fraction decreasing while anisotropy increases proximo-distally throughout the lower limb in all populations. Even within a given limb, trabecular bone does not appear to respond in a stereotypical way in all areas to the loadings associated with a given locomotor behaviour (Carlson et al., 2008; Wallace et al., 2012). Subchondral bone responds to loading of the complementary joint surface, while trabecular bone responds to forces traveling through the bone in question. Furthermore, trabecular bone functional adaption appears to be more localised than that of cortical bone (Rubin et al., 2001, 2002; Judex et al., 2004; Barak et al., 2011). In the human knee, for example, depth-dependent changes in trabecular structural parameters were observed across the first 6 mm of the investigated cores and differences between the medial and lateral compartments were reported (Patel, 2003; Touraine et al., 2017). In this regard, some studies (Fajardo et al., 2007; Shaw and Ryan, 2012; Hébert et al., 2012) have noted the overall complexity in trabecular responses, suggesting that inferred loading environments in skeletal joints may not be decipherable in a straightforward fashion unless specific suites of properties are examined (Ryan and Shaw, 2012).

Studies having comparatively assessed the trabecular organisation of the femoral head in primate taxa, displaying different locomotor behaviours, provide convincing evidence for structural differences in architecture across locomotor groups, where repetitive/stereotypical loading patterns are commonly associated with anisotropic networks and heterogeneous/variable patterns with isotropic trabecular patterns (e.g., Fajardo and Müller, 2001; MacLatchy and Müller, 2002; Ryan and Ketcham, 2002a, b, 2005; Ryan and Krovitz, 2006; Ryan and Walker, 2010; Saparin et al., 2011; Ryan and Shaw, 2012, 2015; Shaw and Ryan, 2012; Raichlen et al., 2015; Ryan et al., 2018; Tsegai et al., 2018). However, to the best of our knowledge, evidence of topographic variation in cancellous network organisation assessed in detail across the different compartments of the proximal femur, is still poorly reported, including in extant Humans.

We plan to extend the analyses summarised in the manuscript HUMEV_2018_160 under review in the *Journal of Human Evolution* (see supra section 3.2.1) by systematically sampling different homologous VOIs across the femoral head, the neck and the great trochanter in the human and chimpanzee extant specimens forming our comparative reference samples, and to compare such results the *P. robustus* SWT1/LB-2 from Swartkrans, whose trabecular architecture is remarkably well preserved (see supra section 3.2.1). With the assumption that each selected VOI represents a functionally related site-specific signature, the goal of

elaborating and expanding this research is to test the hypothesis that, given their ascertained (*Homo* vs. *Pan*) and inferred (*Paranthropus*) locomotory differences, the three taxa do not share the same topographic pattern of structural adaptation. This is probably due to a differential degree in local bone sensitivity exactly resulting from differential multiaxial loadings.

In this perspective, we also plan to preliminarily detail the topographic structural organisation of some proximal femurs already available in our µXCT files representing pathological/clinical cases of individuals who experienced serious imbalance in locomotion (e.g., following one leg amputation). The specimens illustrating these conditions are selected from the R.A. Dart skeletal collection at the University of the Witwatersrand, Johannesburg, the Pretoria Bone Collection stored in the Department of Anatomy at the University of Pretoria and the Department of Anatomy and Histology of the Sefako Makgatho Health Sciences University, Pretoria.

5.2. Cancellous organisation of the australopith coxo-femoral complex

As presented in the introduction of the manuscript HUMEV_2018_160, a suite of features differentiate the australopiths (*Australopithecus* and *Paranthropus*) from the uniquely derived human pelvic condition (rev. in Churchill and Vansickle, 2017; see supra section 3.2.1). These differences broadly result from two main evolutionary steps: the establishment, perhaps since the Late Miocene, of a functional morphology allowing facultative bipedalism to become the obligatory mode of locomotion (e.g., Thorpe et al., 2007; Lovejoy et al., 2009), followed, in the Late Pliocene-Early Pleistocene, by the architectural adjustments necessary to enlarge the birth canal in response to increased encephalisation (Ruff, 1995). Related to this issue, the concept of "obstetrical dilemma" first introduced by Washburn (1960), implies that selective pressures of the structural demands of bipedal gait in the human lineage faced those birthing larger brained neonates. In this evolutionary context, because the hip joint supports weight bearing-related loads and undergoes shape-related biomechanical demands during mobility, variations in pelvic and femoral morphology among past and extant hominins have also been considered in a more comprehensive and broad mechanical and functional perspective (e.g., Lovejoy, 1988; Ruff, 1995, 2017; Lovejoy et al., 2002; Ruff and Higgins, 2013; Warrener, 2017).

Recent evidence of a blend of primitive and modern-like traits characterising the pelves of *A. sediba*, *H. erectus*, *H. naledi* and *H. floresiensis* suggests that the picture may be even more complex than previously assumed (VanSickle, 2016). Because relatively large-brained later hominins might retain an australopith pelvis and hip shape, whereas small-brained older

ones occasionally display some human-like derived features, the deterministic explanation of a brain volume-related adaptation no longer appears as fully satisfactory. In this regard, P. Shipman stated that "the conflict between big-brained babies and upright walking may be more conceptual than real" (Shipman, 2013: 428). She also noted that, as pregnancy may push human mothers to their "metabolic limits" (Ellison, 2009), metabolism, rather than locomotion *s.s.*, might ultimately be a major limiting factor in human birth size. If so, the hominin pelvic evolutionary trajectory(ies) could also have been shaped by several ecological pressures, including gait speed, balance, risk of injury, thermal environment and dietary energy availability (rev. in Wells et al., 2012).

New analytical approaches to elucidate this still unresolved "obstetrical dilemma" thus seem necessary, notably for clarifying the role played by locomotor adaptations in driving hominin pelvic morphology.

The inner structural organisation of the pelvis is intimately related to the balanced requirements for locomotion and obstetrics, both having experienced strong selective pressures across the Plio-Pleistocene. Accordingly, when investigated together as a single functional unit, the cortical and trabecular arrangement of the ilium and of the proximal femur might represent a more sensitive and reliable proxy to deconstruct the complex and multiaxial biomechanical demands at the hominin hip joint.

Distinct functionally related architectural variation in the extant primate cancellous network of the iliac blade has been shown by Correnti (1955) in a classical anatomical study describing two principal systems: the "osteomeric", i.e., limited to circumscribed portions of the bone, and the "idiobadismatic", i.e., gait-related. The gait-related system, which is divided into marginal (ectochoric) and arcuate (internal, or endochoric) sections, reflects significant structural differences related to locomotion. Within the arcuate system, two trabecular structures, especially defined in Humans, are said to assure the absorption, dissipation, and distribution of the loads generated during typical striding gait; These are: (i) the ilio-ischial bundle (iib), originating from the region of the tubercle of the iliac crest, posterior to the anterior spines, and running diagonally downwards and backwards with an arcuate trajectory as far as the ischial tuberosity; (ii) the strong and undivided sacro-pubic bundle (spb), arising from the auricular surface and the posterior superior and posterior inferior iliac spines and running diagonally downwards and forwards along the ilio-pectinal line as far as the pubic symphysis. They converge towards the central-lower portion of the blade of the ilium and finally cross, defining a well-structured chiasma located over the acetabulum (Correnti, 1955; Macchiarelli et al., 1999, 2001; Volpato, 2007) (Fig. 5.2.A).

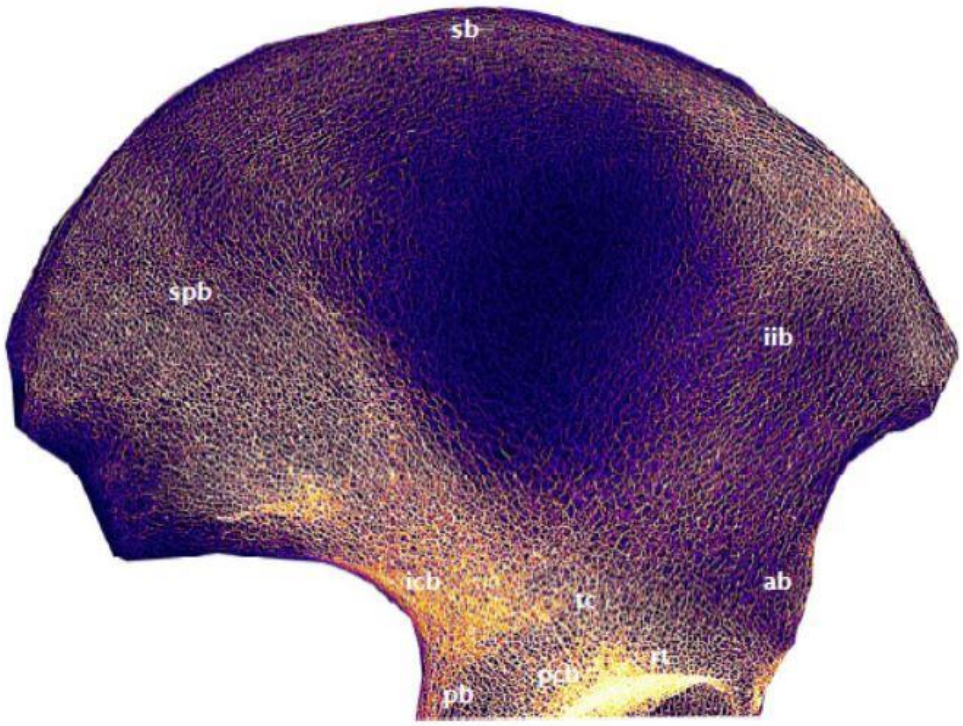

Fig. 5.2.A. Trabecular architecture of the human ilium. ab: anterior bundle; icb: ilio-cotyloid bundle; iib: ilio-ischial bundle; pcb: pericotyloid bundle; pb: posterior bundle; rt: radial trabeculae; sb: superior bundle; spb: sacro-pubic bundle; tc: trabecular chiasma. Dimensions not to scale. (Extracted from Volpato, 2007).

Some human-like trabecular structures are found in the australopith hip bone. They include: an ilio-ischial bundle (iib); a distinct or even strong sacro-pubic bundle (spb); an area of relatively higher density along the superior marginal bundle (sb) located in proximity to the antero-superior rim of the blade; a thin and fan-shaped ilio-cotyloid bundle (icb) arising from the greater sciatic notch margin; and also a supra-acetabular crossing (tc) located at the level of the sciatic notch. However, differences with respect to the human condition are mainly represented by some less developed and less distinct marginal and arcuate trabecular structures, including: a less developed superior (sb) and anterior (ab) marginal bundles running in the superior and anterior margin of the ilium respectively; a less distinct ilio-ischial bundle (iib), consisting of thinner and fewer trabeculae; lower-density supra-acetabular and pericotyloid areas, showing a lower number of radial trabeculae (rt) and a thinner pericotyloid bundle (pcb) respectively; a fan-shaped, rather than diagonal supra-acetabular full crossing (tc); a smaller

distinction between the cancellous network of the supra-acetabular area and the iliac fossa; higher proportion of low-density, open-cell, rod-like structures; and, mostly, a less anisotropic appearance of the cancellous network as a whole (Macchiarelli et al., 1999, 2001) (Fig. 5.2.A, Fig. 5.2.B).

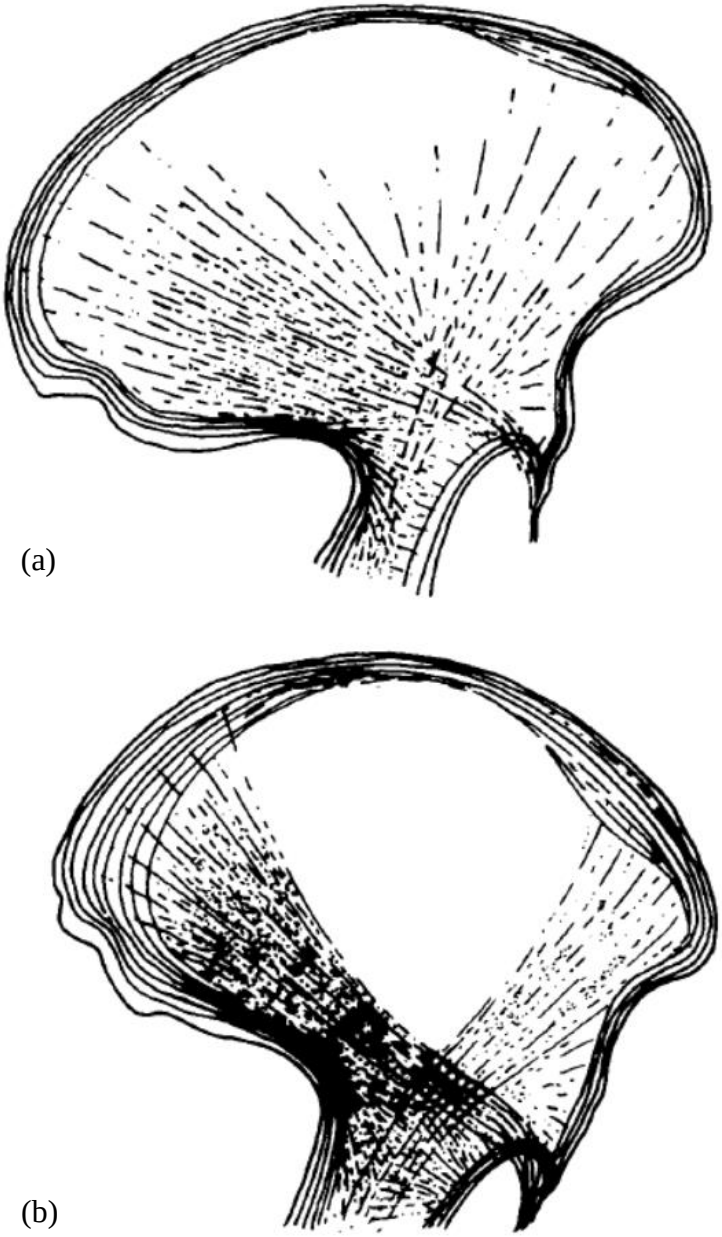

Fig. 5.2.B. Schematic model of the australopith (a) and the human (b) trabecular architecture of the late adolescent-adult ilium (as reconstructed by Macchiarelli et al., 1999). Dimensions not to scale; contours approximate.

Such structures can be roughly figured as consisting of (thinner) spaghetti-, (thicker) tagliatelle-, and (intermediate) linguine-like oriented strings/strips sandwiched within the ilium. Local cortical bone properties of the ilium vary markedly as well (Volpato, 2007). The strings/strips 'move' towards the hip joint, where they 'uninterruptedly' flow into essentially spaghetti-like analogous bundles, finally transmitting the charges to the proximal femoral end.

As noted in the manuscript HUMEV_2018_160, studies involving the australopith proximal femur have increasingly integrated information concerning the arrangement of the cortical and cancellous bone to provide additional evidence on the mechanical environment at the hip joint, thus contributing to the reconstruction of the locomotor behavioural patterns. However, while the australopith upper femoral end has been researched in some studies by using three-dimensional imaging techniques (see Ryan et al., 2018), the endostructural features of the iliac blade in some australopith representatives have been uniquely assessed by radiographs (Macchiarelli et al., 1999, 2001). So far, no study of the inner structural organisation of the hominin hip joint has simultaneously examined, as a functional 3D unit, the combined cortical and trabecular signature of the ilium, on the one hand, and of the femoral head, the neck, the trochanter region and the proximal shaft, on the other hand.

To fill this gap and to progress in the understanding of the adaptive biomechanical demands and evolutionary processes having shaped the hominin coxo-femoral complex as a whole, we plan to comparatively model the cortical and cancellous organisation of the extant human and australopith hip bone and proximal femur as a unitary functional structure by applying finite element analysis (FEA) to our high resolution µXCT records. The results will be compared with strain vectors obtained from FEA simulations of bipedal weight bearing in a simplified model of a hominin pelvis and hip joint warped to vary the form of the birth canal and of the parts of the pelvis and femur that provide attachment (or leverage) for muscles to explore the interplay of obstetric and locomotor demands. These findings should allow to assess the extent to which obstetrically required changes in pelvic and hip joint morphology interact with locomotor demands to determine trabecular architecture.

In addition to the record of the five *P. robustus* proximal femora considered in our manuscript HUMEV_2018_160 (SK 82, SK 97, SK 3121, SKW 19, SWT1/LB-2), we have already scanned at the South African Nuclear Energy Corporation (Necsa) the remains of five australopith hip bones by µXCT (isotropic voxel size ranging from 64 µm to 100 µm) and partially elaborated on it by virtual imaging techniques. These remains are stored at the Ditsong National Museum of Natural History, Pretoria, and at the Evolutionary Studies Institute of the University of the Witwatersrand,

Johannesburg: Sts 14, Sts 65, TM 1605, SK 50, and SK 3155b, sampling both *Australopithecus* and *Paranthropus*.

Critical to our exploratory study is the highly preserved partial ilium TM 1605, attributed to a late adolescent *P. robustus* from Kromdraai (Fig. 5.1.C), which should be articulated by virtual hafting to the similarly well-preserved proximal femur SWT1/LB-2, the specimen having revealed a highly detailed topographic signature of its inner structure. As comparative material, we plan to use some extant human adult hip bones and associated femora selected from the Pretoria Bone Collection at the Department of Anatomy of the University of Pretoria, all lacking any evidence of alteration or pathological change, already available in our files.

The first step of the research will consist of the 3D individualisation of the cortical and trabecular bone components of each fossil and comparative human specimen, by semi-automatic segmentation of the µXCT records with manual correction to generate templates of the iliac and femoral inner structures. Such distinct units will thus be virtually articulated (Fig. 5.2.C). The spaghetti- and tagliatelle-like bundles crossing the coxo-femoral joint will be identified on the composite model and quantitatively assessed for their topographic distribution, extension and orientation. The next step will be to virtually extract a number of VOIs at regular intervals along the bundles forming the integrated coxo-femoral trabecular complex and to measure their textural properties. Following these analytical steps, a simplified FEA model of an average human-australopith pelvis and hip will be constructed. This will be solid and loaded, and constrained according to muscle forces obtained from the biomechanical literature for walking. The predicted organisation of cortical and cancellous bone will then be compared with the modern human and australopith data. A series of experiments will then explore the relationship between pelvic and hip form and bone organisation in the cortical and cancellous regions by warping (birth related and locomotor related) aspects of pelvic anatomy in the model towards the human or australopith morphologies, while keeping constraints and muscle forces the same. These studies will allow us to infer the relative impacts of birth related and locomotor related aspects of form on cortical and trabecular architecture in the pelvis.

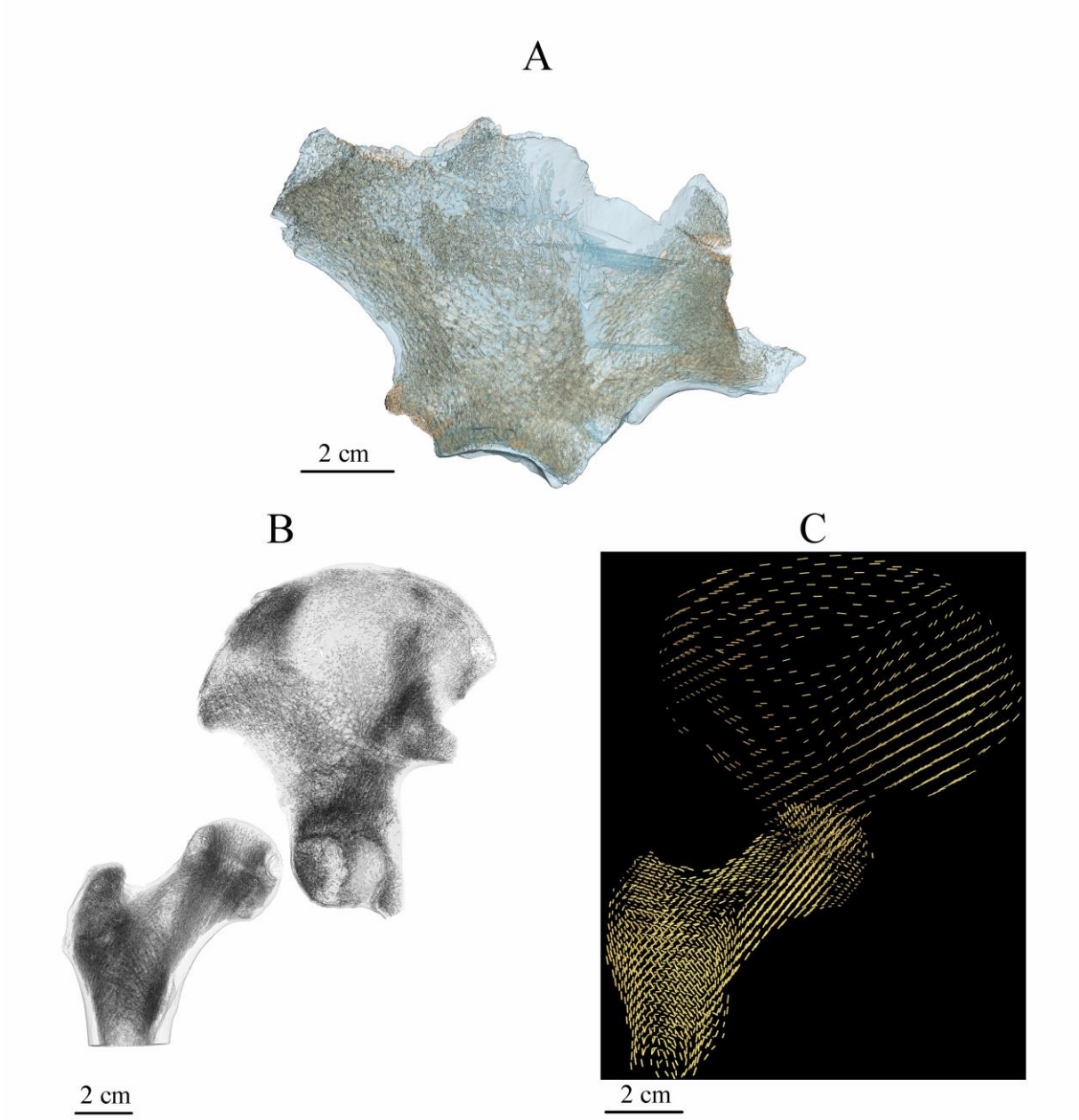

Fig. 5.2.C. µXCT-based lateral view in semi-transparency of the *P. robustus* partial ilium TM 1605 from Kromdraai, showing its preserved inner structure (A); reconstruction in semi-transparency of the articulating femur and pelvis in an extant human individual (female, aged 24 years; spec. from the Pretoria Bone Collection) (B); 3D scalar fields defined on a uniform lattice representing the local cancellous main orientation of the manually articulated (right) femur and hip bone of an extant Human (same individual as B), revealing the main trabecular bundles crossing the blade (C).

In principle, besides other possible details concerning the supra-acetabular "chiasmatic region", we expect to find differences between australopiths and extant Humans in the local arrangement and extension (3D depth) of the sacro-pubic bundle crossing the iliac blade and joining the proximal femur before dividing into vertical and lateral bundles. Accordingly, we will also test the hypothesis that some, likely minor, structural differences of potential locomotory relevance might also exist between *A. africanus* and *P. robustus*, as expression of a slightly different mechanical environment at the coxo-femoral joint. Finally, we expect to clarify the extent to which the structural organisation of the australopith coxo-femoral joint might also reflect individual differences in body mass and shape.

6. References

Aglietti P., Menchetti P.P.M., 1995. Biomechanics of the patellofemoral joint. In: Scuderi G.R. (Ed.), The patella. Springer, New York, pp. 25-48.

Agostini G., Holt B.M., Relethford J.H., 2018. Bone functional adaptation does not erase neutral evolutionary information. Am. J. Phys. Anthropol. 166, 708-729.

Aiello L.C., Dean C., 1990. An introduction to human evolutionary anatomy. Academic Press, New York.

Aiello L.C., Wood B., Key C., Lewis M., 1999. Morphological and taxonomic affinities of the Olduvai ulna (OH 36). Am. J. Phys. Anthropol. 109, 89-110.

Alemseged Z.Y., Coppens Y., Geraads D., 2002. A hominid cranium from Omo: Description and taxonomy of Omo-323-1976-896. Am. J. Phys. Anthropol. 117, 103-112.

Alemseged Z.Y., Spoor F., Kimbel W.H., Bobe R., Geraads D., Reed D., Wynn J.G., 2006. A juvenile early hominin skeleton from Dikika, Ethiopia. Nature 443, 296-301.

Alexander R., Jayes A.S., Maloiy G.M.O., Wathuta E.M., 1979. Allometry of the limb bones of mammals from shrews (Sorex) to elephant (Loxodonta). J. Zool. 189, 305-314.

AlQahtani S.J., Hector M.P., Liversidge H.M., 2010. Brief communication: The London atlas of human tooth development and eruption. Am. J. Phys. Anthropol. 142, 481-490.

Anyonge W., 1993. Body mass in large extant and extinct carnivores. J. Zool. 231, 339-350.

Arambourg C., Coppens Y., 1968. Decouverte d'un australopithecien nouveau dans les gisements de L'Omo (Ethiopie). South Afr. J. Sci. 64, 58-59.

Backwell L.R., Parkinson A.H., Roberts E.M., D'Errico F., Huchet J.-B., 2012. Criteria for identifying bone modification by termites in the fossil record. Palaeogeogr. Palaeoclimatol. Palaeoecol. 337-338, 72-87.

Bacon A.-M., 2000. Principal components analysis of distal humeral shape in Pliocene to recent African hominids: The contribution of geometric morphometrics. Am. J. Phys. Anthropol. 111, 479-487.

Baddeley A., Rubak E., Turner R., 2015. Spatial point patterns: methodology and applications with R. Chapman and Hall/CRC Press, London.

Badoux D.M., 1974. An introduction to biomechanical principles in primate locomotion and structure. In: Jenkins F.A. Jr. (Ed.), Primate locomotion. Academic Press, New York, pp. 1-43.

Balter V., Blichert-Toft J., Braga J., Telouk P., Thackeray J.F., Albarède F., 2008. U-Pb dating of fossil enamel from the Swartkrans Pleistocene hominid site, South Africa. Earth Planet. Sci. Lett. 267, 236-246.

Barak M.M., Black A.M., 2017. Using 3D-printing to evaluate trabecular bone mechanical properties. The FASEB Journal 31, 902-23.

Barak M.M., Lieberman D.E., Hublin J.-J., 2011. A Wolff in sheep's clothing: trabecular bone adaptation in response to changes in joint loading orientation. Bone 49, 1141-1151.

Barak M.M., Lieberman D.E., Hublin J.-J., 2013b. Of mice, rats and men: trabecular bone architecture in mammals scales to body mass with negative allometry. J. Struct. Biol. 183, 123-131.

Barak M.M., Lieberman D.E., Raichlen D., Pontzer H., Warrener A.G., Hublin J.-J., 2013a. Trabecular evidence for a human-like gait in *Australopithecus africanus*. PLoS ONE 8, e77687.

Barak M.M., Sherratt E., Lieberman D.E., 2017. Using principal trabecular orientation to differentiate joint loading orientation in the 3rd metacarpal heads of humans and chimpanzees. J. Hum. Evol. 113, 173-182.

Barak M.M., Weiner S., Shahar R., 2008. Importance of the integrity of trabecular bone to the relationship between load and deformation of rat femora: an optical metrology study. J. Mater. Chem. 18, 3855-3864.

Barak M.M., Weiner S., Shahar R., 2010. The contribution of trabecular bone to the stiffness and strength of rat lumbar vertebrae. Spine 35, 1153-1159.

Bayle P., Bondioli L., Macchiarelli R., Mazurier A., Puymerail L., Volpato V., Zanolli C., 2011. Three-dimensional imaging and quantitative characterization of human fossil remains. Examples from the NESPOS database. In: Macchiarelli R., Weniger G.-C. (Ed.), Pleistocene databases. Acquisition, storing, sharing, vol. 4. Wissenschaftliche Schriften des Neanderthal Museums, Mettmann, pp. 29-46.

Beauchesne P., Agarwal S.C., 2017. A multi-method assessment of bone maintenance and loss in an Imperial Roman population: Implications for future studies of age-related bone loss in the past. Am. J. Phys. Anthropol. 164, 41-61.

Beaudet A., Braga J., De Beer F., Schillinger B., Steininger C., Vodopivec V., Zanolli C., 2016. Neutron microtomography-based virtual extraction and analysis of a cercopithecoid partial cranium (STS 1039) embedded in a breccia fragment from Sterkfontein Member 4 (South Africa). Am. J. Phys. Anthropol. 159, 737-745.

Behrensmeyer A.K., 1978. Taphonomic and ecologic information from bone weathering. Paleobiol. 4, 150-162.

Berger L.R., De Ruiter D.J., Churchill S.E., Schmid P., Carlson K.J., Dirks P.H., Kibii J.M., 2010. *Australopithecus sediba*: a new species of *Homo*-like australopith from South Africa. Science 328, 195-204.

Berger L.R., Pickford M., Thackeray J.F., 1995. A Plio-Pleistocene hominid upper central incisor from the Cooper's site, South Africa. South Afr. J. Sci. 91, 541-542.

Biewener A.A., 1982. Bone strength in small mammals and bipedal birds: do safety factors change with body size? J. Exp. Biol. 98, 289-301.

Biewener A.A., 1990. Biomechanics of mammalian terrestrial locomotion. Science 250, 1097-1103.

Biewener A.A., Fazzalari N.L., Konieczynski D.D., Baudinette R.V., 1996. Adaptive changes in trabecular architecture in relation to functional strain patterns and disuse. Bone 19, 1-8.

Bikle D.D., Halloran B.P., 1999. The response of bone to unloading. J. Bone Miner. Metab. 17, 233-244.

Bikle D.D., Harris J., Halloran B.P., Currier P.A., Tanner S., Morey-Holton E., 1995. The molecular response of bone to growth hormone during skeletal unloading: regional differences. Endocrinology 136, 2099-2109.

Biknevicius A.R., 1993. Biomechanical scaling of limb bones and differential limb use in caviomorph rodents. J. Mammal. 74, 95-107.

Bleuze M.M., 2010. Cross-sectional morphology and mechanical loading in Plio-Pleistocene hominins: implications for locomotion and taxonomy. Ph.D Dissertation, The University of Western Ontario, Ontario.

Bolter D.R., Zihlman A.L., 2012. Skeletal development in *Pan paniscus* with comparisons to *Pan troglodytes*. Am. J. Phys. Anthropol. 147, 629-636.

Bondioli L., Bayle P., Dean C., Mazurier A., Puymerail L., Ruff C., Stock J.T., Volpato V., Zanolli C., Macchiarelli R., 2010. Technical note: Morphometric maps of long bone shafts and dental roots for imaging topographic thickness variation. Am. J. Phys. Anthropol. 142, 328-334.

Bonewald L.F., Johnson M.L., 2008. Osteocytes, mechanosensing and Wnt signaling. Bone, 42, 606-615.

Bonhomme V., Picq S., Gaucherel C., Claude J., 2014. Momocs: outline analysis using R. J. Stat. Softw. 56, 1-24.

Boughner J.C., Dean M.C., Wilgenbusch C.S., 2012. Permanent tooth mineralization in bonobos (*Pan paniscus*) and chimpanzees (*P. troglodytes*). Am. J. Phys. Anthropol. 149, 560-571.

Braga J., 2016. Non-invasive imaging techniques. In: Irish J.D., Scott G.R. (Ed.), A companion to dental anthropology. J. Wiley & Sons, New York, pp. 514-527.

Braga J., Dumoncel J., Duployer B., Tenailleau C., de Beer F., Thackeray J.F., 2016b. The Kromdraai hominins revisited with an updated portrayal of differences between *Australopithecus africanus* and *Paranthropus robustus*. In Kromdraai. A birthplace of *Paranthropus* in the cradle of humankind. Sun Press, Stellenbosch, pp. 49-68.

Braga J., Fourvel J.B., Lans B., Bruxelles L., Thackeray J.F., 2016a. Evolutionary, chrono-cultural and palaeoenvironmental backgrounds to the Kromdraai site: A regional perspective. In: Braga J., Thackeray J.F. (Ed.), Kromdraai: A birthplace of *Paranthropus* in the cradle of humankind. Sun Press, Stellenbosch, pp. 1-16.

Braga J., Thackeray J.F., 2016. Kromdraai: A birthplace of *Paranthropus* in the cradle of humankind. Sun Press, Stellenbosch.

Braga J., Thackeray J.F., 2003. Early *Homo* at Kromdraai B: Probabilistic and morphological analysis of the lower dentition. C. R. Palevol 2, 269-279.

Braga J., Thackeray J.F., Bruxelles L., Dumoncel J., Fourvel J.B., 2017. Stretching the time span of hominin evolution at Kromdraai (Gauteng, South Africa): Recent discoveries. C. R. Palevol 16, 58-70.

Braga J., Thackeray J.F., Dumoncel J., Descouens D., Bruxelles L., Loubes J.M., Kahn J.-L., Stampanoni M., Bam L., Hoffman J., de Beer F., Spoor F., 2013. A new partial temporal bone of a juvenile hominin from the site of Kromdraai B (South Africa). J. Hum. Evol. 65, 447-456.

Brain C.K., 1958. The Transvaal ape-man-bearing cave deposits. Transv. Mus. Mem. 11, 95-99.

Brain C.K., 1975. An interpretation of the bone assemblage from the Kromdraai australopithecine site, South Africa. In: Tuttle R.H. (Ed.), Paleoanthropology, morphology and paleoecology. Mouton Publishers, The Hague, pp. 225-243.

Brain C.K., 1981. The hunter or the hunted. An introduction to African cave taphonomy. The University of Chicago press, Chicago.

Brain C.K., 1993. Swartkrans: A cave's chronicle of early man. Transv. Mus. Monogr. 8.

Bramble D.M., Lieberman D.E., 2004. Endurance running and the evolution of *Homo*. Nature 432, 345-352.

Brimacombe C.S., Kuykendall K.L. Nystrom P., 2015. Epiphyseal fusion in *Pan troglodytes* relative to dental age. Am. J. Phys. Anthropol. 157, 19-29.

Britt B.B., Scheetz R.D., Dangerfield A., 2008. A suite of dermestid beetle traces on dinosaur bone from the Upper Jurassic Morrison Formation, Wyoming, USA. Ichnos: An International Journal for Plant and Animal Traces 15, 59-71.

Brodetti A., Hirsch C., 1956. The weight-bearing capacity of structural elements in femoral necks; second report. Acta orthopaedica Scandinavica 26, 15.

Broom J.T., 1952. *Paranthropus crassidens* type. Transv. Mus. Mem. 6, 1-3.

Broom R., 1938a. The Pleistocene anthropoid apes of South Africa. Nature 142, 377-379.

Broom R., 1938b. Further evidence on the structure of the South African Pleistocene anthropoids. Nature 142, 897-899.

Broom R., 1942. The hand of the Ape-man, *Paranthropus robustus*. Nature 149, 513-514.

Broom R., 1943. An ankle-bone of the Ape-man, *Paranthropus robustus*. Nature 152, 689-690.

Broom R., 1949. Another new type of fossil ape-man. Nature 163, 57.

Broom R., Robinson J.T., 1949. A new type of fossil man. Nature 164, 322-323.

Broom R., Robinson J.T., 1950. Man contemporaneous with the Swartkrans ape-man. Am. J. Phys. Anthropol. 8, 151-156.

Broom R., Schepers G.W.H., 1946. The South African fossil ape-men: The *Australopithecinae*. Transv. Mus. Mem. 2, 18.

Brown B., Walker A., Ward C.V., Leakey R.E., 1993. New *Australopithecus boisei* calvaria from East Lake Turkana, Kenya. Am. J. Phys. Anthropol. 91, 137-159.

Bruxelles L., Maire R., Couzens R., Thackeray J.F., Braga J., 2016. A revised stratigraphy of Kromdraai. In: Braga J., Thackeray J.F. (Ed.), Kromdraai: A birthplace of *Paranthropus* in the cradle of humankind. Sun Press, Stellenbosch, pp. 31-47.

Buie H.R., Campbell G.M., Klinck R.J., MacNeil J.A., Boyd S.K., 2007. Automatic segmentation of cortical and trabecular compartments based on a dual threshold technique for in vivo micro-CT bone analysis. Bone 41, 505-515.

Cameron N., Bogin B., Bolter D., Berger L.R., 2017. The postcranial skeletal maturation of *Australopithecus sediba*. Am. J. Phys. Anthropol. 163, 633-640.

Carlson K.J., Lublinsky S., Judex S., 2008. Do different locomotor modes during growth modulate trabecular architecture in the murine hind limb? Integr. Comp. Biol. 48, 385-393.

Carlson K.J., 2005. Investigating the form-function interface in African apes: Relationships between principal moments of area and positional behaviors in femoral and humeral diaphysis. Am. J. Phys. Anthropol. 127, 312-334.

Carlson K.J., Doran-Sheehy D.M., Hunt K.D., Nishida T., Yamanaka A., Boesch C., 2006. Locomotor behaviour and long bone morphology in individual free-ranging chimpanzees. J. Hum. Evol. 50, 394-404.

Carlson K.J., Jashashvili T., Houghton K., Westaway M.C., Patel B.A., 2013. Joint loads in marsupial ankles reflect habitual bipedalism versus quadrupedalism. PLoS ONE 8, e58811.

Carlson K.J., Judex S., 2007. Increased non-linear locomotion alters diaphyseal bone shape. J. Exp. Biol. 210, 3117-3125.

Carlson K.J., Marchi D., 2014. Reconstructing mobility. Environmental, behavioral, and morphological determinants. Springer, New York.

Carlson K.J., Sumner D., Morbeck M., Nishida T., Yamanaka A., Boesch C., 2008. Role of nonbehavioral factors in adjusting long bone diaphyseal structure in free-ranging *Pan troglodytes*. Int. J. Primatol. 29, 1401-1420.

Carretero J.M., Lorenzo C., Arsuaga J.L., 1999. Axial and appendicular skeleton of *Homo antecessor*. J. Hum. Evol. 37, 459-499.

Chamberlain A.T., Wood B.A., 1987. Early hominid phylogeny. J. Hum. Evol. 16, 119-133.

Chang G., Pakin S.K., Schweitzer M.E., Saha P.K., Regatte R.R., 2008. Adaptations in trabecular bone microarchitecture in Olympic athletes determined by 7T MRI. J. Magn. Reson. Imaging 27, 1089-1095.

Chavaillon J., Piperno M., 2004. Studies on the Early Paleolithic site of Melka Kunture, Ethiopia. Instituto Italiano di Preistoria e Protostoria, Florence.

Chirchir H., Kivell T.L., Ruff C.B., Hublin J.-J., Carlson K.J., Zipfel B., Richmond B.G., 2015. Recent origin of low trabecular bone density in modern humans. Proc. Natl. Acad. Sc. USA 112, 366-371.

Chirchir H., Ruff C.B., Junno J.A., Potts R., 2017. Low trabecular bone density in recent sedentary modern humans. Am. J. Phys. Anthropol. 162, 550-560.

Christen P., Ito K., Ellouz R., Boutroy S., Sornay-Rendu E., Chapurlat R.D., Van Rietbergen B., 2014. Bone remodelling in humans is load-driven but not lazy. Nature communications 5, 4855.

Churchill S.E., Holliday T.W., Carlson K.J., Jashashvili T., Macias M.E., Mathews S., Sparling T.L., Schmid P., de Ruiter D.J., Berger L.R., 2013. The upper limb of *Australopithecus sediba*. Science 340, 1233477.

Churchill S.E., VanSickle C., 2017. Pelvic morphology in *Homo erectus* and early *Homo*. Anat. Rec. 300, 965-977

Clarke R.J., Howell F.C., 1972. Affinities of the Swartkrans 847 hominid cranium. Am. J. Phys. Anthropol. 37, 319-335.

Clegg M., Aiello L.C., 1999. A comparison of the Nariokotome *Homo erectus* with juveniles from a modern human population. Am. J. Phys. Anthropol. 110, 81-93.

Clément G., Geffard-Kuriyama D., 2010. Imaging & 3D in palaeontology and palaeoanthropology. C. R. Palevol 9, 255-470.

Correnti V., 1955. Le basi morfomeccaniche della struttura dell'osso iliaco. Riv. Antropol. 42, 289-336.

Corruccini R.S., 1994. How certain are hominoid phylogenies? The role of confidence intervals in cladistics. In: Corruccini R.S., Ciochon R.L. (Ed.), Integrative paths to the past: Paleoanthropological advances in honor of F. Clark Howell. Englewood Cliffs, Prentice Hall, pp. 167-183.

Cotter M.M., Simpson S.W., Latimer B.M., Hernandez C.J., 2009. Trabecular microarchitecture of hominoid thoracic vertebrae. Anat. Rec. 292, 1098-1106.

Cowin S.C., Moss-Salentijn L., Moss M.L., 1991. Candidates for the mechanosensory system in bone. J. Biomech. Eng. 113, 191-197.

Cullinane D.M., Einhorn T.A., 2002. Biomechanics of bone. Princ. Bone Biol. 1, 17-32.

Culmann K., 1866. Die Graphische Statik. Verlag Von Meyer & Zeller, Zurich, pp. 633.

Cunningham C.A., Black S.M., 2009a. Anticipating bipedalism: trabecular organization in the newborn ilium. J. Anat. 214, 817-829.

Cunningham C.A., Black S.M., 2009b. Development of the fetal ilium - challenging concepts of bipedality. J. Anat. 214, 91-99.

Cunningham C.A., Black S.M., 2010. The neonatal ilium - metaphyseal drivers and vascular passengers. Anat. Rec. 293, 1297-1309.

Cunningham C.A, Scheuer L., Black S., 2016. Developmental juvenile osteology. Academic Press, New York.

Cunningham J.A., Rahman I.A., Lautenschlager S., Rayfield E.J., Donoghue P.C.J., 2014. A virtual world of paleontology. Trends Ecol. Evol. 29, 346-357.

Curnoe D., 2010. A review of early *Homo* in southern Africa focusing on cranial, mandibular and dental remains, with the description of a new species (*Homo gautengensis* sp. nov.). HOMO 61, 151-177.

Curnoe D., Grün R., Taylor L., Thackeray J.F., 2001. Direct ESR dating of a Pliocene hominin from Swartkrans. J. Hum. Evol. 40, 379-391.

Currey J.D., 2002. Bones: Structure and mechanics. Princeton University Press, Princeton.

Currey J.D., 2003. The many adaptations of bone. J. Biomech. 36, 1487-1495.

Dart R.A., 1925. *Australopithecus africanus* the man-ape of South Africa. Nature 115, 195-199.

Davies T.G., Rahman I.A., Lautenschlager S., Cunningham J.A., Asher R.J., Barrett P.M., Bates K.T., Bengtson S., Benson R.B.J., Boyer D.M., Braga J., Bright J.A., Claessens L.P.A.M., Cox P.G., Dong X.-P., Evans A.R., Falkingham P.L., Friedman M., Garwood R.J., Goswami A., Hutchinson J.R., Jeffery N.S., Johanson Z., Lebrun R., Martínez-Pérez C., Marugán-Lobón J., O'Higgins P.M., Metscher B., Orliac M., Rowe T.B., Rücklin M., Sánchez-Villagra M.R., Shubin N.H., Smith S.Y., Starck J.M., Stringer C., Summers A.P., Sutton M.D., Walsh S.A., Weisbecker V., Witmer L.M., Wroe S., Yin Z., Rayfield E.J., Donoghue P.C.J., 2017. Open data and digital morphology. Proc. R. Soc. B 284, 20170194.

Davies T.G., Stock J.T., 2014. The influence of relative body breadth on the diaphyseal morphology of the human lower limb. Am. J. Hum. Biol. 26, 822-835.

Day M.H., 1969. Femoral fragment of a robust australopithecine from the Olduvai Gorge, Tanzania. Nature 221, 230-233.

Day M.H., 1978. Functional interpretations of the morphology of postcranial remains of early African hominids. In: Jolly C.J. (Ed.), African *Hominidae* of the Plio-Pleistocene. St. Martin's Press, New York, pp. 311-345.

Day M.H., Thornton C.M.B., 1986. The extremity bones of *Paranthropus robustus* from Kromdraai B, East Formation Member 3, Republic of South Africa: A reappraisal. Anthropos 23, 91-99.

Dayal M.R., Kegley A.D.T., Štrkalj G., Bidmos M.A., Kuykendall K.L., 2009. The history and composition of the Raymond A. Dart collection of human skeletons at the University of the Witwatersrand, Johannesburg, South Africa. Am. J. Phys. Anthropol. 140, 324-335.

de Ruiter D.J., 2001. A methodological analysis of the relative abundance of hominids and other macromammals from the site of Swartkrans, South Africa. Univ. Witwatersrand, Johannesburg.

de Ruiter D.J., Pickering R., Steininger C.M., Kramers J.D., Hancox E.J., Churchill S.E., Berger L.R., Backwell L., 2009. New *Australopithecus robustus* fossils and associated U-Pb dates from Cooper's Cave (Gauteng, South Africa). J. Hum. Evol. 56, 497-513.

Dean M.C., Smith B.H., 2009. Growth and development of the Nariokotome youth, KNM-WT 15000. In: Grine F.E., Fleagle J.G., Leakey R.E. (Ed.), The first humans - origin and early evolution of the genus *Homo*. Springer, New York, pp. 101-120.

Dean M.C., Wood B.A., 1981. Developing pongid dentition and its use for ageing individual crania in comparative cross-sectional growth studies. Folia Primatologica 36, 111-127.

Delson E., 1988. Chronology of South African australopith site units. In: Grine F.E. (Ed.), Evolutionary history of the ‘‘robust’’ australopithecines. Aldine de Gruyter, New York, pp. 317-324.

Delson E., 1997. One skull does not make a species. Nature 389, 445-446.

Demes B., Jungers W.L., 1993. Long bone cross-sectional dimensions, locomotor adaptations and body size in prosimian primates. J. Hum. Evol. 25, 57-74.

Demes B., Jungers W.L., Walker C., 2000. Cortical bone distribution in the femoral neck of strepsirhine primates. J. Hum. Evol. 39, 367-379.

DeSilva J.M., 2009. Functional morphology of the ankle and the likelihood of climbing in early hominins. Proc. Natl. Acad. Sci. USA 106, 6567-6572.

DeSilva J.M., Devlin M.J., 2012. A comparative study of the trabecular bony architecture of the talus in humans, non-human primates, and *Australopithecus*. J. Hum. Evol. 63, 536-551.

DeSilva J.M., Gill C.M., Prang T.C., Bredella M.A., Alemseged Z., 2018. A nearly complete foot from Dikika, Ethiopia and its implications for the ontogeny and function of *Australopithecus afarensis*. Sci. Adv. 4, eaar7723.

DeSilva J.M., Holt K.G., Churchill S.E., Carlson K.J., Walker C.S., Zipfel B., Berger L.R., 2013. The lower limb and mechanics of walking in *Australopithecus sediba*. Science 340, 1232999.

Di Vincenzo F., Rodriguez L., Carretero J.M., Collina C., Geraads D., Piperno M., Manzi G., 2015. The massive fossil humerus from the Oldowan horizon of Gombore I, Melka Kunture (Ethiopia, >1.39 Ma). Quat. Sc. Rev. 122, 207-221.

Diogo R., Potau J.M., Pastor J.F., 2013. Photographic and descriptive musculoskeletal atlas of chimpanzees: with notes on the attachments, variations, innervation, function and synonymy and weight of the muscles. CRC Press.

Diogo R., Potau J.M., Pastor J.F., Ferrero E.M., Bello G., Barbosa M., Wood B.A., 2012. Photographic and descriptive musculoskeletal atlas of gibbons and siamangs (*Hylobates*): with notes on the attachments, variations, innervation, synonymy and weight of the muscles. CRC Press.

Frelat M.A., Shaw C.N., Sukhdeo S., Hublin J.-J., Benazzi S., Ryan T.M., 2017. Evolution of the hominin knee and ankle. J. Hum. Evol. 108, 147-160.

Domínguez-Rodrigo M., Pickering T.R., Baquedano E., Mabulla A., Mark D.F., Musiba C., Bunn H.T., Uribelarrea D., Smith V., Diez-Martin F., Pérez-González A., Sánchez P., Santonja M., Barboni D., Gidna A., Ashley G., Yravedra J., Heaton J.L, Carmen Arriaza M., 2013. First partial skeleton of a 1.34-million-year-old *Paranthropus boisei* from Bed II, Olduvai Gorge, Tanzania. PLoS ONE 8, e80347.

Doran D.M., 1997. Ontogeny of locomotion in mountain gorillas and chimpanzees. J. Hum. Evol. 32, 323-344.

Doube M., Klosowski M.M., Wiktorowicz-Conroy A.M., Hutchinson J.R., Shefelbine S.J., 2011. Trabecular bone scales allometrically in mammals and birds. Proc. R. Soc. B. 278, 3067-3073.

Dowdeswell M.R., Jashashvili T., Patel B.A., Lebrun R., Susman R.L., Lordkipanidze D., Carlson K.J., 2016. Adaptation to bipedal gait and fifth metatarsal structural properties in *Australopithecus*, *Paranthropus*, and *Homo*. In: Macchiarelli R., Zanolli C. (Ed.), Hominin biomechanics, virtual anatomy and inner structural morphology: From head to toe. A tribute to Laurent Puymerail. C. R. Palevol 16, 585-599.

Dusseldorp G., Lombard M., Wurz S., 2013. Pleistocene *Homo* and the updated Stone Age sequence of South Africa. South Afr. J. Sci. 109, 1-7.

Ellison P.T., 2009. On Fertile Ground: A natural history of human reproduction. Harvard University Press, Cambridge, MA.

Emonet E.G., Tafforeau P., Chaimanee Y., Guy F., De Bonis L., Koufos G., Jaeger J.-J., 2012. Three-dimensional analysis of mandibular dental root morphology in hominoids. J. Hum. Evol. 62, 146-154.

Eriksen E.F., 1986. Normal and pathological remodeling of human trabecular bone: three dimensional reconstruction of the remodeling sequence in normals and in metabolic bone disease. Endocr. Rev. 7, 379-408.

Eriksen E.F., 2010. Cellular mechanisms of bone remodelling. Rev. Endocr. Metab. Disord. 11, 219-227.

Fajardo R.J., Desilva J.M., Manoharan R.K., Schmitz J.E., Maclatchy L.M., Bouxsein M.L., 2013. Lumbar vertebral body bone microstructural scaling in small to mediumsized strepsirhines. Anat. Rec. 296, 210-226.

Fajardo R.J., Müller R., 2001. Three-dimensional analysis of nonhuman primate trabecular architecture using micro-computed tomography. Am. J. Phys. Anthropol. 115, 327-336.

Fajardo R.J., Müller R., Ketcham R.A., Colbert M., 2007. Nonhuman anthropoid primate femoral neck trabecular architecture and its relationship to locomotor mode. Anat. Rec. 290, 422-436.

Feldesman M.R., 1982. Morphometric analysis of the distal humerus of some Cenozoic catarrhines: the late divergence hypothesis revisited. Am. J. Phys. Anthropol. 59, 73-95.

Fleagle J.G., 2013. Primate adaptation and evolution. Academic Press, New York.

Fox J.C., Keaveny T.M., 2001. Trabecular eccentricity and bone adaptation. J. Theor. Biol. 212, 211-221.

Frelat M.A., Shaw C.N., Sukhdeo S., Hublin J.-J., Benazzi S., Ryan T.M., 2017. Evolution of the hominin knee and ankle. J. Hum. Evol. 108, 147-160.

Frost H.M., 1987. Bone ‘mass’ and the ‘mechanostat’: a proposal. Anat. Rec. 219, 1-9.

Frost H.M., 1988. Structural adaptations to mechanical usage. A proposed “three-way rule” for bone modeling. Vet. Comp. Orthop. Traumatol. 1, 80-85.

Frost H.M., 1999. An approach to estimating bone and joint loads and muscle strength in living subjects and skeletal remains. Am. J. Hum. Biol. 11, 437-455.

Frost H.M., 2003. Bone's mechanostat: a 2003 update. The anatomical record part A: discoveries in molecular, cellular, and evolutionary biology 275, 1081-1101.

Galilei G., 1638. Discourses and mathematical demonstrations relating to two new sciences. Appresso gli Elsevirii, Leiden.

Gallotti R., Mussi M., 2015. The unknown Oldowan: ~1.7-million-year-old standardized obsidian small tools from Garba IV, Melka Kunture, Ethiopia. PLoS ONE 10, e0145101.

Gebo D.L., 1992. Plantigrady and foot adaptation in African apes: implications for hominid origins. Am. J. Phys. Anthropol. 89, 29-58.

Gebo D.L., Schwartz G.T., 2006. Foot bones from Omo: implications for hominid evolution. Am. J. Phys. Anthropol. 129, 499-511.

Gibbon R.J., Rayne T., Sutton M.B., Heaton J.L., Kuman K., Clarke R.J., Brain C.K., Granger D.E., 2014. Quaternary geochronology cosmogenic nuclide burial dating of hominin-bearing Pleistocene cave deposits at Swartkrans, South Africa. Quat. Geochron. 24, 10-15.

Gibson L.J., 1985. The mechanical behaviour of cancellous bone. J. Biomech. 18, 317-328.

Goldstein S.A., Goulet R., McCubbrey D., 1993. Measurement and significance of three-dimensional architecture to the mechanical integrity of trabecular bone. Calcif. Tissue Int. 53, S127-S133.

Goodfellow J., Hungerford D.S., Zindel M.A.R.C., 1976. Patello-femoral joint mechanics and pathology. 1. Functional anatomy of the patello-femoral joint. J. Bone Joint Surg. 58, 287-290.

Gosman J.H., Stout S.D., Larsen C.S., 2011. Skeletal biology over the life span: a view from the surfaces. Am. J. Phys. Anthropol. 146, 86-98.

Gowlett J.A.J., Harris J.W.K., Walton D., Wood B.A., 1981. Early archaeological sites, hominid remains and traces of fire from Chesowanja, Kenya. Nature 294, 125-129.

Grausz H.M., Leakey R.E.F., Walker A.C., Ward C.V., 1988. Associated cranial and postcranialbones of *Australopithecus boisei*. In: Grine F.E. (Ed.), Evolutionary history of the ‘‘robust’’ australopithecines. Aldine de Gruyter, New York, pp. 127-132.

Green D.J., Alemseged Z., 2012. *Australopithecus afarensis* scapular ontogeny, function, and the role of climbing in human evolution. Science 338, 514.

Grine F.E., 1982. A new juvenile hominid (Mammalia: Primates) from Member 3, Kromdraai Formation, Transvaal, South Africa. Ann. Transv. Mus. 33, 165-239.

Grine F.E., 1985. Australopithecine evolution: The deciduous dental evidence. In: Delson E. (Ed.), Ancestors: The hard evidence. Alan R. Liss, New York, pp. 153-167.

Grine F.E., 1988. Evolutionary history of the “robust” australopithecines. Adline de Gruyter, New York, pp. 509-520.

Grine F.E., 1989. New hominid fossils from the Swartkrans formation (1979-1986 excavations): Craniodental specimens. Am. J. Phys. Anthropol. 79, 409-449.

Grine F.E., 2005. Early *Homo* at Swartkrans, South Africa: a review of the evidence and an evaluation of recently proposed morphs. South Afr. J. Sc. 101, 43-52.

Grine F.E., Jacobs R.L., Reed K.E., Plavcan J.M., 2012. The enigmatic molar from Gondolin, South Africa: Implications for *Paranthropus* paleobiology. J. Hum. Evol. 63, 597-609.

Grine F.E., Jungers W.L., Schultz J., 1996. Phenetic affinities among early *Homo* crania from East and South Africa. J. Hum. Evol. 30, 189-225.

Grine F.E., Smith H.F., Heesy C.P., Smith E.J., 2009. Phenetic affinities of Plio-Pleistocene *Homo* fossils from South Africa: Molar cusp proportions. In: Grine F.E., Fleagle J.G., Leakey R.E. (Ed.), The first humans. Origin and early evolution of the genus *Homo*. Springer, Dordrecht, pp. 49-62.

Grine F.E., Susman R.L., 1991. Radius of *Paranthropus robustus* from Member 1, Swartkrans Formation, South Africa. Am. J. Phys. Anthropol. 84, 229-248.

Guldberg R.E., Caldwell N.J., Guo X.E., Goulet R.W., Hollister S.J., Goldstein S.A., 1997. Mechanical stimulation of tissue repair in the hydraulic bone chamber. J. Bone Miner. Res. 12, 1295-1302.

Gupta A, Bayraktar H.H., Fox J.C., Keaveny T.M., Papadopoulos P., 2007. Constitutive modelling and algorithmic implementation of a plasticity-like model for trabecular bone structures. Comput. Mech. 40, 61-72.

Haile-Selassie Y., Latimer B.M., Alene M., Deino A.L., Gibert L., Melillo S.M., Saylor B.Z., Scott G.R., Lovejoy C.O., 2010. An early *Australopithecus afarensis* postcranium from Woranso-Mille, Ethiopia. Proc. Natl. Acad. Sci. 107, 2121.

Hall B.K., 1985. Research and the development and structure of the skeleton since the publication of Bones. An introduction to Bones: a study of the development and structure of the vertebrate skeleton by Murray PDF (originally published in 1936, reissued 1985). Cambridge University Press, Cambridge.

Harcourt-Smith W.E.H., 2016. Early hominin diversity and the emergence of the genus *Homo*. J. Anthropol. Sciences 94, 19-27.

Harcourt-Smith W.E.H., Aiello L.C., 2004. Fossils, feet and the evolution of human bipedal locomotion. J. Anat. 204, 403-416.

Harmon E., 2009. Size and shape variation in the proximal femur of *Australopithecus africanus*. J. Hum. Evol. 56, 551-559.

Harrison L.C.V., Nikander R., Sikiö M., Luukkaala T., Helminen M.T., Ryymin P., Soimakallio S., Eskola H.J., Dastidar P., Sievänen H., 2011. MRI texture analysis of femoral neck: detection of exercise load-associated differences in trabecular bone. J. Magn. Reson. Imaging 34, 1359-1366.

Harrison T., Kweka A., 2011. Paleontological localities on the Eyasi Plateau, including Laetoli. In: Harrison T. (Ed.), Paleontology and geology of Laetoli: human evolution in context: volume 1: geology, geochronology, paleoecology and paleoenvironment. Springer, Dordrecht, pp. 17-45.

Harrison T., 2011. Hominins. In: Harrison T. (Ed.), Paleontology and geology of Laetoli: human evolution in context (Fossil hominins and the associated fauna, vol. 2). Springer, Dordrecht, pp. 141-188.

Hatala K.G., Roach N.T., Ostrofsky K.R., Wunderlich R.E., Dingwall H.L., Villmoare B.A., Green D.J., Harris J.W.K., Braun D.R., Richmond B.G., 2016. Footprints reveal direct evidence of group behavior and locomotion in *Homo erectus*. Sci. Rep. 6, 28766.

Havill L.M., Allen M.R., Bredbenner T.L., Burr D.B., Nicolella D.P., Turner C.H., Warren D.M., Mahaney M.C., 2010. Heritability of lumbar trabecular bone mechanical properties in baboons. Bone 46, 835-840.

Heaton J.L., 2006. Taxonomy of the Sterkfontein *Cercopithecinae*: The *Papionini* of Members 2 and 4 (Gauteng, South Africa). Ph.D Dissertation, Indiana University, Bloomington.

Hébert D., Lebrun R., Marivaux L., 2012. Comparative three-dimensional structure of the trabecular bone in the talus of primates and its relationship to ankle joint loads generated during locomotion. Anat. Rec. 295, 2069-2088.

Herries A.I.R., Curnoe D., Adams J.W., 2009. A multi-disciplinary seriation of early *Homo* and *Paranthropus* bearing palaeocaves in southern Africa. Quat. Int. 202, 14-28.

Hill A., Ward S., 1988. Origin of the Hominidae: the record of African large hominoid evolution between 14 My and 4 My. Am. J. Phys. Anthropol. 31, 49-83.

Hlusko L.J., Reiner W.B., Njau J.K., 2015. A one-million-year-old hominid distal ulna from Olduvai Gorge, Tanzania. Am. J. Phys. Anthropol. 158, 36-42.

Hollister S.J., Brennan J.M., Kikuchi N., 1994. A homogenization sampling procedure for calculating trabecular bone effective stiffness and tissue level stress. J. Biomech. 27, 433-444.

Homminga J., van Reitbergen B., Lochmüller E.M., Weinans H., Eckstein F., Huiskes R., 2004. The osteoporotic vertebral structure is well adapted to the loads of daily life, but not to infrequent 'error' loads. Bone 34, 510-516.

Howell F.C., 1978. Hominidae. In: Maglio V.J., Cooke H.B.S. (Ed.), Evolution of African mammals. Harvard University Press, Cambridge, pp. 154-248.

Huiskes R., 2000. If bone is the answer, then what is the question? J. Anat. 197, 145-56.

Huiskes R., Ruimerman R., van Lenthe G.H., Janssen J.D., 2000. Effects of mechanical forces on maintenance and adaptation of form in trabecular bone. Nature 405, 704-706.

Ibáñez-Gimeno P., De Esteban-Trivigno S., Jordana X., Manyosa J., Malgosa A., Galtés I., 2013. Functional plasticity of the human humerus: Shape, rigidity, and muscular entheses. Am. J. Phys. Anthropol. 150, 609-617.

Ingham S., de Carvalho R., Martins C.Q., Lertwanich P., Abdalla R., Smolinski P., Lovejoy C.O., Fu F., 2015. Anterolateral ligament anatomy: a comparative anatomical study. Knee Surg. Sports Traumatol. Arthrosc. 25, 1048-1054.

Ireland A., Maden-Wilkinson T., Ganse B., Degens H., Rittweger J., 2014. Effects of age and starting age upon side asymmetry in the arms of veteran tennis players: a cross-sectional study. Osteoporos. Int. 25, 1389-1400.

Jacobs C.R., 2000. The mechanobiology of cancellous bone structural adaptation. J. Rehab. Research. Devel. 37, 209-216.

Jashashvili T., Dowdeswell M.R., Lebrun R., Carlson K.J., 2015. Cortical structure of hallucal metatarsals and locomotor adaptations in hominoids. PLoS ONE 10, e0117905.

Jilka R.L., 2003. Biology of the basic multicellular unit and the pathophysiology of osteoporosis. Med. Pediatr. Oncol. 41, 182-185.

Jolly C.J., 1970. The seed eaters: a new model for hominid differentiation based on a baboon analogy. Man 5, 5-26.

Jones H.H., Priest J.D., Hayes W.C., Tichenor C.C., Nagel D.A., 1977. Humeral hypertrophy in response to exercise. J. Bone Joint Surg. A 59, 204-208.

Judex S., Garman R., Squire M., Donahue L.R., Rubin C., 2004. Genetically based influences on the site-specific regulation of trabecular and cortical bone morphology. J. Bone Miner. Res. 19, 600-606.

Jungers W.L., Burr D.B., 1994. Body size, long bone geometry and locomotion in quadrupedal monkeys. Zeitschrift für Morphologie und Anthropologie, 89-97.

Kabel J., van Rietbergen B., Odgaard A., Huiskes R., 1999. Constitutive relationships of fabric, density, and elastic properties in cancellous bone architecture. Bone 25, 481-486.

Kapandji A.I., 2011. The physiology of the joints. Vol. 2. The lower limb. 6th ed. Elsevier, Edinburgh.

Kappelman J., Ketcham R.A., Pearce S., Todd L., Akins W., Colbert M.W., Feseha M., Maisano J.A., Witzel A., 2016. Perimortem fractures in Lucy suggest mortality from fall out of tall tree. Nature 537, 503-507.

Karlsson C., Obrant K.J., Karlsson M.K., 2001. Pregnancy and lactation confer reversible bone loss in humans. Osteoporos. Int. 12, 828-834.

Karlsson M.K., Linden C., Karlsson C., Johnell O., Obrant K., Seeman E., 2000. Exercise during growth and bone mineral density and fractures in old age. Lancet 355, 469-470.

Kaszycka K.A., 2002. Status of Kromdraai: Cranial, mandibular and dental morphology, systematic relationships, and significance of the Kromdraai hominids. Editions du Cahiers de Paleoanthropologie, CNRS, Paris.

Katoh T., Griffin M.P., Wevers H.W., Rudan J., 1996. Bone hardness testing in the trabecular bone of the human patella. J. Arthroplasty 11, 460-468.

Kay R.F., McHenry H.M., 1973. Humerus of robust *Australopithecus*. Science 182, 396-396.

Keaveny T.M., Morgan E.F., Niebur G.L., Yeh O.C., 2001. Biomechanics of trabecular bone. Annu. Rev. Biomed. Eng. 3, 307-333.

Kelley J., Bolter D., 2013. Growth, development, and life history in hominin evolution. In: Begun D. (Ed.), A companion to palaeoanthropology. Wiley-Liss, New York, pp. 97-117.

Keyser A.W., 2000. The Drimolen skull: The most complete australopithecine cranium and mandible to date. South Afr. J. Sci. 96, 189-193.

Keyser A.W, Menter C.G., Moggi-Cecchi J., Pickering T.R., Berger L.R., 2000. Drimolen: A new hominid-bearing site in Gauteng, South Africa. South Afr. J. Sc. 96, 193-197.

Kimbel W.H., 2007. The species and diversity of australopiths. In: Henke W., Tattersall I. (Ed.), Handbook of paleoanthropology. Springer, Berlin Heidelberg, pp. 1539-1573.

Kimbel W.H., Rak Y., Johanson D.C., 2004. The skull of *Australopithecus afarensis*. Oxford University Press, Oxford.

Kivell T.L., 2016. A review of trabecular bone functional adaptation: What have we learned from trabecular analyses in extant hominoids and what can we apply to fossils? J. Anat. 228, 569-594.

Kivell T.L., Davenport R., Hublin J. J., Thackeray J.F., Skinner M.M., 2018a. Trabecular architecture and joint loading of the proximal humerus in extant hominoids, *Ateles*, and *Australopithecus africanus*. Am. J. Phys. Anthropol, in press.

Kivell T.L., Dunmore C.J., Stephens N.B., Spoor F., Hublin J.-J., Skinner M.M., 2018b. Trabecular bone structure of the *Australopithecus afarensis* A.L. 438-1 metacarpals and implications for skeletal age and hand use. PESHE 7, 100.

Komza K., Kivell T.L., Skinner M.M., 2018. Unique forms of locomotion in Swartkrans hominins: An analysis of the trabecular structure of the first metatarsal. Am. J. Phys. Anthropol. 165, 144.

Kozma E.E., Webb N.M., Harcourt-Smith W.E., Raichlen D.A., D'Août K., Brown M.H., Finestone E.M., Ross S.R., Aerts P., Pontzer H., 2018. Hip extensor mechanics and the evolution of walking and climbing capabilities in humans, apes, and fossil hominins. Proc. Natl. Acad. Sc., 201715120.

Kullmer O., Sandrock O., Abel R., Schrenk F., Bromage T.G., Juwayeyi Y.M., 1999. The first *Paranthropus* from the Malawi Rift. J. Hum. Evol. 37, 121-127.

Kumakura H., 1989. Functional analysis of the biceps femoris muscle during locomotor behaviour in some primates. Am. J. Phys. Anthropol. 79, 379-391.

Kuman K., Clarke R.J., 2000. Stratigraphy, artefact industries, and hominid associations for Sterkfontein Member 5. J. Hum. Evol. 38, 827-847.

Kuman K., Field A.S., Thackeray J.F., 1997. Discovery of new artefacts at Kromdraai. S. Afr. J. Sci. 93, 187-193.

Kuykendall K.L., 1996. Dental development in chimpanzees (*Pan troglodytes*): the timing of tooth calcification stages. Am. J. Phys. Anthropol. 99, 135-157.

L'Abbé E.N., Loots M., Meiring J.H., 2005. The Pretoria bone collection: A modern South African skeletal sample. Homo 56, 197-205.

Lague M.R., 2002. Another look at shape variation in the distal femur of *Australopithecus afarensis*: implications for taxonomic and functional diversity at Hadar. J Hum Evol. 42, 609-626.

Lague M.R., 2014. The pattern of hominin postcranial evolution reconsidered in light of size-related shape variation of the distal humerus. J. Hum. Evol. 75, 90-109.

Lague M.R., 2015. Taxonomic identification of Lower Pleistocene fossil hominins based on distal humeral diaphyseal cross-sectional shape. PeerJ 3, e1084.

Lague M.R., Jungers W.L., 1996. Morphometric variation in Plio-Pleistocene hominid distal humeri. Am. J. Phys. Anthropol. 101, 401-427.

Lanyon L., Skerry T., 2001. Perspective: postmenopausal osteoporosis as a failure of bone's adaptation to functional loading: a hypothesis. J. Bone Min. Res. 16, 1937-1947.

Lazenby R.A., Cooper D.M., Angus S., Hallgrímsson B., 2008. Articular constraint, handedness, and directional asymmetry in the human second metacarpal. J. Hum. Evol. 54, 875-885.

Le Cabec A., Tang N., Tafforeau P., 2015. Accessing developmental information of fossil hominin teeth using new synchrotron microtomography-based visualization techniques of dental surfaces and interfaces. PLoS ONE 10, e0123019.

Le Gros Clark W.E., 1947. Observations on the anatomy of the fossil Australopithecinae. J. Anat. 81, 300.

Leakey L.S.B., 1959. A new fossil skull from Olduvai. Nature 184, 491-493.

Leakey M.D., 1970. Stone artefacts from Swartkrans. Nature 225, 1222-1225.

Leakey R.E.F., 1971. Further evidence of Lower Pleistocene hominids from East Rudolf, North Kenya. Nature 231, 241-245.

Leakey R.E.F., 1972. Further evidence of Lower Pleistocene hominids from East Rudolf, North Kenya, 1971. Nature 237, 264-269.

Leakey R.E.F., Walker A., 1988. New *Australopithecus boisei* specimens from East and West Lake Turkana, Kenya. Am. J. Phys. Anthropol. 76, 1-24.

Ledger M., Holtzhausen L.M., Constant D., Morris A.G., 2000. Biomechanical beam analysis of long bones from a late 18th century slave cemetery in Cape Town, South Africa. Am. J. Phys. Anthropol. 112, 207-216.

Levangie P.K., Norkin C.C., 2005. Joint structure and function: A comprehensive analysis. F.A. Davis, Philadelphia.

Levenston M.E., Beaupré G.S., Jacobs C.R., Carter D.R., 1994. The role of loading memory in bone adaptation simulations. Bone 15, 177-186.

Lieberman D.E., 1996. How and why humans grow thin skulls: experimental evidence for systemic cortical robusticity. Am. J. Phys. Anthropol. 101, 217-236.

Lieberman D.E., 1997. Making behavioral and phylogenetic inferences from hominid fossils: considering the developmental influence of mechanical forces. Annu. Rev. Anthropol. 26, 185-210.

Lieberman D.E., Pearson O.M., Polk J.D., Demes B., Crompton A.W., 2003. Optimization of bone growth and remodeling in response to loading in tapered mammalian limbs. J. Exp. Biol. 206, 3125-3138.

Lieberman D.E., Polk J.D., Demes B., 2004. Predicting long bone loading from cross-sectional geometry. Am. J. Phys. Anthropol. 123, 156-171.

Lockwood C.A., Menter C.G., Moggi-Cecchi J., Keyser A.W., 2007. Extended male growth in a fossil hominin species. Science 318, 1443-1446.

Lordkipanidze D., Jashashvili T., Vekua V., Ponce de Leon M.S., Zollikofer C.P.E., Rightmire G.P., Pontzer H., Ferring R., Oms O., Tappen M., Bukhsianidze M., Agusti J., Kahlke R., Kiladze G., Martinez-Navarro B., Mouskhelishvili A., Nioradze M., Rook L., 2007. Postcranial evidence from early *Homo* from Dmanisi, Georgia. Nature 449, 305-310.

Lovejoy C.O., 1975. Biomechanical perspectives on the lower limb of early hominids. In: Tuttle R.H. (Ed.), Primate functional morphology and evolution. Mouton, Paris, pp. 291-326.

Lovejoy C.O., 1988. Evolution of human walking. Sci. Am. 259, 118-125.

Lovejoy C.O., 2005. The natural history of human gait and posture. Part 2. Hip and thigh. Gait & Post. 21, 113-124.

Lovejoy C.O., 2007. The natural history of human gait and posture: Part 3. The knee. Gait & Post. 25, 325-341.

Lovejoy C.O., Cohn M.J., White T.D., 1999. Morphological analysis of the mammalian postcranium: A developmental perspective. Proc. Natl. Acad. Sc. USA 96, 13247-13252.

Lovejoy C.O., Heiple K.G., Burstein A.H., 1973. The gait of *Australopithecus*. Am. J. Phys. Anthropol. 38, 757-780.

Lovejoy C.O., Meindl R.S., Ohman J.C., Heiple K.G., White T.D., 2002. The Maka femur and its bearing on the antiquity of human walking: Applying contemporary concepts of morphogenesis to the human fossil record. Am. J. Phys. Anthropol. 119, 97-133.

Lovejoy C.O., Suwa G., Spurlock L., Asfaw B., White T., 2009. The pelvis and femur of *Ardipithecus ramidus*: the emergence of upright walking. Science 326, 71e1-71e6

Macchiarelli R., Bondioli L., 2000. Multimedia dissemination of the "Isola Sacra" human paleobiological project: reconstructing lives, habits, and deaths of the "ancient Roman people" by means of advanced investigative methods. In: Proceedings of 2nd International Congress on Science and Technology for the Safeguard of Cultural Heritage in the Mediterranean Basin Vol. 2, pp. 1075-1080.

Macchiarelli R., Bondioli L., Galichon V., Tobias P., 1999. Hip bone trabecular architecture shows uniquely distinctive locomotor behaviour in South African australopithecines. J. Hum. Evol. 36, 211-232.

Macchiarelli R., Rook L. Bondioli L., 2001. Comparative analysis of the iliac trabecular architecture in extant and fossil Primates by means of digital image processing techniques: implications for the reconstruction of fossil locomotor behaviours. In: de Bonis L., Koufos G., Andrews P. (Ed.), Hominoid evolution and climatic change in Europe. Phylogeny of the neogene hominoid primates of Eurasia. Cambridge University Press, Cambridge, pp. 60-101.

Macchiarelli R., Weniger G.-C., 2011. Pleistocene Databases. Acquisition, Storing, Sharing. Wissenschaftliche Schriften des Neanderthal Museums 4, Mettmann.

Macho G.A., Shimizu D., Jiang Y., Spears I.R., 2005. *Australopithecus anamensis*: A finite-element approach to studying the functional adaptations of extinct hominins. Anat. Rec. 283, 310-318.

Macintosh A.A., Pinhasi R., Stock J.T., 2017. Prehistoric women's manual labor exceeded that of athletes through the first 5500 years of farming in Central Europe. Sci. Adv. 3, eaao3893.

MacKenzie K., 1994. History of events leading to palaeontological excavations of Gondolin, Alias ''Mackenzie Cave''. Pal. News 10, 23-24.

MacLatchy L., Müller R., 2002. A comparison of the femoral head and neck trabecular architecture of *Galago* and *Perodicticus* using micro-computed tomography (microCT). J. Hum. Evol. 43, 89-105.

Maguire J.M., Pemberton D., Collett M.H., 1980. The Makapansgat limeworks grey breccia: hominids, hyaenas, hystricids or hillwash? Palaeontologia Africana 23, 75-98.

Maquer G., Musy S.N., Wandel J., Gross T., Zysset P.K., 2015. Bone volume fraction and fabric anisotropy are better determinants of trabecular bone stiffness than other morphological variables. J. Bone Min. Res. 30, 1000-1008.

Marchi D., 2005. The cross-sectional geometry of the hand and foot bones of the *Hominoidea* and its relationship to locomotor behaviour. J. Hum. Evol. 49, 743-761.

Marchi D., 2015. Using the morphology of the hominoid distal fibula to interpret arboreality in *Australopithecus afarensis*. J. Hum. Evol. 85, 136-148.

Marchi D., Proctor D.J., Huston E., Nicholas C.L., Fischer F., 2017. Morphological correlates of the first metacarpal proximal articular surface with manipulative capabilities in apes, humans and South African early hominins. In: Macchiarelli R., Zanolli C. (Ed.), Hominin biomechanics, virtual anatomy and inner structural morphology: From head to toe. A tribute to Laurent Puymerail. C. R. Palevol 16, 645-654.

Marchi D., Sparacello V.S., Holt B.M., Formicola V., 2006. Biomechanical approach to the reconstruction of activity patterns in Neolithic Western Liguria, Italy. Am. J. Phys. Anthropol. 131, 447-455.

Marchi D., Walker C.S., Wei P., Holliday T.W., Churchill S.E., Berger L.R., DeSilva J.M., 2017. The thigh and leg of *Homo naledi*. J. Hum. Evol. 104, 174-204.

Mariani P.P., Puddu G., Ferretti A., 1978. Jumper's knee. Ital. J. Orthopaed. Traumat. 4, 85-93.

Marotti G., Ferretti M., Muglia M.A., Palumbo C., Palazzini S., 1992. A quantitative evaluation of osteoblast-osteocyte relationships on growing endosteal surface of rabbit tibiae. Bone 13, 363-368.

Martin R.B., Burr D.B., 1989. Structure, function and adaptation of bone. Raven Press, New York.

Martin R.B., Burr D.B., Sharkey N.A., 1998. Skeletal tissue mechanics. Springer-Verlag, New York.

Martín-Francés L., Martinón-Torres M., Gracia-Téllez A., Bermúdez de Castro J.M., 2016. Evidence of trauma in a ca. 1-million-year-old patella of *Homo antecessor*, Gran Dolina-Atapuerca (Spain). C. R. Palevol 15, 1011-1016.

Masouros S.D., Bull A.M.J., Amis A.A., 2010. Biomechanics of the knee joint. Orthopaed. Trauma 24, 84-91.

Matarazzo S.A., 2015. Trabecular architecture of the manual elements reflects locomotor patterns in primates. PLoS ONE 10, e0120436.

Maureille B., Gómez-Olivencia A., Couture-Veschambre C., Madelaine S., Holliday T., 2015. Nouveaux restes humains provenant du gisement de Regourdou (Montignac-sur-Vézère, Dordogne, France). Paléo 26, 117-138.

Mazurier A., 2006. Relations entre comportement locomoteur et variation cortico-trabéculaire du plateau tibial chez les Primates: analyse quantitative noninvasive à haute réolution (SR-μCT) et applications au registre fossile. Ph.D Dissertation, Université de Poitiers, Poitiers.

Mazurier A., Nakatsukasa M., Macchiarelli R., 2010. The inner structural variation of the primate tibial plateau characterized by high-resolution microtomography. Implications for the reconstruction of fossil locomotor behaviours. C. R. Palevol 9, 349-359.

Mazurier A., Volpato V., Macchiarelli R., 2006. Improved noninvasive microstructural analysis of fossil tissues by means of SR-microtomography. Appl. Phys. A. Mater. Sci. Process. 83, 229-233.

McHenry H.M., 1971. Multivariate analysis of early hominid humeri. In: Giles E., Friedlaender J.S. (Ed.), The measures of man. Cambridge, Harvard University, pp. 338-371.

McHenry H.M., 1973. Early hominid humerus from East Rudolf, Kenya. Science 180, 739-741.

McHenry H.M., 1975a. The ischium and hip extensor mechanism in human evolution. Am. J. Phys. Anthropol. 43, 39-46.

McHenry H.M., 1975b. Biomechanical interpretation of the early hominid hip. J. Hum. Evol. 4, 343-355.

McHenry H.M., 1975c. A new pelvic fragment from Swartkrans and the relationship between the robust and gracile australopithecines. Am. J. Phys. Anthropol. 43, 245-262.

McHenry H.M., 1976. Fossil hominid femora and the evolution of walking. Nature 259, 657-658.

McHenry H.M., 1978. Fore- and hindlimb proportions in Plio-Pleistocene hominids. Am. J. Phys. Anthropol. 49, 15-22.

McHenry H.M., Brown C.C., 2008. Side steps: the erratic pattern of hominin postcranial change through time. J. Hum. Evol. 55, 639-651.

McHenry H.M., Brown C.C., McHenry L.J., 2007. Fossil hominin ulnae and the forelimb of Paranthropus. Am. J. Phys. Anthropol. 134, 209-218.

McHenry H.M., Corruccini R.S., 1975. Distal humerus in hominoid evolution. Folia Primatol. 23, 227-244.

McHenry H.M., Corruccini R.S., Howell F.C., 1976. Analysis of an early hominid ulna from the Omo Basin, Ethiopia. Am. J. Phys. Anthropol. 44, 295-304.

McKee J.K., Thackeray J.F., Berger L.R., 1995. Faunal assemblage seriation of Southern African Pliocene and Pleistocene fossil deposits. Am. J. Phys. Anthropol. 96, 235-250

McMahon T., 1973. Size and shape in biology: elastic criteria impose limits on biological proportions, and consequently on metabolic rates. Science 179, 1201-1204.

Mehlman P.T., Doran D.M., 2002. Influencing western gorilla nest construction at Mondika Research Center. Int. J. Primatol. 23, 1257-1285.

Menter C.G., Kuykendall K.L., Keyser A.W., Conroy G.C., 1999. First record of hominid teeth from the Plio-Pleistocene site of Gondolin, South Africa. J. Hum. Evol. 37, 299-307.

Middleton K.M., Shubin C.E., Moore D.C., Carter P.A., Garland T., Swartz S.M., 2008. The relative importance of genetics and phenotypic plasticity in dictating bone morphology and mechanics in aged mice: Evidence from an artificial selection experiment. Zool. 111, 135-147.

Mikuni-Takagaki Y., 1999. Mechanical responses and signal transduction pathways in stretched osteocytes. J. Bone Miner. Metab. 17, 57-60.

Mittra E., Rubin C., Qin Y., 2005. Interrelationship of trabecular mechanical and microstructural properties in sheep trabecular bone. J. Biomech. 38, 1229-1237.

Moggi-Cecchi J., Menter C., Boccone S., Keyser A., 2010. Early hominid dental remains from the Plio-Pleistocene site of Drimolen, South Africa. J. Hum. Evol. 58, 374-405.

Moorrees C.F., Fanning E.A., Hunt E.E. Jr. 1963. Age variation of formation stages for ten permanent teeth. J. Dent. Res. 42, 490-502.

Morgan E.F., Keaveny T.M., 2001. Dependence of yield strain of human trabecular bone on anatomic site. J. Biomech. 34, 569-577.

Morimoto N., Ponce de León M.S., Zollikofer C.P.E., 2011. Exploring femoral diaphyseal shape variation in wild and captive chimpanzees by means of morphometric mapping: A test of Wolff's Law. Anat. Rec. 294, 589-609.

Morris A.G., 1984. Osteological analysis populations of the cape and Western Africa. Ph.D. Dissertation, University of the Witwatersrand, Johannesburg.

Nadell J.A., Shaw C.N., 2015. Phenotypic plasticity and constraint along the upper and lower limb diaphyses of *Homo sapiens*. Am. J. Phys. Anthropol. 159, 410-422.

Napier J.R., 1964. The evolution of bipedal walking in the hominids. Arch. Biol. (Liege) 75, 673-708.

Nguyen N.H., Pahr D.H., Gross T., Skinner M.M., Kivell T.L., 2013. The biomechanical role of trabecular bone in the siamang (Symphalangus syndactylus) manual proximal phalanx. Eur. Soc. Study Hum. Evol. 3, 162.

Nguyen N.H., Pahr D.H., Gross T., Skinner M.M., Kivell T.L., 2014. Micro-finite element (lFE) modeling of the siamang (Symphalangus syndactylus) third proximal phalanx: the functional role of curvature and the flexor sheath ridge. J. Hum. Evol. 67, 60-75.

Nisell R., 1985. Mechanics of the knee. A study of joint and muscle load with clinical applications. Acta Orthop. Scandinava 56, 1-42.

Odgaard A., Kabel J., van Reitbergen B., Dalstra M., Huiskes R., 1997. Fabric and elastic principal directions of cancellous bone are closely related. J. Biomech. 30, 487-495.

Ohman J.C., Krochta T.J., Lovejoy C.O., Mensforth R.P., Latimer B., 1997. Cortical bone distribution in the femoral neck of hominoids: Implications for the locomotion of *Australopithecus afarensis*. Am. J. Phys. Anthropol. 104, 117-131.

Oxnard C.E., 1971. Tensile forces in skeletal structures. J. Morph. 134, 425-436.

Parkinson A.H., 2016. Traces of insect activity at Cooper's D fossil site (Cradle of Humankind, South Africa). Ichnos 23, 322-339.

Partridge T.C., 1982. Some preliminary observations on the stratigraphy and sedimentology of the Kromdraai B hominid site. Palaeoecol. Afr. 15, 3-12.

Patel B.A, 2005. The hominoid proximal radius: re-interpreting locomotor behaviors in early hominins. J. Hum. Evol. 48, 415-432.

Patel B.A., Carlson K.J., 2007. Bone density spatial patterns in the distal radius reflect habitual hand postures adopted by quadrupedal primates. J. Hum. Evol. 52, 130-141.

Patel V., Issever A.S., Burghardt A., Laib A., Ries M., Majumdar S., 2003. MicroCT evaluation of normal and osteoarthritic bone structure in human knee specimens. J. Orthop. Res. 21, 6-13.

Paternoster L., Lorentzon M., Lehtimäki T., Eriksson J., Kähönen M., Raitakari O., Laaksonen M., Sievänen H., Viikari J., Lyytikäinen L.-P., Mellström D., Karlsson M., Ljunggren O., Grundberg E., Kemp J.P., Sayers A., Nethander M., Evans D.M., Vandenput L., Tobias J.H., Ohlsson C., 2013. Genetic determinants of trabecular and cortical volumetric bone mineral densities and bone microstructure. PLoS Genetics 9, e1003247.

Patterson B., Howells W., 1967. Hominid humeral fragment from early Pleistocene of northwestern Kenya. Science 156, 64-66.

Pearson O.M., Lieberman D.E., 2004. The aging of Wolff's law: Ontogeny and responses to mechanical loading in cortical bone. Yearb. Phys. Anthropol. 47, 63-99.

Pebesma E.J., 2004. Multivariable geostatistics in S: The gstat package. Computers & Geosciences 30, 683-691.

Pennycuick C.J., 1967. The strength of the pigeon's wing bones in relation to their function. J. Exp. Biol. 46, 219-233.

Pettersson U., Nilsson M., Sundh V., Mellström D., Lorentzon M., 2010. Physical activity is the strongest predictor of calcaneal peak bone mass in young Swedish men. Osteoporos. Int. 21, 447-455

Pickering T.R., Heaton J.L., Clarke R.J., Sutton M.B., Brain C.K., Kuman K., 2012. New hominid fossils from Member 1 of the Swartkrans formation, South Africa. J. Hum. Evol. 62, 618-628.

Pickering T.R., Kramers J.D., Hancox P.J., de Ruiter D.J., Woodhead J.D., 2011. Contemporary flowstone development links early hominin bearing cave deposits in South Afric. Earth Plan. Sc. Letters 306, 23-32.

Pickford M., 2013. The diversity, age, biogeographic and phylogenetic relationships of Plio-Pleistocene suids from Kromdraai, South Africa. Ann. Ditsong Nat. Mus. Nat. Hist. 3, 11-32.

Pina M., 2016. Unravelling the positional behaviour of fossil hominoids: Morphofunctional and structural analysis of the primate hindlimb. Ph.D Dissertation, Universidad Autònoma de Barcelona, Barcelona.

Pina M., Alba D.M., Almécija S., Fortuny J., Moyà-Solà S., 2012. Brief communication: Paleobiological inferences on the locomotor repertoire of extinct hominoids based on femoral neck cortical thickness: The fossil great ape hispanopithecus laietanus as a test-case study. Am. J. Phys. Anthropol. 149, 142-148.

Pina M., Alba D.M., Almécija S., Moyà-Solà S., 2011. Is the cortical thickness of the femoral neck a diagnostic trait for inferring bipedalism? Paleontol. Evol. Memoria especial 5, 313-317.

Pina M., Almécija S., Alba D.M., O'Neill M.C., Moyà-Solà S., 2014. The middle Miocene ape Pierolapithecus catalaunicus exhibits extant great ape-like morphometric affinities on its patella: Inferences on knee function and evolution. PLoS ONE 9, e91944.

Platzer W., 2008. Color atlas of human anatomy. Locomotor System. Stuttgart Thieme, New York.

Polk J.D., Blumenfeld J., Ahlumwalia D., 2008. Knee posture predicted subchondral apparent density in the distal femur: an experimental validation. Anat. Rec. 291, 293-302.

Pontzer H., Lieberman D.E., Momin E., Devlin M.J., Polk J.D., Hallgrímsson B., Cooper D.M. L., 2006. Trabecular bone in the bird knee responds with high sensitivity to changes in load orientation. J. Exp. Biol. 209, 57-65.

Pouydebat E., Laurin M., Gorce P., Bels V., 2008. Evolution of grasping among anthropoids. J. Evol. Biol. 21, 1732-1743

Prat S., Brugal J.-P., Roche H., Texier P.-J., 2003. Nouvelles découvertes de dents d'hominidés dans le Membre Kaitio de la Formation de Nachukui (1.65-1.9 Ma) ouest du Lac Turkana (Kenya). C. R. Palevol 2, 685-693.

Preuschoft H., 1970. Functional anatomy of the lower extremity. In: G. Bourne (Ed.), The chimpanzee. Basel/München/New York, Karger, pp 221-294.

Preuschoft H., Tardieu C., 1996. Biomechanical reasons for the divergent morphology of the knee joint and the distal epiphyseal suture in hominoids. Folia Primatologica 66, 82-92.

Puymerail L., 2011. Caractérisation de l'endostructure et des propriétés biomécaniques de la diaphyse fémorale: la signature de la bipédie et la reconstruction des paléo-répertoires posturaux et locomoteurs des hominines. Ph.D Dissertation, Muséum national d'Histoire naturelle, Paris.

Puymerail L., 2013. The functionally-related signatures characterizing the endostructural organisation of the femoral shaft in modern humans and chimpanzee. C. R. Palevol 12, 223-231.

Puymerail L., Bondioli L., Engda B., Mazurier A., Macchiarelli R., 2014. The Early Pleistocene human distal humerus from Gombore I, Melka Kunture (Upper Awash basin, Ethiopia). Cortical bone topography and structural organization. Int. Symp. The Afr. Hum. Foss. Rec. Toulouse, 15-16

Puymerail L., Ruff C.B., Bondioli L., Widianto H., Trinkaus E., Macchiarelli R., 2012. Structural analysis of the Kresna 11 *Homo erectus* femoral shaft (Sangiran, Java). J. Hum. Evol. 63, 741-749.

Radovčić J., Smith F.H., Trinkaus E., Wolpoff M.H., 1988. The Krapina hominids. An illustrated catalog of skeletal collection. Croatian Natural History Museum, Zagreb.

Rafferty K.L., 1998. Structural design of the femoral neck in primates. J. Hum. Evol. 34, 361-383.

Rafferty K.L., Ruff C.B., 1994. Articular structure and function in *Hylobates*, *Colobus*, and *Papio*. Am. J. Phys. Anthropol. 94, 395-408.

Raichlen D.A., Gordon A.D., Foster A.D., Webber J.T., Sukhdeo S.M., Scott R.S., Gosman J.H., Ryan T.M., 2015. An ontogenetic framework linking locomotion and trabecular

bone architecture with applications for reconstructing hominin life history. J. Hum. Evol. 81, 1-12.

Rak Y., 1983. The australopithecine face. Academic Press, New York.

Rak Y., Kimbel W.H., 1991. On the squamosal suture of KNM-WT 17000. Am. J. Phys. Anthropol. 85, 1-6.

Rak Y., Kimbel W.H., 1993. Reply to Drs. Walker, Brown and Ward. Am. J. Phys. Anthropol. 90, 506-507.

Raux P., Townsend P.R., Miegel R., Rose R.M., Radin E.L., 1975. Trabecular architecture of the human. J. Biomech. 8, l-7.

Rein T.R., Harrison T., Carlson K.J., Harvati K., 2017. Adaptation to suspensory locomotion in *Australopithecus sediba*. J. Hum. Evol. 104, 1-12.

Remis M., 1995. Effects of body size and social context on the arboreal activities of lowland gorillas in the Central African Republic. Am. J. Phys. Anthropol. 97, 413-433.

Rhodes J.A., Knüsel C.J., 2005. Activity-related skeletal change in medieval humeri: Cross-sectional and architectural alterations. Am. J. Phys. Anthropol. 128, 536-546.

Richmond B.G., Jungers W.L., 2008. Orrorin tugenensis femoral morphology and the evolution of hominin bipedalism. Science 319, 1662-1665.

Robinson J.T., 1954. The genera and species of the *Australopithecinae*. Am. J. Phys. Anthropol. 12, 181-200.

Robinson J.T., 1972. Early hominid posture and locomotion. University of Chicago Press, Chicago

Robling A.G., Hinant F.M., Burr D.B., Turner C.H., 2002. Improved bone structure and strength after long-term mechanical loading is greatest if loading is separated into short bouts. J. Bone Min. Res. 17, 1545-1554.

Rockoff S.D., Sweet E., Bleustein J., 1969. The relative contribution of trabecular and cortical bone to the strength of human lumbar vertebrae. Calcif. Tissue Res. 3, 163-175.

Rockwell L.C., 1994. Shape differences of the elbow joint between male and female large-bodied hominoids including humans. Am. J. Phys. Anthropol. S18, 171.

Rogers R.R., LaBarbera M., 1993. Contribution of internal bony trabeculae to the mechanical properties of the humerus of the pigeon (Columba livia). J. Zoo. 230, 433-441.

Rook L., Bondioli L., Köhler M., Moyà-Solà S., Macchiarelli R., 1999. Oreopithecus was a bipedal ape after all: evidence from the iliac cancellous architecture. Proc. Natl. Acad. Sc. USA 96, 8795-8799.

Rothman J.M., Van Soest P.J., Pell A.N., 2006. Decaying wood is a sodium source for mountain gorillas. Biol. Lett. 2, 321-324.

Rubin C.T., Lanyon L.E., 1985. Regulation of bone mass by mechanical strain magnitude. Calcif. Tissue Int. 37, 411-417.

Rubin C.T., McLeod K.J., Bain S.D., 1990. Functional strains and cortical bone adaptation: epigenetic assurance of skeletal integrity. J. Biomech. 23, 43-54.

Rubin C.T., Turner A.S., Bain S., Mallinckrodt C., McLeod K., 2001. Anabolism: low mechanical signals strengthen long bones. Nature 412, 603-604.

Rubin C.T., Turner A.S., Mallinckrodt C., Jerome C., Mcleod K., Bain S., 2002. Mechanical strain, induced noninvasively in the high-frequency domain is anabolic to cancellous bone, but not cortical bone. Bone 30, 445-452

Ruff C.B., 1988. Hindlimb articular surface allometry in *Hominoidea* and *Macaca*, with comparisons to diaphyseal scaling. J. Hum. Evol. 17, 687-714.

Ruff C.B., 1995. Biomechanics of the hip and birth in early *Homo*. Am. J. Phys. Anthropol. 98, 527-574.

Ruff C.B., 2002. Long bone articular and diaphyseal structure in old world monkeys and apes. I: Locomotor effects. Am. J. Phys. Anthropol. 119, 305-342.

Ruff C.B., 2008a. Femoral/humeral strength in early African *Homo erectus*. J. Hum. Evol. 54, 383-390.

Ruff C.B., 2008b. Biomechanical analyses of archaeological human skeletons. In: Katzenberg M.A., Saunders S.R. (Ed.), Biological anthropology of the human skeleton. Alan R. Liss, New York, pp. 183-206.

Ruff C.B., 2009. Relative limb strength and locomotion in *Homo habilis*. Am. J. Phys. Anthropol. 138, 90-100

Ruff C.B., 2017. Mechanical constraints on the hominin pelvis and the "obstetrical dilemma". Anat. Rec. 30, 946-955.

Ruff C.B., Burgess M.L., Junno J.A., Mudakikwa A., Zollikofer C.P., Ponce de León M.S., McFarlin, S.C., 2018b. Phylogenetic and environmental effects on limb bone structure in gorillas. Am. J. Phys. Anthropol. 166, 353-372.

Ruff C.B., Burgess M.L., Ketcham R.A., Kappelman J., 2016. Limb bone structural proportions and locomotor behavior in AL 288-1 ("Lucy"). PLoS ONE 11, e0166095.

Ruff C.B., Burgess M.L., Squyres N., Junno J.A., Trinkaus E., 2018a. Lower limb articular scaling and body mass estimation in Pliocene and Pleistocene hominins. J. Hum. Evol. 115, 85-111.

Ruff C.B., Higgins R., 2013. Femoral neck structure and function in early hominins. Am. J. Phys. Anthropol. 150, 512-525.

Ruff C.B., Holt B.H., Trinkaus E., 2006. Who's afraid of the big bad Wolff?: 'Wolff's law' and bone functional adaptation. Am. J. Phys. Anthropol. 129, 484-498.

Ruff C.B., Holt B.H., Trinkaus E., 2006. Who's afraid of the big bad Wolff? Wolff's Law and bone functional adaptation. Am. J. Phys. Anthropol. 129, 484-498.

Ruff C.B., Jones H.H., 1981. Bilateral asymmetry in cortical bone of the humerus and tibia sex and age factors. Hum. Biol. 53, 69-86.

Ruff C.B., McHenry H.M., Thackeray J.F., 1999. Cross-sectional morphology of the SK 82 and 97 proximal femora. Am. J. Phys. Anthropol. 109, 509-521.

Ruff C.B., Puymerail L., Macchiarelli R., Sipla J., Ciochon R.L., 2015. Structure and composition of the Trinil femora: functional and taxonomic implications. J. Hum. Evol. 80, 147-158.

Ruff C.B., Trinkaus E., Walker A., Larsen C.S., 1993. Postcranial robusticity in *Homo*. I: Temporal trends and mechanical interpretation. Am. J. Phys. Anthropol. 91, 21-53.

Ruff C.B., Walker A., Trinkaus E., 1994. Postcranial robusticity in *Homo*. III: Ontogeny. Am. J. Phys. Anthropol. 65, 191-197.

Ruimerman R., Hilbers P., Van Rietbergen B., Huiskes R., 2005. A theoretical framework for strain-related trabecular bone maintenance and adaptation. J. biomech. 38, 931-941.

Ryan T.M., Carlson K.J., Gordon A.D., Jablonski N., Shaw C.N., Stock J.T., 2018. Human-like hip joint loading in *Australopithecus africanus* and *Paranthropus robustus*. J. Hum. Evol. 121, 12-24.

Ryan T.M., Ketcham R.A., 2002a. The three-dimensional structure of trabecular bone in the femoral head of strepsirrhine primates. J. Hum. Evol. 43, 1-26.

Ryan T.M., Ketcham R.A., 2002b. Femoral head trabecular bone structure in two omomyid primates. J. Hum. Evol. 43, 241-263.

Ryan T.M., Ketcham R.A., 2005. Angular orientation of trabecular bone in the femoral head and its relationship to hip joint loads in leaping primates. J. Morph. 265, 249-263.

Ryan T.M., Krovitz G.E., 2006. Trabecular bone ontogeny in the human proximal femur. J. Hum. Evol. 51, 591-602.

Ryan T.M., Shaw C.N., 2012. Unique suites of trabecular bone features characterize locomotor behaviour in human and nonhuman anthropoid primates. PLoS ONE 7, e41037.

Ryan T.M., Shaw C.N., 2013. Trabecular bone microstructure scales allometrically in the primate humerus and femur. Proc. R. Soc. B 280, 20130172.

Ryan T.M., Shaw C.N., 2015. Gracility of the modern *Homo sapiens* skeleton is the result of decreased biomechanical loading. Proc. Natl. Acad. Sci. USA 112, 372-377.

Ryan T.M., Sukhdeo S., 2016. KSD-VP-1/1: Analysis of the postcranial skeleton using high-resolution computed tomography. In: Haile-Selassie Y., Su D.E. (Ed.), The postcranial anatomy of *Australopithecus afarensis*. Springer, Dordrecht, pp. 39-62.

Ryan T.M., van Rietbergen B., 2005. Mechanical significance of femoral head trabecular bone structure in *Loris* and *Galago* evaluated using micromechanical finite element models. Am. J. Phys. Anthropol. 126, 82-96.

Ryan T.M., Walker A., 2010. Trabecular bone structure in the humeral and femoral heads of anthropoid primates. Anat. Rec. 293, 719-729.

Saers J.P.P., Cazorla-Bak Y., Shaw C.N., Stock J.T., Ryan T.M., 2016. Trabecular bone structural variation throughout the human lower limb. J. Hum. Evol. 97, 97-108.

Sakaue K., 1997. Bilateral asymmetry of the humerus in Jomon people and modern Japanese. Anthropol. Sci. 105, 231-246.

Sanchez S., Ahlberg P.E., Trinajstic K.M., Mirone A., Tafforeau P., 2012. Three-dimensional synchrotron virtual paleohistology: A new insight into the world of fossil bone microstructures. Microsc. Microanal. 18, 1095-1105.

Saparin P., Scherf H., Hublin J.-J., Fratzl P., Weinkamer R., 2011. Structural adaptation of trabecular bone revealed by position resolved analysis of proximal femora of different primates. Anat. Rec. 294, 55-67.

Sarringhaus L.A., Stock J.T., Marchant L.F., McGrew W.C., 2005. Bilateral asymmetry in the limb bones of the chimpanzee (*Pan troglodytes*). Am. J. Phys. Anthropol. 128, 840-845.

Schaller G.E., 1963. The mountain *Gorilla*. Chicago University Press, Chicago.

Scherf H., 2007. Locomotion-related femoral trabecular architectures in primates. Ph.D Dissertation, Technische Universität, Berlin.

Scherf H., 2008. Locomotion-related femoral trabecular architectures in primates- high resolution computed tomographies and their implications for estimations of locomotor preferences of fossil primates. In: Endo I., Frey R. (Ed.), Anatomical imaging. Springer, Tokyo, pp. 39-59.

Scherf H., Harvati K., Hublin J.-J., 2013. A comparison of proximal humeral cancellous bone of great apes and humans. J. Hum. Evol. 65, 29-38.

Schillinger B., Beaudet A., Fedrigo A., Grazzi F., Kullmer O., Laaß M., Makowska M.,I Werneburg I., Zanolli C., 2018. Neutron imaging in cultural heritage research at the FRM II reactor of the Heinz Maier-Leibnitz Center. J. Imaging 4, 22.

Schindler O.S., Scott W.N., 2011. Basic kinematics and biomechanics of the patella-femoral joint. Part 1: The native patella. Acta Orthop. Belg. 77, 421-431.

Schoenau E., 2005. From mechanostat theory to development of the" Functional Muscle-Bone-Unit". J. Musculoskelet. Neuronal Interact. 5, 232.

Schroer K., Wood B., 2015. The role of character displacement in the molarization of hominin mandibular premolars. Evol. 69, 1630-1642.

Schultz A.H., 1953. The relative thickness of the long bones and the vertebrae in primates. Am. J. Phys. Anthropol. 11, 277-312.

Schwartz G.T., 2012. Growth, development, and life history throughout the evolution of *Homo*. Curr. Anthro. 53, S395-S408.

Schwartz J.H., Tattersall I., 2003. The human fossil record, volume 2. Craniodental morphology of genus *Homo* (Africa and Asia). Wiley-Liss, New York.

Scott J.E., Lockwood C.A., 2004. Patterns of tooth crown size and shape variation in great apes and humans and species recognition in the hominid fossil record. Am. J. Phys. Anthropol. 125, 303-319.

Selker F., Carter D.R., 1989. Scaling of long bone fracture strength with animal mass. J. biomech. 22, 1175-1183.

Senut B., 1979. Comparison des hominidés de Gomboré IB et de Kanapoi: deux pièces du genre *Homo*? Bull. Mem. Soc. Anthropol. Paris 6, 111-117.

Senut B., 1981a. Outlines of the distal humerus in hominoid primates: Application to some Plio-Pleistocene hominids. In: Chiarelli B., Corruccini R.S. (Ed.), Primate evolutionary biology. Springer-Verlag, Berlin, pp. 81-92.

Senut B., 1981b. Humeral outlines in some hominoid primates and in Plio-Pleistocene hominids. Am. J. Phys. Anthropol. 56, 275-283.

Senut B., 1986. Long bones of the primate upper limb: Monomorphic or dimorphic? Hum. Evol. 1, 7-22.

Senut B., and Tardieu C., 1985. Functional aspects of Plio-Pleistocene hominid limb bones. In: Delson E. (Ed.) Ancestors: The hard evidence. Alan R. Liss, New York, pp. 193-201.

Šešelj M., 2017. Brief communication: An analysis of dental development in Pleistocene *Homo* using skeletal growth and chronological age. Am. J. Phys. Anthropol. 163, 531-541.

Shaw C.N., Ryan T.M., 2012. Does skeletal anatomy reflect adaptation to locomotor patterns? Cortical and trabecular architecture in humans and nonhuman anthropoids. Am. J. Phys. Anthropol. 147, 187-200.

Shaw C.N., Stock J.T., 2009. Habitual throwing and swimming correspond with upper limb diaphyseal strength and shape in modern human athletes. Am. J. Phys. Anthropol. 140, 160-172.

Shaw C.N., Stock J.T., 2013. Extreme mobility in the Late Pleistocene? Comparing limb biomechanics among fossil *Homo*, varsity athletes and Holocene foragers. J. Hum. Evol. 64, 242-249.

Shipman P., 2013. Why is human childbirth so painful? Am. Scient. 101, 426-429.

Shipman P., Rose J. 1983. Early hominid hunting, butchering, and carcass-processing behaviours: approaches to the fossil record. J. Anthropol. Archaeol. 2, 57-98.

Simkin A., Ayalon J., Leichter I., 1987. Increased trabecular bone density due to bone-loading exercises in potstmenopausal osteoporotic women. Calcif. Tissue Int. 40, 59-63.

Sinclair K.D., Farnsworth R.W., Pham T.X., Knight A.N., Bloebaum R.D., Skedros J.G., 2013. The artiodactyl calcaneus as a potential "control bone" cautions against simple interpretations of trabecular bone adaptation in the anthropoid femoral neck. J. Hum. Evol. 64, 366-379.

Skedros J.G., Baucom S.L., 2007. Mathematical analysis of trabecular "trajectories" in apparent trajectorial structures: The unfortunate historical emphasis on the human proximal femur. J. Theor. Biol. 244, 15-45.

Skedros J.G., Hunt K.J., Bloebaum R.D., 2004. Relationships of loading history and structural and material characteristics of bone: development of the mule deer calcaneus. J. Morph. 259, 281-307.

Skedros J.G., Knight A.N., Farnsworth R.W., Bloebaum R.D., 2012. Do regional modifications in tissue mineral content and microscopic mineralization heterogeneity adapt trabecular bone tracts for habitual bending? Analysis in the context of trabecular architecture of deer calcanei. J. Anat. 220, 242-255.

Skelton R.R., McHenry H.M., 1992. Evolutionary relationships among early hominids. J. Hum. Evol. 23, 309-349.

Skerry T.M., 2000. Biomechanical influences on skeletal growth and development. In: O'Higgins P., Cohn M.S. (Ed.), Development, growth and evolution: implications for the study of the hominid skeleton. Academic Press, London, pp 29-39.

Skerry T.M., 2008. The response of bone to mechanical loading and disuse: fundamental principles and influences on osteoblast/osteocyte homeostasis. Arch. Biochem. Biophys. 473, 117-123.

Skerry T.M., Lanyon L.E., 1995. Interruption of disuse by short duration walking exercise does not prevent bone loss in the sheep calcaneus. Bone 16, 269-274.

Skinner M.M., Kivell T.L., Potze S., Hublin J.J., 2013. Microtomographic archive of fossil hominin specimens from Kromdraai B, South Africa. J. Hum. Evol. 64, 434-447.

Skinner M.M., Stephens N.B., Tsegai Z.J., Foote A.C., Nguyen N.H., Gross T., Pahr D.H., Hublin J.-J., Kivell T.L., 2015. Human-like hand use in *Australopithecus africanus*. Science 347, 395-399.

Smith B.H., 1993. The physiological age of KNM-WT 15000. In: Walker A., Leakey R. (Ed.), The Nariokotome *Homo erectus* skeleton. Harvard University Press, Cambridge, MA, pp. 195-220.

Sparacello V., Marchi D., 2008. Mobility and subsistence economy: a diachronic comparison between two groups settled in the same geographical area (Liguria, Italy). Am. J. Phys. Anthropol. 136, 485-495.

Spoor F., Wood B., Zonneveld F., 1994. Implications of early hominid labyrinthine morphology for evolution of human bipedal locomotion. Nature 369, 645-648.

Standring S., 2008. Gray's anatomy: The anatomical basis of clinical practice. Elsevier Health Sciences, UK.

Stauber M., Rapillard L., van Lenthe G.H., Zysset P., Müller R., 2006. Importance of individual rods and plates in the assessment of bone quality and their contribution to bone stiffness. J. Bone Min. Res. 21, 586-595.

Stern J.T., 2000. Climbing to the top: A personal memoir of *Australopithecus afarensis*. Evol. Anthropol. 9, 113.

Stock J.T., 2006. Hunter-gatherer postcranial robusticity relative to patterns of mobility, climatic adaptation, and selection for tissue economy. Am. J. Phys. Anthropol. 131, 194-204.

Stock J.T., Pfeiffer S., 2001. Linking structural variability in long bone diaphyses to habitual behaviors: foragers from the southern African Later Stone Age and the Andaman Islands. Am. J. Phys. Anthropol. 115, 337-348.

Strait D.S., Grine F.E., 2004. Inferring hominoid and early hominid phylogeny using craniodental characters: The role of fossil taxa. J. Hum. Evol. 47, 399-452.

Strait D.S., Grine F.E., Fleagle J.G., 2015. Analyzing hominin phylogeny: Cladistic approach. In: Henke W., Tattersall I. (Ed.), Handbook of paleoanthropology. Springer, Berlin Heidelberg, pp. 1989-2014.

Strait D.S., Grine F.E., Moniz M.A., 1997. A reappraisal of early hominid phylogeny. J. Hum. Evol. 32, 17-82.

Strait D.S., Mongle C.S., Grine F.E., 2018. The systematics of robust australopiths. Am. J. Phys. Anthropol. 165, 267-268.

Straus W.L., 1948. The humerus of *Paranthropus robustus*. Am. J. Phys. Anthropol. 6, 285-313.

Su A., Carlson K.J., 2017. Comparative analysis of trabecular bone structure and orientation in South African hominin tali. J. Hum. Evol. 106, 1-18.

Su A., Wallace I.J., Nakatsukasa M., 2013. Trabecular bone anisotropy and orientation in an Early Pleistocene hominin talus from East Turkana, Kenya. J. Hum. Evol. 64, 667-677.

Susman R.L., 1988. New postcranial remains from Swartkrans and their bearing on the functional morphology and behavior of *Paranthropus robustus*. In: Grine F.E. (Ed.), The evolutionary history of the ‘"robust" australopithecines. Aldine de Gruyter, New York, pp. 149-172.

Susman R.L., 1989. New hominid fossils from the Swartkrans formation (1979-1986 excavations): craniodental specimens. Am. J. Phys. Anthropol. 79, 451-474.

Susman R.L., 2004. Swartkrans; a cave's chronicle of early man. Hominid postcranial remains from Swartkrans. Transv. Mus. Monogr. 8, 117-136.

Susman R.L., Brain T.M., 1988. New first metatarsal (SKX 5017) from Swartkrans and the gait of *Paranthropus robustus*. Am. J. Phys. Anthropol. 77, 7-15.

Susman R.L., de Ruiter D.J., 2004. New hominin first metatarsal (SK 1813) from Swartkrans. J. Hum. Evol. 47, 171-181.

Susman R.L., de Ruiter D., Brain C.K., 2001. Recently identified postcranial remains of Paranthropus and early *Homo* from Swartkrans Cave, South Africa. J. Hum. Evol. 41, 607-629.

Sutton M.B., Pickering T.R., Pickering R., Brain C.K., Clarke R.J., Heaton J.L., Kuman K., 2009. Newly discovered fossil- and artifact-bearing deposits, uranium-series ages, and Plio-Pleistocene hominids at Swartkrans Cave, South Africa. J. Hum. Evol. 57, 688-696.

Sutton M.D., 2008. Tomographic techniques for the study of exceptionally preserved fossils. Proc. R. Soc. B 275, 1587-1593.

Suwa G., 1988. Evolution of the ‘‘robust’’ australopithecines in the Omo succession: Evidence from mandibular premolar morphology. In: Grine F.E. (Ed.), Evolutionary history of the ‘‘robust’’ australopithecines. Aldine de Gruyter, New York, pp. 199-222.

Suwa G., Asfaw B., Beyene Y., White T.D., Katoh S., Nagaoka S., Nakaya H., Uzawa K., Renne P., Woldegabriel G., 1997. The first skull of *Australopithecus boisei*. Nature 389, 489-492.

Suwa G., Wood B.A., White T.D., 1994. Further analysis of mandibular molar crown and cusp areas in Pliocene and early Pleistocene hominids. Am. J. Phys. Anthropol. 93, 407-426.

Swartz S.M., Parker A., Huo C., 1998. Theoretical and empirical scaling patterns and topological homology in bone trabeculae. J. Exp. Biol. 201, 573-590.

Sylvester A., 2013. A geometric morphometric analysis of the medial tibial condyle of African hominids. Anat. Rec. 296, 1518-1525.

Szalay F.S., 1971. Biological level of organization of the Chesowanja robust australopithecine. Nature 234, 229-230.

Tallman M., 2013. Forelimb to hindlimb shape covariation in extant hominoids and Plio-Pleistocene hominins. Anat Rec. 296, 290-304.

Tallman M., 2016. Shape ontogeny of the distal femur in the *Hominidae* with implications for the evolution of bipedality. PLoS ONE11, e0148371.

Tardieu C., 1999. Ontogeny and phylogeny of femoro-tibial characters in humans and hominid fossils: Functional influence and genetic determinism. Am. J. Phys. Anthropol. 110, 365-377.

Taylor W.R., Heller M.O., Bergmann G., Duda G.N., 2004. Tibio-femoral loading during human gait and stair climbing. J. Orthop. Res. 22, 625-632.

Thackeray J.F., Braga J., Sénégas F., Gommery D., Potze S., Senut B., 2005. Discovery of a humerus shaft from Kromdraai B: Part of the skeleton of the type specimen of *Paranthropus robustus* Broom, 1938? Ann. Transv. Mus. 42, 92-93.

Thackeray J.F., de Ruiter D.J., Berger L.R., Van Der Merwe N.J., 2001. Hominid fossils from Kromdraai: A revised list of specimens discovered since 1938. Ann. Transv. Mus. 38, 43-56.

Thackeray J.F., Kirschvink J.L., Raub T.D., 2002. Palaeomagnetic analyses of calcified deposits from the Plio-Pleistocene hominid site of Kromdraai, South Africa. South Afr. J. Sci. 98, 537-540.

Thompkins R.J., 1977. Early hominid postcrania and locomotor adaptations. Kroeber Anthropol. Soc. Pap. 50, 85-104.

Thorpe S.K.S., Holder R.L., Crompton R.H., 2007. Origin of human bipedalism as an adaptation for locomotion on flexible branches. Science 316, 1328-1331.

Tobias P.V., 1967. The cranium and maxillary dentition of *Australopithecus* (*Zinjanthropus*) *boisei*. Cambridge University Press, Cambridge.

Tobias P.V., 1988. Numerous apparently synapomorphic features in *Australopithecus robustus*, *Australopithecus boisei* and *Homo habilis*: Support for the Skelton McHenry-Drawhorn hypothesis. In: Grine F.E. (Ed.), Evolutionary history of the ‘‘robust’’ australopithecines. Aldine de Gruyter, New York, pp. 293-308.

Toumi H., Higashiyama I., Suzuki D., Kumai T., Bydder G., McGonagle D.D., Emery P., Fairclough J., Benjamin M., 2006. Regional variations in human patellar trabecular architecture and the structure of the proximal patellar tendon enthesis. J. Anat. 208, 47-57.

Toumi H., Larguech G., Filaire E., Pinti A., Lespessailles E., 2012. Regional variations in human patellar trabecular architecture and the structure of the quadriceps enthesis: A cadaveric study. J. Anat. 220, 632-637.

Touraine S., Bouhadoun H., Engelke K., Laredo J.D., Chappard C., 2017. Influence of meniscus on cartilage and subchondral bone features of knees from older individuals: A cadaver study. PLoS ONE 12, e0181956.

Townsend P.R., Rose R.M., Radin E.L., Raux P., 1977. The biomechanics of the human patella and its implications for chondromalacia. J. Biomech. 10, 403-407.

Townsend P.R., Raux P., Rose R.M., Miegel R.E., Radin E.L., 1975. The distribution and anisotropy of the stiffness of cancellous bone in the human patella. J. Biomech. 8, 363-367.

Trinkaus E., 2018. The palaeopathology of the Ohalo 2 Upper Paleolithic human remains: A reassessment of its appendicular robusticity, humeral asymmetry, shoulder degenerations, and costal lesion. Int. J. Osteoarchaeol. 28, 143-152.

Trinkaus E., Churchill S.E., 1999. Diaphyseal cross-sectional geometry of Near Eastern Middle Palaeolithic humans: the humerus. J. Archaeol. Science 26, 173-184.

Trinkaus E., Churchill S.E., Ruff C.B., 1994. Postcranial robusticity in *Homo*. II: Humeral bilateral asymmetry and bone plasticity. Am. J. Phys. Anthropol. 93, 1-34.

Trinkaus E., Churchill S.E., Ruff C.B., 1994. Postcranial robusticity in *Homo*. II: Humeral bilateral asymmetry and bone plasticity. Am. J. Phys. Anthropol. 93, 1-34

Trinkaus E., Churchill S.E., Ruff C.B., Vandermeersch B., 1999. Long bone shaft robusticity and body proportions of the Saint-Césaire 1 Châtelperronian Neanderthal. J. Archaeol. Science 26, 753-773.

Trinkaus E., Ruff C.B., 2012. Femoral and tibial diaphyseal cross-sectional Geometry in Pleistocene *Homo*. PaleoAnthropology 2012, 13-62.

Tsegai Z.J., Kivell T.L., Gross T., Nguyen N.H., Pahr D.H., Smaers J.B., Skinner M.M., 2013. Trabecular bone structure correlates with hand posture and use in hominoids. PLoS ONE 8, e78781.

Tsegai Z.J., Skinner M.M., Gee A.H., Pahr D.H., Treece G.M., Hublin J.-J., Kivell T.L., 2017. Trabecular and cortical bone structure of the talus and distal tibia in *Pan* and *Homo*. Am. J. Phys. Anthropol. 163, 784-805.

Tsegai Z.J., Skinner M.M., Pahr D.H., Hublin J.-J., Kivell T.L., 2016. Systemic patterns of trabecular structure in *Homo* and *Pan*: Evaluating inter-and intraspecific variability across anatomical sites. Am. J. Phys. Anthropol. 159, 318-319.

Tsegai Z.J., Skinner M.M., Pahr D.H., Hublin J.-J., Kivell, T.L., 2018. Systemic patterns of trabecular bone across the human and chimpanzee skeleton. J. Anat. 232, 641-656.

Turner A.S., 2001 Animal models of osteoporosis - necessity and limitations. Eur. Cell. Mater. 1, 66-81.

Turner A.S., Wood B., 1993a. Taxonomic and geographic diversity in robust australopithecines and other African Plio-Pleistocene larger mammals. J. Hum. Evol. 24, 147-168.

Turner A.S., Wood B., 1993b. Comparative palaeontological context for the evolution of the early hominid masticatory system. J. Hum. Evol. 24, 301-318.

Turner C.H., 1998. Three rules for bone adaptation to mechanical stimuli. Bone 23, 399-407.

Turner C.H., Pavalko F.M., 1998. Mechanotransduction and functional response of the skeleton to physical stress: the mechanisms and mechanics of bone adaptation. J Orthop. Sci. 3, 346-355.

Ulrich D., van Reitbergen B., Laib A., Ruegsegger P., 1999. The ability of three-dimensional structural indices to reflect material aspects of trabecular bone. Bone 25, 55-60.

Val A., Stratford D.J., 2015. The macrovertebrate fossil assemblage from the Name Chamber, Sterkfontein: Taxonomy, taphonomy and implications for site formation processes. Palaeont. Afr. 50, 1-17.

Val A., Taru P., Steininger C., 2014. New taphonomic analysis of large-bodied primate assemblage from Cooper's D, Bloubank valley, South Africa. The South Afr. Archaeol. Bull. 69, 49-58.

van der Meulen M.C.H., Ashford M.W. Jr., Kiralti B.J., Bachrach L.K., Carter D.R., 1996. Determinant of femoral geometry and structure during adolescent growth. J. Orthop. Res. 14, 22-29.

van der Meulen M.C.H., Beaupré G.S., Carter D.R., 1993. Mechanobiologic influences in long bone cross-sectional growth. Bone 14, 63-642.

van der Meulen M.C.H., Carter D.H., 1995. Developmental mechanics determine long bone allometry. J. Theor. Biol. 172, 323-327.

van Rietbergen B., Müller R., Ulrich D., Rüegsegger P., Huiskes R., 1999. Tissue stresses and strain in trabeculae of the canine proximal femur can be quantified from computer reconstructions. J. Biomech. 32, 165-73.

van Rietbergen B., Odgaard A., Kabel J., Huiskes R., 1998. Relationships between bone morphology and bone elastic properties can be accurately quantified using high-resolution computer reconstructions. J. Orthop. Res. 16, 23-28.

van Rietbergen B., Weinans H., Huiskes R., Odgaard A., 1995. A new method to determine trabecular bone elastic properties and loading using micromechanical finite element models. J. Biomech. 28, 69-81.

VanSickle C., 2016. An updated prehistory of the human pelvis recent fossil discoveries are raising new questions about how the modern human pelvis developed its unique shape. Sci. Am. 104, 354-361.

Vekua A., Lordkipanidze D., Rightmire G.P., Agusti J., Ferring R., Maisuradze G., Mouskhelishvili A., Nioradze M., Ponce de Leon M., Tappen M., Merab Tvalchrelidze M., Zollikofer C., 2002. A new skull of early *Homo* from Dmanisi, Georgia. Science 297, 85-89.

Viola T.B., 2002. Locomotion dependent variation in the trabecular pattern of the hominoid proximal femur. Am. J. Phys. Anthropol. 117, 160.

Volkman S.K., Galecki A.T., Burke D.T., Paczas M.R., Moalli M.R., Miller R.A., Goldstein S.A., 2003. Quantitative trait loci for femoral size and shape in a genetically heterogeneous mouse population. J. Bone Miner. Res. 18, 1497-1505.

Volpato V., 2007. Morphogenèse des propriétés texturales du tissu osseux et environnement biomécanique: caractérisation non invasive du réseau trabéculaire et de l'os cortical du squelette appendiculaire de mammifères actuels et fossiles, hominidés inclus. Ph.D Dissertation, Université de Poitiers.

Volpato V., Couture C., Macchiarelli R., Vandermeersch B., 2011. Endostructural characterisation of the Regourdou 1 Neanderthal proximal arm: bilateral asymmetry and handedness. In: Condemi S., Weniger G.-C. (Ed.), Continuity and discontinuity in the peopling of Europe. Springer, Dordrecht, pp. 175-178.

Volpato V., Macchiarelli R., Guatelli-Steinberg D., Fiore I., Bondioli L., Frayer D.W., 2012. Hand to mouth in a Neandertal: right-handedness in Regourdou 1. PLoS ONE 7, e43949.

Vrba E.S., 1975. Some evidence of chronology and palaeoecology of Sterkfontein, Swartkrans and Kromdraai from the fossil Bovidae. Nature 254, 301-304.

Vrba E.S., 1981. The Kromdraai australopithecine site revisited in 1980: Recent investigations and results. Ann. Transv. Mus. 33, 17-60.

Vrba E.S., 1982. Gondolin site, Broederstroom, progress report. Progress Report to the National Monuments Council, Ref. #TM 3/6/9/1.

Vrba E.S., Panagos D.C., 1982. New perspectives on taphonomy, palaeoecology and chronology of the Kromdraai apeman. Palaeoecol. Afr. 15, 13-26.

Walker A.C., Brown B., Ward S.C., 1993. Squamosal suture of cranium KNMWT 17000. Am. J. Phys. Anthropol. 90, 501-505.

Walker A.C., Leakey R.E., 1993. The Nariokotome *Homo erectus* Skeleton. Harvard University Press, Cambridge, MA.

Walker A.C., Leakey R.E., Harris J.M., Brown F.H., 1986. 2.5 Myr *Australopithecus boisei* from west of Lake Turkana, Kenya. Nature 322, 517-522.

Wallace I.J., Middleton K.M., Lublinsky S., Kelly S.A., Judex S., Garland T., Demes B., 2010. Functional significance of genetic variation underlying limb bone diaphyseal structure. Am. J. Phys. Anthropol. 143, 21-30.

Wallace I.J., Tommasini S.M., Judex S., Garland T. Jr., Demes B., 2012. Genetic variations and physical activity as determinants of limb bone morphology: An experimental approach using a mouse model. Am. J. Phys. Anthropol. 148, 24-35.

Ward C.V., 2002. Interpreting the posture and locomotion of *Australopithecus afarensis*: Where do we stand? Am. J. Phys. Anthropol. 119, 185-215.

Ward C.V., 2013. Postural and locomotor adaptations of *Australopithecus* species. In: Reed K.E., Fleagle J.G., Leakey R.E. (Ed.), The paleobiology of *Australopithecus*. Springer, Dordrecht, pp. 235-245.

Ward C.V., Ruff C.B., Walker A., Teaford M.F., Rose M.D., Nengo I.O., 1995. Functional morphology of Proconsul patellas from Rusinga Island, Kenya, with implications for other Miocene-Pliocene catarrhines. J. Hum. Evol. 29, 1-19.

Warden S.J., Bogenschutz E.D., Smith H.D., Gutierrez A.R., 2009. Throwing induces substantial torsional adaptation within the midshaft humerus of male baseball players. Bone 45, 931-941.

Warrener A.G., 2017. Hominin hip biomechanics: changing perspectives. Anat. Rec. 300, 932-945.

Washburn S.L., 1960. Tools and human evolution. Sci. Am. 203, 62-75.

Watson V., 1993. Composition of the Swartkrans bone accumulations, in terms of skeletal parts and animals represented. In: Brain C.K. (Ed.), Swartkrans: A cave's chronicle of early man. Transvaal Museum, Pretoria, pp. 35-73.

Weber G.W., 2015. Virtual Anthropology. Yrbk. Phys. Anthrpol. 156, 22-42.

Wells J.C., DeSilva J.M., Stock J.T., 2012. The obstetric dilemma: An ancient game of Russian roulette, or a variable dilemma sensitive to ecology? Am. J. Phys. Anthropol. 149, 40-71.

Werner C., Iversen B.F., Therkildsen M.H., 1988. Contribution of the trabecular component to mechanical strength and bone mineral content of the femoral neck. An experimental study on cadaver bones. Scandinavian Journal of Clinical and Laboratory Investigation 48, 457-460.

White T.D., Falk D., 1999. A quantitative and qualitative reanalysis of the endocast from the juvenile *Paranthropus* specimen L338y-6 from Omo, Ethiopia. Am. J. Phys. Anthropol. 110, 399-406.

Wolff J., 1870. Uber die innere architektur der knochen und ihre bedeutung für die frage vom knochenwachstum. Arch. Pathol. Anat. Physiol. Klin. Med. 50, 389-453.

Wood B.A., 1988. Are 'robust' australopithecines a monophyletic group? In: Grine F.E. (Ed.), Evolutionary history of the ''robust'' australopithecines. Aldine de Gruyter, New York, pp. 269-284.

Wood B.A., 1991. Koobi Fora research project. Hominid cranial remains, Vol. 4. Clarendon Press, Oxford.

Wood B.A., 2015. Wiley-Blackwell student dictionary of human evolution. J. Wiley & Sons, New York.

Wood B.A., Boyle E.K., 2016. Hominin taxic diversity: Fact or fantasy? Am. J. Phys. Anthropol. 159, 37-78.

Wood B.A., Constantino P., 2007. *Paranthropus boisei*: Fifty years of evidence and analysis. Am. J. Phys. Anthropol. 134, 106-132.

Wood B.A., Lieberman D.E., 2001. Craniodental variation in *Paranthropus boisei*: a developmental and functional perspective. Am. J. Phys. Anthropol. 116, 13-25.

Wood B.A., Schroer K., 2013. In: Begun D.R. (Ed.), A companion to paleoanthropology. Wiley-Blackwell, West Sussex, pp. 457-478.

Wood B.A., Schroer K., 2017. *Paranthropus*: Where do things stand? In: Marom A., Hovers E. (Ed.), Human paleontology and prehistory. Springer, Cham, pp. 95-107.

Yeni Y.N., Zinno M.J., Yerramshetty J.S., Zauel R., Fyhrie D.P., 2011. Variability of trabecular microstructure is age-, gender-, race- and anatomic sitedependent and affects stiffness and stress distribution properties of human vertebral cancellous bone. Bone 49, 886-894.

Yokley T.R., Churchill S.E., 2006. Archaic and modern human distal humeral morphology. J. Hum. Evol. 51, 603-661.

Zanolli C., Pan L., Dumoncel J., Kullmer O., Kundrát M., Liu W., Macchiarelli R., Mancini L., Schrenk F., Tuniz C., 2018. Inner tooth morphology of *Homo erectus* from Zhoukoudian. New evidence from an old collection housed at Uppsala University, Sweden. J. Hum. Evol. 116, 1-13.

Zeininger A., Patel B.A., Zipfel B., Carlson K.J., 2016. Trabecular architecture in the StW 352 fossil hominin calcaneus. J. Hum. Evol. 97, 145-158.

Zihlman A.L., Bolter D.R., Boesch C., 2007. Skeletal and dental growth and development in chimpanzees of the Taï National Park, Côte D'Ivoire. J. Zool. 273, 63-73.

Zipfel B., Berger L.R., 2009. Partial hominin tibia (StW 396) from Sterkfontein, South Africa. Palaeont. Afr. 44, 71-75.

Zipfel B., DeSilva J.M., Kidd R.S., Carlson K.J., Churchill S.E., Berger L.R., 2011. The foot and ankle of *Australopithecus sediba*. Science, 1202703.

Caractérisation multi-site de la distribution osseuse corticale et de l'organisation du réseau trabéculaire du squelette postcrânien de* Paranthropus robustus*: implications taxonomiques, fonctionnelles et paléobiologiques.

RESUME:
Le taxon du Pléistocène inférieur *Paranthropus robustus*, dont l'holotype est le spécimen TM 1517, a été défini en 1938 par le paléontologue R. Broom suite à la découverte d'éléments crâniens et postcrâniens sur le site de Kromdraai, Gauteng, en Afrique du Sud. Depuis, d'autres sites sud-africains ont contribué à l'extension de son hypodigme et fourni la preuve de sa contemporanéité à l'échelle macro-régionale avec des représentants des taxons *Australopithecus* et *Homo*. L'identification des hominines étant principalement basée sur l'analyse de la variation morphologique des éléments cranio-dentaires, un enjeu majeur dans l'étude des assemblages fossiles des sites sud-africains concerne donc l'identification et l'attribution taxinomique de restes isolés et/ou fragmentaires du squelette axial et appendiculaire non associés à des éléments cranio-dentaires. Il en résulte que plusieurs aspects fonctionnels et paléobiologiques du squelette postcrânien de *P. robustus* restent à préciser.

Au moyen de la microtomographie à rayons X, de l'imagerie virtuelle et d'analyses quantitatives en deux-trois dimensions, nous avons entrepris un projet de recherche visant à explorer, extraire et les patrons d'organisation endostructurale de spécimens fossiles communément, ou préliminairement, attribués à *P. robustus*. Sur une base comparative, nous visons à (i) identifier quelques caractéristiques osseuses endostructurales propres à ce taxon, qui pourraient fournir un cadre de référence pour l'attribution de spécimens fossiles isolés; (ii) déconstruire l'environnement biomécanique ayant façonné l'arrangement de l'os cortical et trabéculaire au niveau des articulations du coude, de la hanche et du genou; (iii) évaluer le degré de variation et, dans la mesure du possible, les différences liées au sexe et à l'âge.

L'échantillon étudié comprend quatre huméri distaux (TM 1517g, SK 24600, SKX 10924, SKX 34805), cinq fémurs proximaux (SK 82, SK 97, SK 3121, SKW 19, SWT1/LB-2), une patella (SKX 1084), des éléments additionnels échantillonnant l'assemblage TM 1517 (l'ulna proximale TM 1517e, la phalange distale d'hallux TM 1517k) et deux ilia (TM 1605, SK 50) provenant des sites de Kromdraai et Swartkrans. Le matériel comparatif comprend des Humains fossiles et actuels et des représentants des taxons *Pan*, *Gorilla* et *Papio*.

La distribution corticale de l'humérus distal offre un exemple de signal contrasté entre morphologie externe et interne, dénotant deux morphotypes endostructuraux: le premier est partagé par les fossiles sud-africains attribués à *P. robustus* et aux premiers représentants du genre *Homo*, alors que le second distingue le spécimen *H. erectus* de notre étude, qui se rapproche de la condition humaine actuelle. L'analyse comparative de l'assemblage de fémurs proximaux de Swartkrans a permis l'identification de certaines caractéristiques jusqu'alors non décrites (y compris des différences liées au sexe), notamment au niveau du col fémoral, indiquant une cinématique de la marche chez *Paranthropus* distincte de celle humaine, mais suggérant également de possibles différences biomécaniques de l'articulation de la hanche par rapport à *A. afarensis* et *A. africanus*. La signature endostructurale extraite de la patella non complète SKX 1084, initialement attribuée à un individu *P. robustus* de petite taille, ne permet pas de rejeter son statut taxinomique. Enfin, la recherche non-invasive à haute résolution de traces d'une fusion récente, ou incomplète, de l'épiphyse de TM 1517g, de TM 1517e et de TM 1517k soutient l'hypothèse que certains éléments de l'assemblage odonto-squelettique de Kromdraai répertorié TM 1517, comprenant l'holotype de *P. robustus*, échantillonne un seul individu adolescent-jeune adulte présentant un modèle de maturation plus proche de la condition observée chez les chimpanzés que chez les Humains actuels.

MOTS CLES: *Paranthropus robustus*; squelette postcrânien; os cortical; os trabéculaire; micro-tomographie à rayons X ; morphologie fonctionnelle

Multi-site characterisation of cortical bone distribution and cancellous network organisation in the **Paranthropus robustus** *postcranial skeleton: Taxonomic, functional and paleobiological implications.*

ABSTRACT:
The Early Pleistocene taxon *Paranthropus robustus*, represented by the holotype TM 1517, was established in 1938 by the paleontologist R. Broom following the discovery of craniodental and postcranial remains at the cave site of Kromdraai, in Gauteng, South Africa. Since, other Southern African sites have contributed to the extension of its hypodigm, providing evidence for its chronological overlap in the macro-region with representatives of the taxa *Australopithecus* and *Homo*. As species identification in the hominin fossil record is commonly based on the comparative assessment of craniodental anatomy and morphological variation, the rarity in the hominin-bearing South African cave assemblages of unambiguously associated craniodental and postcranial remains usually complicates the task of identifying isolated and fragmentary elements from the axial and the appendicular skeleton. Consequently, different functionally- and paleobiologically-related aspects of the *P. robustus* postcranial skeleton remain poorly known.

By means of techniques of high resolution X-ray micro-tomography and virtual imaging coupled with two-three-dimensional quantitative analyses, in this research project we explored, extracted and assessed the patterns of endostructural organisation in some fossil specimens commonly, or tentatively, attributed to *P. robustus*. On comparative ground, we aim at (i) identifying some endostructural bony features characteristic of this taxon, if any, thus tentatively providing a reference framework for the attribution of isolated fossil specimens; (ii) deconstructing the biomechanical (loading) environment having shaped the cortical and cancellous bone arrangement at the elbow, the hip, and the knee joints; (iii) assessing variation and, whenever possible, sex- and age-related differences.

The investigated sample consists of four distal humeri (TM 1517g, SK 24600, SKX 10924, SKX 34805), five proximal femora (SK 82, SK 97, SK 3121, SKW 19, SWT1/LB-2), a patella (SKX 1084), some additional elements from the assemblage labelled TM 1517 (the proximal ulna TM 1517e, the distal hallucial phalanx TM 1517k), and two ilia (TM 1605, SK 50) from the sites of Kromdraai and Swartkrans. The comparative material used in this project consists of fossil and extant humans and of representatives of the taxa *Pan*, *Gorilla* and *Papio*.

Cortical bone distribution at the distal humerus offers an example of contrasting signal between the outer and the inner morphology, indicating two endostructural morphotypes: the first is shared by *P. robustus* and South African Early *Homo*, while the second clearly sets apart the *H. erectus* representative used in this study, which more closely approximates the extant human condition. The comparative analysis of the assemblage of proximal femora from Swartkrans–allowed the identification of some previously unreported features (including likely sex-related differences), especially at the femoral neck, indicating a gait kinematics in *Paranthropus* distinct from the human one, but also suggesting possible hip joint loading differences with respect to *A. afarensis* and *A. africanus*. The endostructural signature extracted from the partial patella SKX 1084, originally attributed to a small-bodied *P. robustus*, did not allow rejection of its suggested taxonomic status. Finally, the high-resolution noninvasive search for any remnant of a recent, or even still incomplete, epiphyseal closure in TM 1517g, TM 1517e and TM 1517k supports the suggestion that the odontoskeletal assemblage from Kromdraai labelled TM 1517, which includes the *P. robustus* holotype, actually samples a single late adolescent-young adult individual displaying a maturational pattern closer to the chimp than to the extant human condition.

KEYWORDS: *Paranthropus robustus*; postcranial skeleton; cortical bone; trabecular bone; X-ray micro-tomography; functional morphology